Technical
University of
Denmark

# Ship Collision Damage

Marie Lützen
PhD thesis
December 2001

Department of
Mechanical
Engineering

MEK

Maritime
Engineering

# Ship Collision Damages

Marie Lützen

TECHNICAL UNIVERSITY OF DENMARK
DEPARTMENT OF MECHANICAL ENGINEERING
MARITIME ENGINEERING
DECEMBER 2001

*Published in Denmark by*
Technical University of Denmark



*Maritime Engineering*
*Department of Mechanical Engineering*
*Technical University of Denmark*
*Studentertorvet, Building 101E, DK-2800 Kgs. Lyngby, Denmark*
*Phone +45 4525 1360, Telefax +45 4588 4325*
*E-mail: maritime.engineering@mek.dtu.dk*
*WWW: http://www.mek.dtu.dk/*

Publication Reference Data
*Lützen, M.*
*Ship Collision Damages*
*PhD Thesis*
*Technical University of Denmark, Maritime Engineering.*
*December, 2001*
*ISBN 87-89502-60-4*
*Keywords: Ship collisions, probabilistic damage stability, damage statistics, simulation*

# Preface

This thesis is submitted as a partial fulfilment of the requirements for the Danish Ph.D degree. The work has been performed at the Section of Maritime Engineering, the Technical University of Denmark, during the period from September 1998 to December 2001. The project was supervised by Professor Preben Terndrup Pedersen, whose help and guidance are highly appreciated.

The study was financially supported by the Technical University of Denmark and this support is gratefully acknowledged.

Special thanks to Preben Terndrup Pedersen, Bo Cerup Simonsen, Jørgen Juncher Jensen and Peter Friis Hansen for several inspiring discussions and suggestions.

Thanks to my colleagues at the Department, friend and family for invaluable help and support. Special thanks to Søren for his support and understanding during the entire study.

Marie Lützen
Kgs. Lyngby, December, 2001

This page is intentionally left blank.

# Executive Summary

The purpose of this thesis has been to develop a rational procedure for analysis of ship collisions, addressing all types of ships and damage scenarios.

The covered main aspects are:

1. Deterministic analysis of ship collisions
2. Numerical Monte Carlo based simulations of ship collisions for estimation of distributions for the damage to the struck vessel and of the energy released for crushing
3. Analysis of damage statistics related to ship collisions
4. A new proposal for damage stability regulation using the probabilistic approach

The work concerning deterministic analysis of ship collisions includes the following main aspects:

- Presentation of a collision model based on the principle of splitting the collision problem into an internal and an external analysis, where the external analysis deals with the movements of the two vessels and the interaction with the surrounding water during the collision, whereas the internal analysis or the internal mechanics is concerned with the response of the structure. The internal mechanics is described in more detail and the calculation procedure is validated by formerly performed experiments on double hull-structures
- Establishment of models for describing the geometry of the striking bow and the structure of the side of the struck vessel. The bow geometry is idealised so that the geometry can be described by few parameters, still covering with sufficient accuracy almost all existing bows. The side structure modelling is based on the principle that the area of the struck ship which is effected by the collision is restricted to the area touched by the bow of the striking vessel.

- Three programs have been developed for the deterministic analysis:
  - Damage to the struck vessel
    The results from the developed program have been compared to results from other programs for analysis of collisions. In order to investigate the sensitivity of the collision analysis, the effect of changing the striking location and the design of the side of the struck vessel have been analysed
  - Damage to the striking vessel
    Two models for bow crushing have been presented, one dealing with longitudinally stiffened bows, the other with transversely stiffened bows. The bow strengths for the two differently stiffened vessels have been compared
  - Damage to both vessels
    A sensitivity analysis has been carried out using a series of computer simulations of collisions involving 11 different ships, five striking and six struck, in order to determine when the energy released for crushing is absorbed by the bow of the striking vessel or by the side structure of the struck vessel

The work concerning numerical Monte Carlo based simulations of ship collisions includes the following main aspects:

- Establishment of a probabilistic method for determination of damage and energy distributions. The probabilistic analysis is based on input distributions of striking vessels, velocities, striking locations and collision angles. This input can be separated into three groups, the struck vessel, the striking vessels and the collision scenarios. The input parameters for these groups are analysed in detail
- The probabilistic method has been used for the following analyses:
  - Fifteen different struck vessels have been subjected to the damage analysis giving distributions for the damage lengths and penetrations
  - Distributions for energy to be absorbed by crushing of the ship's structure have been calculated for vessels sailing in worldwide trade, the Straits of Dover and Gibraltar and the eastern and western routes through the Great Belt

A damage database containing information on past collisions, collected within the European research program HARDER has been analysed with respect to collision type, the relation between the struck and the striking vessel and the relation between damage parameters and the main particulars of the struck vessel.

Based on findings from the numerical simulations and the analysis of the damage statistics a new proposal for damage stability regulation using the probabilistic approach is given.

# Synopsis

Formålet med dette studium har været udvikling af en rationel procedure til analyse af skibskollisioner. Analysen inkluderer alle typer af skibe og kollisionsscenarier.

Arbejdet er delt i fire hovedområder:

1. Deterministisk analyse af skibskollisioner
2. Numeriske, Monte Carlo baserede simuleringer af skibskollisioner. Hovedformålet er her etablering af skadesfordelinger på det ramte skib og fordelinger for den kollisionsenergi, der skal optages i skibets struktur ved knusning og deformation
3. Behandling af skadesstatistik vedrørende skibskollisioner
4. Udvikling af forslag til et nyt sæt af lækstabilitetsregler

De væsentligste aspekter af arbejdet med den deterministiske analyse af skibskollisioner er:

- Præsentation af en kollisionsmodel, hvor den ydre dynamik og den indre mekanik behandles i to adskilte analyser. Den ydre dynamik behandler skibenes bevægelser under kollisionen, herunder interaktionen med det omgivende vand. Formålet med denne analyse er at bestemme tabet af kinetisk energi. I analysen af den indre mekanik behandles knusning og deformationer af skibsstrukturen, herunder energioptaget
- Etablering af modeller til beskrivelse af bovgeometrien på det rammende skib og sidestrukturen i den ramte skibsside
- Udvikling af tre programmer til bestemmelse af skader på skibe:
  - Skader på det ramte skib
    Resultater fra dette program sammenlignes med resultater fra andre kollisionsprogrammer. Herudover er der udført sensitivitetsanalyser angående placering af kontaktpunkt og det strukturelle design af ramte skib

  - Skader på rammende skib
    Præsentation af to forskellige modeller til bestemmelse af bovdeformation på henholdsvis tværskibs- og langskibs-afstivede skibe. Styrken af de to bovafstivningstyper er sammenlignet
  - Skader på både ramte og rammende skib
    Analyser hvor både det ramte og det rammende skib deformerer under kollisionen. Tredive forskellige kollisionsscenarier er undersøgt. Disse kollisioner involverer fem rammende og seks ramte skibe.

De væsentligste aspekter i arbejdet vedrørende numerisk simulering af skibskollisioner er:

- Etablering af en probabilistisk metode til bestemmelse af skades- og kollisionsenergifordelinger. Den probabilistiske metode bygger på kendte fordelinger af rammende skibe, hastigheder, kontaktpunkter og kollisionsvinkler. Forslag til disse inputfordelinger er fundet bl.a. ved hjælp af skibs- og skadesdatabaseanalyser
- Den udviklede probabilistiske metode er bl.a. anvendt til følgende:
  - Fordelinger for skadeslængder og indtrængninger er fundet for femten forskellige ramte skibe
  - Fordelinger for kollisionsenergi er beregnet for skibe, der sejler i fri fart gennem Dover eller Gibraltar strædet samt gennem den vestlige eller østlige rute i Storebælt

En skadesdatabase indeholdende informationer om tidligere observerede kollisioner er etableret i forbindelse med det europæiske forskningsprojekt HARDER. Denne database er benyttet til etablering af skadesstatistik og til bestemmelse af relationer mellem ramte og rammende skibe samt mellem ramte skibe og skadesstørrelser.

Baseret på numeriske simuleringer og analyse af skadesstatistik er der udarbejdet et forslag til et nyt sæt af lækstabilitetsregler.

# Contents

# Chapter 1

# Introduction

## 1.1 Overview and Background

The overall goal of this thesis is to develop rational procedures for analysis of ship collisions, addressing all types of ships and damage scenarios. The procedure ends up giving methods for both deterministic and probabilistic analyses of damages to vessels.

The vessels of today have a built-in passive safety based mainly on the damage stability regulations, which either build on traditional deterministic methods or on the more modern probabilistic approach. In the usual deterministic procedure, all relevant one- or two-compartment damages must be analysed in order to verify compliance with the requirements in the regulations. This may be reasonable for ships with a standard compartmentation, but may lead to either too unsafe or too conservative ship designs. A way out of this dilemma may be the probabilistic approach, where all possible damages are considered and weighed with regard to survivability.

The first international probabilistic concept for damage stability regulation, Resolution A.265, IMO (1971), was adopted by IMO in 1971. The probabilistic rules were an optional alternative to the deterministic passenger vessel regulation in the SOLAS Convention and were developed for passenger vessels only. The passenger vessel regulation was in 1990 followed by the adoption of subdivision and damage stability rules for dry cargo vessels, SOLAS (1990), also based on the probabilistic concept. While the probabilistic rules for cargo vessels are generally based on the same overall principles and damage statistics as the passenger vessel rules, there are some differences, specially the treatment of the vertical extent of damage.

The damage statistics for the passenger vessel A.265 regulation is based on data collected for casualties occurring in the 1950's and 1960's and covers vessels commonly used at that time. These vessels were considerably different from the ship design of today. Many of the

vessels were often designed with many decks. Even though the shortcomings of the statistics were well known, the same statistics was used for the dry cargo regulation in 1990. The shortcomings mainly arise from lack of updating the statistics, but also from the fact that the statistics is based on only 296 ship collisions.

The International Maritime Organization (IMO) is currently seeking to harmonise the damage stability regulation for all types of vessels using the probabilistic damage stability concept. Following, introduction of the probabilistic damage stability requirements of dry cargo ships, SOLAS Part B-1, IMO put on their work program for harmonisation of all damage stability requirements in SOLAS, using a probabilistic concept of survival. The main framework of these new harmonised regulations should follow the concept of SOLAS Part B-1, but include the main features of IMO Res. A.265 and the current deterministic regulations of SOLAS Chapter 8, also referred to as SOLAS 90.

In parallel with the activity within IMO, a European research program entitled HARDER, "Harmonization of Rules and Design Rationale", was initiated, see Harder (2000). The project, which was begun in 2000, is presently carried out to investigate systematically the validity, robustness, consistency, and impact of all aspects of the harmonised probabilistic damage stability regulations.

A part of the work presented in this thesis is also included in technical reports from the research project HARDER.

## 1.2 Objectives and Scope of the Work

With the overall objective of improving the safety of ship's structures with respect to accidental loads, the present thesis focuses on ship collisions.

The basic modelling of a given collision is quite complex and involves the coupled effects of:

- The global motion of the two ships during the collision
- Hydrodynamic forces from the surrounding water, arising from ship accelerations
- Friction between the bow of the striking vessel and the side of the struck vessel
- Large plastic deformation of the involved structures
- Fracture and propagation of cracks in the structure

Depending on the level of detail, each of these effects can be complex to model and predict theoretically. Therefore, it is essential to simplify carefully the modelling as much as possible with due consideration to the desired level of accuracy.

A well known theoretical model for prediction of collision damage is due to Minorsky (1959). He separated the collision problem into two, namely the external dynamics and the internal mechanics. The external dynamics deals with the global motion of the vessels and the interaction with the surrounding water during the collision, whereas the internal mechanics is concerned with the response of the structure. The present theoretical collision model is based on the same idea of splitting the problem into an internal and an external analysis. When both the rigid body dynamics and the crushing internal mechanics are known the damage to the struck vessel can be determined by comparison of the results from the two analyses.

When the struck and the striking vessels are known, a deterministic analysis can be performed and a quite accurate estimate of the damage can be made. In the Monte Carlo approach the deterministic calculations are carried out for many different choices of striking vessels and collision scenarios along the above-mentioned lines, so that the probability distribution for the damage to the struck vessel and for the energy released for crushing can be determined.

Casualty statistics related to ship collisions has been collected in order to update the original damage database from IMO. This statistics has been used to analyse the historical distributions of damage locations and damage sizes.

The results from the analysis of the damage statistics have been compared to results from numerical simulation. The outcome of these analyses is new proposals for damage distributions regarding both striking locations, damage sizes and maximum upper extent of damage. These distributions have been used to establish a new proposal for the damage stability regulations for vessels by using the probabilistic approach.

The thesis is composed as follows:

In Chapter 2 a framework for risks associated with collisions is presented.

Chapter 3 gives the model for the external dynamics, which deals with the movements of the two vessels and the interaction with the surrounding water during the collision. The aim of this analysis is to estimate the fraction of the kinetic energy which is released for crushing of the structure.

In Chapter 4 the crushing analysis or the internal mechanics is presented. The chapter starts with a presentation of the principles of modelling the bow of the striking vessel and the structure on the side of the struck vessel. The crushing analysis deals with the deformation of the side of the struck vessel and the bow of the striking vessel. It is very difficult to obtain a precise calculation of the internal mechanics as the collision strength of a ship is governed by a complex mixture of buckling, yielding, tension, tearing, rupture and brittle failure of materials. Owing to this complexity of the problem, a simplified but rational method is used to determine the energy absorption in the ship's structure. The results from the method are compared to experimental results.

Chapter 5 introduces a method for prediction of damage to vessels in a collision event. The collision analyses are purely deterministic. The chapter starts with a description of the program modelling. Three programs have been developed for the deterministic analysis: one predicting the damage to the struck vessel, the second predicting the of damage to the striking vessel and the third predicting the damage to both vessels. The program structure is described in detail, including the necessary input and the program output. The results from the developed programs have been compared to results from other programs for analysis of collisions. In order to investigate the sensitivity of the collision analysis, the effect of changing the striking location and the design of the side of the struck vessel have been analysed. The last section of the chapter deals with minor damages to vessels. The minor damages may arise at sea during collision with floating objects or by contact with obstacles during manoeuvring in harbour areas. The question of how large permanent deformation can be accepted without having the vessel repaired is raised in this section.

In Chapter 6 the probabilistic method for determination of damage distributions is presented. The probabilistic program or calculation method is build up around the deterministic program calculating damage to the struck vessel introduced in Chapter 5. The analysis concerns one particular struck vessel. The input for the striking vessels and for the collision scenarios differs from the deterministic analysis. In the probabilistic analysis not only one striking vessel or one particular collision scenario is enough. Therefore, the input parameters for these groups are analysed in detail. Output from the program is distributions for the damage to the struck vessel and for the energy released for crushing. Fifteen different struck vessels have been subjected to the damage analysis. In the energy analysis five cases have been investigated, namely struck vessels in worldwide trade, in the Straits of Dover and Gibraltar and the eastern and western routes through the Great Belt.

Chapter 7 starts with a short description of the damage database, collected within the European research program HARDER. The database is analysed with regard to collision type, the relation between the struck and the striking vessel and the relation between the damage parameters and the main particulars of the struck vessel.

In Chapter 8 the results from the numerical simulation, regarding the distributions of damage sizes, are compared to the distributions obtained from the damage statistics.

In Chapter 9 the damage distributions have been used to establish a new proposal for the damage stability regulations for vessels by using the probabilistic approach. The main concept of the probabilistic damage stability regulation from A.265 and SOLAS part B-1 is used for determination of the subdivision index $A$. The current method for calculation of the index is validated using the damage statistics, and new proposals for parameters contained in the expression for $A$ are given. The chapter includes small application examples, where the new parameter proposals are compared to current regulation.

Chapter 10 contains the conclusions.

# Chapter 2

# Risk Analysis of Collisions

Shipping regulations have over many years been developed on the basis of some significant marine accidents. Therefore, the regulations are mostly concentrated on reducing the consequences. Often this can be an effective method, but in some circumstances it may be better to reduce the likelihood of an accident occurring.

The ship collision analysis may be performed in three steps: estimation of the probability of collisions, the consequences and finally recommendations for decision-making.

**Probability of a Collision**

When the probability of a collision is to be determined all factors related to the risk of a collision must be identified. In the present analysis a method of splitting the probability of a collision into two separate analyses is used. First the number of possible ship collisions is estimated, if no aversive manoeuvres are made. The result from this analysis is mostly concerned with the waterway and the size of the involved vessels. Then the causation probability or the fraction of the possible collisions, which result in a collision event is estimated. The causation probability is influenced by a large number of factors related both to the waterway, the involved vessels and to the human factor. Methods of analyses for finding the causation factor may include e.g. fault trees or Bayesian networks.

When all factors related to the risk of a collision are identified, they can be separated into two groups. The first group contains the factors which can be controlled. Factors in this group may be denoted as risk control options. The other group contains factors which cannot be controlled. Factors in this group are mainly related to the environmental conditions.

The factors concerning estimation of the probability of a collision are described in more detail in Section 2.1.

### Consequence Estimation

Factors which may reduce or increase the consequences of the collision must be found. The consequences cannot only be related to the structural deformation of the vessel. Also human safety, the effect on the environment, the economic consequences, the reputation of the shipping company and the amount and the type of the oil outflow may be included in this analysis.

The ship collision consequences are described in more detail in Section 2.2.

### Recommendations for Decision Making

A way of evaluating the collision risk could be an analysis of the combination of the frequency and the consequences of collision, Figure 2.1 illustrates the model. To bring a vessel from an intolerable to an acceptable situation may be performed by reducing the frequencies and/or the consequences of the collisions. The diagram shown in Figure 2.1 is called the risk diagram or the ALARP (As Low As Reasonable Practicable) diagram. By this method the risk involved in shipping can be compared with other transportation forms.

The risk assessment or the cost-benefit analysis may provide a decision tool or recommendations for specific risk reduction measures, either preventive as vessel traffic systems (VTS) or protective as new design criteria for the structure of the involved vessels. Making a cost-benefit analysis could be a way of quantifying the consequences, in this process it is needed to quantify values for statistical life, pollution and property. The term cost-benefit refers to the costs of risk reduction in relation to the achieved benefits.

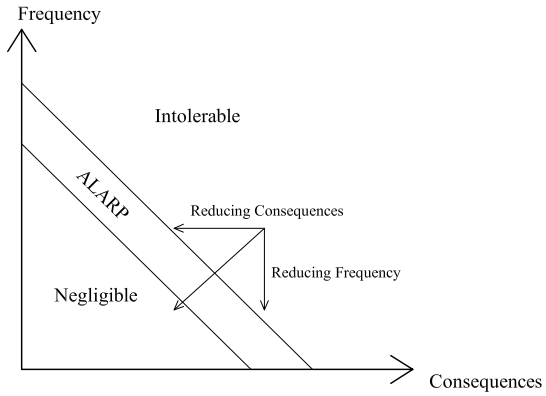


Figure 2.1: *The ALARP diagram.*

Not only is the overall collision analysis result interesting, but also other analyses concerning the collision event may be performed, e.g.:

- Comparison of ship structures for better energy absorption
- Effect of human errors, technical failures and environmental conditions

- Comparison of waterways or traffic regulation systems
- Cost-benefit analysis of given fixed shipping routes
- Comparison in connection with route planning

## 2.1 Ship Collision Probability

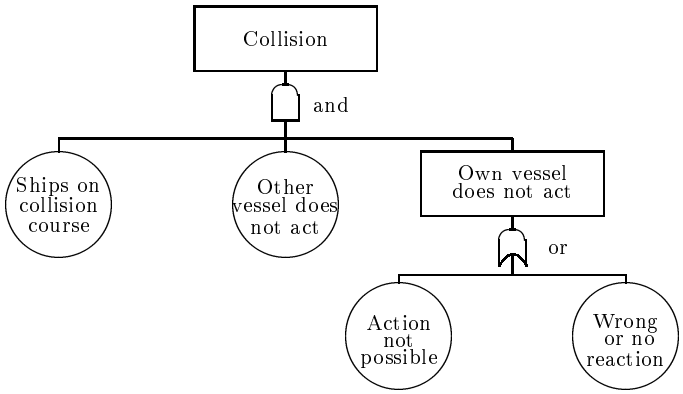


Figure 2.2: *Procedure for determining the probability of collision.*

The probability of a collision is described by the fault tree in Figure 2.2. If two vessels collide it is required that the vessels are on collision course and none of the vessels make any action to avoid the situation. The probability of no action, given that the other vessel as well does not act, is called the causation factor, which can also be defined as the fraction of the collision candidates, which result in an accident.

The probability of a collision can be determined from the number of possible ship collisions and be estimated as

$$P[collision] = 1 - e^{-N_{ship-ship}}$$

where $N_{ship-ship}$ is the expected number of ship to ship collisions, which can be determined as

$$N_{ship-ship} = P_c N_a$$

Here $P_c$ is the causation probability, and the number of possible ship collisions is denoted $N_a$. A more detailed description of these parameters will be given in Sections 2.1.1 and 2.1.3.

The number of possible ship collisions may be ignored during the analysis by assuming that all vessels will experience the same level of traffic during their lifetime. This sounds reasonable if the same sizes and types of vessels are compared, which is the case in many analyses. But a calculation of choosing alternative routes between two ports requires a

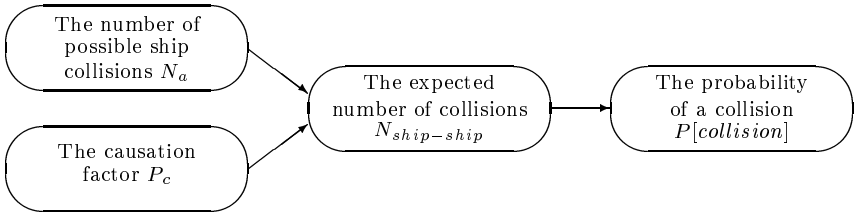


Figure 2.3: *Probability of collision.*

calculation of possible collision candidates, which is also the case in connection with a cost-benefit analysis of a given fixed shipping route. An analysis of a traffic system may include analyses of technical, navigational and environmental issues and the types and sizes of vessels passing that particular location.

The following three sections deal with the identification of factors related to the risk of a collision, finding the causation probability and determining of the number of possible ship collisions in a particular area.

### 2.1.1 Collision Risk Factors

The first step of the analysis is to define the system of interest. This means - define the structure, group the elements and define their relationship - define the output from the system and the impacts of interest.

Determination of the probability analysis of a collision requires combination of knowledge and modelling of risk, involving human factors, the nature of the waterway, description and modelling of the ship structure deformation, global motions of the vessels and technical installations, both in connection with the waterway and on board the vessels.

Reducing the probability of a collision may also be referred to as preventing the vessels from collisions. Preventing a vessel from accidents is one of the main objectives of the shipping industry, as accidents in many cases will result in loss of life, lost operational time, lost income and insurance claims from passengers, authorities or cargo owners.

This section includes an analysis of factors which may influence the probability of a collision. These factors are here separated into three main groups:

- The waterway system including environmental conditions
- The involved vessels
- Human factors

The vessels cannot be analysed isolated from the waterway. Likewise the waterway cannot be analysed isolated from the vessel, and both the ship and the waterway are complex systems involving physical and human elements and are extremely interdependent. However, to identify factors related to risk and later to identify where to implement actions of prevention, it seems to be a good separation.

The factors influencing the risk of a collision are shown in Figures 2.4 - 2.6, where they are separated into the three main groups: the waterway system, the involved vessels and human factors. Some of the factors are difficult to change, but most of the factors mentioned in the following can be considered as risk control options, which can be used as parameters in cost-benefit analyses.

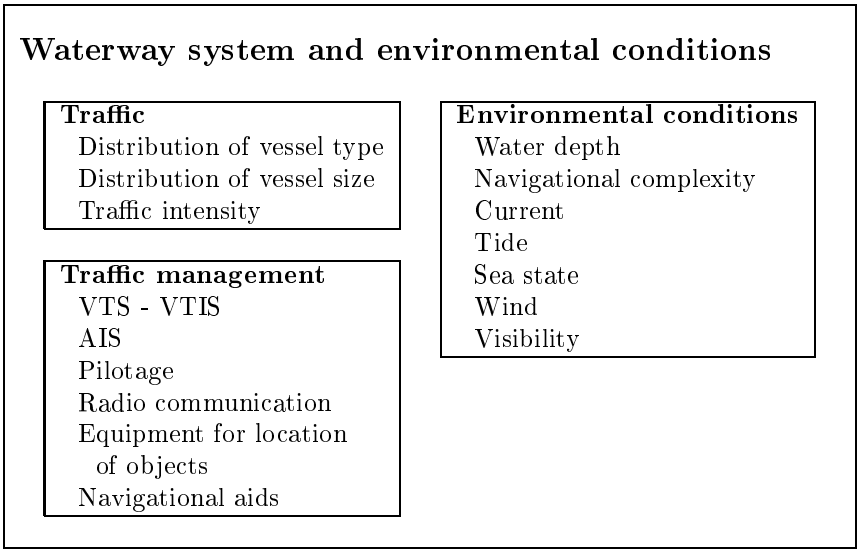


Figure 2.4: *Influence of the waterway system on the probability of a collision.*

### Waterway System and Environmental Conditions

The waterway system is analysed considering the traffic in that particular area, the management of the waterway system and the environmental conditions. The analysis of the traffic includes information about the types and sizes of passing vessels and of the traffic intensity. Factors describing the traffic can normally not be changed, as they are a result of the surrounding harbours.
Most regions in the world are not restricted in navigation, only the rules of the sea apply. Other areas are equipped with a vessel traffic system (VTS) or pilotage as a mandatory or voluntary system. VTSs are land-based marine vessel systems usually operated by government authorities. The main objective is to ensure safe navigation in restricted shipping areas, such as coastal waters, heavy traffic areas, and areas of difficult navigation. The management of the VTSs varies depending on the size and the navigational difficulties of the location, but generally the system is equipped with radars for location of objects and vessels and has equipment for inspection of navigational aids as buoys, light houses etc. Most VTSs have mandatory or voluntary reporting systems, where radio communication is often used.

Most of the factors involved in the management of the traffic can be changed and they are therefore risk control options.
Environmental conditions may also be considered. The navigational conditions may be restricted because of the water depth or the complexity of the waterway. Current and wind may set the vessel, or the visibility can be restricted because of heavy rain, fog, smoke, or sea spray. In this case the complexity of the waterway and perhaps the water depth can be risk control options, whereas the other factors normally cannot be changed.

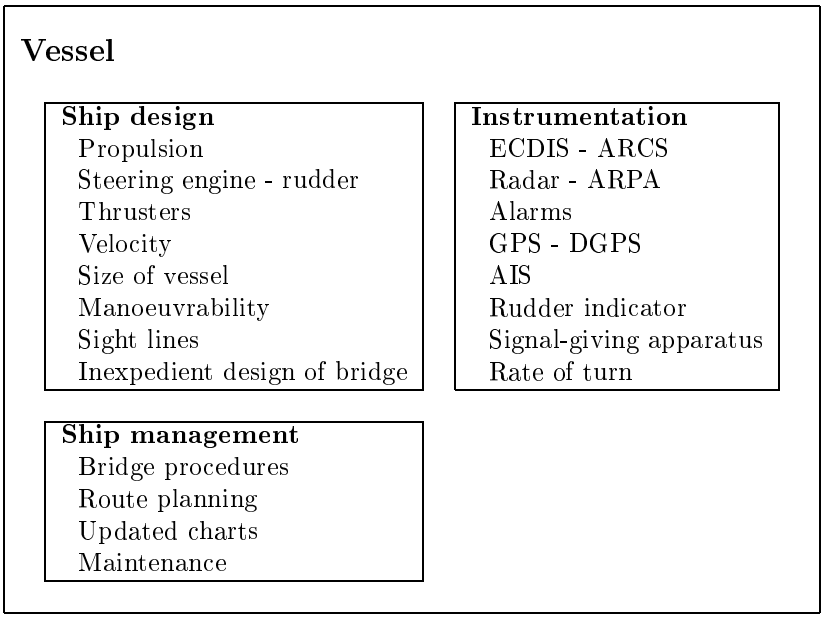


Figure 2.5: *Influence of the vessel on the probability of a collision.*

### The Vessel

The vessel analysis includes design, instrumentation and management. The design and the instrumentation are directly related to the particular vessel, whereas the management of the vessel may both be related to the crew on board and the shipping company. The International Maritime Organization (IMO) has laid down conventions and guidelines for education of the crew on board, guidelines for the equipment, and contingency planning for emergencies. The maintenance of both the vessel and the equipment on board is normally examined by classification societies or authorities at regular intervals.
The introduction of the automatic identification system (AIS) on ships and on shore-based VTS stations may in the future have a large impact on the number of accidents at sea. The system makes it possible to identify and track vessels from other vessels and from shore stations. Unfortunately, the system cannot be reliable before all vessels are equipped with AIS transponders, which might take several years.
All factors involved in describing the vessel system are risk control options, except for the size of the vessel.

### Human Factors

The human factors resulting in ship collisions are normally due to the officer on watch, but also the communication on board the vessel is of great importance. Multi-cultural crew with several languages makes it important to have one and only one language of communication. The human factors, which can be seen in Figure 2.6, are explained in more detail in Section 2.1.3 regarding the causation probability. All factors are here risk control options.

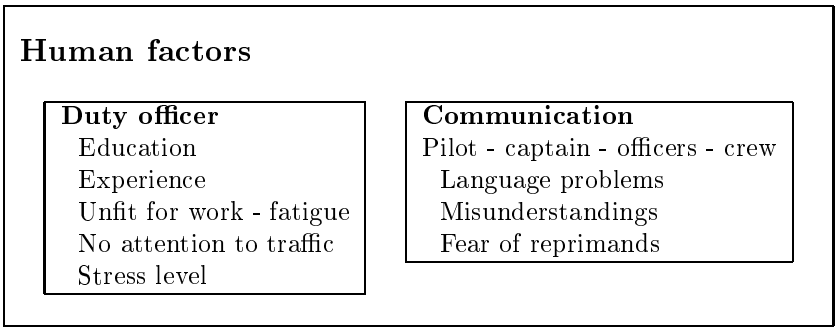


Figure 2.6: *Influence of human factors on the probability of a collision.*

## 2.1.2 The Number of Possible Ship Collisions

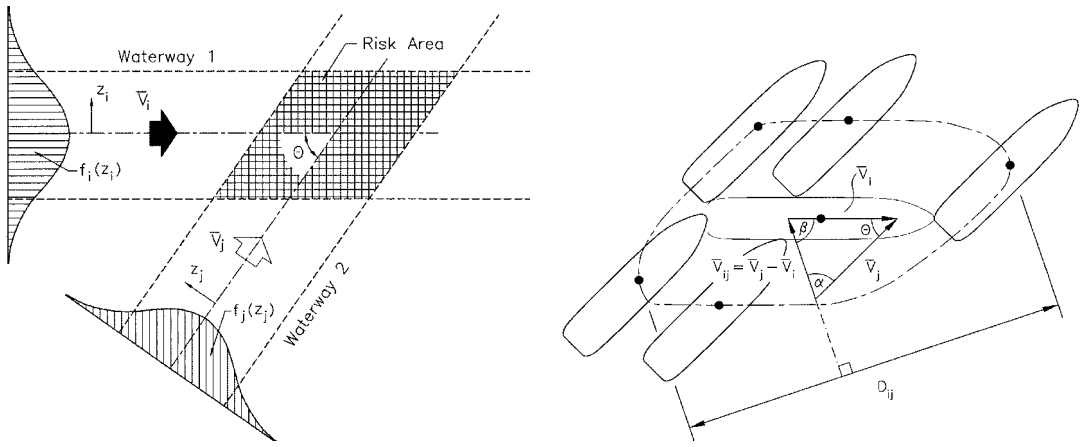


Figure 2.7: *Left: waterway intersection. Right: definition of collision diameter (Pedersen, 1995).*

The number of possible ship collisions, $N_a$, is here defined as the number of collisions if no aversive manoeuvres are made. A method for determining the number $N_a$ for the purpose of comparing alternative routes or estimating the navigational difficulties of waterways has been presented by Pedersen (1995). It is seen from this reference and also from Figure 2.7 that by summing all the class "$j$" ships of waterway 2 on collision course with all relevant

class "$i$" ships during the time $\Delta t$, the following expression can be obtained

$$N_a = \sum_i \sum_j \int \int_{\Omega(z_i z_j)} \frac{Q_i^{(1)} Q_j^{(2)}}{V_i^{(1)} V_j^{(2)}} f_i^{(1)}(z_i) f_j^{(2)}(z_j) V_{ij} D_{ij} dA \Delta t$$

Here $Q_j^{(2)}$ is the traffic flow (i.e. the number of ships per unit of time) of class "$j$" in waterway 2, $V_j^{(2)}$ is the associated speed. The lateral distribution of the ship traffic of class "$j$" in waterway 2 is denoted $f_j^{(2)}$, $D_{ij}$ is the geometrical collision diameter defined in Figure 2.7, and finally the relative velocity is defined $V_{ij}$.

### 2.1.3 The Causation Probability

The causation probability, $P_c$, is the fraction of the collision candidates resulting in an accident. This number can be estimated on the basis of statistical accident data, but another approach is to analyse the cause leading to human inaction or external failures by e.g. fault trees or Bayesian networks.

The causation probability is the conditional distribution of no action from own vessel, given that the other vessel does no act. The reason for no action can be separated into: a) that action is not possible or b) action is possible but the officer on watch does not act or makes a wrong decision. These events are a mixture of mechanical failures, human errors or failures due to environmental conditions. The input 'action not possible' is a mixture of mechanical failures and environmental conditions. The mechanical failures are engine, steering engine, rudder or thruster problems. These failures might depend on the maintenance of the vessel or the experience and the education of the crew. The environmental conditions are related to the waterway or location, where the route might be restricted by sea depth, bridge pillars etc. Also sudden wind squalls or current might surprise the captain or officer on watch. Some failure states for 'wrong or no reaction' are described in Table 2.1. It is seen that both the waterway system, the vessel and the human factors are represented.
The waterway or the location can be presented as both visible and invisible, the traffic intensity and the number of possible collision candidates are factors given directly from the location, but also other causes leading to failure states are affected by the location. If the vessel is passing a trafficked area, the officer on watch will probably be more attentive and aware of the situation. The human factors such as experience and education are as well related to many failure states, but also a factor as fear of reprimands, which is not directly mentioned, may be of great importance. Examples are: the lookout is afraid of warning the officer, or the officer is afraid of warning the captain or calling for an extra officer in case of heavy traffic or illness. Many failures may arise from the lack of competence on board the vessel. That is ships, operated with lack of control systems, e.g. bridge procedures, under a pressure to maintain a schedule, fear of reprimands for pointing out faults or defects, or not observing rules on time of rest etc. These failures can in many cases be traced back to the management of the shipping company.

Friis Hansen and Pedersen (1998) have by use of a Bayesian network estimated the causation factor for meetings between conventional vessels to be $P_c = 9.0 \cdot 10^{-5}$.

| **Failure state** | **Causes** |
|---|---|
| Incompetence | Experience |
| | Education |
| | Incorrect reading of instruments |
| | Violation of rules of the sea |
| | Incorrect evaluation of current and wind |
| Paralysed | Experience |
| | Education |
| No observation by lookout | Lookout does not respond |
| | Language problems |
| | Misunderstandings |
| Poor visibility | Heavy rain |
| | Smoke |
| | Fog |
| | Sea spray |
| | Blind angles |
| No attention to traffic | Paper work |
| | Inexpedient bridge design |
| | Alcohol or the like |
| | Fallen asleep |
| | Fire |
| | Tuning of instruments |
| | Radio communication |
| | Changing of the watch |
| | Chat |
| | Tiredness |
| Unfit for work | Sudden illness |
| | Illness |
| Stress | Personal problems |
| | Heavy traffic intensity |
| | Alarms or noise |
| ARPA knowledge | Misunderstandings |
| | Refreshment rate of data |
| Radar status | Sea clutter |
| | Rain clutter |
| | Heavy traffic (fishing area) |
| Radar failure | Mechanical failure |
| Radar not started | |

Table 2.1: *Failure states - causes leading to no action during a collision.*

## 2.2 Ship Collision Consequences

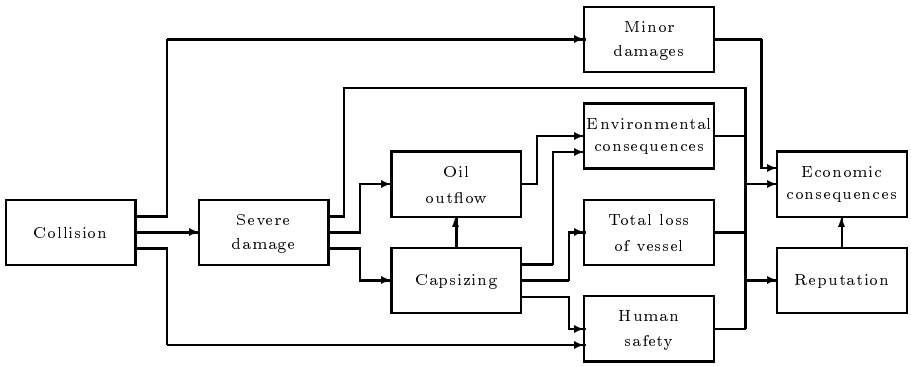


Figure 2.8: *Consequences of a collision.*

The consequences of a collision, see Figure 2.8, can be separated into consequences for the vessel as minor damages, severe damage or total loss, consequences for human safety or for the environment. From these may follow consequences for the shipping company in the form of a bad reputation or economic consequences. The individual consequences are described in more detail in the following.

- Human safety
  Human safety is normally not directly affected by a collision, but in the case of severe damage to the vessel, the vessel may capsize and lives may be lost. Especially, collisions involving passenger ships may result in a high risk. Minor injuries may also arise during the collision, mainly due to de-acceleration. Loss of lives or injuries may result in a bad reputation for the vessel and the company and have consequences.

- Consequences for the vessel
  The consequences for the vessel can be separated into four cases, minor and severe damage, capsizing, and total loss of the vessel. Minor damage does not result in unacceptably large permanent deformations of the vessel. The damage will be repaired during the next call to a shipyard and the vessel will not be delayed. No other consequences will arise from a minor damage. Severe damage is damage to the vessel resulting in fracture of the ship's hull. The consequence is repair of the vessel, which has economic consequences. The vessel will normally be delayed and cargo owners or passengers might consider the use of another shipping company the next time. Fracture of the hull may also result in oil outflow leading to environmental consequences or stability problems, which may again result in capsizing of the vessel. Capsizing can be a result of severe damage, but a vessel may also capsize due to reduced stability in connection with water inflow from smaller damages. Capsizing might cause oil outflow and have environmental consequences. A result of a total loss will normally be both economic and problems of reputation.

- Environmental consequences
  Environmental consequences arising from oil outflow may be separated into three categories. First the consequences for the commercial industry as fish farms, fisheries, tourist industry etc., second the restoration consequences as cleaning of beaches and harbours, birds and animals, and third the consequences of non-commercial value as loss of recreation areas, social losses and ecological losses.

- Consequences of reputation
  A collision involving environmental pollution can result in bad publicity. Authorities, cargo owners or passengers might be influenced by the press, especially nowadays when the political consumer is in focus. Also a delay of the vessel may lead to a bad reputation, and cargo owners or passengers might consider the use of another shipping company the next time. A bad reputation is normally followed by economic consequences.

- Economic consequences
  The consequences of an oil outflow may not only be related to the amount and the type of the outflow, also the impact or fate and effect of a spill may be included in the analysis. A way to quantify the consequences of a collision could be to estimate the involved costs. These costs may arise from commercial losses or restoration claims from a third party, costs for the shipowner or noncommercial values.

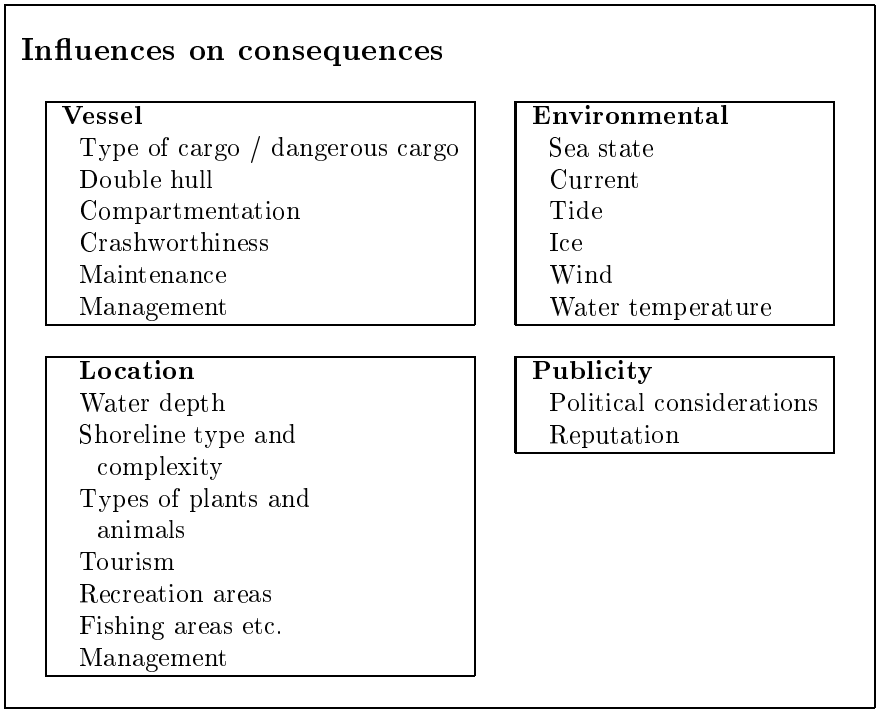


Figure 2.9: *Factors influencing the consequences of a collision.*

When a collision has taken place, the extent of the damage as well as the consequences of the damage may be affected by human factors or actions, the cargo characteristics, the nature of

the ocean and the coastline and other physical conditions, see Figure 2.9. The environmental conditions such as the sea state, the wind, the current or the tide may influence the size of the area which will be affected. The presence of ice or low water temperature will make it more difficult to clean up the location. Also the type of coast, sand, rocks etc. or the complexity of the coastline may affect the cleaning time. The consequences may be influenced by the location, for instance the presence of protected animals or plants, recreation areas, tourism or fishing industry. The amount of oil outflow or the consequences may be affected by human actions. If the crew on board the vessel are well trained and are familiar with emergency plans immediate actions can be taken on board the vessel, authorities can be warned and the response time for start of cleaning might be reduced. But also the compartmentation and the crashworthiness of the vessel can have a great influence on the amount of oil outflow.

More crashworthy vessels may reduce the amount of oil outflow, but normally more crashworthy vessels have an increased volume of steel in the structure, which increases the total lightweight of the vessel. This might increase the fuel oil consumption and be followed by environmental consequences. Use of new materials or new design or use of a buoyancy medium in the wing tanks may in the future decrease the consequences of a collision.

# Chapter 3

# The External Dynamics of Ship Collisions

The external dynamics analysis deals with the movements of the two vessels and the interaction with the surrounding water during collision. The aim of the external dynamics is to estimate the fraction of the kinetic energy which is released for rupture and plastic deformation in the vessels. An analytical method for determination of the energy loss in ship-ship collision has been developed by Pedersen and Zhang (1998). Here the estimation of the energy loss for dissipation in structural deformations is based on an analytical method where the energy is expressed in closed-form solutions. The most important idealisations are that only surge, sway and yaw motions are considered and that the influence of the hydrodynamic forces arising when the ship accelerates is approximated by simple added mass coefficients.

The separation of the collision problem into two individual problems, the internal mechanics and the external dynamics, is only possible when the structural systems and the surrounding water can be handled as an undamped system, by use of the theory for absolutely inelastic collision between two vessels. Previous comparison with complete time domain analysis (Zhang, 1999) has shown good results using the simplified procedure for the external dynamics. The procedure is based on a rigid body mechanism, where it is assumed that there is negligible strain energy for deformation outside the contact region, and that this region is local and small. This implies that the collision can be considered as instantaneous and each body is assumed to exert an impulsive force on the other at the point of contact. The model includes friction between the impacting surfaces so that situations with glancing blows can be identified. At the start of the calculation, the ships are supposed to have forward motion. The subsequent sliding and rebounding in the water plane during the collision are analysed.

The characteristics of the external dynamics depend on various aspects for a given collision, namely the main particulars of the struck and the striking vessels and a collision scenario

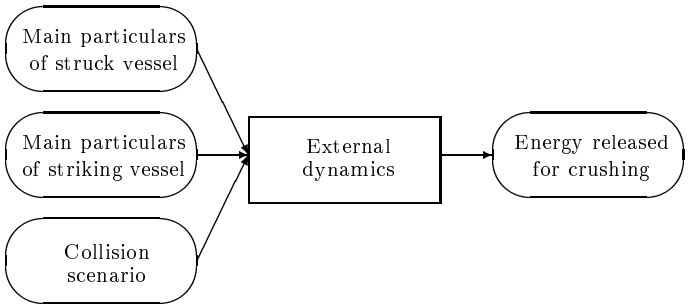


Figure 3.1: *Determination of energy released for crushing.*

describing the collision angle, the impact location and the velocity of both vessels, see Figure 3.1.

The theoretical analysis model for determining the external dynamics or the energy released for crushing of the ship's structure is described in detail in this chapter. The chapter ends with a small example.

## 3.1 The External Dynamics Theory

To illustrate the assumptions behind the method a striking ship ($B$), which sails at a forward speed of $V_{b1}$ and a speed of $V_{b2}$ in the sway direction, is considered. This vessel collides with a struck ship ($A$), sailing at a forward speed of $V_{ax}$ and a sway speed of $V_{ay}$ .

The theory makes use of three different coordinate systems. An $xyz$-coordinate system is fixed to the sea bottom. The $z$-axis points in a direction out of the water surface, the $x$-axis lies in the symmetry plane of the struck ship pointing towards the bow, and the origin of the $xyz$-system is placed so that the section amidships is in the $yz$-plane at the moment $t = 0$. The origin of a $\xi\eta$-system is located at the impact point $C$, the $\xi$-direction is normal to the impact surface, the angle between the $x$-axis and the $\eta$-axis is $\alpha$, and the angle between the $x$-axis and the 1-axis is $\beta$, see Figure 3.2.

The loss in kinetic energy is determined in six steps:

1. The equations of motion of the striking and the struck ships due to the impact force components are set up
2. The acceleration and the relative acceleration of the impact point are determined
3. The relative velocities before and after the collision are determined for the two ships
4. The impact impulses are calculated

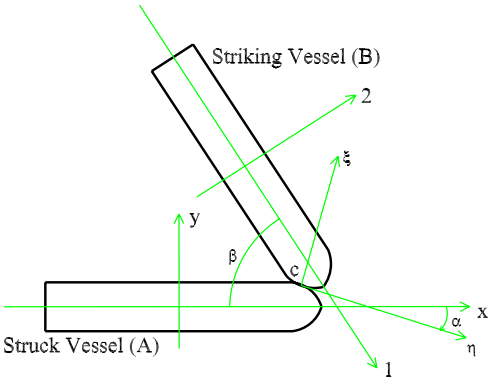


Figure 3.2: *The coordinate system used for analysis of the collision.*

5. From the ratio between the impact impulses it can be determined whether the two ships stick together or they slide against each other
6. The loss in kinetic energy is determined

If the collision angle is very small or large, the ships may glance against each other. Therefore, it is necessary to consider the friction between the two vessels. If the coefficient of friction is denoted $\mu_0$ and if $|\mu_0| \geq |\mu|$, then the two vessels stick together, otherwise if $|\mu_0| < |\mu|$ the vessels slide against each other.

The parameter $\mu$ is the ratio between the impact impulses, see Pedersen and Zhang (1998);

$$\mu = \frac{I_{\eta 0}}{I_{\xi 0}} = \frac{D_\xi \dot{\eta}(0) - K_\xi[\dot{\xi}(0) - \dot{\xi}(T)]}{K_\eta[\dot{\xi}(T) - \dot{\xi}(0)] - D_\eta \dot{\eta}(0)]} \tag{3.1}$$

The relative velocities immediately after the collision in the $\xi$- and the $\eta$-direction can be expressed by the velocities $V_a$ and $V_b$, which are the velocities before the collision for the struck and the striking ship, respectively.

$$\begin{aligned} \dot{\xi}(0) &= V_{ax}\sin(\alpha) + V_{ay}\cos(\alpha) + V_{b1}\sin(\beta-\alpha) - V_{b2}\cos(\beta-\alpha) \\ \dot{\eta}(0) &= V_{ax}\cos(\alpha) - V_{ay}\sin(\alpha) - V_{b1}\cos(\beta-\alpha) - V_{b2}\sin(\beta-\alpha) \end{aligned}$$

At the end of the collision ($t = T$), it is assumed that the vessels may rebound from each other in the $\xi$-direction.

$$\dot{\xi}(T) = -e\dot{\xi}(0)$$

Here $e$ is the coefficient of restitution.

The constants $D_\xi$, $D_\eta$, $K_\xi$ and $K_\eta$ are determined by

$$D_\xi = \frac{D_{a\xi}}{M_a} + \frac{D_{b\xi}}{M_b} \quad ; \quad D_\eta = \frac{D_{a\eta}}{M_a} + \frac{D_{b\eta}}{M_b}$$

$$K_\xi = \frac{K_{a\xi}}{M_a} + \frac{K_{b\xi}}{M_b} \quad ; \quad K_\eta = \frac{K_{a\eta}}{M_a} + \frac{K_{b\eta}}{M_b}$$

where

$$\begin{aligned}
D_{a\xi} &= \frac{\sin^2(\alpha)}{(1+m_{ax})} + \frac{\cos^2(\alpha)}{(1+m_{ay})} + \frac{1}{(1+j_a)R_a^2}(y_c\sin(\alpha) - (x_c - x_a)\cos(\alpha))^2 \\
D_{a\eta} &= \frac{\sin(\alpha)\cos(\alpha)}{(1+m_{ax})} - \frac{\sin(\alpha)\cos(\alpha)}{(1+m_{ay})} \\
&\quad + \frac{1}{(1+j_a)R_a^2}(y_c\sin(\alpha) - (x_c - x_a)\cos(\alpha))(y_c\cos(\alpha) + (x_c - x_a)\sin(\alpha))
\end{aligned}$$

$$\begin{aligned}
D_{b\xi} &= \frac{\sin^2(\beta-\alpha)}{(1+m_{b1})} + \frac{\cos^2(\beta-\alpha)}{(1+m_{b2})} + \frac{1}{(1+j_b)R_b^2}((y_c - y_b)\sin(\alpha) - (x_c - x_b)\cos(\alpha))^2 \\
D_{b\eta} &= -\frac{\sin(\beta-\alpha)\cos(\beta-\alpha)}{(1+m_{b1})} + \frac{\sin(\beta-\alpha)\cos(\beta-\alpha)}{(1+m_{b2})} \\
&\quad + \frac{1}{(1+j_b)R_b^2}((y_c - y_b)\sin(\alpha) - (x_c - x_b)\cos(\alpha)) \\
&\quad ((y_c - y_b)\cos(\alpha) + (x_c - x_b)\sin(\alpha))
\end{aligned}$$

$$\begin{aligned}
K_{a\xi} &= \frac{\sin(\alpha)\cos(\alpha)}{(1+m_{ax})} - \frac{\sin(\alpha)\cos(\alpha)}{(1+m_{ay})} \\
&\quad + \frac{1}{(1+j_a)R_a^2}(y_c\sin(\alpha) - (x_c - x_a)\cos(\alpha))(y_c\cos(\alpha) + (x_c - x_a)\sin(\alpha)) \\
K_{a\eta} &= \frac{\cos^2(\alpha)}{(1+m_{ax})} + \frac{\sin^2(\alpha)}{(1+m_{ay})} \\
&\quad + \frac{1}{(1+j_a)R_a^2}(y_c\cos(\alpha) + (x_c - x_a)\sin(\alpha))^2
\end{aligned}$$

$$\begin{aligned}
K_{b\xi} &= -\frac{\sin(\beta-\alpha)\cos(\beta-\alpha)}{(1+m_{b1})} + \frac{\sin(\beta-\alpha)\cos(\beta-\alpha)}{(1+m_{b2})} \\
&\quad + \frac{1}{(1+j_b)R_b^2}((y_c - y_b)\sin(\alpha) - (x_c - x_b)\cos(\alpha)) \\
&\quad ((y_c - y_b)\cos(\alpha) + (x_c - x_b)\sin(\alpha)) \\
K_{b\eta} &= \frac{\cos^2(\beta-\alpha)}{(1+m_{b1})} + \frac{\sin^2(\beta-\alpha)}{(1+m_{b2})} \\
&\quad + \frac{1}{(1+j_b)R_b^2}((y_c - y_b)\cos(\alpha) + (x_c - x_a)\sin(\alpha))^2
\end{aligned}$$

here $M_a$ and $M_b$ are the mass of the struck and the striking ship, respectively. The radius of the ship mass inertia around the centre of gravity is $R_a$ or $R_b$ and the coordinate of the centre of gravity of the struck ship is $(x_a, 0)$. The coordinate for the impact point is $(x_c, y_c)$, the added mass coefficient for surge is $m_{ax}$ or $m_{b1}$ and the added mass coefficient for sway is $m_{ay}$ or $m_{b2}$.

**Sliding Case**

In the case where the ratio between the two impact impulses, $\mu$, see Eq. (3.1), is greater than the coefficient of friction, $\mu_0$, between the two vessels, the ships are assumed to slide against each other. The energy released in this case can be expressed as

$$\begin{aligned} E_\xi &= \frac{1}{2}\frac{1}{D_\xi + \mu_0 D_\eta}(1-e^2)[\dot{\xi}(0)]^2 \\ E_\eta &= \frac{1}{2}\frac{1}{\frac{1}{\mu_0}K_\xi + K_\eta}[(\dot{\eta}(0))^2 - \dot{\eta}(T))^2] \end{aligned}$$

where the glancing speed after the collision $\dot{\eta}(T)$ can be expressed as

$$\dot{\eta}(T) = \dot{\eta}(0) - \frac{K_\xi + \mu_0 K_\eta}{D_\xi + \mu_0 D_\eta}[\dot{\xi}(0) - \dot{\xi}(T)]$$

**Sticking Case**

In the case where the coefficient of friction, $\mu_0$, is greater than the ratio between the two impact impulses, the two vessels will stick together and the energy can be determined as

$$\begin{aligned} E_\xi &= \frac{1}{2}\frac{1}{D_\xi + \mu D_\eta}\dot{\xi}(0)^2 \\ E_\eta &= \frac{1}{2}\frac{1}{\frac{1}{\mu}K_\xi + K_\eta}[\dot{\eta}(0)]^2 \end{aligned}$$

**Added Mass Coefficients**

The added mass coefficients $m_{ax}$, $m_{ay}$, $j_a$ and $m_{b1}$, $m_{b2}$, $j_b$, taking into account the interaction effects between the ships and the surrounding water, depend on the hull form of the ships and the impact duration etc. For simplicity, Minorsky (1959) proposed the use of a constant value of the added mass coefficients of ships for the sway motion: $m_{ay} = 0.4$.

Motora (1971) conducted a series of model tests and a hydrodynamic analysis of the added mass coefficient for the sway motion. He found that the added mass coefficient varies during the collision in the range of $m_{ay} = 0.4 - 1.3$. The longer the duration, the larger the value

of the coefficient. However, if the collision duration is very short, the value assumed by Minorsky (1959) may be correct. The added mass coefficient for the forward motion is small compared to the mass of the ship. It is found to be $m_{ax} = 0.02 - 0.07$. The added mass coefficient for the yaw motion of the ship, $j_a$, is found to be $j_a = 0.21$ (Zhang, 1999).

For simplicity, the added mass coefficients are taken to be: $m_{ax} = m_{b1} = 0.05$ (surge motion), $m_{ax} = m_{b1} = 0.85$ (sway motion) and $j_a = j_b = 0.21$ (yaw motion) in the examples of the present calculations. The radius of inertia is taken to be a quarter of the ship's length: $R_a = L_a/4$ and $R_b = L_b/4$.

## 3.2 Application Example

### Collision between Two Similar Ro-Ro Vessels

Two similar Ro-Ro vessels sailing at the same forward speed of 5.0 m/s collide at different impact angles and in different striking locations along the length of the struck vessel.

Dimensions of the Ro-Ro vessels :

| | |
|---|---|
| Length $[m]$ | 150.0 |
| Breadth $[m]$ | 27.0 |
| Draught $[m]$ | 6.0 |
| Displacement $[mt]$ | 15800 |

The angle $\alpha$ and the breadth of the ship forwards are determined from the assumption that the shape of the bow can be approximated to a parabola $y = C \cdot x^2$, where $C$ equals 0.16. The coefficient of friction between the two ships is assumed to be $\mu_0 = 0.6$.

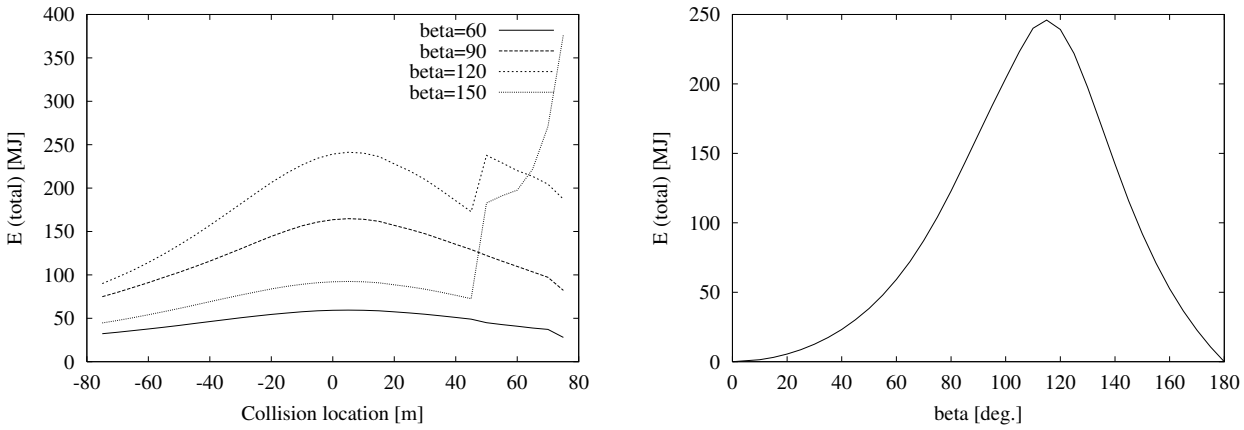


Figure 3.3: *Left: Total energy loss as a function of striking location for various collision angles. Right: Total energy loss for collision amidships as a function of the collision angle.*

In Figure 3.3 (left) the total loss in kinetic energy is shown as a function of striking location for various collision angles. The figure show that the impact angle and location have a significant influence on the loss in energy. It is seen that if the ships have courses towards each other, the energy loss is significantly higher for a collision in the forward part of the struck ship. The right diagram in Figure 3.3 shows the total energy loss for collision amidships as a function of the collision angle. An energy peak is seen for a collision angle around $120^o$, which is a result of both vessels having forward motion.

This page is intentionally left blank.

# Chapter 4

# The Internal Mechanics of Ship Collisions

The internal analysis or the internal mechanics deals with the deformation of the side of the struck vessel and the bow of the striking vessel. It is very difficult to obtain a precise calculation of the internal mechanics as the collision strength of a ship is governed by a complex mixture of buckling, yielding, tension, tearing, rupture and brittle failure of materials.

There are two classes of theoretical methods, which can be used to predict the damage caused by a collision: the finite element method and simplified, analytical methods often referred to as 'super-element methods'. Experiments are normally too costly to be used for other purposes than validation of theory. Recent work has shown that the finite element method can be used to perform both ship collision and grounding analyses, see for example Kuroiwa (1996), Kitamura (2001) or Sano et al. (1996). Although problems of fracture have not yet been fully resolved, the solutions of a finite element analysis can be detailed and accurate. However, the finite element modelling requires a massive effort both as regards modelling and computer power so for many practical problems it is prohibitively expensive, especially if stochastic simulation of a large number of accidents is required. The other group of methods covers a range of procedures, which are so sufficiently simple that they can be used in hand calculations. The most famous of these methods was proposed by Minorsky (1959). The basic idea is that the absorbed energy is a simple linear function of the volume of deformed material. Several modifications have been proposed to widen the applicability or the accuracy of the method. Most recently Pedersen and Zhang (2000) introduced parameters for the structural layout in a formula similar to Minorsky's formula. At a more detailed level, many papers over the past have proposed fundamental, closed form solutions to various impact problems involving structural crushing and deformation. For example Wierzbicki and Abramowicz (1983), Abramowicz (1994) and Amdahl (1982) have developed several fundamental solutions, which can be used to estimate the energy absorption in axial crushing of plate intersections like X-forms, T-forms etc. Likewise other solutions are known for indentation into shell plating, crushing of a deck or a deep web

girder. These special solutions, often referred to as super-element solutions, are known to predict the energy absorption quite accurately.

This chapter presents methods for determination of energy absorption due to crushing and deformation of the ship's structure during a collision and estimation of the resulting damage to the vessels. The method used for analysis of collision events is based on the super-element approach.

It is common practice to assume that the bow of the striking ship does not deform during the impact. Obviously, this assumption is very convenient for the analysis but at the same time it is known that the assumption does not always hold true, see for example Lehmann and Yu (1995) and Lützen et al. (2000). A part of the present chapter is used to investigate the limits of validity for this assumption. Therefore, both the striking bow and the side of the struck ship are modelled.

When both the energy to be absorbed, determined by the external dynamics analysis presented in Chapter 3, and the energy absorbed by structural deformation are known, the damage to the struck and the striking vessels can be determined. As the theory for the internal mechanics is based on an indentor incrementing into the ship's structure, the geometry of the striking bow will be an important factor. Therefore this chapter starts with a presentation of the simplified bow geometry model. This section is followed by a description of the area of contact between the two vessels and the method for estimation of the damage.

Section 4.3 deals with the super-element approach to the internal mechanics. The different types of elements are described and crushing forces are estimated. The next two sections deal with energy absorption of the side structure and the bow structure during the collision. The sections start with modelling of the structure and end with some application examples. In the last section the theory is combined in a model for prediction of damage to both vessels involved in the collision.

## 4.1 The Geometry of the Bow of the Striking Ship

The bow of the striking vessel can be separated into two different types, a conventional bow and a bulbous bow. The geometry of the two types of bows is idealised so that the geometry can be described by few parameters, still covering with sufficient accuracy almost all existing ship's bows, see Figure 4.1.

**The Conventional Striking Bow**

The basic data for describing the assumed conventional bow consists of the stem angle, $\varphi$, the breadth of the ship, $B$, the uppermost deck height, $H_{deck}$, and some deck and bottom constants, $B_d$ and $B_b$, describing the shape of the deck and the bottom. The forecastle deck and the bottom are here assumed to have the form of parabolas.

A typical bow shape for the conventional bow is given by Scharrer (1996). If the length, the breadth and the height of the striking vessel are known, the bow shape can be approximated from:

| | | | |
|---|---|---|---|
| Deck coefficient | $B_d$ | = | $0.576\frac{L}{B^2}$ |
| Bottom coefficient | $B_b$ | = | $1.645\frac{L}{B^2}$ |
| Stem angle | $\tan(\phi)$ | = | $24.376\frac{H}{L}$ |

**The Bulbous Striking Bow**

The bulbous bow can be divided into two parts, a conventional bow and a bulb. The bulb is assumed to have the form of an elliptic parabola, see Figure 4.1. In the local coordinate system with origin in the bulb tip, the bulb is described as

$$\frac{x_1}{R_L} = \frac{y_1^2}{{R_H}^2} + \frac{z_1^2}{{R_V}^2} \tag{4.1}$$

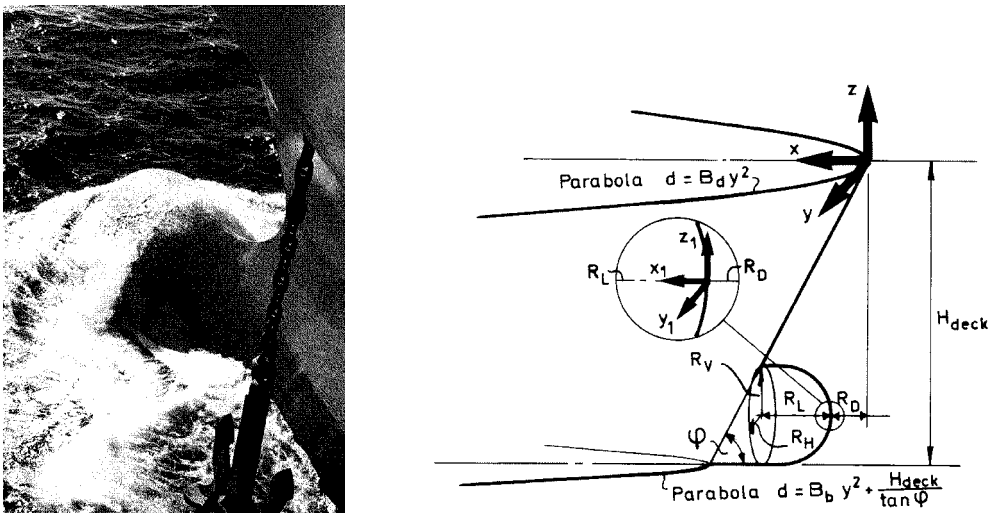


Figure 4.1: *Bulbous bow.*

The basic data for describing the assumed bulbous bow consists of the parameters describing the conventional part of the bow plus some bulb parameters: The length of the bulb, $R_L$, the vertical radius of the bulb, $R_V$, the horizontal radius of the bulb, $R_H$, and the distance between the bulb tip and the foremost part of the bow, $R_D$, see also Figure 4.1.

If the bulb design is unknown the following parameters may be used, Zhang (1999):

$$R_L = 0.3 \cdot H_{deck} \qquad R_V = 0.125 \cdot H_{deck} \qquad R_H = 0.05 \cdot H_{deck}$$

Scharrer (1996) has also proposed a typical bow shape for the bulbous bow. If the length, the breadth and the height of the striking vessel are known the bow shape can be estimated from:

| | | | |
|---|---|---|---|
| Deck coefficient | $B_d$ | = | $0.579\frac{L}{B^2}$ |
| Bottom coefficient | $B_b$ | = | $15.946\frac{L}{B^2}$ |
| Stem angle | $\tan(\phi)$ | = | $14.644\frac{H}{L}$ |
| Bulb parameters | $R_D$ | = | $8.26 \cdot 10^{-3}L$ |
| | $R_L$ | = | $3.51 \cdot 10^{-2}L$ |
| | $R_V$ | = | $0.243H$ |
| | $R_H$ | = | $0.143B$ |

## 4.2 The Area of Contact and Damage Size Estimation

The striking vessel will penetrate the side of the struck vessel. At the moment of impact the relative direction is determined by the velocities and the courses of the two vessels, where the penetration angle, $\gamma$, into the struck vessel can be determined as

$$\cos\gamma = \frac{U_b\cos\beta - U_a}{\sqrt{U_a^2 + U_b^2 - 2U_aU_b\cos\beta}}$$

The parameters $U_a$ and $U_b$ are the surge velocity of the struck and the striking vessel, respectively, and $\beta$ is the collision angle. The method is purely geometrical and allows no rotation of the vessels.

The length of the hole is taken as the difference between the foremost and the aftermost intersection between the bow or the bulb and the side of the struck vessel. The damage height is taken as the distance of the uppermost point to the lowest point of the hole, and the damage location is taken as the point with the deepest penetration into the struck vessel.

When the side of the struck vessel is modelled it is assumed that only elements in contact with the striking bow need to be included in the analysis. This seems reasonable in studies of pictures of past collision accidents, where the damage corresponds very well to the imprint of the bow, see Figure 4.2. Therefore, it is here assumed that the area of contact only depends on the bow geometry of the striking vessel, the draught of both of the vessels and the penetration. Figure 4.3 shows the imprints from different conventional bows. If the striking vessel is equipped with a bulbous bow, the imprint of the top of the bow will be as that of a conventional bow. The bulb, which is here assumed to have the form of an elliptic parabola, will have an imprint corresponding to that of an ellipse. In case of a bulbous bow the damage may be separated into two holes, a lower hole created by the bulb and an upper hole created by the top of the bow, in this case a normal approximation is to merge the two holes into one.

Figure 4.2: *Imprints on side of struck vessel, left bulb, right bow.*

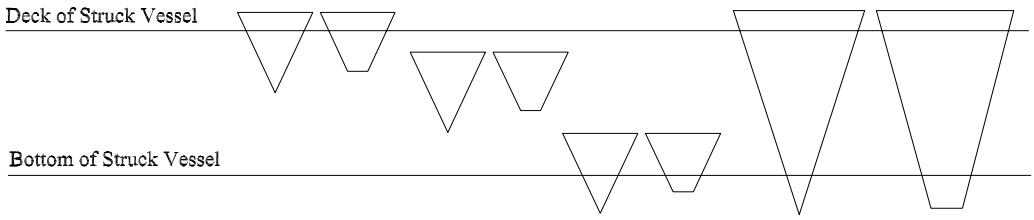


Figure 4.3: *Imprints on side of struck vessel caused by striking vessels with conventional bow.*

## 4.3 Super Elements

The model for the internal mechanics is based on a set of so-called super elements. Each element represents an assembly of structural components and contains solutions for the structural behaviour of this assembly under deep collapse.

The super elements used in this model are:

**1** Lateral loading of plates resulting in deflection and rupture

**2** Crushing of intersecting structural elements (T- or X-elements)

**3** In-plane crushing and tearing of plates

**4** Lateral loading of beams resulting in deflection and rupture

An example of a super-element load case can be described as: The bow strikes between two transverse frames. First the side plating will deflect and later fracture. After initiation of fracture the solution for concertina tearing of the side shell can be used to determine the resistance. After a certain penetration the bow hits some deep stiffeners, which will deflect as beams. Later on the bow may come into contact with transverse bulkheads or frames. When this happens, the main resistance comes from crushing of intersections between e.g. deck and bulkheads. These intersections are modelled as T- or X-elements. This example illustrates that use of the super-element solution calls for adaptive or successive discretisation. During the collision the bow of the striking vessel is incremented into the side of the struck ship, at each step the side structure of the struck vessel is discretised into super elements. By summing up the crushing force of each super element, it is possible to determine the total contact load between the two involved vessels and the total amount of absorbed energy.

The next sections will give a short description of the different super elements and where they can be found in a ship structure.

**1. Lateral Loading of Plates Resulting in Deflection and Rupture**

Plates are structural elements at the ship's side, the inner ship's side, the longitudinal bulkheads or the longitudinal floors. The horizontal boundary of a plate can be the weather deck, mid-decks, inner bottom, bottom or stringer decks. The vertical boundary of a plate can be transverse bulkheads, frames at the side, girders or transverse floors. If stiffeners are attached to the plate they will form a boundary until they are in contact with the striking ship. After contact smaller stiffeners will in this model be smeared out, and the plate will be considered orthotropic. Larger stiffeners will be considered as beams.

The model for lateral loading of plates follows Wierzbicki and Simonsen (1996).

Consider a rectangular plate deformed by a point load, where the distances from the point of loading to the four edges of the plate are denoted $R_1$, $R_2$, $R_3$ and $R_4$, respectively, see

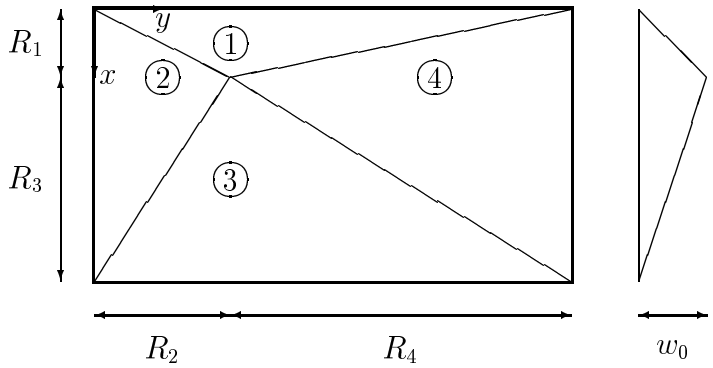


Figure 4.4: *Deformation pattern for a rectangular plate.*

Figure 4.4. The plate is subjected to an increasing deflection $w_0$ at the point of loading. Large deflections are assumed, which implies that the bending resistance can be neglected. The purpose of the analysis is to determine the force, $P$, necessary to deform the plate.

The plate is divided into four triangular parts, which extend from the point of impact to the corners of the plate. The deformation mode assumed for the left section of part 1 of the plate, see Figure 4.4, which satisfies the clamped boundary condition, is as follows:

$$w = w_0 \frac{xy}{R_1 R_2}$$

The Lagrangian strain tensor $\epsilon_{\alpha\beta}$ is defined by

$$\epsilon_{\alpha\beta} = \frac{1}{2}\left(u_{\alpha,\beta} + u_{\beta,\alpha}\right) + \frac{1}{2} w_{,\alpha} w_{,\beta}$$

where $u$ is the component of the in-plane displacement, and $w$ denotes the out-of-plane displacement. The in-plane component is neglected and the strain component and its increments resulting from the displacement are

$$\begin{aligned}
\epsilon_{xx} &= \tfrac{1}{2}\left(\tfrac{dw}{dx}\right)^2 = \tfrac{1}{2}\tfrac{w_0^2 y^2}{(R_1 R_2)^2} & \dot{\epsilon}_{xx} &= \tfrac{\dot{w}_0 w_0 y^2}{(R_1 R_2)^2} \\
\epsilon_{yy} &= \tfrac{1}{2}\left(\tfrac{dw}{dy}\right)^2 = \tfrac{1}{2}\tfrac{w_0^2 x^2}{(R_1 R_2)^2} & \dot{\epsilon}_{yy} &= \tfrac{\dot{w}_0 w_0 x^2}{(R_1 R_2)^2} \\
\epsilon_{xy} &= \tfrac{1}{2}\tfrac{dw}{dx}\tfrac{dw}{dy} = \tfrac{1}{2}\tfrac{w_0^2 xy}{(R_1 R_2)^2} & \dot{\epsilon}_{xy} &= \tfrac{\dot{w}_0 w_0 xy}{(R_1 R_2)^2}
\end{aligned} \tag{4.2}$$

The rate of the external loading must be equal to the rate of energy dissipation in the plate. Using the von Mises yield criterion this requirement is expressed by

$$P\dot{w}_0 = \frac{2}{\sqrt{3}}\sigma_0 t \int_A \sqrt{\dot{\epsilon_{xx}}^2 + \dot{\epsilon_{yy}}^2 + \dot{\epsilon_{xx}}\dot{\epsilon_{yy}} + \dot{\epsilon_{xy}}^2}\, dA \tag{4.3}$$

where $P$ is the external load and $A$ is the area of the plate.

Substituting the increments of Eqs. (4.2) into Eq. (4.3) gives the following expression:

$$P_{1,left} = \frac{2}{\sqrt{3}}\sigma_0 t \frac{w_0}{(R_1 R_2)^2} \int_0^{R_2} \int_0^{\frac{R_1}{R_2}y} (x^2 + y^2) dx dy = \frac{1}{6\sqrt{3}}\sigma_0 t w_0 \left[\frac{R_1}{R_2} + 3\frac{R_2}{R_1}\right]$$

The same procedure is used for the rest of the plate, and the forces are summed to give the total force acting on the plate.

$$P = \frac{2\sigma_0 t}{3\sqrt{3}} w_0 A \left[\frac{1}{R_1 R_3} + \frac{1}{R_2 R_4}\right]$$

If the plate is orthotropic the force-deflection function can be expressed as

$$P = \frac{1}{6\sqrt{3}} w_0 A \left[\frac{3N_{0y} + N_{0x}}{R_1 R_3} + \frac{3N_{0x} + N_{0y}}{R_2 R_4}\right]$$

where $N_{0x}$ and $N_{0y}$ are the membrane yield forces in the $x-$ and $y-$direction, respectively. See Wierzbicki and Simonsen (1996).

After rupture a special plate element is used, which takes into account that the plate may be intact with membrane tension or be fractured in the longitudinal, in the transverse or in both directions. See Scharrer (1996).

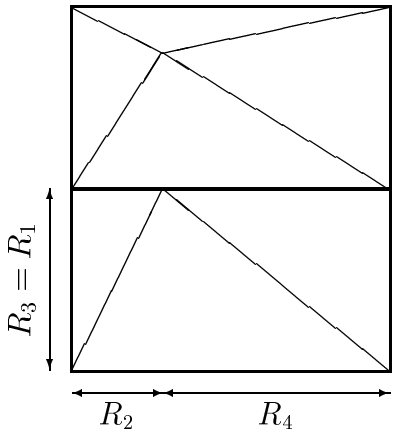


Figure 4.5: *Deformation pattern for two plates. The first plate of contact and the plate below.*

If the boundary of the plate is touched by the striking bow, the part of the plate belonging to this boundary will be omitted. The rest of the plate will still be included until rupture. A new plate, situated below or to the side, is now to be included. In Figure 4.5 the deformation pattern for a plate below the first plate of contact is shown. The resistance of this plate can now be calculated as

$$P_{new} = 0 \cdot P_1 + P_2 + \frac{1}{2} \cdot P_3 + \frac{1}{2} \cdot P_4$$

where $P_1$, $P_2$, $P_3$ and $P_4$ are the resistance of each of the four plate parts. The new distances for $R_1$, $R_2$, $R_3$ and $R_4$ are defined in Figure 4.5.

If the striking ship has a bulbous bow, first a conventional ship without bulb is considered and all the plates in contact with the bow are found. Then the plates in contact with the bulb are found. If both the bow and the bulb touch the same plate, only the largest deflection is considered.

**2. Crushing of Intersecting Structural Elements (T- or X-elements)**

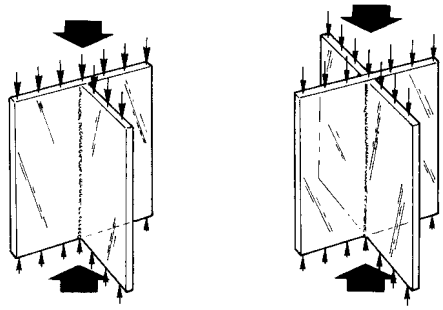

Figure 4.6: *Deformation of T- and X-elements.*

Crushing elements can be found in the following places :

| | |
|---|---|
| Intersections between | |
| weather deck, bottom | / transv. bulkhead (T) |
| | / girder (T) |
| | / frames at side (T) |
| mid deck, inner bottom | / transv. bulkhead (X) |
| | / girder (X) |
| | / frames at side (X) |
| bottom | / transv. floors (T) |
| | / transv. frames (T) |
| inner bottom | / transv. floors (T) |
| stringer deck | / girders (X) |
| | / transv. bulkhead (X) |

Furthermore, all transverse stiffeners at weather deck, mid-decks, inner bottom, bottom and bulkheads are crushed as either T- or X-elements.

When the crushing resistance of the elements shall be determined it is assumed that the material is perfectly plastic, characterised by the flow stress $\sigma_0$. The model used for the crushing forces follows Amdahl (1982) and Kirkegaard (1993).

The T- or the X-element is included from the moment the point of intersection is touched for the first time. The starting length of the crushing element flanges is half the distance

between the individual crushing elements. The flange length is reduced if part of the flange is outside the area of consideration. If the same element is in contact with both the bow and the bulb the element with the largest deformation is included in the model. There are a number of possible deformation modes of a T- or an X-element. Both the T- and the X-elements are here assumed to collapse in the straight edge mechanism mode, where the flanges remain straight in the intersection line. Thus, there will be no interaction between the flanges. The mean crushing force for a T-element, $P_T$, and for an X-element, $P_X$, can be determined from

$$\frac{P_T}{M_0} = 25.6\left(\frac{c}{t}\right)^{\frac{1}{2}} + 6.46 \qquad \frac{P_X}{M_0} = 34.2\left(\frac{c}{t}\right)^{\frac{1}{2}} + 8.61$$

where $c$ is the average flange length and $t$ the average flange thickness. The plastic bending moment per unit flange length, $M_0$, is calculated as $M_0 = \frac{\sigma_0 t^2}{4}$.

**3. In-Plane Crushing and Tearing of Plates**

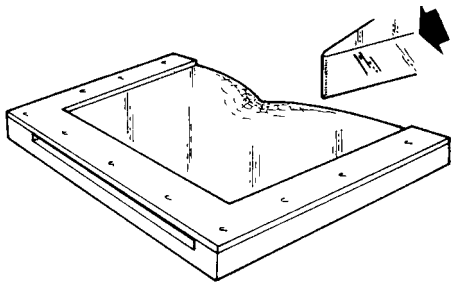

Figure 4.7: *In-plane deformation of plate.*

This section is concerned with deep plastic collapse of plates subjected to local in-plane loads. Crushing of plates can be idealised by simple geometrical modes of deformation. A model suggested by Simonsen and Ocakli (1999) is used. When a deck is loaded by a point load it will first collapse plastically with folds extending to the nearest boundaries. After a certain penetration, the plate will fracture and it will continue to fold up in front of the bow like a concertina.

Plates which can be crushed during a collision can be found in the following places:

| | |
|---|---|
| Horizontal plates | Part of weather deck, mid decks, inner bottom, bottom and stringer decks |
| Vertical plates | Part of transverse bulkheads, frames at side, girders and transverse floors |

The length of the crushed plate between two crushing elements is defined in the previous section. If the boundary of the plate element is touched, the crushing plate is omitted and the intersection element will take over.

Transverse stiffeners, stiffeners parallel to the direction of penetration, are crushed axially. The theory for crushing elements of this type, is dealt with in the previous section. Longitudinal stiffeners are included in the model by smearing out the volume of the stiffener in the longitudinal direction, resulting in an orthotropic plate.

According to Simonsen and Ocakli (1999) the load-deformation relation can be expressed by

$$P = 1.56\ \sigma_0\ t^{5/3}\frac{b_1+b_2}{(b_1b_2)^{1/3}} + 0.518\ \sigma_0\ t_{eq}^{4/3}\frac{b_1+b_2}{(b_1b_2)^{2/3}}\left[1+\frac{w}{1.51(b_1b_2t)^{1/3}}\right]\ f(w)$$

where $w$ is the deflection. The thickness of the plate is $t$. This thickness is corrected for every new involved longitudinal, which volume is smeared out to give the equivalent thickness $t_{eq}$. The distances from the load point to the boundaries are denoted $b_1$ and $b_2$. The involved function, $f$, depends on the depth of the plate and is defined as

$$f(w) = \begin{cases} w\left(1+\dfrac{w}{4H}\right) & \text{for} \quad w \le D \\ D\left(1+\dfrac{w}{2H}-\dfrac{D}{4H}\right) & \text{for} \quad w > D \end{cases}$$

where $D$ is the depth of the plate, and $H$ is the folding length, which can be determined as

$$H = 0.377\sqrt[3]{b_1b_2t}$$

After rupture the folding mode changes to concertina tearing. Wierzbicki (1995) found that concertina tearing can be expressed as

$$P_m = 4.33\sigma_0 t^{5/3}\left(\frac{b_1+b_2}{2}\right)^2 + \frac{8}{3}R_c t$$

where $R_c$ is the fracture toughness. The fracture toughness for mild steel is in the range $R_c = 300 - 1000\ N/mm$.

**4. Lateral Loading of Beams Resulting in Deflection and Rupture**

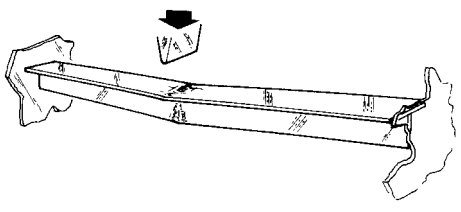

Figure 4.8: *Deep collapse of beam.*

Only deep stringers attached to the ship's side are considered as beams. The boundary can be transverse bulkheads, girders or frames.

The beam first fails by forming a mechanism of plastic hinges. In order to obtain the yield condition for a beam, it is necessary to find the combinations of the bending moment and the membrane force, which cause the cross-section of a perfectly plastic beam to become fully plastic, see for example Jones (1989). Here a simple model is used to estimate the switch between the two modes. The ultimate load $P$ of a fully clamped beam with a plastic moment $M_p$ can be expressed as

$$P = 2M_p \left( \frac{1}{b_1} + \frac{1}{b_2} \right) \tag{4.5}$$

where $b_1$ and $b_2$ are the distances from the point of loading to the boundaries.

In pure tension the resistance of a beam can be expressed as

$$P = N_p w_0 \left( \frac{1}{b_1} + \frac{1}{b_2} \right) \tag{4.6}$$

where $N_p$ is the fully plastic axial force.

By use of Eqs. (4.5) and (4.6) and requiring continuity for the function $P$, the resistance can be expressed as

$$P = \begin{cases} 2M_p \left( \frac{1}{b_1} + \frac{1}{b_2} \right) & \text{for} \quad w_0 \leq \frac{2M_p}{N_p} \\ N_p w_0 \left( \frac{1}{b_1} + \frac{1}{b_2} \right) & \text{for} \quad w_0 > \frac{2M_p}{N_p} \end{cases}$$

Fracture of the beam will occur when the critical strain is reached. After fracture the resistance of the beam will be reduced to zero.

## 4.4 Modelling of the Internal Mechanics in the Side Structure

Modelling of the internal mechanics in the side structure is based on the principle that the area of the struck ship which is affected by the collision is restricted to the area touched by the bow of the striking vessel, see Section 4.2. For the simplified analysis the structure in contact with the bow is divided into its structural components or super elements, e.g. plates, crushing elements or beams. By summing up the crushing force of each super element, it is possible to determine the total contact load between the two involved vessels.

In order to allow fast input, or description of the structure, it is assumed that all elements can be located only longitudinally, transversely or vertically, and that the material is described by Young's modulus, the flow stress, the fracture toughness and the critical strain to fracture. The critical strain to fracture can for most ship structure be set to 5-10

When the side structure of the struck vessel is defined, it is separated into two types, principal and secondary structure. The principal structure can be stiffened by secondary structure; the secondary structure cannot be stiffened further.

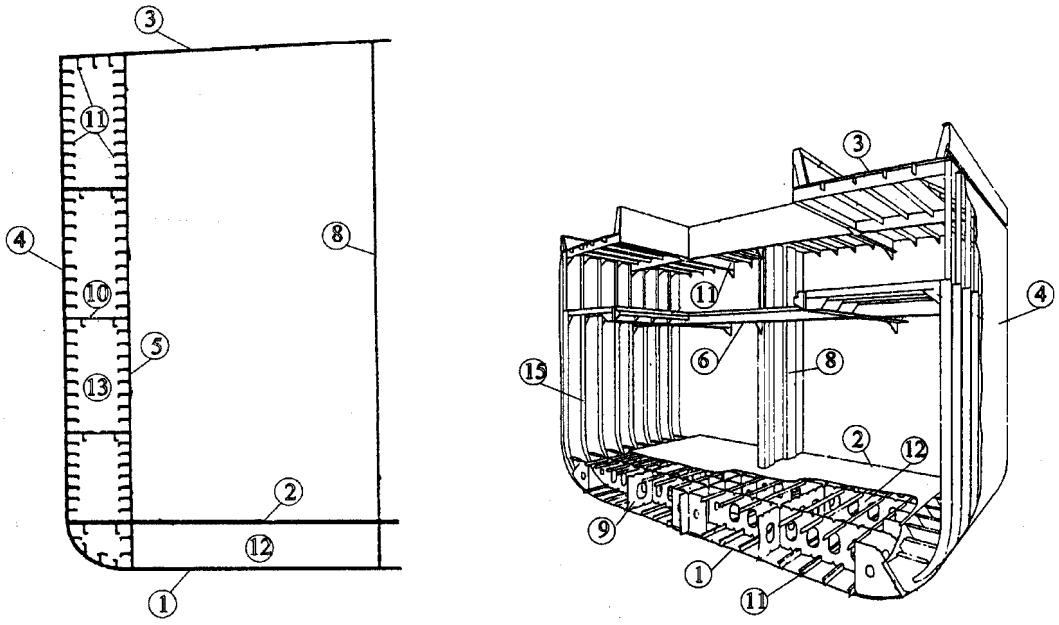


Figure 4.9: *Definition of ship's structure.*

**Principal Structure**

**1** The ship's bottom
**2** The inner bottom
**3** The weather deck
**4** The ship's side
**5** The inner side
**6** Mid-deck
**7** Transverse bulkhead
**8** Longitudinal bulkhead

**Longitudinal Secondary Structure**

**9** Floor
**10** Stringer
**11** Stiffener

**Transverse Secondary Structure**

**12** Floor
**13** Girder

**14** Frame
**15** Stiffener

**Calculation Elements**
For simplification of the analysis, the pre-defined ship's structure is divided into four categories, namely longitudinal elements, which extend all the way between fore and aft of the ship, transverse elements extending from top to bottom, single elements and elements for further penetration. The calculation elements can easily be transformed into super elements during bow penetration.

| Long. elements | Transv. elements | Single elements |
|---|---|---|
| Bottom | Transv. bulkhead | Transv. stiffeners at bottom |
| Mid-deck | Frames at side | Transv. stiffeners at mid-deck |
| Weather deck | Transv. stiffeners at side | Transv. stiffeners at weather deck |
| Inner bottom | Girders | Transv. stiffeners at transverse bulkheads |
| Stringers | | Transv. stiffeners at inner bottom |
| Long. stiffeners | | Transv. floors |

| Elements for further penetration |
|---|
| Long. bulkhead stiffened vertically or horizontally |
| Longitudinals at weather deck, mid deck, inner bottom and bottom |
| Vertical stiffeners at transv. bulkhead |
| Longitudinal floors |
| Inner side stiffened vertically or horizontally |

### 4.4.1 Validation Examples based on Structural Elements

**Double Hull Test by Nagasawa and Tani (1977)**

Nagasawa and Tani (1977) carried out experiments simulating an indentation of a bridge pillar into the side of a vessel. The vessels were both transversely and longitudinally stiffened. Five tests were performed.

The indentor or the bridge pillar was a cylinder with a radius of 300 or 450 mm. A parabola approximates the form of the indentor or the pillar. By use of the Taylor expansion the circular indentation can be described by

$$y = Ar^2 \qquad \text{where} \quad A = \frac{1}{2R} \quad \text{and } R \text{ is the radius of the indentor.}$$

**Transversely Stiffened Vessels**

Three tests were performed with a transversely stiffened side construction.

Principal dimensions / parameters not changed during the tests:

- Height of ship's side is 800 mm
- Depth of frames is 45 mm
- Spacing between transverse frames is 55 mm
- Material yield stress is 250 $MPa$

The thickness of the structural components and the radius of the indentor were varied in the three tests according to Table 4.1.

Figures 4.10 to 4.12 show the comparison between measured and calculated values for the load and the absorbed energy as a function of the penetration. The figures show good agreement between measured and calculated values.

Table 4.1: *Variable parameters for transversely stiffened side.*

| | Side plate thickness $[mm]$ | Deck / bottom thickness $[mm]$ | Transv. frames thickness $[mm]$ | Indentor radius $[mm]$ |
|---|---|---|---|---|
| T1 | 1.2 | 1.2 | 1.6 | 450 |
| T2 | 1.6 | 1.6 | 2.3 | 450 |
| T3 | 1.2 | 1.2 | 1.6 | 300 |

**Longitudinally Stiffened Vessels**

Two tests were performed with a longitudinally stiffened side construction. The structure was not changed during the test, only the radius of the indentor was varied. In test no. 4 the radius was 450 mm and in test no. 5 it was 300 mm.

Principal dimensions / parameters not changed during the tests:

- Height of ship's side is 800 mm
- Depth of frames is 80 mm
- Spacing between transverse frames is 319 mm
- Material yield stress is 250 $MPa$
- Thickness of bottom, side and deck plating is 1.6 mm
- The longitudinals are flat bars 35 x 1.2 mm with a spacing of 67 mm

Figures 4.13 to 4.14 show the comparison between measured and calculated values for the load and the absorbed energy as a function of the penetration. A good agreement between measured and calculated values is seen.

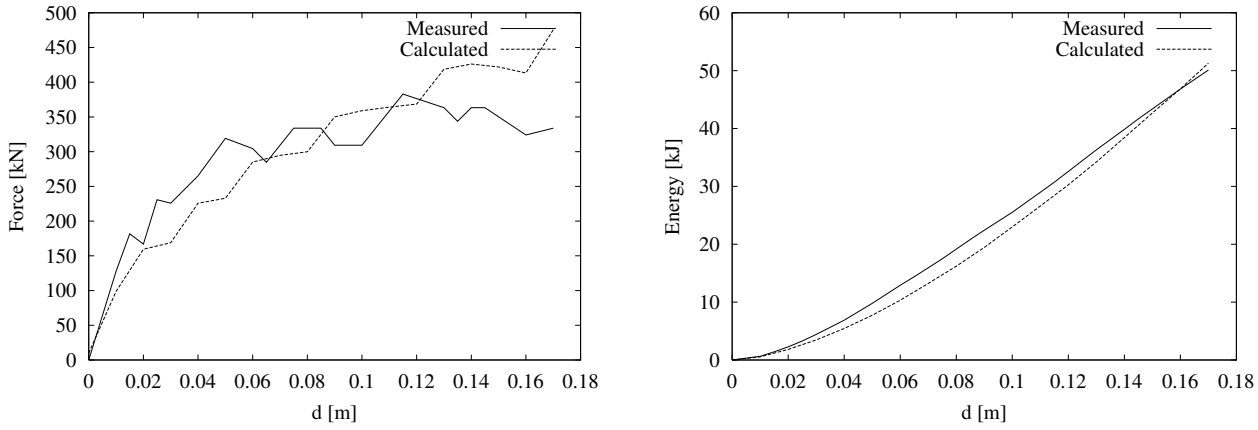


Figure 4.10: *Calculated and measured load and energy absorption versus penetration, exp. T1.*

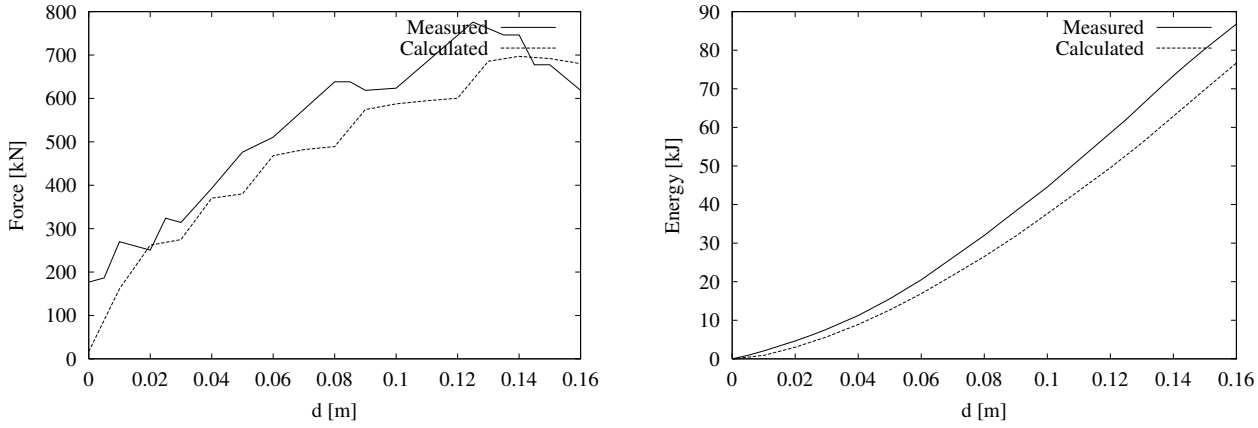


Figure 4.11: *Calculated and measured load and energy absorption versus penetration, exp. T2.*

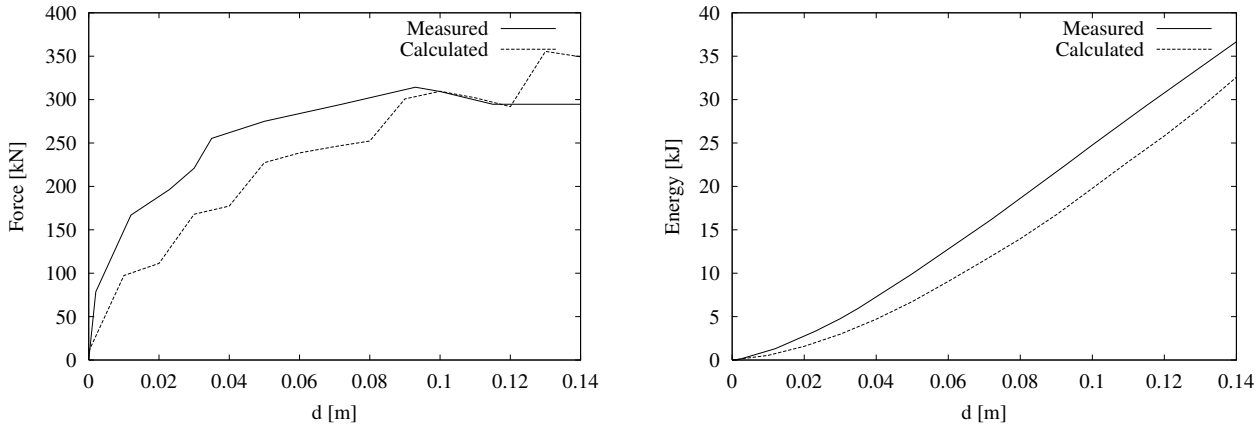


Figure 4.12: *Calculated and measured load and energy absorption versus penetration, exp. T3.*

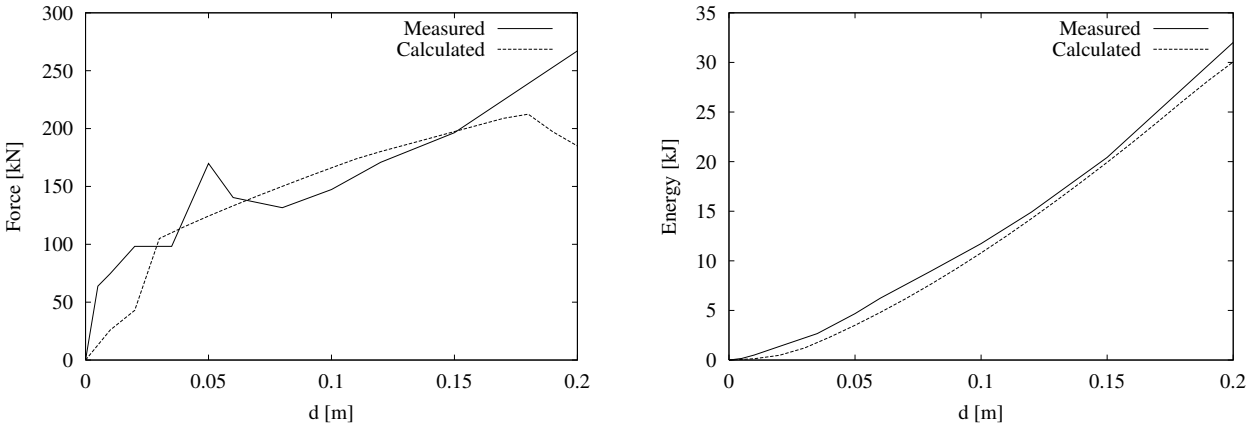


Figure 4.13: *Calculated and measured load and energy absorption versus penetration, exp. L4.*

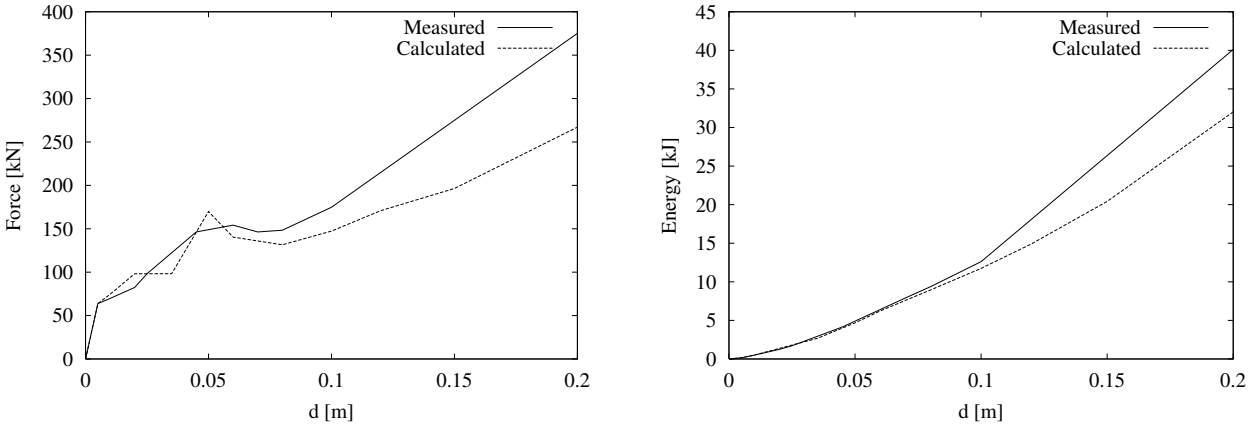


Figure 4.14: *Calculated and measured load and energy absorption versus penetration, exp. L5.*

### Double-Hull Test by Amdahl and Kavlie (1992)

Amdahl and Kavlie (1992) performed model tests simulating a double hull indented by a rigid hexagonal body. The tests originally simulated grounding, but the tests are also useful in side collision analysis.

Two different structures were examined.

### Model 1

The geometry is shown in Figure 4.15.

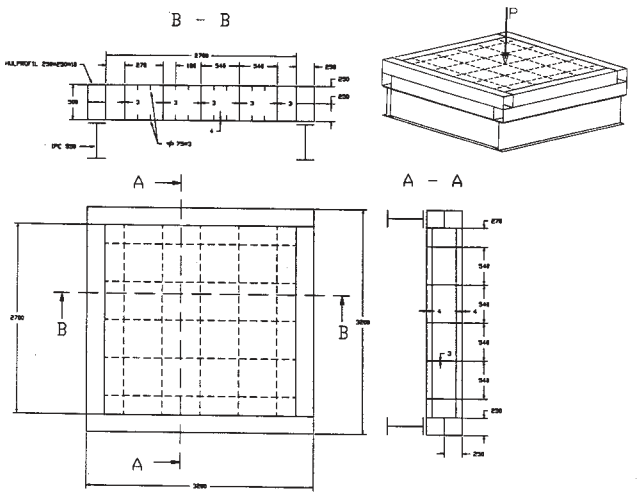


Figure 4.15: *Model 1 (Amdahl and Kavlie (1992)).*

| | | | |
|---|---|---|---|
| Side Shell | $t = 4mm$ | | $\sigma_0 = 390MN/m^2$ |
| Inner side shell | $t = 4mm$ | | $\sigma_0 = 390MN/m^2$ |
| Frames | $t = 3mm$ | Spacing $= 548mm$ | $\sigma_0 = 380MN/m^2$ |
| Stringer decks | $t = 4mm$ | Spacing $= 540mm$ | $\sigma_0 = 380MN/m^2$ |
| Longitudinals | $75\ x\ 3mm$ | Spacing $= 180mm$ | $\sigma_0 = 405MN/m^2$ |

The fracture strain is not given but is set to 7%.

The geometry of the indentor was not specified in detail ("hexagonal truncated cone"), but it was stated that the indentor came into contact with the nearest girders and floors after a penetration of 207 mm. The distance from the striking point to these members was 540 mm. A bulb with a length of 0.6m here approximates the indentor. The vertical radius of the bulb can then be calculated as

$$R_V = R_L \frac{(x)^2}{d} = 0.6 \frac{(0.540)^2}{0.207}$$

The horizontal radius must be $\frac{\sqrt{3}}{2}$ times smaller to obtain the best agreement with a hexagonal cone.

The bulb or the indentor can then be described by the following parameters:

$$R_L = 0.6\ m \qquad R_V = 0.846\ m \qquad R_H = 0.732\ m$$

The results from the experiment and the calculation are shown in Figure 4.16. It is seen that there is a good agreement between measured and calculated values. Small differences may arise from the geometry approximation of the indentor.

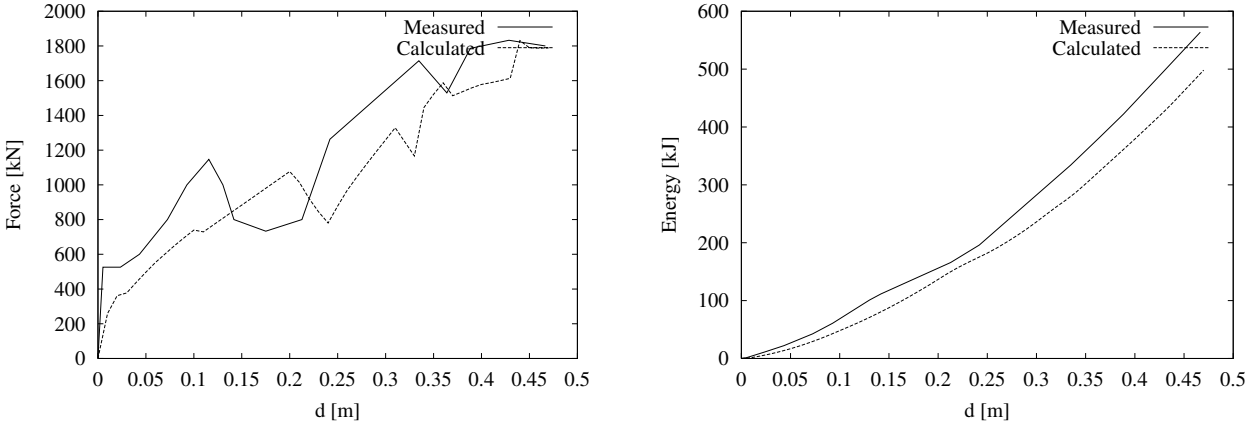


Figure 4.16: *Calculated and measured load and energy absorption versus penetration, experiment with model 1.*

### Model 2

The geometry is shown in Figure 4.17.

| | | | |
|---|---|---|---|
| Side Shell | $t = 4mm$ | | $\sigma_0 = 380MN/m^2$ |
| Inner side shell | $t = 4mm$ | | $\sigma_0 = 380MN/m^2$ |
| Frames | $t = 3mm$ | Spacing $= 540mm$ | $\sigma_0 = 400MN/m^2$ |
| Stringer decks | $t = 4mm$ | Spacing $= 1530mm$ | $\sigma_0 = 400MN/m^2$ |
| Longitudinals | $75x3mm$ | Spacing $= 180mm$ | $\sigma_0 = 350MN/m^2$ |

The three middle frames are equipped with stiffeners. The centre frame is equipped with a stiffener for every longitudinal, the other frames for every second longitudinal, the stiffeners are flat bars 40 $X$ 3 $mm$. Se also figure 4.17. The fracture strain is not given but is set to 7%.

The indentor has the same dimensions as the indentor in the model 1 experiment.

The results from the experiment and the calculation are given in Figure 4.18. It is seen that there is a good agreement between measured and calculated values.

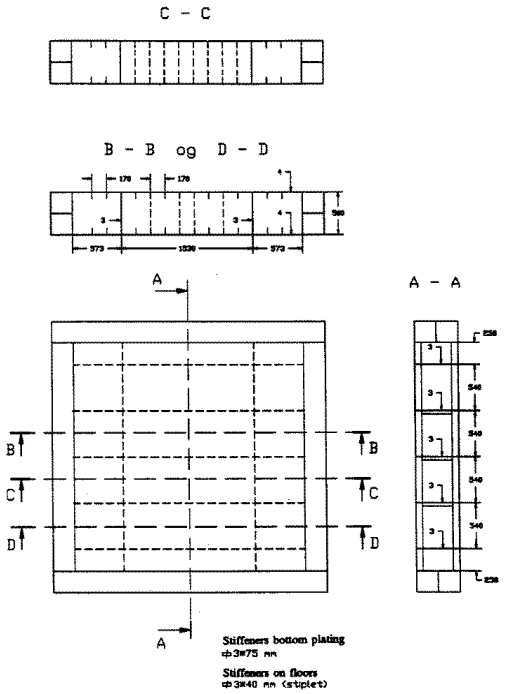


Figure 4.17: *Model 2 (Amdahl and Kavlie (1992)).*

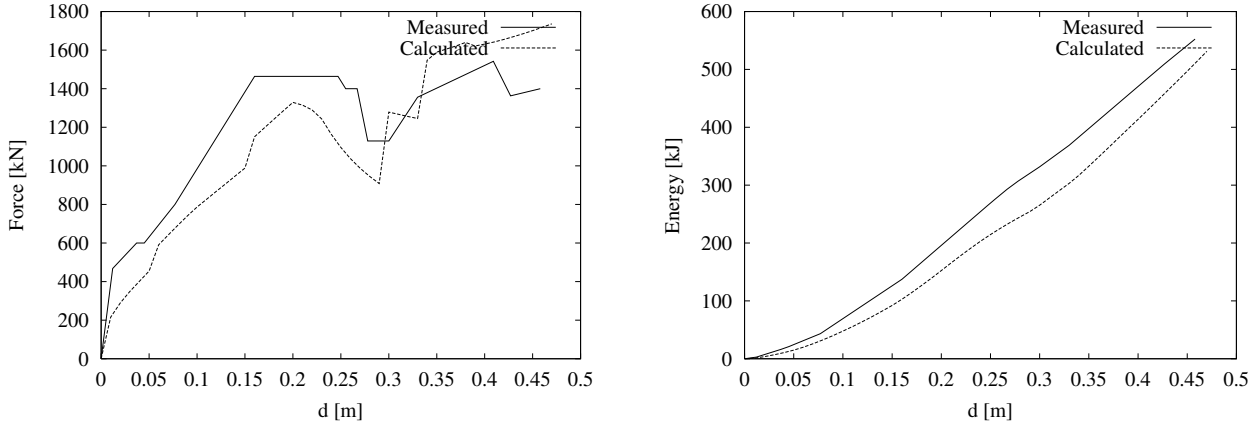


Figure 4.18: *Calculated and measured load and energy absorption versus penetration, experiment with model 2.*

## 4.5 Modelling of the Mechanics of Bow Crushing

The analysis of bow crushing will here be separated into two parts. One dealing with longitudinal stiffened bows, the other with transversely stiffened bows.

Figure 4.19: *Bulb deformation of M/S Tadeusz Koseiuszko (Lehmann and Yu (1995)).*

### Deformation of Longitudinally Stiffened Bow

A method for determination of impact loads as a function of deformation for bow collisions against rigid walls has been developed by Pedersen et al. (1993). The method is based on a modification of Amdahl's method (Amdahl, 1982), which has been established on the basis of theoretical considerations of energy dissipated during plastic deformation of basic super elements. The formula for the average crushing strength is given by

$$\sigma_c = 2.42\sigma_0 \left[\frac{n_{AT}t^2}{A}\right]^{0.67} \left[0.87 + 1.27\frac{n_c + 0.31n_T}{n_{AT}} \left(\frac{A}{(n_c + 0.31n_T)t^2}\right)^{0.25}\right]^{0.67} \tag{4.7}$$

The total crushing load is found by multiplying by the associated cross-sectional area of the deformed steel material $F_c = \sigma_c A$. Other symbols:

| | |
|---|---|
| $\sigma_c$ | average crushing strength of bow |
| $\sigma_0$ | flow stress |
| $t$ | average plate thickness of cross-section under consideration |
| $A$ | cross-sectional area of deformed steel material |
| $n_c$ | number of cruciforms or X-sections |
| $n_T$ | number of T-sections |
| $n_{AT}$ | number of angle- and T-sections |

### Deformation of Transversely Stiffened Bow

The method developed by Pedersen et al. (1993), Eq. (4.7), is by Lehmann and Yu (1995) said not to be suitable for transversely stiffened bows. They developed a method based on a study of crushing of conical shell structures. The shell plating of the bulb is idealised as a series of short conical shells with different cone angles. The average crushing load for each shell is given by

$$F_c = 2.09\sigma_0 t^2 \left[\frac{2\pi R_i}{L} + \frac{L}{t} + (\pi + 2\phi)\tan\phi + 1\right] \tag{4.8}$$

List of symbols:

| | |
|---|---|
| $\sigma_0$ | ultimate strength of steel |
| $t$ | plate thickness |
| $L$ | frame spacing |
| $R_i$ | effective radius |
| $\phi$ | conic angle |

Internal elements such as decks and longitudinal bulkheads are treated as super elements, where the crushing strength is calculated by use of Eq. (4.7).

### Comparison of Formulas for Bow Crushing

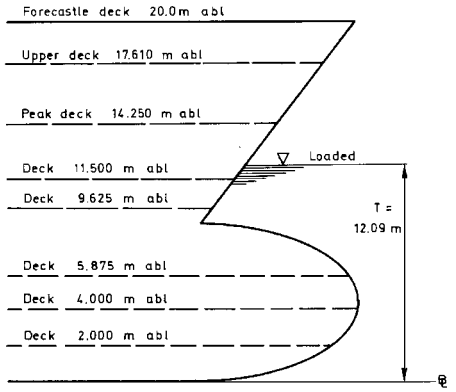


Figure 4.20: *Bow geometry of a 51,800 DWT bulk carrier.*

The two equations, Eq. (4.7) and Eq. (4.8) are compared for a transversely stiffened bow. The crushing load is calculated for a 51,800 DWT bulk carrier. Main data and bow geometry are found in Appendix A, Table A.1, and the scantlings of the transversely stiffened bulb are found in Appendix A, Table A.2 and Figure 4.20. The forces calculated by the two equations are quite similar, as seen by a comparison of the force-deformation curves in Figure 4.21.

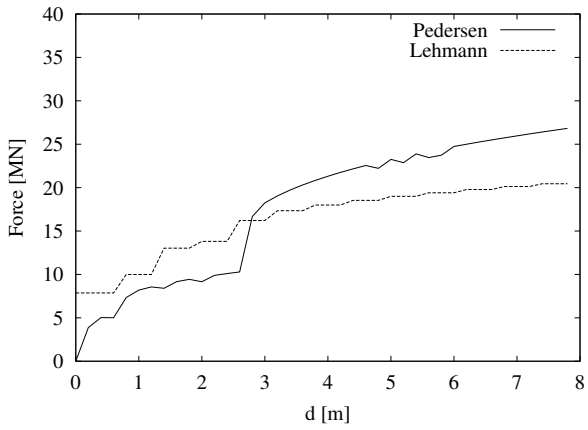


Figure 4.21: *Comparison of Eqs. (4.7) and (4.8). Crushing of the bulb of a 51,800 DWT bulk carrier (transversely stiffened).*

### Comparison of Longitudinally and Transversely Stiffened Bows

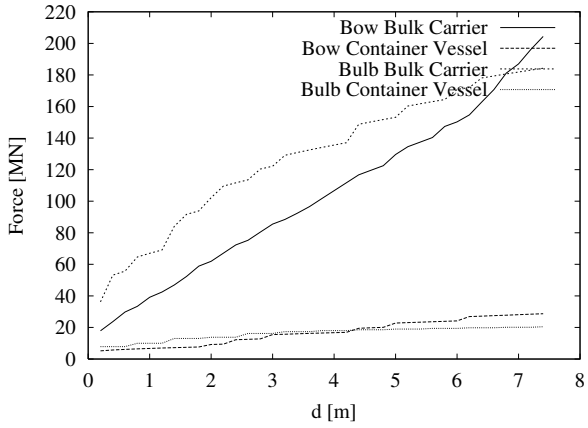


Figure 4.22: *Calculated load deflection curve for the 40,000 DWT container vessel (longitudinally stiffened) and the 51,800 DWT bulk carrier (transversely stiffened).*

Before a presentation of the effect of the crushing deformation of the bow of the striking vessel, the variation in bow strength for two differently stiffened vessels is considered. The two vessels to be compared are a container vessel of 40,000 DWT with high ice class and a bulk carrier of 51,800 DWT. The geometrical data for the two vessels is shown in Appendix A, Table A.1, the scantling data for the container vessel is given in Pedersen et al. (1993) and the structural data for the bulk carrier is found in Appendix A, Table A.2 and Figure 4.20.

The two vessels are comparable in size and geometry, but the structural layout of the two bows is different. The method of calculation is the model developed by Pedersen et al. (1993), see Eq. (4.7). The result is that the bow of the bulk carrier, which is transversely stiffened,

shows a significantly lower resistance, as seen by comparison of the force-penetration curves in Figure 4.22.

## 4.6 Deformation of both Striking and Struck Vessel

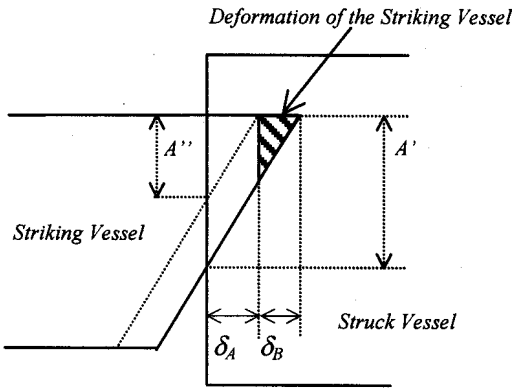


Figure 4.23: *Deformation of vessels during collision. The A's relate to areas not lengths.*

The analysis of collision scenarios, where both the striking and the struck vessel can be damaged, is carried out in penetration steps. Only one of the involved vessels can be deformed in each step. By a comparison of the crushing forces for respectively the bow and the side, it can be determined which vessel deforms during the considered step. Before calculation of the deformation of the two vessels the following calculations are carried out:

1. Force-penetration curve $F_{struck}(\delta_A)$ for the struck vessel, where the striking vessel is rigid

2. Force-penetration curve $F_{striking}(\delta_B)$ for the striking vessel, where the struck vessel is rigid

If the striking vessel is equipped with a bulbous bow, the analysis of the crushing forces is separated into a bulb analysis and an analysis of the top of the bow above the bulb. A commonly used procedure for taking into account the deformation of the bow is to compare the two above mentioned force-penetration curves, $F_{struck}(\delta_A)$ and $F_{striking}(\delta_B)$, at each step. This approach, however, only includes a very limited level of interaction. In reality, the force-penetration curve for the side of the struck vessel is a function of the deformation of the bow, and vice versa. This stronger interaction is taken into account by comparing the forces $F_A$ and $F_B$, which are determined as

Struck vessel $F_A = F_{struck}(\delta_A)\frac{A'}{A''}$

Striking vessel $F_B = F_{striking}(\delta_A + \delta_B)$

where

| | |
|---|---|
| $F_A$ | force to crush the struck vessel |
| $F_B$ | force to crush the striking vessel |
| $F_{struck}$ | force from the force-penetration curve for struck vessel, where the striking vessel is rigid |
| $F_{striking}$ | force from the force-penetration curve for striking vessel, where the struck vessel is rigid |
| $\delta_A$ | penetration into the struck vessel |
| $\delta_B$ | deformation of the striking vessel |
| $A'$ | cross-sectional area of the striking vessel taken at a distance of $\delta_A + \delta_B$ from bow or bulb tip |
| $A''$ | cross-sectional area of the striking vessel taken at a distance of $\delta_A$ from bow or bulb tip |

See also Figure 4.23.

The forces on the struck and the striking vessel $F_A$ and $F_B$ are compared

- If $F_A > F_B$
  deformation of striking vessel, $\delta_B$, is increased
- If $F_B > F_A$
  deformation of struck vessel, $\delta_A$, is increased

The reason for correcting the resistance of the struck vessel is that if the bow is deformed, the resistance is approximately equal to the force on the side times the ratio between the areas. For a single-hull vessel the correction will have nearly no influence, but for a double-hull vessel, there will be some corrections when the bow penetrates the inner side, see Figure 4.23. When the deformation patterns of the struck and the striking vessel are known, the total absorbed energy can be calculated by integration and compared with the energy calculated by the external dynamics, see Chapter 3.

This page is intentionally left blank.

# Chapter 5

# Deterministic Analysis of Collisions

This chapter presents a method for prediction of damage to vessels in a collision event. The analyses are purely deterministic, as both the struck and the striking vessel are known. The method is based on the external dynamics and the internal mechanics described in detail in Chapters 3 and 4.

The chapter starts with a description of the program modelling. Three programs have been developed for the deterministic analysis. The program structure is described in detail, including the necessary input and the program output.

The results from the developed program have been compared to results from other programs for analysis of collisions. Two series of comparisons are made. First results for force and energy absorption as function of the penetration are presented for a collision between two Ro-Ro vessels. The comparison is made between calculation models developed by Hysing (1995) (Det Norske Veritas), Scharrer (1996) (Germanischer Lloyd) and the present model. Then the results from the present model are compared to results obtained by use of three other collision models: DAMAGE developed by Wierzbicki and Simonsen in connection with the Joint MIT-Industry Program on Tanker Safety, ALPS/SCOL developed by Prof. Paik in Korea and SIMCOL, Simplified Collision Model, developed by Prof. Brown from Virginia Tech.

In order to investigate the sensitivity of the collision analysis, the effect of changing the striking location and the design of the side of the struck vessel have been analysed.

The last section in this chapter deals with minor damages to vessels. Minor damages may arise at sea during collision with floating objects or by contact with obstacles during manoeuvring in harbour areas. The question of how large permanent deformation can be accepted without repair of the vessel is raised in this section. See also Lützen (2001).

## 5.1 The Tools - Damages in Collision Events

Three programs for deterministic analysis of collisions are developed.

1. Deformation of the struck vessel, see Section 5.1.1
2. Deformation of the bow of the striking vessel, see Section 5.1.2
3. Deformation of both vessels, see Section 5.1.3

In the first program, deformation of the struck vessel, the bow of the striking vessel is assumed to be rigid, whereas the side of the struck vessel is assumed to be rigid in the second program regarding deformation of the bow of the striking vessel.

All the programs make use of a subroutine for calculation of the energy released for crushing, see Chapter 3 on external dynamics.

The programs are all written in the Microsoft Visual C++ language.

### 5.1.1 Program 1: Deformation of the Struck Vessel

The overall goal of the first program is to determine the resistance of the side structure, the energy released for crushing and the damage to the struck vessel. Subroutines calculating the external dynamics and the internal mechanics are used for the program. The input parameters for the program are information on the main particulars and the structural design of the struck vessel, the main particulars and the bow geometry of the striking vessel and finally a collision scenario describing the striking location, the collision angle and the velocity of both the struck and the striking vessel, see Figure 5.1.

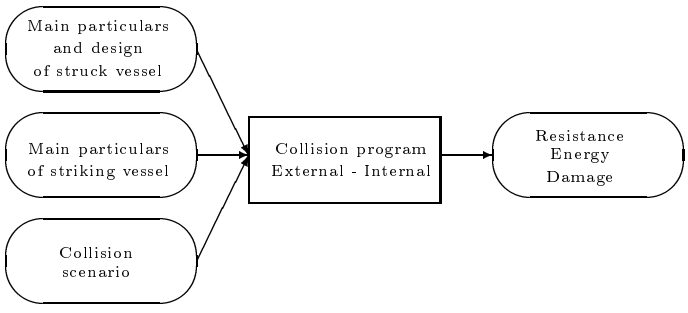


Figure 5.1: *Determination of energy released for crushing.*

A flow chart for the developed program is shown in Figure 5.2.

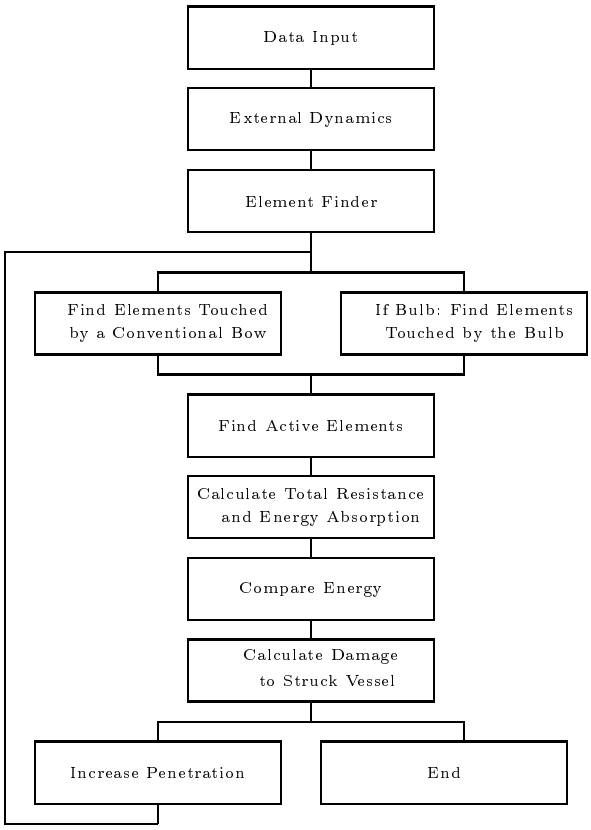


Figure 5.2: Collision program - damage to side of struck vessel.

**Data Input** Three data files must be provided for the program

- Structural layout of the struck vessel
- Main particulars of both vessels, including bow geometry of the striking vessel
- Description of the collision scenario

The files are described in detail in Appendix B.

**External Dynamics** Calculates the energy to be absorbed using rigid body dynamics

**Element Finder** Finds all super elements at the side of the struck vessel such as membrane plates, in-plane deformation of plates, X- or T-elements and beams

**Find Elements Touched by a Conventional Bow** Finds all involved elements touched by the striking bow

**If Bulb: Find Elements Touched by the Bulb** If the bow of the striking vessel is equipped with a bulb, all elements in contact with the bulb are found

**Find Active Elements** For elements in contact with both the bow and the bulb, it is here determined which to neglect and which to include in the analysis

**Calculate Total Resistance and Energy Absorption** By summing up the crushing forces of each super element, the total contact load between the two involved vessels is determined. The absorbed energy is found by integration of the force-deformation curve

**Compare Energy** The energy calculated by the external dynamics and the internal mechanics is compared

**Calculate Damage to Struck Vessel** The damage to the struck vessel is determined

**Increase Penetration** If the energy calculated by the external dynamics is greater than the absorbed energy, the penetration is increased and the calculation loop is continued

**End** The penetration into the struck vessel stops when the energy absorbed by structural deformation reaches the loss in kinetic energy calculated by the external dynamics

Output from the program is the damage length, the damage height and the penetration. The damage is calculated for a penetration corresponding to a situation where all energy determined by the external dynamics is absorbed in the structure of the struck vessel. The total resistance and the absorbed energy are given as a function of the penetration into the struck vessel. The resistance for respectively the bulb and the top of the bow areas is also given as a function of the penetration.

### 5.1.2 Program 2: Deformation of the Bow of the Striking Vessel

The overall goal of the second program is to determine the total resistance of the striking bow and from this estimate the energy absorbed during deformation. The method of calculation is a model developed by Pedersen et al. (1993), see Section 4.5.

**Data Input** Two files must be provided for the program:

- Structure in the bow of the striking vessel
- Bow geometry of striking vessel

The files are described in detail in Appendix B.

**Structural Component Finder** Finds all structural elements in the striking bow

**Find Elements and Area at Conventional Bow** All involved elements in the striking bow are found. The number of X-, T- and L-elements is determined and the resistance for a given indentation is calculated

**Find Elements and Area at Bulb** If the bow of the striking vessel is equipped with a bulb, all construction parts in the bulb are found and the resistance is calculated

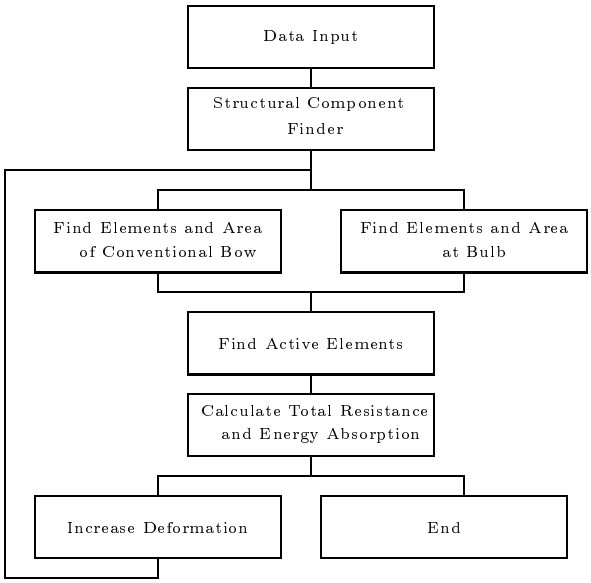


Figure 5.3: Collision program - damage to bow of striking vessel.

**Find Active Elements** Elements used in both the bow and the bulb analysis are found. It is here determined which to neglect and which to include in the analysis

**Calculate Total Resistance and Energy Absorption** By summing up the crushing forces of the bulb and the top of the bow, the total contact load is determined. The force-deformation curve is integrated to give the absorbed energy

**Increase Deformation** If the deformation is below a pre-defined level the deformation is increased

**End** The penetration into the struck vessel stops when the pre-defined level for deformation is reached

The output from the program is the total resistance and the absorbed energy given as a function of the deformation of the bow of the striking vessel. The resistance and the areas for respectively the bulb and the top of the bow are also given as functions of the deformation.

### 5.1.3 Program 3: Deformation of Both Vessels

Collision events where both the striking and the struck vessel can be damaged are analysed in the third program. By a comparison of the crushing forces for respectively the bow and the side of the struck vessel, it can be determined which vessel deforms. For further details of the theory and symbols, see Section 4.6.

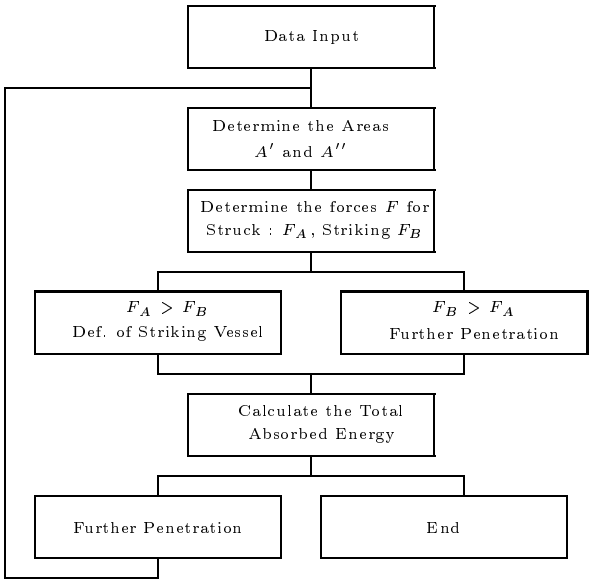


Figure 5.4: Collision program - damage to both the struck and the striking vessel.

**Data Input** Two files must be provided for the program:

- Struck vessel, $F_{bulb}$, $F_{bow}$, $F_{total}$
- Striking vessel, $F_{bulb}$, $F_{bow}$, $F_{total}$, $Areas$

Furthermore, the energy from the external dynamics must be given. The files are outputs from the programs described in Sections 5.1.1 and 5.1.2.

**Determine the Areas $A'$ and $A''$** Calculation of the cross-sectional area of the striking vessel for given penetrations

**Determine the Forces $F_A$ and $F_B$** Determination of the force to crush the struck vessel, $F_A$, and the force to crush the striking vessel, $F_B$

**$F_A > F_B$ and $F_B > F_A$** Determination of which vessel will deform in this particular penetration step

**Calculate the Total Absorbed Energy** Calculation of the energy absorbed in both the struck and the striking vessel

**Further Penetration** Increase of increment

**End** The deformation of the vessels stops when all the energy determined by the external dynamics is absorbed in the structure of the two vessels

Output from the program is the deformation of the bulb and the bow of the striking vessel and the penetration into the struck vessel.

## 5.2 Comparison of Different Collision Programs

Two series of comparisons are made in this section. First a comparison of force and energy absorption as a function of the penetration for a collision between two Ro-Ro vessels is presented, the comparison is made between calculation models developed by Hysing (1995), Scharrer (1996) and the present model. Then the results from the present model have been compared to results obtained using three other collision models.

It is in all examples assumed that the bow of the striking vessel is rigid, which means that only the side of the struck vessel will deform.

### 5.2.1 Comparison of Force and Energy Curves for a Ro-Ro Vessel

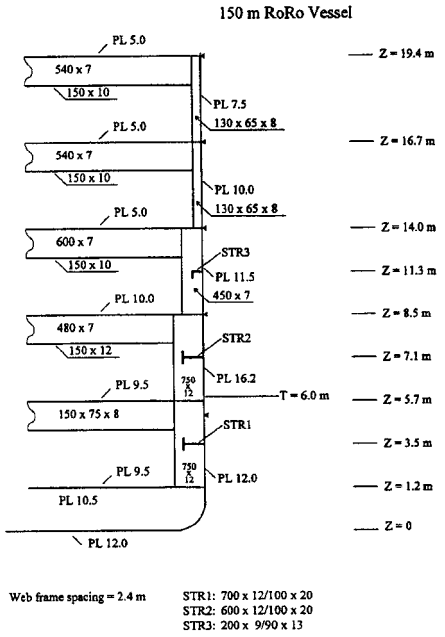


Figure 5.5: *Midship section of the Ro-Ro vessel (Hysing (1995)).*

Scharrer (1996) and Hysing (1995) made a series of calculations where striking vessels with conventional and bulbous bows strike Ro-Ro vessels in oblique collisions. The results from some of their examples are here compared with the results from the present method.

**Struck Vessel**

The main particulars of the Ro-Ro vessel are shown in the table below.

| $L_{pp}$ [m] | $B$ [m] | $T$ [m] | $\Delta$ [tonnes] |
|---|---|---|---|
| 150.00 | 27.0 | 6.0 | 15800 |

The critical rupture strain of the structure is taken to be 5% and the yield strain of the steel to be $235N/mm^2$. Scharrer and Hysing also used these parameters. The impact point is located between two frames. The detailed structure of the midship section is shown in Figure 5.5.

### Striking Vessel

Four situations are analysed, a ballast and a fully loaded condition with both a conventional and a bulbous bow. The displacements of the vessels are not given but are estimated by a block coefficient of 0.65. The main particulars of the striking vessel for the two loading conditions are shown in Table 5.1.

Table 5.1: *Main particulars of striking vessel.*

| | $L_{pp}$ [m] | $B$ [m] | $T$ [m] | $\Delta$ [t] | $H_{deck}$ [m] | $B_d$ [m$^{-1}$] | $B_b$ [m$^{-1}$] | $\phi$ [$^0$] |
|---|---|---|---|---|---|---|---|---|
| Ballast, conv. bow | 160.00 | 24.6 | 6.41 | 16800 | 16.3 | 0.15 | 0.43 | 68 |
| Loaded, conv. bow | 160.00 | 24.6 | 9.11 | 24000 | 16.3 | 0.15 | 0.43 | 68 |
| Ballast, bulbous bow | 160.00 | 24.6 | 6.41 | 16800 | 16.3 | 0.15 | 4.22 | 56 |
| Loaded, bulbous bow | 160.00 | 24.6 | 9.11 | 24000 | 16.3 | 0.15 | 4.22 | 56 |

If the striking vessel is equipped with a bulbous bow, the bulb parameters are taken to be

$$R_L = 5.6\text{m} \qquad R_V = 4.0\text{m} \qquad R_H = 3.5\text{m} \qquad R_D = 1.3\text{m}$$

See Section 4.1 for a description of the bulb parameters.

### Calculation Results

The force and energy absorption as a function of the penetration calculated by Hysing, Scharrer and by the present method are shown in Figures 5.6-5.8. Considering the complexity of the problem, the comparisons indicate that good agreement has been achieved.

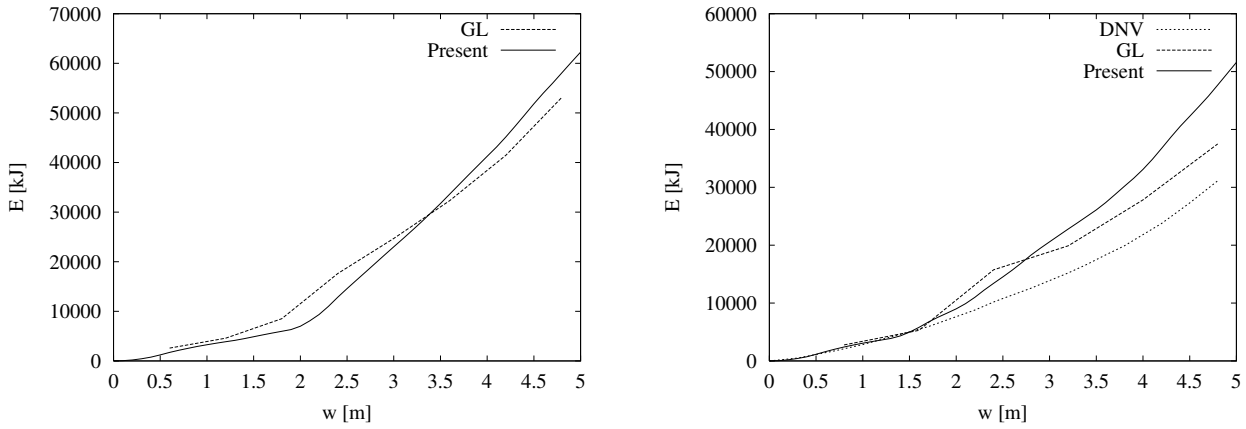


Figure 5.6: *Energy absorption of struck vessel, striking vessel with bulb : Left loaded, right ballast.*

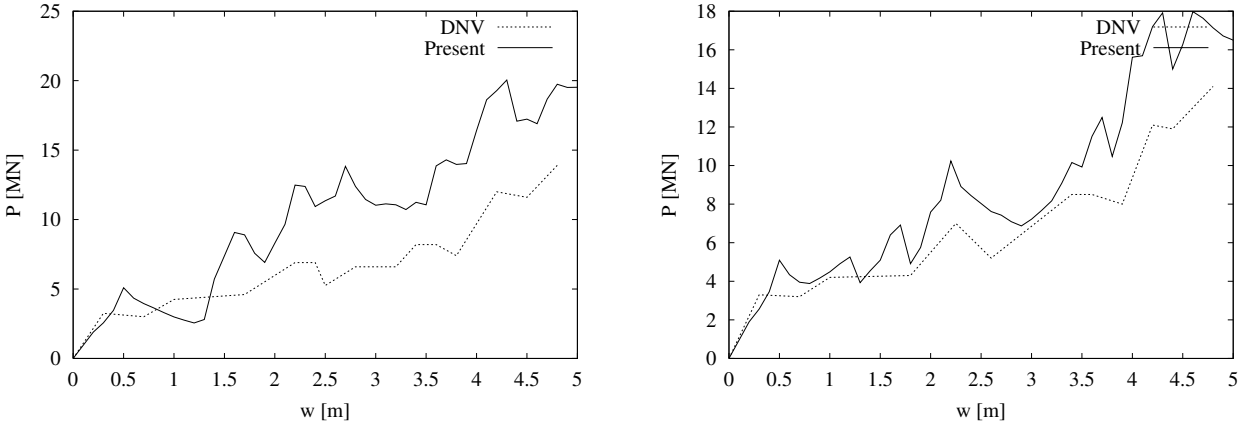


Figure 5.7: *Forces, ballast condition: Left striking vessel with bulb, right striking vessel without bulb.*

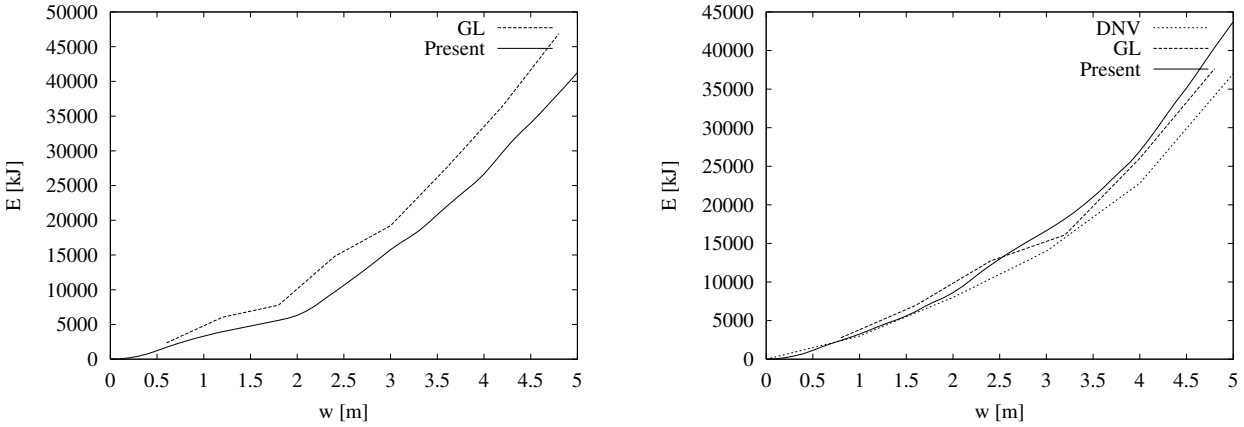


Figure 5.8: *Energy absorption of struck vessel, striking vessel without bulb: Left loaded, right ballast.*

### 5.2.2 Comparison of Calculation Models Using a Tanker

The results from the present model are compared to results obtained by three other quite recent collision models: DAMAGE developed in connection with the Joint MIT-Industry Program on Tanker Safety, ALPS/SCOL developed by Prof. Paik in Korea and SIMCOL (Simplified Collision Model) developed by Prof. Brown from Virginia Tech. A short description of the models, except the present model, is given in the following sections. See also Brown et al. (2000).

**DAMAGE Ver. 4.0 (Abramowicz and Sinmao (1999),Simonsen (1999))**
The DAMAGE 4.0 collision model solves the external problem uncoupled from the internal problem and applies the calculated absorbed energy to plastic deformation of the struck vessel. Forward motion of the struck vessel is assumed to be zero and only right angle collisions are considered. Determination of the external dynamics is based on the rigid body mechanism. The model for the internal mechanics is based on the super element method.

**ALPS/SCOL (Paik et al. (2000), Paik and Pedersen (1996))**
ALPS/SCOL is a coarse-mesh 3-D non-linear finite element code using super elements based on the Idealised Structural Unit Method (ISUM). The analysis of the external dynamics and the internal mechanics is performed separately. The velocity of the struck vessel is assumed to be zero. The added masses for the struck and the striking vessels used in the external analysis are directly calculated based on ships of similar type and size by use of a computer program based on linear strip theory.

**SIMCOL (Chen (2000))**
SIMCOL (Simplified Collision Model) uses a time-domain simultaneous solution of the external dynamics and the internal mechanics similar to a method originally proposed by Hutchison (1986). The external model uses a three-degree-of-freedom system for ship dynamics. The internal model determines forces from side and bulkhead structures using mechanisms adapted from a Rosenblatt study (McDermott et al. (1974)). Crake, Rawson and Brown (Rawson et al. (1998), Crake (1995)) developed the first version of SIMCOL as a part of the work of SNAME Ad Hoc Panel #3. Based on further research, improvements were made by Chen and Brown at Virginia Tech (Chen (2000)). The program determines the energy absorbed by the crushing and tearing of decks, bottom and stringers using a Minorsky correlation.

**Comparison**

The four programs have been used for modelling the same collision scenarios involving a double-hull tanker as the struck vessel and a bulk carrier as the striking vessel.

**The Struck and the Striking Vessels**

The baseline struck vessel used for comparison is a 150,000 DWT double-hull tanker. The tanker is modelled to be consistent with the dimensions of the 150,000 DWT reference

tanker in the IMO Interim Guidelines (IMO, 1995). HECSALV and Safehull have been used to develop the details of the design to ensure that the arrangement satisfies the IMO regulations and that the structural design satisfies classification requirements.

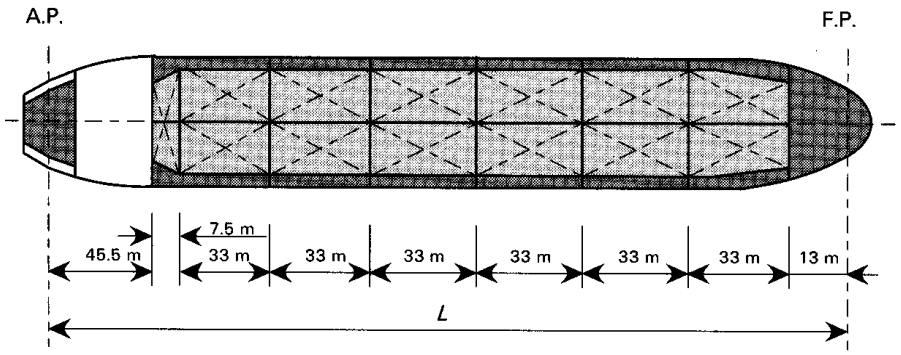


Figure 5.9: *Baseline tanker, 150,000 DWT double-hull tanker, (IMO, 1995).*

Main particulars of the 150,000 DWT double-hull tanker:

| | | |
|---|---|---|
| Dead weight | 150,000 | tonnes |
| Displacement | 178,867 | tonnes |
| Length | 264.00 | m |
| Breadth | 48.00 | m |
| Depth | 24.00 | m |
| Draught | 16.80 | m |

A description of the scantlings and the material parameters is found in Appendix A, Table A.3.

The striking vessel is a 150,000 DWT bulk carrier. The geometry of the bow of the vessel is found in Appendix A, Table A.1. The scantlings are described in detail in Pedersen et al. (1993). The bow of the striking vessel is in all the calculations assumed to be rigid.

### Model Test Matrices

Three scenario test matrices are used in the comparison study. Since the focus of the test is on the penetration, zero speed of the struck vessel is used in all the cases. Scenarios for the test matrices are described in Table 5.2.

### Results

Representative results from the matrices 1-3 are shown in Figures 5.10 -5.12. The figures show the transverse penetration into struck vessel as a function of the particular variables in each matrix. The results reveal a difference between the models. DAMAGE generally predicts the lowest penetration and ALPS/SCOL generally the highest. The difference may reflect the different bow model geometry resulting in more or less crushing elements, but unfortunately this has not been examined further.

Table 5.2: *Test matrices.*

| | Struck vessel speed [knt] | Striking vessel speed [knt] | Collision angle [deg] | Striking location [m from ⊗] |
|---|---|---|---|---|
| Matrix 1 | 0 | 3,4,5,6,7 | 90 | -62.5, 29.5, 3.5, 36.5, 69.5, 102.5 |
| Matrix 2 | 0 | 3,4,5,6,7 | 90 | 1.85, 2.675, 3.5, 4.325, 5.15 |
| Matrix 3 | 0 | 3,4,5,6,7 | 45, 60, 75, 90, 105, 120, 135 | 3.5 |

Results from matrix 1, Figure 5.10, show to a great extent the effect of the external dynamics, i.e. most energy has to be absorbed around midships. SIMCOL shows a large variation in the penetration as a function of the global striking location, particularly at low energy collisions. ALPS/SCOL has a similar, but lesser tendency.

Results from matrix 2, Figure 5.11, show the reduction in the penetration when the striking location is on the web (3.5 m). The reduction is most significant for the SIMCOL, the other programs reveal a similar tendency, but less pronounced decrease. The results are remarkably consistent, maybe because of the relatively wide bow of the striking vessel compared to the web frame spacing.

In matrix 3, Figure 5.12, the penetration is shown as a function of the collision angle. The striking location is on the web nearest midships (3.5 m). The current version of DAMAGE is only able to consider right angle collisions, so DAMAGE is not used in this matrix. The figures show the effect of the external dynamics. In the considered cases, the velocity of the struck vessel is zero, which results in the deepest penetration for a right angle collision.

## 5.3 Sensitivity Analysis for a Crude Oil Carrier

In order to investigate the sensitivity of the collision analysis results, this section presents numerical analyses of the effect of changing the striking location and the design of the side of the struck vessel.

It is in all the examples assumed that the bow of the striking vessel is rigid, which means that only the side of the struck vessel will deform.

The first part deals with the striking location. The following changes have been investigated: a) the local collision location relative to the web framing, b) the global longitudinal striking location along the hull girder, and finally c) the vertical striking location, i.e. the influence of the loading condition of the involved vessels.

The second part of the analysis deals with the design of the struck vessel. The influence of the following parameters on the energy absorption is investigated: the thickness of the side

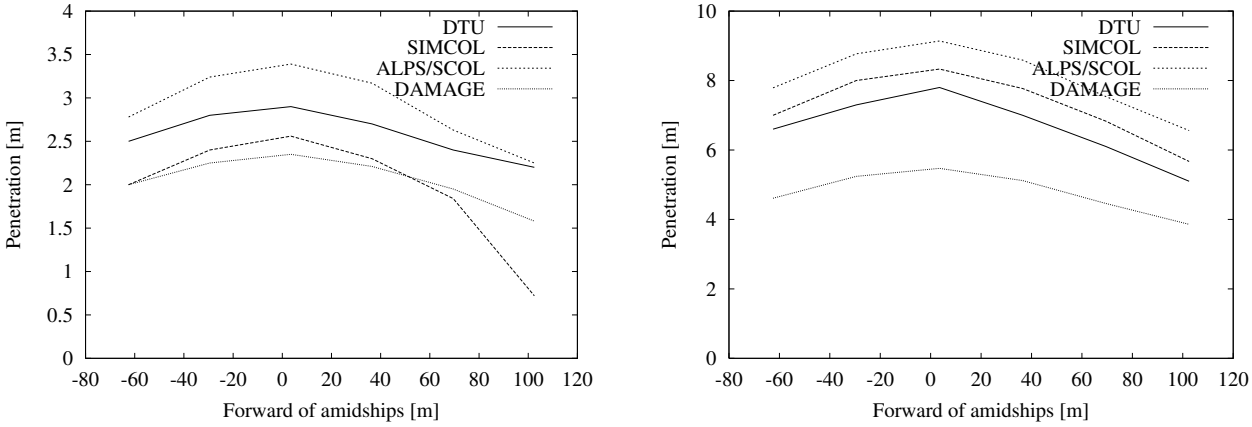


Figure 5.10: *Matrix 1 : Left $V_b = 3.0$ knots, right $V_b = 7.0$ knots.*

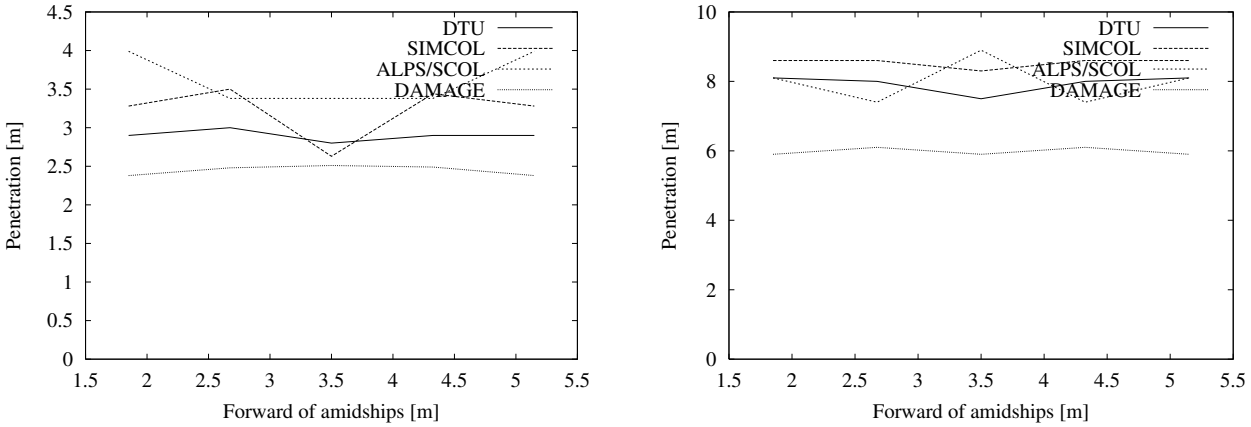


Figure 5.11: *Matrix 2 : Left $V_b = 3.0$ knots, right $V_b = 7.0$ knots. Web frame at 3.5m.*

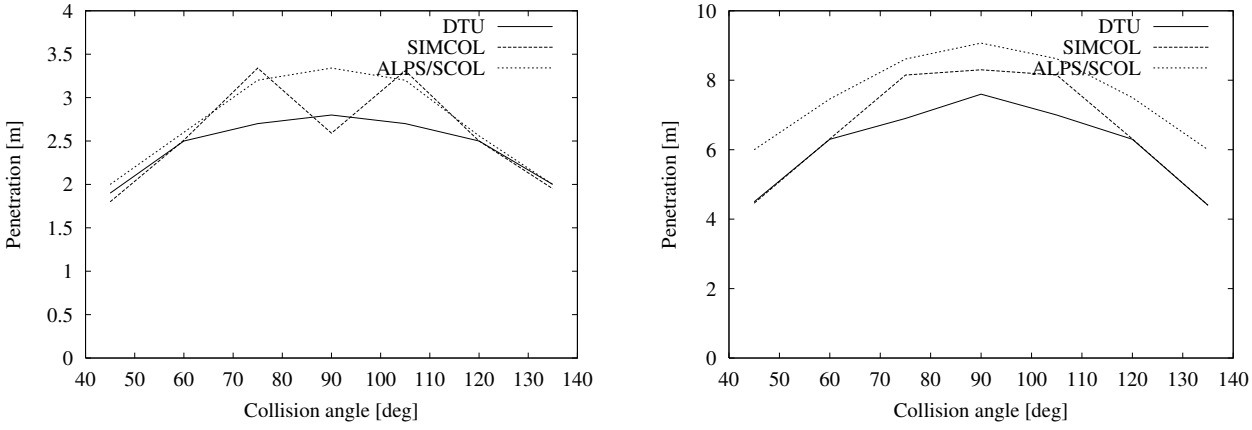


Figure 5.12: *Matrix 3 : Left $V_b = 3.0$ knots, right $V_b = 7.0$ knots.*

shell, the thickness and spacing of the frames, and the thickness and spacing of the stringer decks.

Two specific vessels have been treated in all the sensitivity analyses. The struck vessel is a 105,400 DWT double hull crude oil carrier. The main data for this vessel is:

| | | |
|---|---|---|
| Length | 234.0 | m |
| Breadth | 42.0 | m |
| Depth | 21.0 | m |
| Draught | 14.9 | m |
| Displacement | 122,870 | t |

A description of the scantlings is found in Appendix A, Tables A.4 and A.5, see also Figure 5.13.

The striking vessel is a 40,000 DWT container vessel with high Baltic ice class (DNV ice class 1B). Main data and bow geometry are found in Appendix A, Table A.1. The scantlings are found in Pedersen et al. (1993).

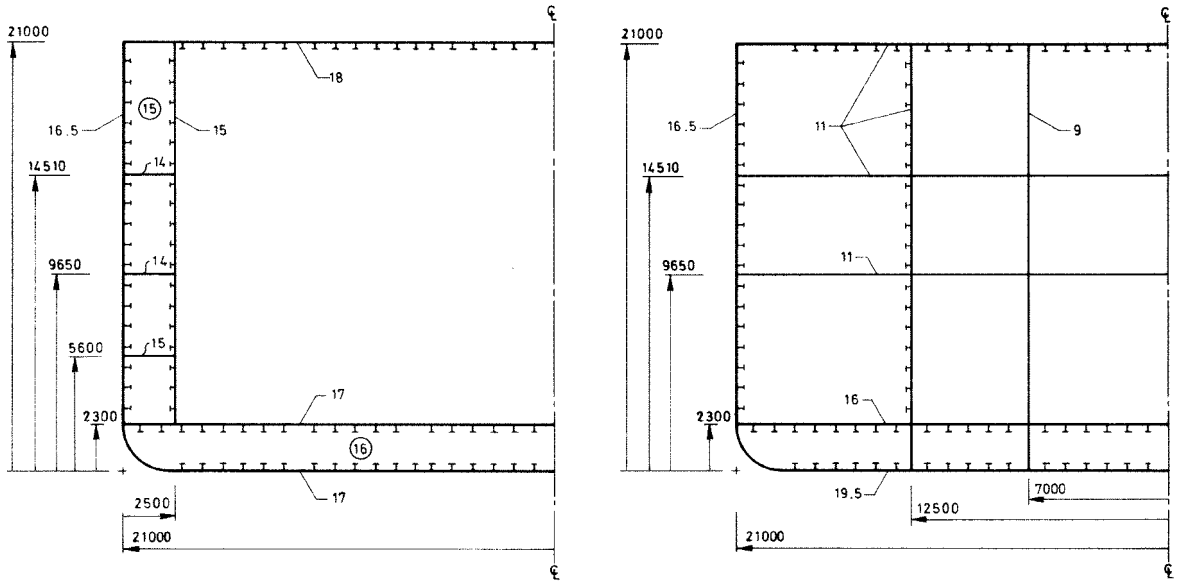


Figure 5.13: *Scantlings of 105,400 DWT crude oil carrier. Left: cargo hold section. Right: engine section.*

### 5.3.1 Sensitivity to the Striking Location

#### Sensitivity to Longitudinal Striking Location (Local)

To determine the effect of either striking a transverse web frame or having the collision point between two web frames, a right angle collision is considered. The struck vessel has zero speed. The striking vessel has a velocity of 3, 5 or 7 knots. Both vessels are fully loaded. The collision locations are all placed in the tank amidships. Figure 5.14 (left) shows the penetration into the struck vessel as a function of the striking location. The plan view of the side structure of the double-hull side of the tanker is also depicted in Figure 5.14. The penetration patterns for the 5- and 7-knot collision speeds are similar. A decrease in penetration occurs, when the striking location is between two frames. The main reason for this decrease in penetration is that when the bow is between two frames, it will early come into contact with both frames. The case where the velocity of the striking vessel is 3 knots is different. The deepest penetration occurs if the striking location is between two frames. The main absorption of energy will in this case be from plates in tension as crushing elements are touched late in the process. A decrease in frame spacing or a striking vessel with a more slender form will cause the curves to be more flat.

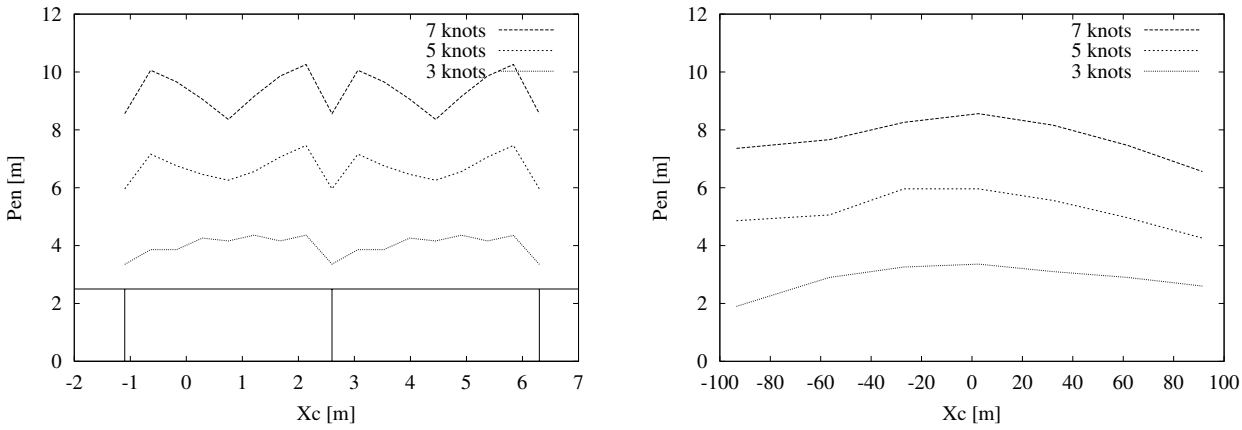


Figure 5.14: *Penetration into a 105,400 DWT crude oil carrier as a function of striking location (left local, right global).*

#### Sensitivity to Longitudinally Striking Location (Global)

It will now be investigated whether it is important to model in detail the variation of the contact point along the length of the hull. Figure 5.14 (right) shows the results of such an analysis. The penetration into the struck double-hull crude oil tanker is plotted as a function of the striking location. The striking positions are in the centre of each cargo tank at a frame and in the centre of the engine room aft. The collision is again a right angle collision, where the struck vessel has zero speed. The striking vessel has a velocity of 3, 5 or 7 knots. Both vessels are fully loaded. The figure shows the effect of the external dynamics,

i.e. most energy has to be absorbed around the midships. In the aft part of the struck vessel, which is a single-hull section in the engine region, there is a slight modification in the penetration pattern. For the 3-knots case, there will be a decrease in the penetration, which is due to the relatively thick mid -decks in the engine section and only few crushing elements being touched in the hold region. In the 5-knots case the penetration will increase in the engine region. In this case many elements will be crushed in the hold section, whereas only mid-decks are touched in the engine section. The penetration curve is flattening in the 7-knots case, where the bow will penetrate a longitudinal bulkhead in the engine section.

**Sensitivity to the Vertical Striking Location**

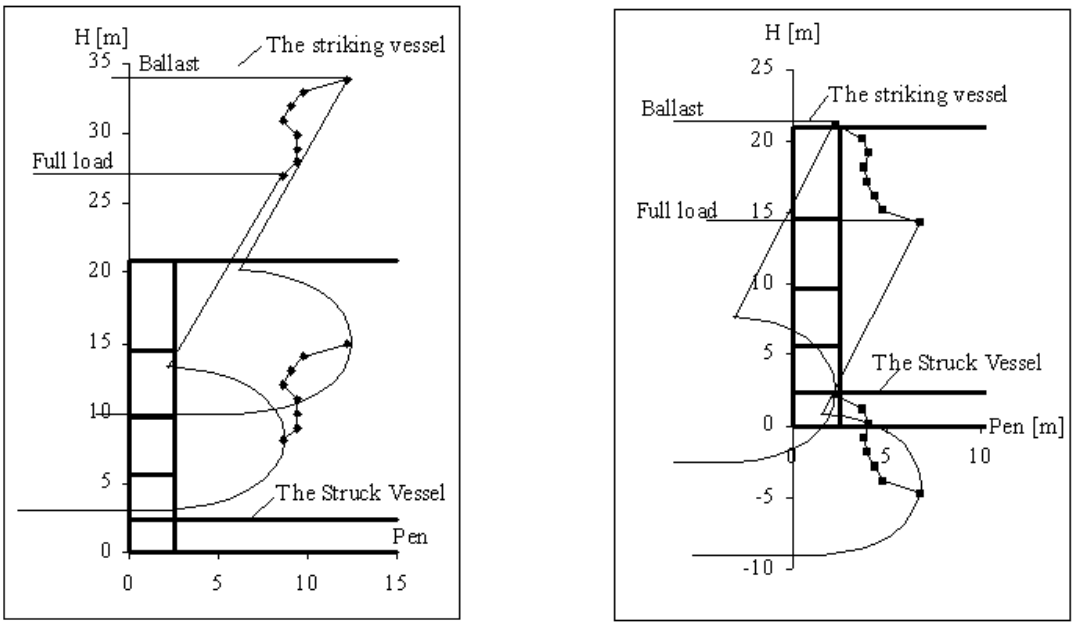


Figure 5.15: *Penetration into struck vessel, varying draught of striking vessel. Left: struck vessel fully loaded. Right: struck vessel in ballast.*

In order to analyse the importance of the vertical striking location in a collision, the same two vessels are considered, i.e. the striking 40,000 DWT container vessel and the 105,400 DWT crude oil carrier described earlier. Again the collision is a right angle collision with zero speed of the struck double hull tanker. The striking container vessel has a velocity of 7 knots. The crude oil carrier is either fully loaded or in ballast, as these conditions are normal for tankers. The crude oil carrier has a displacement of 17,000 tons and a draught of 2.1 m in ballast. The calculations show that the largest penetration occurs, when the crude oil carrier is fully loaded and the container vessel is in ballast. This is partly a result of the external dynamics and partly because the striking vessel only touches the upper part of the struck vessel. Figure 5.15 shows the envelopes of maximum penetration at varying draught of striking vessel, the positions of bulb tip and bow tip are marked in the cross-section of the struck vessel. It is remarkable that the only situation, where the striking vessel does not penetrate the inner side of the struck ship is when both the crude oil carrier and the

container vessel are in ballast, which is not a normal situation for a container vessel. The large penetration is also remarkable, considering that the velocity, 7 knots, is close to the lowest manoeuvrable speed for the container vessel.

### 5.3.2 Sensitivity to the Design

Five studies on changing the design of the struck ship's side have been carried out. In all the analyses the absorbed energy is calculated from the start of the impact until the striking bow reaches the inner hull plating. This case corresponds to a penetration of 2.5 m. The absorbed energy is compared to the energy as if the design was unchanged.

Figures 5.16 and 5.17 show the energy ratio $E_{ratio} = \frac{E_{abs}^{new}}{E_{abs}^{unchanged}}$ versus the increase in plate thickness for side plating, stringer decks and frames. As it would be expected, the resistance of the side structure is improved by increasing thickness. From the figures it is seen that the energy absorption may be increased by 10-12 % by increasing the thickness of the structural parts by 30 % (ex. 15 mm to 19.5 mm).

The number of stringer decks is increased in steps from three to six. The three-deck-case is calculated twice, first where the decks are in their original location and then where the stringer deck locations are equally distributed between the inner bottom and the weather deck. The frame spacing is reduced in steps until 20 % of the original spacing. In Tables 5.3 and 5.4 it is seen that a decreasing spacing of frames or stringer decks is not always followed by an increase in energy absorption. When the spacing is reduced, the lengths of the plates at the side shell are also reduced, which may result in fracture for a smaller penetration. If the spacing is strongly decreased, which is followed by an increasing number of crushing elements (X or T) touched by the striking bow, the energy ratio is again increased.

Table 5.3: *Stringer deck spacing.*

| Number of decks | 3 (orig.) | 3 | 4 | 5 | 6 |
|---|---|---|---|---|---|
| Spacing | 4.05 / 4.86 | 4.675 | 3.74 | 3.12 | 2.67 |
| Energy ratio | 1 | 1.04 | 1.29 | 0.76 | 1.01 |

Table 5.4: *Frame spacing.*

| Spacing | 3.70 | 3.33 | 2.96 | 2.59 | 2.22 | 1.85 | 1.48 | 1.11 | 10.74 |
|---|---|---|---|---|---|---|---|---|---|
| Energy ratio | 1 | 0.97 | 0.95 | 0.92 | 0.89 | 0.84 | 0.77 | 0.98 | 1.13 |

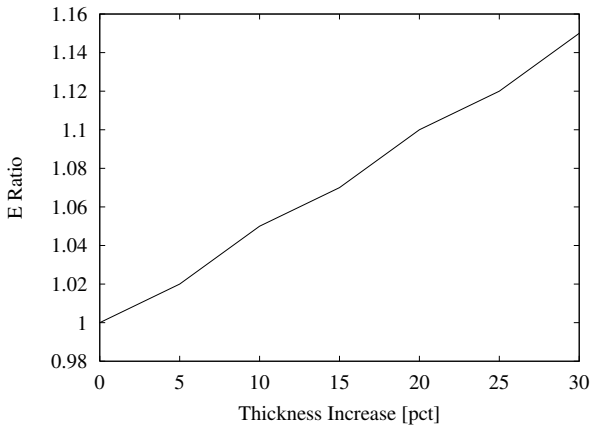


Figure 5.16: *Changing thickness of side shell.*

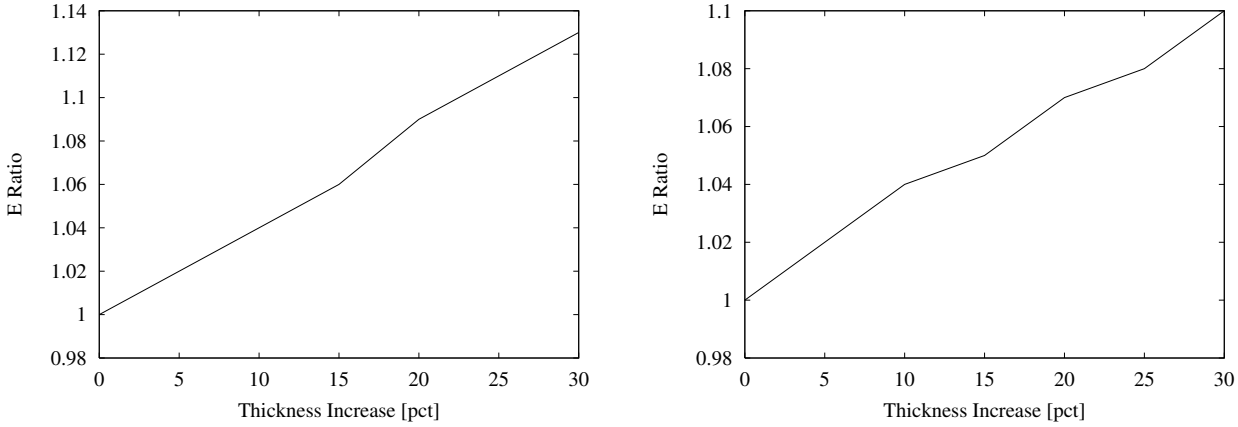


Figure 5.17: *Changing thickness of plates. Left: stringer decks. Right: frames.*

## 5.4 Reduction in Penetration Due to Bow Deformation

In this section a sensitivity analysis is carried out using a series of computer simulations of collisions involving 11 different ships in order to determine when the energy released for crushing is absorbed by the bow of the striking vessel or absorbed by the side structure of the struck vessel. Five different striking vessels are considered:

1. 150,000 DWT bulk carrier (L = 274 m)
2. 40,000 DWT container vessel (L = 212 m)
3. 3,000 DWT general cargo vessel (L = 78 m)
4. 2,000 DWT tanker (L = 69 m)
5. 500 DWT coaster (L = 41 m)

The main particulars and geometry parameters of these five vessels are given in Appendix A, Table A.1. The bow scantlings are found in Pedersen et al. (1993).

The present analysis is based on striking vessels with relatively strong bow structures. Since most ships have bulbous bows and since bulbous bows are known to exert high collision resistance, all the ships are analysed with bulbous bows. In order to obtain upper bounds for the local bow collision loads the scantlings given in Pedersen et al. (1993) were taken so that the vessels could obtain a Baltic ice class (DNV ice class 1B). To get sufficient ice strength the bulbous bows on all five vessels are designed with longitudinal stiffeners at decks, longitudinal bulkheads and outer shells. Ships without ice strengthening normally have a transverse stiffening system such as the bulk carrier bow described in Section 4.5.

Six different struck vessels are considered. The struck vessels are separated into two groups, tankers and Ro-Ro vessels. The tanker group consists of three vessels with lengths of 103 m, 198 m and 317 m, respectively. The vessel of 103 m is transversely stiffened, whereas the two other vessels are longitudinally stiffened. The main particulars and the most important structure are seen in Appendix A, Table A.6. The three Ro-Ro vessels are ships examined by Hysing (1995) and Scharrer (1996) in the Joint North-West European Research Project.

Main particulars for three Ro-Ro vessels:

| | | Ro-Ro 1 | Ro-Ro 2 | Ro-Ro 3 |
|---|---|---|---|---|
| Length | [m] | 58.0 | 150.0 | 180.0 |
| Breadth | [m] | 13.0 | 27.0 | 31.5 |
| Depth | [m] | 9.7 | 19.4 | 21.1 |
| Draught | [m] | 3.5 | 6.0 | 7.0 |
| Displacement | [t] | 1,600 | 15,800 | 27,000 |

The scantlings are found in reports by Scharrer (1996) and Hysing (1995). Also for this analysis the collision is a right angle collision, where the struck vessel has zero speed. The striking vessel has a velocity of 4.0 m/s. In all cases the striking position is the frame nearest midships of the struck vessel.

Main particulars for the three single hull tankers :

| | | Tanker 1 | Tanker 2 | Tanker 3 |
|---|---|---|---|---|
| Length | $[m]$ | 103.0 | 198.0 | 317.0 |
| Breadth | $[m]$ | 15.5 | 29.9 | 56.6 |
| Depth | $[m]$ | 6.9 | 14.9 | 31.5 |
| Draught | $[m]$ | 5.8 | 11.1 | 22.5 |
| Displacement | $[t]$ | 7,400 | 52,400 | 330,300 |

The scantlings for the three tankers are found in Appendix A, Table A.6.

Table 5.5 (left numbers) shows the penetration into the struck vessel, when the striking vessel is assumed to be rigid. The table proves to a great extent the effect of the external

dynamics, i.e. the penetration is increased when the struck vessel has a larger displacement, but there are exceptions. The penetration of the container vessel into the large tanker of 317 m is smaller than the penetration into the tanker of 198 m, which is due to the difference in height of the two tankers. The top of the large tanker will be crushed earlier than that of the medium tanker, which means that the struck vessel will absorb more energy. For the smaller vessels, i.e. the general cargo vessel, the tanker and the coaster impacting the smallest tanker, and the coaster impacting the smallest Ro-Ro vessel, the effect of a weak shell plate penetrated by slender vessels with only a few frames touched is seen. Table 5.5 (right numbers) shows the calculated penetration into the struck vessel, when the actual strength of the bow is considered. A large reduction in the penetration for the three smaller striking vessels is seen, whereas the bow of the ice-strengthened bulk carrier and the container vessel does not deform. The big reduction in penetration for the tanker striking the smallest Ro-Ro vessel is partly due to a relatively weak bow, where the forepart deforms before it penetrates rigidly into the side of the struck vessel, and partly due to the external dynamics. The same situation is seen for the coaster impacting the small Ro-Ro vessel.

Table 5.5: *Penetration into struck vessel. Left numbers: striking vessel rigid. Right numbers: actual penetration. *The bulk carrier penetrates the whole breadth of the vessel. Lower numbers: Non-dimensional penetration (%).*

| **Struck vessels** \ **Striking vessels** | Bulk carrier, L = 274 m<br>Δ = 174,850 t, B = 47.0 m | Container vessel, L=212 m<br>Δ = 54,000 t, B = 32.2 m | General cargo, L = 78 m<br>Δ = 4,594 t, B = 16.0 m | Tanker, L = 69 m<br>Δ = 3,016 t, B = 12.3 m | Coaster, L = 41 m<br>Δ = 886 t, B= 9.0 m |
|---|---|---|---|---|---|
| Tanker 1, L = 103 m<br>Δ = 7,400 t, B = 15.5 m | 4.56/4.56<br>29.4/29.4 | 7.87/7.87<br>50.8/50.8 | 4.30/4.30<br>27.7/27.7 | 3.03/2.83<br>19.5/18.3 | 1.63/0.10<br>10.5/0.6 |
| Tanker 2, L = 198 m<br>Δ = 52,400 t, B = 29.9 m | 16.10/16.10<br>53.8/53.8 | 19.31/19.31<br>64.6/64.6 | 2.30/1.30<br>7.7/4.3 | 1.50/0.30<br>5.0/1.0 | 0.70/0.20<br>2.3/0.7 |
| Tanker 3, L = 317 m<br>Δ = 330,300 t, B = 56.6 m | */*<br>100.0/100.0 | 10.98/10.98<br>19.4/19.4 | 3.50/1.70<br>6.2/3.0 | 2.10/0.10<br>3.7/0.2 | 0.80/0.10<br>1.4/0.2 |
| Ro-Ro 1, L = 58 m<br>Δ = 1,600 t, B = 13.0 m | 3.32/3.32<br>25.5/25.5 | 3.00/3.00<br>23.1/23.1 | 2.40/2.40<br>18.5/18.5 | 2.00/0.10<br>15.4/0.8 | 1.50/0.20<br>11.5/1.5 |
| Ro-Ro 2, L = 150 m<br>Δ = 15,800 t, B = 27.0 m | 8.60/8.60<br>31.9/31.9 | 7.40/7.40<br>27.4/27.4 | 3.60/2.80<br>13.3/10.4 | 2.10/1.80<br>7.8/6.7 | 1.00/0.50<br>3.7/1.9 |
| Ro-Ro 3, L = 180 m<br>Δ = 27,000 t, B = 31.5 m | 9.00/9.00<br>28.6/28.6 | 8.20/8.20<br>26.0/26.0 | 3.70/3.60<br>11.7/11.4 | 2.30/1.90<br>7.3/6.0 | 1.20/0.40<br>3.8/1.3 |

## 5.5 Minor Damages

Insurance company statistics shows that large sums are paid every year for repair of minor contact damages. Minor ship impacts may arise at sea during collision with floating objects or by contact with obstacles during manoeuvring in harbour areas.

When a ship collides with a floating object energy is released for structural deformation of the vessel. Floating objects can be cargo lost from other ships such as containers and barrels or nature-made objects as logs or floating ice bits. Loss of deck cargo may happen in bad weather due to insufficient lashing combined with large motion or green water on deck. The risk of colliding with a floating object depends on factors as the size and the geometrical form of the object. Weather conditions and traffic density will influence the possibility of detection of the object.

Most minor impacts occur during berthing manoeuvres in the harbour, or when the vessel is alongside or passing narrow canals or locks. During harbour manoeuvres the vessel is exposed to many forces, which may arise from own propulsion, mooring lines, wind, current, swell, etc. To avoid unintended contact, the control options available for the navigator during berthing of the vessel are e.g. rudder, thrusters, winches, anchors, and occasionally tug assistance. In such a complex situation it is not surprising that the frequency of severe impacts to a large extent depends on the experience and the education of the crew. Since impacts cannot be avoided, it is necessary to design ships so that a certain robustness of the hull structure is ensured.

The calculation of the external dynamics is based on a method developed by Pedersen and Zhang (1998), see Chapter 3. The method is developed for ship-ship collisions, but may as well be used for ship-object collisions and for vessels impacting a quay. When the energy released for structural deformation during the impact is known, the next step is to apply the internal mechanics analysis to prediction of the resulting structural deformation. Structural elements such as plates or beams may withstand a pressure above the limit for elastic deformation without unacceptably large permanent deformation after unloading. The permanent deformation, which may be accepted, depends on the design and the type of the vessel. Hughes (1981) has as a design criterion suggested that a permanent deformation of the plate thickness is acceptable for merchant ships. If the vessel has been exposed to larger deformation, ship repair may be required. As the velocity of a vessel is relatively small, dynamic effects can be neglected.

Two application examples will be presented. The first example deals with a fender system impact during a harbour manoeuvre. Contact forces and energy absorbed by the system during the manoeuvre are calculated, and the maximum safe berthing velocity for the vessel is estimated. Secondly a collision with a floating object will be illustrated by an example where an ice-strengthened bulk carrier impacts a small iceberg. The plastic deformation of the bow is given as a function of the mass of the iceberg and the velocity of the striking vessel. For both examples the energy absorbed by elastic deformation of the ship structure is negligible as in the rest of the study.

### 5.5.1 Application Example: Harbour Manoeuvre

The manoeuvre of berthing a vessel is so difficult that the frequency of accidents is very high. The increase in the size of vessels has made berthing manoeuvres even more difficult. Special problems are related to large vessels, which are not able to enter some harbours and therefore must berth in locations exposed to waves, swell and currents.

#### Berthing Velocities

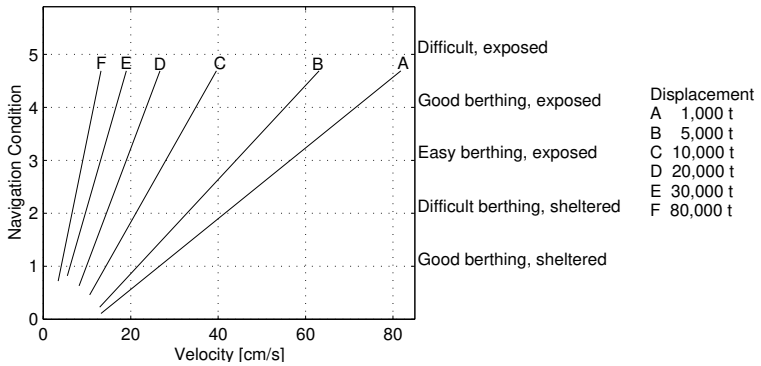


Figure 5.18: *Berthing velocity as a function of navigational conditions for tankers of various displacements, data from Pianc (1984).*

In the berthing procedure the vessel is moved slowly towards the quay by tugs, thrusters or mooring winches. During this procedure, the wind may push the vessel towards the quay with a speed above what is desirable, or a strong current may cause the vessel to drift in an undesirable direction. Berthing forces are a function of the vessel momentum and the berthing velocity, where the impact velocity depends on the navigational condition, the difficulties of berthing and the location of the quay. Figure 5.18 shows an empirical relation between navigational conditions and velocity for tankers of various displacements. The diagram is based on field data analysed by Pianc (1984).

#### The Fender System

The type and the size of a fender system in a specific harbour are mainly determined with respect to the following considerations:

- The fender system must be capable of absorbing the loss in kinetic energy during the procedure of berthing the vessel. If berthing the quay is difficult, the requirements of energy absorption are stricter, as the velocity of the vessel may be increased
- If only small movements of the vessel are allowed during the loading/discharging procedure, a fender with small deformation for large energy absorption is required
- The size of the reaction force and the contact area of the fender must be considered together with the design strength of the weakest part of the side shell

From these considerations it can be concluded that the design of a fender system is highly dependent on the vessels expected to berth at a particular quay.

**Berthing a Tanker of 150 m in Length**

| Main particulars of the vessel: | | | Scantlings: | | |
|---|---|---|---|---|---|
| Length ($L$) | 150.0 | m | Frame spacing | 3000 | mm |
| Breadth ($B$) | 23.4 | m | Plate thickness | 18 | mm |
| Draught ($T$) | 9.7 | m | Spacing between longitudinals | 600 | mm |
| Displacement ($\Delta$) | 27721 | t | Longitudinals | 180 x 80 x 12/12 | |
| | | | Yield strength | 235 | MPa |

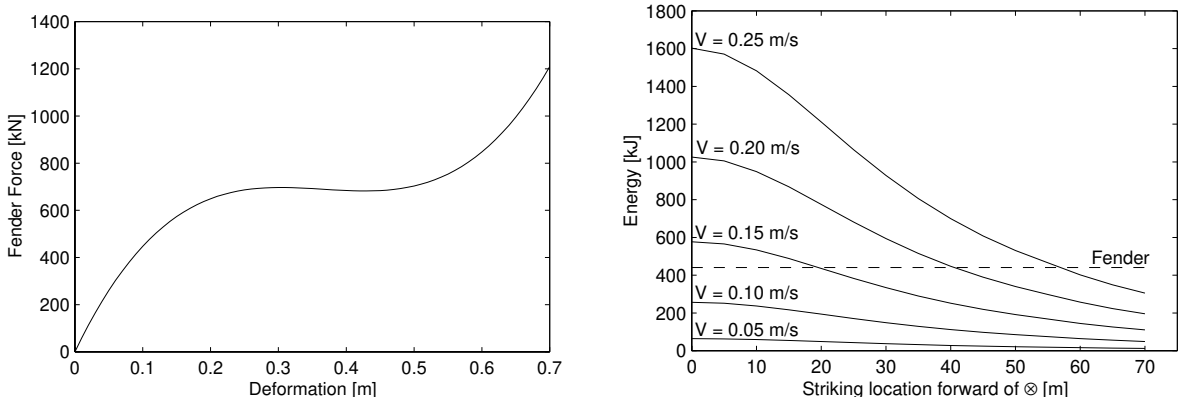


Figure 5.19: *Left: Deformation diagram for fender. Right: Energy to be absorbed by the fender as a function of the collision location forward of midship for various velocities.*

The added mass coefficients are assumed to be 0.05 for surge, 0.85 for sway and 0.21 for yaw motion. The coefficient of friction between the fender and the side of the vessel is taken to be 0.6. It is assumed that the vessel is berthed as parallel to the quay as possible, but that only one fender is in contact with the side of the vessel. The design berthing velocity for a tanker of approx. 30,000 t is of the size 0.1 to 0.2 m/s. (See Figure 5.18). The smallest velocity is for berthing at sheltered quays and good berthing, the largest velocity for difficult berthing at exposed quays.

The loss in kinetic energy or the energy to be absorbed by the fender as a function of the collision location forward of midship is shown in Figure 5.19. The velocity is taken to be 0.05 m/s to 0.15 m/s. It is assumed that the quay is equipped with a fender system of the buckling type (Derucher, 1983), the deformation diagram for this fender type is shown in Figure 5.19 (left).

According to Agerschou and Lundgren (1983), the design height and length of a fender are based on the size and the type of vessels, which will berth at a particular quay. For tankers of 10,000 to 100,000 DWT the ratio between the fender height and the longitudinal spacing should not be less than about two. For this example the smallest height is chosen. According to Agerschou and Lundgren (1983), this will give a length equal to the frame spacing. The

limit strength for the side shell is calculated and compared to the fender reaction force. The energy absorbed by the fender, before the force reaches the limit strength of the side shell, may now be calculated by integration.

The limit strength is calculated to be 1117 kN, which for the chosen fender system gives an energy absorption of 441 kJ for a travelled distance of 0.68 m. From Figure 5.19, where both the energy to be absorbed and the maximum allowable energy absorbed by the fender are shown, it is seen that at a berthing velocity of 0.13 m/s the fender can absorb all energy regardless of the striking location. A velocity of 0.13 m/s relates to a berthing condition referred to as easy berthing at exposed quays.

### 5.5.2 Application Example: Collision with a Floating Object

A collision between a vessel and a floating object will be illustrated by an example where a bulk carrier impacts a small iceberg.

The struck vessel is a 150,000 DWT bulk carrier of the high ice class (DNV ice class 1B). The scantlings are found in Pedersen et al. (1993).

The main particulars of the vessel are:

| | | |
|---|---|---|
| Length ($L$) | 274.0 | m |
| Breadth ($B$) | 47.0 | m |
| Draught ($T$) | 15.96 | m |
| Displacement ($\Delta$) | 174,850 | t |
| Service speed ($V$) | 15 | knots |

The floating object is in this example a cylindrical iceberg. The added mass coefficients for the cylinder are assumed to be one for both the surge and the sway motions, whereas the coefficient for yaw is zero. The radius of inertia may be taken to be $R = \frac{r}{\sqrt{2}}$, where $r$ is the cylinder radius. The object is assumed to be rigid, which means that the loss in kinetic energy during the collision must be transformed into deformation of the bow of the vessel. The density of ice and water is 920 $kg/m^3$ and 1025 $kg/m^3$ respectively, and the height above the water level of the iceberg or the cylinder is in all cases assumed to be 0.3 m, which means that the object can hardly be seen visually or by radar. The coefficient of friction between ice and steel can according to Bruun (1989) be taken to be 0.2.

The highest local loads will occur in a head-on collision. But it is not necessarily this situation, which will induce the highest stresses or cause damage, as the bow is the strongest part of the vessel. Higher stresses or larger damages may occur by glancing impacts on the side of the bow. Therefore, a situation like this is analysed for the side. The striking location is assumed to be 7 m aft of the forward perpendicular where the breadth of the vessel is 6 m. The form of the bow is such that the angle between the centre line and the side of the vessel is $15^o$. The bow region is longitudinally stiffened. The frame spacing is 3200 mm, the

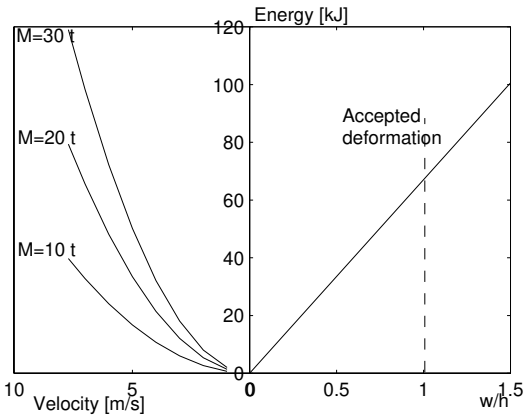


Figure 5.20: *Left: Energy to be absorbed as a function of the velocity of the bulk carrier for various masses of the iceberg. Right: Absorbed energy in the side shell versus the ratio between permanent deformation and plate thickness.*

plate thickness 33 mm and the longitudinal stiffeners are T-stiffeners (400 x 100 x 19/19) with a spacing of 600 mm. The yield strength of the steel is 315 MPa.

The energy absorbed due to crushing of the side shell as a function of the ratio between the permanent deformation and the plate thickness $w/h$ is shown in Figure 5.20, which also shows the loss in kinetic energy during the collision calculated by use of the external dynamics. It is assumed that the vessel has a velocity up to its service speed of 15 knots, and a permanent deformation of the size of the plate thickness is accepted. Figure 5.20 shows that a collision with an object of 10 t is acceptable without reducing the velocity of the vessel. If the velocity is reduced to 13 knots a collision with a 20 t object is acceptable.

# Chapter 6

# Probabilistic Analysis of Collision Damages, Monte Carlo Simulation

The probability of a damage can be found as

$$P[damage] = P[collision] \cdot P[damage|collision]$$

where $P[collision]$ is the probability of a collision and $P[damage|collision]$ the consequence prediction in the form of structural failure in case of a collision. The expression damage or structural failure can be defined in several ways. It may refer to the fracture of the side shell or the inner side shell, or a hole in the vessel of predefined dimensions.

The consequence of the collision $P[damage|collision]$ can be written as

$$P[damage|collision] = \sum_{V_A} \sum_{type} \sum_{L_B} \sum_{loading} \sum_{bow} \sum_{V_B} \sum_{x_c} \sum_{\beta}$$

$$P[damage|struck\ vessel, striking\ vessel, V_A, V_B, x_c, \beta] \cdot P[struck\ vessel] \cdot$$

$$P[V_A|struck\ vessel] \cdot P[type|striking\ vessel, route] \cdot P[L_B|striking\ vessel, route] \cdot$$

$$P[loading|striking\ vessel] \cdot P[bow\ shape|striking\ vessel] \cdot P[V_B|striking\ vessel] \cdot P[x_c] \cdot P[\beta]$$

The individual parameters in the expression can be described as

$P[damage|struck\ vessel, striking\ vessel, V_a, V_b, x_c, \beta]$ The probability of damage given struck vessel, striking vessel and a collision scenario, where the collision scenario involves the striking location, the collision angle and the velocity of both vessels

$P[struck\ vessel]$ The probability that the struck vessel is present (equal one)

$P[V_A|struck\ vessel]$ The probability of a specific velocity of the struck vessel, given the struck vessel

$P[type|striking\ vessel, route]$ The probability of a ship type of the striking vessel given a specific route or a predefined distribution of vessel

$P[L_B|striking\ vessel, route]$ The probability of a length of the striking vessel given a specific route or a predefined distribution of vessel

$P[loading|striking\ vessel]$ The probability of a specific loading condition given the striking vessel

$P[bow\ shape|striking\ vessel]$ The probability that the striking vessel is equipped with a conventional bow or a bulbous bow, given striking vessel

$P[V_B|striking\ vessel]$ The probability of a specific velocity of the striking vessel, given the striking vessel

$P[x_c]$ The probability of a specific striking location at the struck vessel

$P[\beta]$ The probability of a specific collision angle

The numerical simulation or the calculation method is built around the deterministic program calculating damage to struck vessel, see 5.1.1.

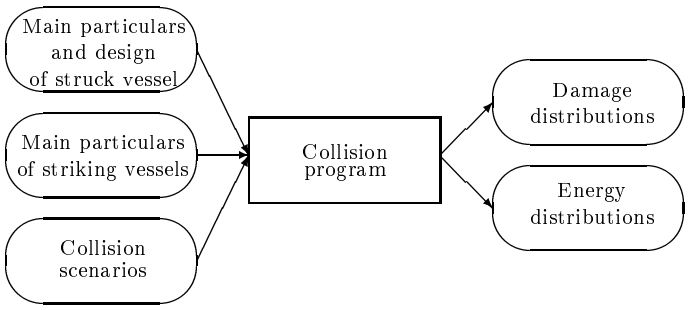


Figure 6.1: *Determination of energy released for crushing.*

When input is to be prepared for the above probabilistic calculation, it will ease the clearness, if the input parameters are arranged into three groups: a) the struck vessel, b) information about the striking vessels and c) a group dealing with the collision scenarios, see Figure 6.1.

The simulation program is the same as described in Section 5.1.1 regarding the external dynamics and the internal mechanics, but the calculation is now made for a series of collisions. In practice, these calculations are carried out by use of a Monte Carlo simulation, where many different choices of striking vessels and collision scenarios are considered to establish probability distributions for the damage to the struck vessel and for the energy released for

crushing. The simulation is stopped when 99.9 percent of the total energy is absorbed or the penetration into the struck vessel reaches the centre line of the struck vessel. For very few of the collisions, the side plating will deform but not fracture. These collisions can easily be separated from the analysis, but it is decided not to do so as the onset fracture depends much on the local collision point. If the point is e.g. near a frame the fracture may start in the initial collision phase, whereas the deformation before fracture may be larger if the point of contact is at the middle of two frames.

The analysis is for one particular struck vessel. The input parameters will here be the main particulars and the structural design. Input for this group will not be described further in this chapter, as it is described in Section 5.1.1.

The input for the striking vessels and for the collision scenarios differs from the deterministic analysis. Therefore, the input parameters for these groups will be described in more detail.

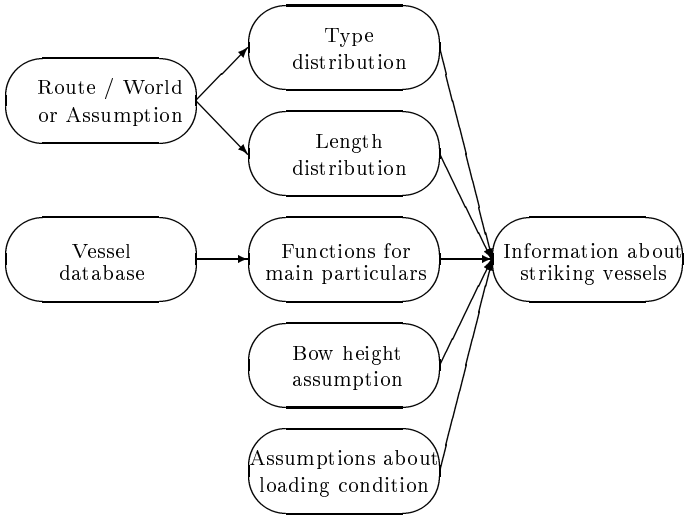


Figure 6.2: *Information flow for determination of striking vessels.*

Five different ship traffic patterns have been investigated, namely vessels in worldwide trade, the Straits of Dover and Gibraltar and the eastern and western routes through the Great Belt. The parameters describing the traffic are the distribution of ship types and the distribution of lengths within each type. A detailed description and analysis of the world fleet and the four different European shipping routes are given in Section 6.1.

Data from a database containing ship characteristics for the world fleet has been analysed to find relations for length versus breadth, draught, depth, displacement and service speed for each type of vessel, see Section 6.2.

In Section 6.3 proposals for distributions of striking vessel are given. If the type and the length of a vessel are known from the analyses in Sections 6.1 and 6.2 or from other assumptions, the rest of the main particulars can easily be determined by use of the information from Section 6.2, where functions for main particulars are estimated for given ship type and

length. The remaining input parameters such as bow heights and loading conditions are also discussed in this section. The information flow for determination of the striking vessels can be seen in Figure 6.2.

The results from the probabilistic analyses are shown in the last two sections in this chapter. First the damage distribution is given for 15 struck vessels of different types, sizes and structural designs. See also Lützen (2001). Then the distribution of energy to be absorbed in the struck vessel or the energy dissipation value calculated for vessels sailing in worldwide trade or on specific European traffic routes. See also Lützen and Rusaas (2001), Lützen and Pedersen (2000) and Lützen and Clausen (2000).

An overall view of the flow in the probabilistic approach to calculation of damages and energy released for crushing is given in Figure 6.3.

## 6.1 Shipping Routes

### Vessels in Worldwide Trade

A database containing ship characteristics for the world fleet has been purchased from LMIS (2000). The database consists of approx. 87,000 ships in service all over the world and is the complete database of all ships in service with an IMO number. The ships are divided into two main categories: a group of conventional merchant ships and a group of fishing vessels and specialised ships. The database has been analysed to derive distributions of ship types in the world fleet and to describe the distribution of lengths within each ship type.

It is decided to leave out of the study some types of vessels because their number is either very small or their movement patterns are atypical. The ship types left out are e.g. sailing vessels, twin-hull/hydrofoil ships, drilling vessels, tugs, ice-breakers, supply vessels and dredgers. Thus, the remaining vessels can be divided into ten fairly homogeneous groups:

1. Bulk carriers
2. Cargo vessels
3. Chemical tankers
4. Container vessels
5. Gas tankers
6. Passenger vessels
7. Reefer vessels
8. Ro-Ro vessels
9. Tankers
10 Fishing vessels

The distribution of ship types in the world fleet is shown in Figure 6.4.

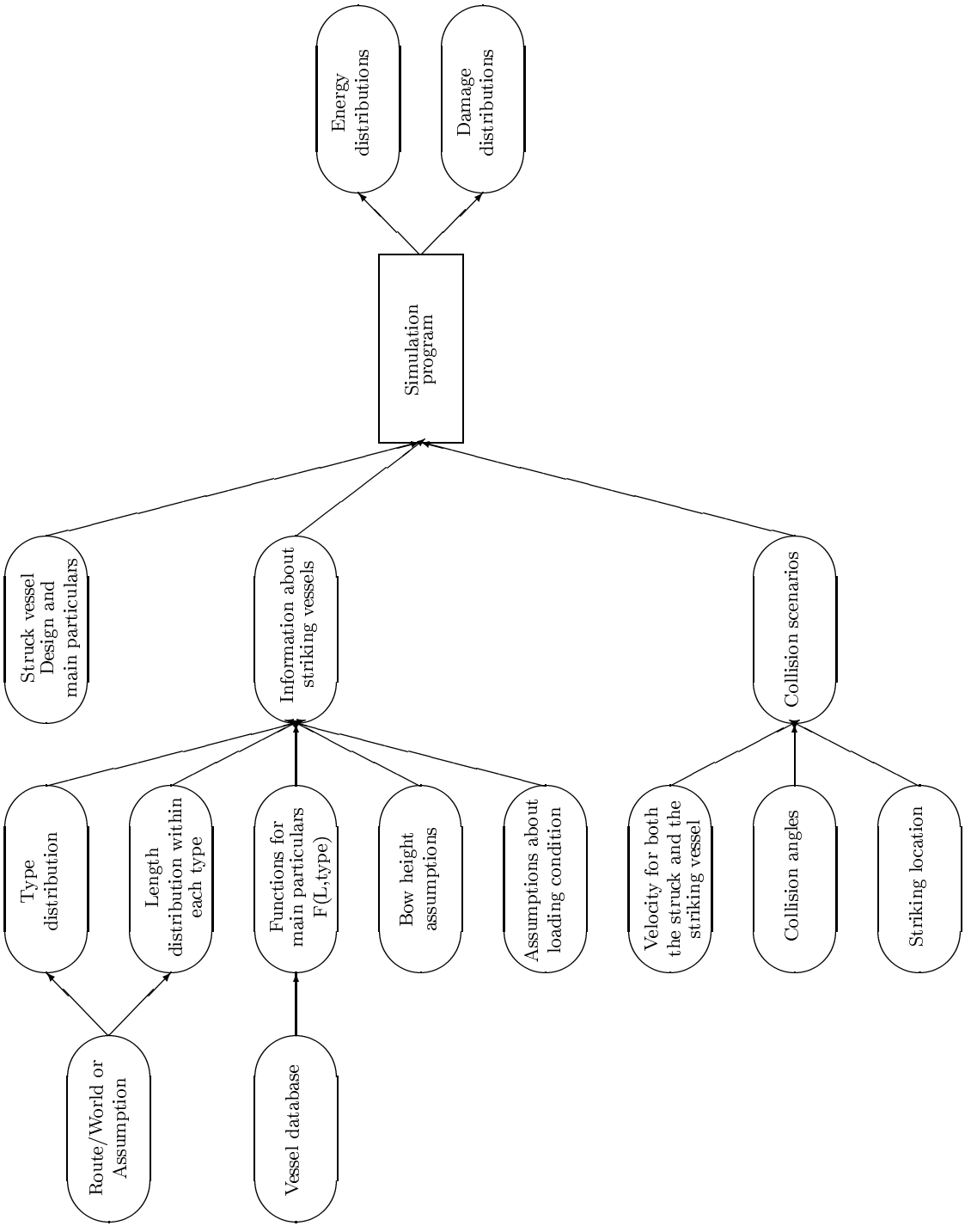


Figure 6.3: *Information flow for determination of distributions for damage and energy.*

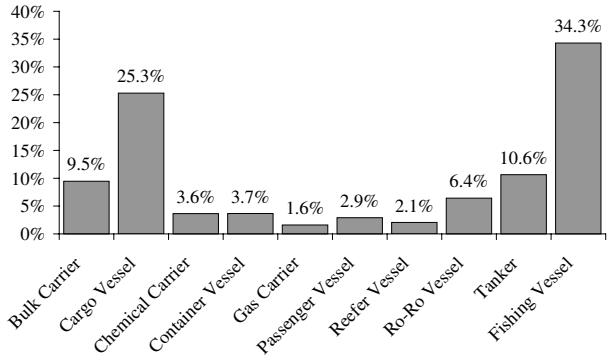


Figure 6.4: *Distribution of types in worldwide trade.*

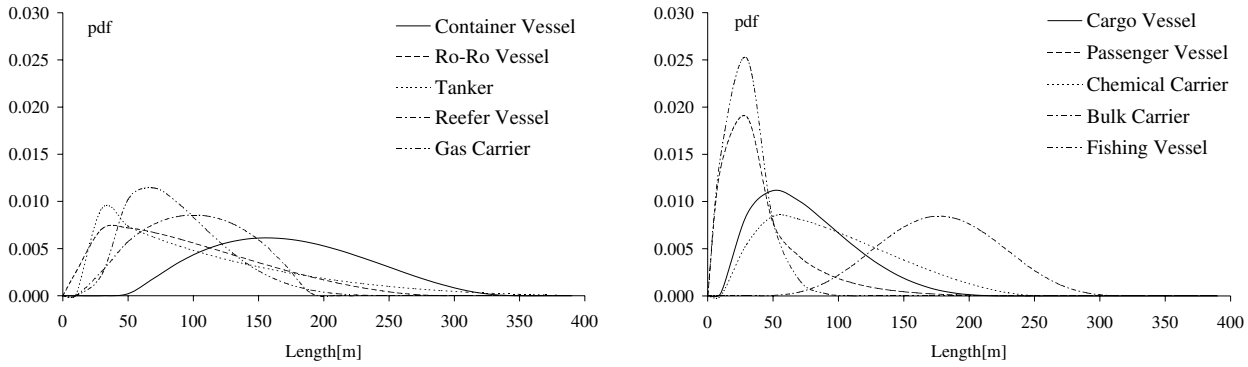


Figure 6.5: *Distribution of lengths for vessels in worldwide trade.*

The distribution of lengths for each ship type has been approximated by a beta probability function. The beta distribution is described by two parameters $\alpha$ and $\beta$ in a restricted interval $[L_{min};L_{max}]$:

$$f(x) = \frac{1}{(L_{max} - L_{min})^{\alpha+\beta-1} B(\alpha,\beta)} (x - L_{min})^{\alpha-1} (L_{max} - x)^{\beta-1}$$

where

$$B(\alpha,\beta) = \int_0^1 t^{\alpha-1}(1-t)^{\beta-1} dt$$

Subjects of the constraints: $\alpha > 0 \quad \beta \geq 0 \quad L_{min} \leq x \leq L_{max}$

Mean value: $\mu = L_{min} + (L_{max} - L_{min}) \dfrac{\alpha}{\alpha+\beta}$

Standard deviation: $\sigma = (L_{max} - L_{min}) \dfrac{\alpha}{\alpha+\beta} \sqrt{\dfrac{\beta}{\alpha(\alpha+\beta+1)}}$

Based on data fitting, numerical results for the parameters $\alpha$, $\beta$, $L_{min}$ and $L_{max}$ are given in Table 6.1 for each ship type in the world fleet. Furthermore, values for the mean value and the standard deviation are given. Diagrams for the resulting distributions for all types of vessels are shown in Figure 6.5.

Table 6.1: *Parameters defining the beta function for each type of vessel in worldwide trade.*

| Ship type | $\alpha$ | $\beta$ | $L_{min}$ [m] | $L_{max}$ [m] | $\mu$ [m] | $\sigma$ [m] |
|---|---|---|---|---|---|---|
| Bulk carrier | 6.0 | 6.3 | 20 | 343 | 178 | 44 |
| Cargo Vessel | 1.6 | 4.5 | 18 | 239 | 75 | 37 |
| Chemical Carrier | 1.2 | 2.8 | 24 | 254 | 95 | 47 |
| Container Vessel | 2.2 | 3.2 | 50 | 347 | 172 | 58 |
| Gas Carrier | 1.8 | 6.4 | 30 | 298 | 88 | 36 |
| Passenger Vessel | 1.4 | 15.8 | 17 | 316 | 41 | 19 |
| Reefer Vessel | 1.8 | 1.9 | 20 | 187 | 102 | 39 |
| Ro-Ro Vessel | 1.2 | 2.9 | 11 | 292 | 95 | 57 |
| Tanker | 1.3 | 5.1 | 20 | 458 | 109 | 65 |
| Fishing Vessel | 1.5 | 14.1 | 10 | 206 | 29 | 14 |
| Total Fleet | 1.4 | 10.0 | 10 | 458 | 65 | 42 |

### Specific European Shipping Routes

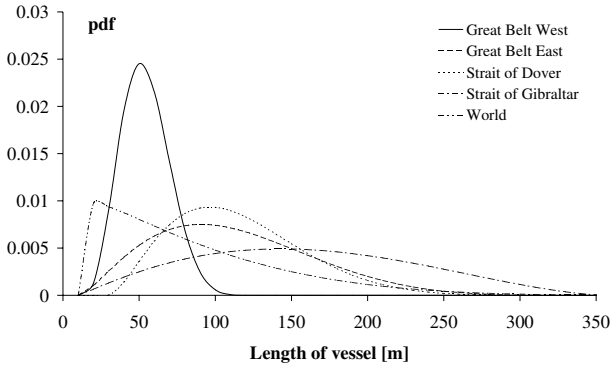


Figure 6.6: *Probability distribution function of ship's lengths for different routes, all types taken together.*

Vessels in four different routes, the Straits of Dover (LMIS (2000)) and Gibraltar (Dovre Safetec Ltd. (1996)) and the eastern and western routes through the Great Belt (MSR Consultants (1990)), have been investigated. The data for the Great Belt and the Strait of Gibraltar includes a large group of vessels specified as other vessels, they will in this report be handled as cargo vessels.

The distribution of ship types is shown in Table 6.2 and the probability distribution for lengths of all vessels taken together is shown in Figure 6.6.

Table 6.2: *Distribution of ship types (in percent) for vessels in worldwide trade and four different European shipping routes.*

| Ship type | Great Belt West | Great Belt East | Strait of Dover | Strait of Gibraltar | World |
|---|---|---|---|---|---|
| Bulk carrier | 0.0 | 11.8 | 10.6 | 17.4 | 9.5 |
| Cargo Vessel | 84.4 | 55.2 | 41.8 | 47.0 | 25.2 |
| Chemical Carrier | 1.4 | 3.4 | 10.2 | 6.0 | 3.6 |
| Container Vessel | 2.1 | 6.3 | 12.9 | 7.6 | 3.7 |
| Gas Carrier | 0.6 | 1.5 | 3.9 | 3.1 | 1.6 |
| Passenger Vessel | 0.0 | 0.0 | 0.4 | 0.6 | 2.9 |
| Reefer Vessel | 0.0 | 0.0 | 5.2 | 0.0 | 2.1 |
| Ro-Ro Vessel | 0.0 | 0.0 | 7.0 | 5.8 | 6.4 |
| Tanker | 11.5 | 21.8 | 7.8 | 12.4 | 10.6 |
| Fishing Vessel | 0.0 | 0.0 | 0.2 | 0.0 | 34.3 |

## 6.2 Ship Database - Finding Main Particulars

Data from the ship characteristics database described in Section 6.1 has been analysed to find simple linear relations for length versus other main particulars of each type of vessel.

Also a neural network is established. The network can be used as a design tool for preliminary estimation of main particulars of a ship. The main particulars for all types of vessels can be estimated if the loading capacity is known. The power of using a neural network as design tool is illustrated by two design examples.

A description of the distributions of ship types of striking vessels and lengths within each type for both vessels in worldwide trade and for vessels in specific European routes is given in Section 6.1.

### 6.2.1 Empirical Relations Defining the Main Particulars of Vessels

Data from the ship characteristics database (LMIS) has been analysed to find empirical relations for length versus breadth, draught, depth, displacement and service speed for each type of vessel.

**Estimation of Breadth, Draught, Depth and Speed**

The breadth, draught, depth and speed parameters are estimated as piecewise linear functions of the ship's length, $L$.

For $L_{min} < L \leq a \quad Parameter = b \cdot L + c$
For $a < L \leq L_{max} \quad Parameter = d \cdot L + e$

The parameter may be the breadth, $B$, the draught, $T$, the depth, $H$ and the speed, $V$. The constants $L_{min}$, $L_{max}$, $a$, $b$, $c$, $d$, and $e$ are defined in the Tables 6.3 to 6.5. The functions are optimised by use of a least squared error method.

Table 6.3: *$L_{min}$ and $L_{max}$ for all vessel types.*

| | Bulk carrier | Cargo vessel | Chemical carrier | Container vessel | Gas carrier | Passenger vessel | Reefer vessel | Ro-Ro vessel | Tanker | Fishing vessel |
|---|---|---|---|---|---|---|---|---|---|---|
| $L_{min}$ | 50.0 | 30.0 | 40.0 | 50.0 | 40.0 | 20.0 | 20.0 | 20.0 | 20.0 | 10.0 |
| $L_{max}$ | 350.0 | 250.0 | 250.0 | 350.0 | 300.0 | 325.0 | 175.0 | 300.0 | 450.0 | 200.0 |

Table 6.4: *Regression coefficients for breadth, draught, depth and speed functions.*

| | | Bulk carrier | Cargo vessel | Chemical carrier | Container vessel | Gas carrier |
|---|---|---|---|---|---|---|
| Breadth | a | 2.500E+02 | | | 2.0000E+02 | |
| | b | 1.2980E-01 | 1.2624E-01 | 1.5875E-01 | 1.3500E-01 | 1.4890E-01 |
| | c | 3.5000E+00 | 2.5205E+00 | | 3.3090E+00 | 1.1285E+00 |
| | d | 2.4780E-01 | | | 6.0000E-02 | |
| | e | -2.6000E+01 | | | 1.8309E+01 | |
| Draught | a | | | | 1.7500E+02 | 1.9000E+02 |
| | b | 5.6802E-02 | 5.4447E-02 | 6.0488E-02 | 5.7749E-02 | 5.9776E-02 |
| | c | 3.7748E-01 | 4.1417E-01 | 3.7832E-01 | | 1.2035E-01 |
| | d | | | | 2.5484E-02 | |
| | e | | | | 5.6465E+00 | 1.1478E+01 |
| Depth | a | | | | | |
| | b | 8.2350E-02 | 7.5784E-02 | 9.2575E-02 | 7.5074E-02 | 9.6915E-02 |
| | c | | 4.3451E-01 | -1.1233E+00 | 8.7679E-01 | -1.2610E+00 |
| | d | | | | | |
| | e | | | | | |
| Speed | a | 1.7500E02 | | 1.2500E+0.2 | 1.7500E+02 | 1.2500E+02 |
| | b | 3.5714E-02 | 5.1366E-02 | 5.0000E-02 | 6.5000E-02 | 5.5512E-02 |
| | c | 8.7500E+00 | 7.5553E+00 | 8.0000E+00 | 8.0000E+00 | 8.2239E+00 |
| | d | | | 1.0000E-02 | 4.0000E-02 | 2.3530E-02 |
| | e | 1.5000E+01 | | 1.3000E+01 | 1.2375E+01 | 1.2222E+01 |

Table 6.5: *Regression coefficients for breadth, draught, depth and speed functions.*

| | | Passenger vessel | Reefer vessel | Ro-Ro vessel | Tanker | Fishing vessel |
|---|---|---|---|---|---|---|
| Breadth | a | | | | | |
| | b | 1.1061E-01 | 1.2678E-01 | 1.2366E-01 | 1.6200E-01 | 1.1272E-01 |
| | c | 4.0980E+00 | 2.4045E+00 | 4.7894E+00 | -3.4600E-01 | 3.7327E+00 |
| | d | | | | | |
| | e | | | | | |
| Draught | a | | | | | |
| | b | 3.1369E-02 | 5.3084E-02 | 4.1820E-02 | 5.8702E-02 | 4.2759E-02 |
| | c | 9-1779E-01 | 7.0971E-01 | 4.5817E-01 | 2.0258E-01 | 1.6595E+00 |
| | d | | | | | |
| | e | | | | | |
| Depth | a | | | | | |
| | b | 6.6372E-02 | 8.4033E-02 | 8.8445E-02 | 8.7197E-02 | 5.7808E-02 |
| | c | 6.1000E-01 | | -6.0103E-01 | -9.1950E-01 | 1.6138E+00 |
| | d | | | | | |
| | e | | | | | |
| Speed | a | 1.5000E+02 | | 1.2500E+02 | 1.7000E+02 | 7.5000E+01 |
| | b | 7.0000E-02 | 9.0369E-02 | 1.0000E-01 | 4.1176E-02 | 8.2885E-02 |
| | c | 9.0000E+00 | 6.1217E+00 | 6.2000E+00 | 8.0000E+00 | 8.0000E+00 |
| | d | 1.6667E-02 | | | | 2.3630E-02 |
| | e | 1.7000E+01 | | 1.8700E+01 | 1.5000E+01 | 1.2444E+01 |

### 6.2.2 Using a Neural Network to Define the Main Particulars of Vessels

Neural networks are designed to learn the relations between inputs and outputs. Once the network has been trained, it can be used to predict the output parameters related to chosen input parameter(s), and thus a properly trained neural network can be used for generalisation/interpolation.

A feedforward neural network consists of a number of layers each transferring the weighted sum of its inputs to the next layer through transfer functions. Along with the weighted sum, a constant, also called bias, enters into the transfer function, see Figure 6.7. Each layer may have several inputs and outputs, and all but the first layer use the output from another layer as input. The weights and biases are found in the learning phase, where an optimisation procedure using the program MATLAB (Demuth and Beale (1998)) minimises the output error, given known inputs and outputs.

**Neural Network Topology**

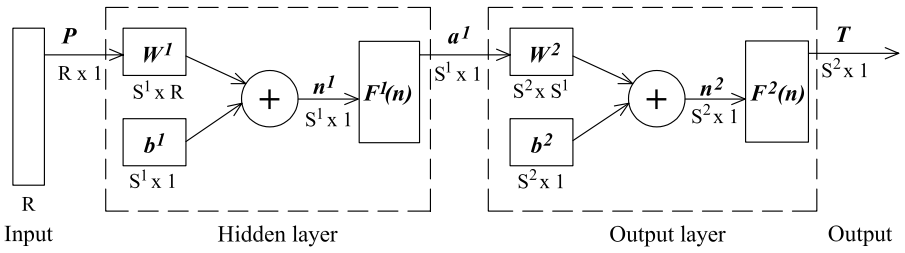


Figure 6.7: *Structure of a neural network.*

Normally, networks with biases, sigmoid layers and a linear output layer can approximate any continuous function to an arbitrary accuracy. A network of this type is therefore chosen for this work. More specifically, the network used is a two-layer feedforward net with an input vector, one hidden layer, an output layer and an output vector. See Figure 6.7. The input vector is $\boldsymbol{P}$ and has the dimension $R$. Each of the two layers consist of $S^x$ neurons or outputs, where $x$ refers to the layer number. The input vector for each layer is connected to the neurons through a weight matrix, $\boldsymbol{W^x}$. This weighted input is summed by the biases, $\boldsymbol{b^x}$, to yield the input, $\boldsymbol{n^x}$, for the transfer functions, $\boldsymbol{F^x}$.

Thus, the outputs from the hidden layer are

$$\boldsymbol{a^1} = \boldsymbol{F^1}\left(\boldsymbol{W^1} \cdot \boldsymbol{P} + \boldsymbol{b^1}\right) \tag{6.1}$$

where the transfer function is chosen to be the sigmoid function:

$$F^1(n) = \frac{1}{1 + e^{-n}} \tag{6.2}$$

The output $\mathbf{a^1}$ is a vector of the length $S^1$.

The output layer can in a similar way be expressed as

$$\begin{aligned} \boldsymbol{T} &= \boldsymbol{F^2}\left(\boldsymbol{W^2}\cdot\boldsymbol{a^1}+\mathbf{b^2}\right) \\ &= \boldsymbol{F^2}\left(\boldsymbol{W^2}\cdot\boldsymbol{F^1}\left(\boldsymbol{W^1}\cdot\boldsymbol{p}+\boldsymbol{b^1}\right)+\boldsymbol{b^2}\right) \end{aligned} \tag{6.3}$$

using the linear transfer function

$$F^2(n) = n$$

The data is normalised to assume values in the range [-1,1] to improve the learning convergence. Each of the parameters are normalised by use of

$$\text{Normalised value} = \frac{2\cdot(\text{Real Value - Min. Value})}{\text{Max. Value - Min. Value}} - 1$$

The outputs from the network are returned through an equivalent postprocess to obtain real output values.

The network is trained by use of Bayesian regularisation (Foresee and Hagen (1997), MacKay (1992)). This is a backpropagation method, which updates the weight and bias values according to the Levenberg-Marquardt optimisation. It minimises a combination of squared errors and weights and determines the correct combination to produce a network which generalises well.

**Single-Input Example**

In the following, a neural network is used to predict the main particulars of container vessels. When the prediction is made on the basis of just one input parameter, this must in some sense be the governing one, in this case the TEU capacity. Relations are found for length, $L$, breadth, $B$, velocity, $V$, draught, $D$, depth, $H$, and displacement, $\Delta$.

A network structure as shown in Figure 6.7 is used. It is found that the output of the network agrees well with the given data, i.e. no over-fitting when the number of nodes or neurons in the hidden layer is three ($S^1 = 3$). As only one input is given ($R$=1), the number of neurons in the output layer must be six ($S^2 = 6$), one for each output. With one hidden layer and one output layer, the weights, biases and normalisation can be described by two (bias) vectors and four (normalisation and weight) matrices.

The loading capacity (TEU) is assigned to the input, $\boldsymbol{P}$, and the output vector, $\boldsymbol{T}$, is

$$\mathbf{T} = \begin{pmatrix} \text{Length} & (L) \\ \text{Breadth} & (B) \\ \text{Speed} & (V) \\ \text{Draught} & (D) \\ \text{Depth} & (H) \\ \text{Displacement} & (\Delta) \end{pmatrix}$$

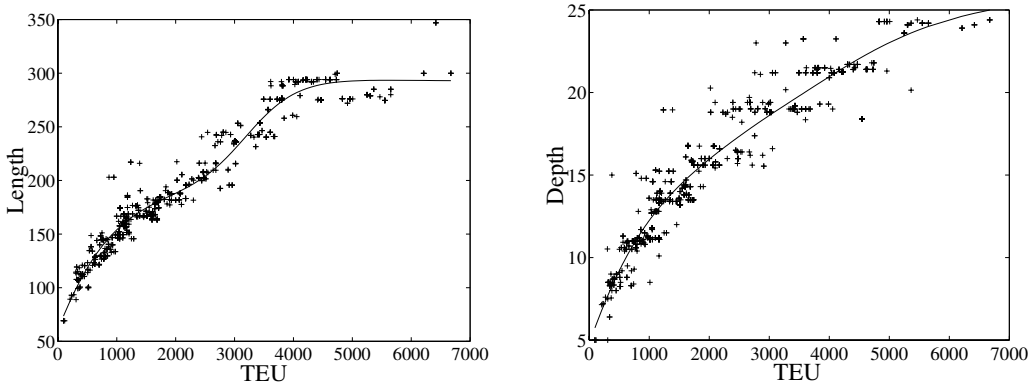


Figure 6.8: *Design parameters for container vessels, neural network.*

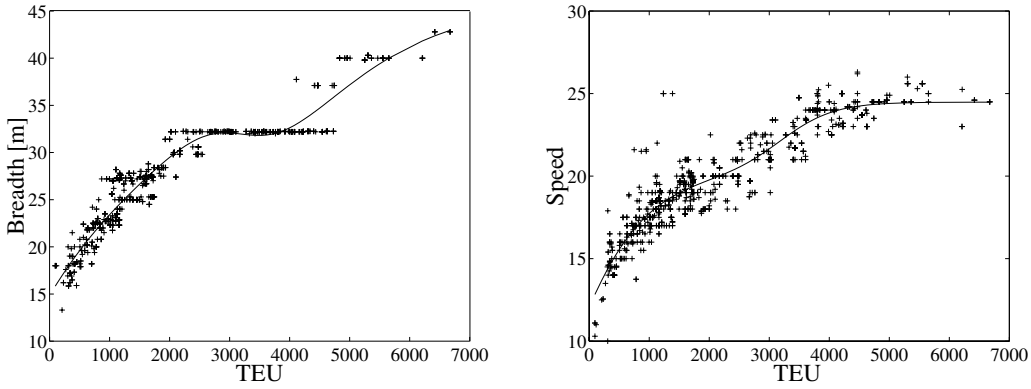


Figure 6.9: *Design parameters for container vessels, neural network.*

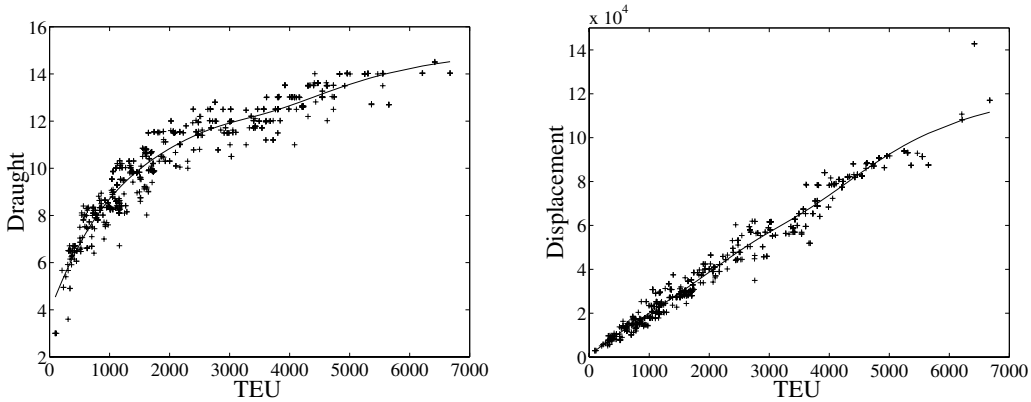


Figure 6.10: *Design parameters for container vessels, neural network.*

The normalisation matrices for the input $P$ and the output $\boldsymbol{T}$ are

| Input $P[min\ max]$ | Output $\boldsymbol{T}[min\ max]$ |
|---|---|
| $\begin{bmatrix} 95 & 6673 \end{bmatrix}$ | $\begin{bmatrix} 69.2 & 347.0 \\ 13.3 & 42.8 \\ 10.0 & 26.3 \\ 3.0 & 14.5 \\ 5.0 & 24.4 \\ 295.5 & 142800 \end{bmatrix}$ |

The weight matrices and bias vectors are

| Hidden layer | | Output layer | |
|---|---|---|---|
| Weight, $\boldsymbol{W^1}$ | Bias, $\boldsymbol{b^1}$ | Weight, $\boldsymbol{W^2}$ | Bias, $\boldsymbol{b^2}$ |
| $\begin{bmatrix} 2.52475 \\ 7.36627 \\ 4.93392 \end{bmatrix}$ | $\begin{pmatrix} 0.08000 \\ 0.40853 \\ 5.86986 \end{pmatrix}$ | $\begin{bmatrix} -0.08923 & 0.79895 & 3.03311 \\ 2.87692 & -1.09129 & 1.68256 \\ -0.01008 & 0.54992 & 3.15126 \\ 1.18918 & -0.23417 & 3.38025 \\ 1.42872 & -0.08277 & 3.01379 \\ 1.94908 & -0.27382 & 0.59050 \end{bmatrix}$ | $\begin{pmatrix} -3.13720 \\ -2.26198 \\ -2.91564 \\ -3.25505 \\ -3.20148 \\ -1.57929 \end{pmatrix}$ |

The values predicted by the neural network are shown in Figures 6.8 - 6.10 where also the data from the database is shown. The vectors and matrices for other types of ships are presented in Appendix C.

The neural network described in this section is compared to different other methods for prediction of main particulars for preliminary ship design, see Clausen et al. (2001a) and Clausen et al. (2001b).

**Multiple Input**

For multiple inputs, a designated neural network has to be learned for given inputs and outputs. The ability of the networks to use multiple inputs is demonstrated by the examples below.

The main particulars of a 4100 TEU container vessel shall be estimated. The neural network predicts the following main particulars: ($L$, $B$, $V$, $D$, $H$, $\Delta$) = (283.0 m, 33.0 m, 23.9 knt, 12.7 m, 21.2 m, 75,729 t). It is further specified that the ship must not exceed the maximum dimensions of the Panama Canal ($L \leq 294.2, B \leq 32.2, D \leq 13.4$) m. The Panmax requirements are not fulfilled by the estimates produced by the single-input neural network as the breadth is too wide, so a network with TEU and breadth as input is trained. In this network, a fixed breadth of 32.2 m and a TEU capacity of 4100 are pre-defined and the following main particulars are estimated: ($L$, $V$, $D$, $H$, $\Delta$) = (281.1 m, 24.0 knt, 12.8 m, 20.8 m, 78,347 t).

As another example, a smaller container vessel having a capacity of 1000 TEU is considered. The neural network predicts the following main particulars: ($L$, $B$, $V$, $D$, $H$, $\Delta$) = (154.0 m, 23.4 m, 17.7 knt, 8.7 m, 12.2 m, 19,993 t). By further requiring that the draught is limited to 8.5 m, a neural network with capacity and draught as input is trained where the draught

input is set to 8.5 m. The predicted parameters are: ($L$, $V$, $D$, $H$, $\Delta$) = (152.7 m, 23.3 m, 17.6 knt, 12.1 m, 19,684 t). Additionally, it is required that the ship in question should have a service speed of minimum 18 knots. By training a neural network with known capacity, draught and velocity the remaining parameters will be ($L$, $B$, $H$, $\Delta$) = (151.6 m, 23.3 m, 12.1 m, 19,722 t).

## 6.3 Proposals for Distribution of Striking Vessels

For the final description of the striking vessels, the distribution of ship types and lengths must be known for the considered shipping area. When the length and the type of a vessel are given the remaining main particulars are easily estimated by the linear regression or the neural network described in Section 6.2. Not only must the length and type distribution be known, also the bow height and the loading condition must be considered. Analyses of these parameters are given in this section.

In the length and ship type analysis in this section reference will be made to a damage database handled in Section 7.1.

**Length and Type Distribution**

The database from LMIS (2000), see Section 6.1, has been used as a basis for description of the distribution of lengths and ship types of striking vessels. Two different proposals will be given here. For both studies all fishing vessels are left out. Even though these vessels are normally sailing in restricted and trafficked waters their velocities are slow and manoeuvres atypical, which in most cases will make them the struck vessel. The differences between the two proposals can be summarised as:

Analysis 1,. Striking vessels with a length greater than 50 m
In analysis 1 all vessels of a length below 50 m are left out, which gives the final number of vessels of approx. 41,000. The percentage distributions of types of striking vessels and lengths of all the included vessels are shown in Figure 6.11.

Analysis 2. Relation between struck and striking vessels
Vessels of all lengths are included in the analysis. The relation between the lengths of the struck and the striking vessels is examined using the damage database described in detail in Section 7.1. The length of the struck vessel versus the length of the striking vessel is shown in Figure 6.12 (left). The figure shows a wide scatter, but also a tendency towards that small vessels are struck by other small vessels and larger vessels by larger vessels is observed. If the lengths of the struck vessels are separated into three intervals, $L \leq 100, 100 < L \leq 160$ and $L > 160$, the tendency is clearer, see Figure 6.12 right. In Figure 6.13 the distribution of the length of the striking vessel is shown for a given length interval of the struck vessel.

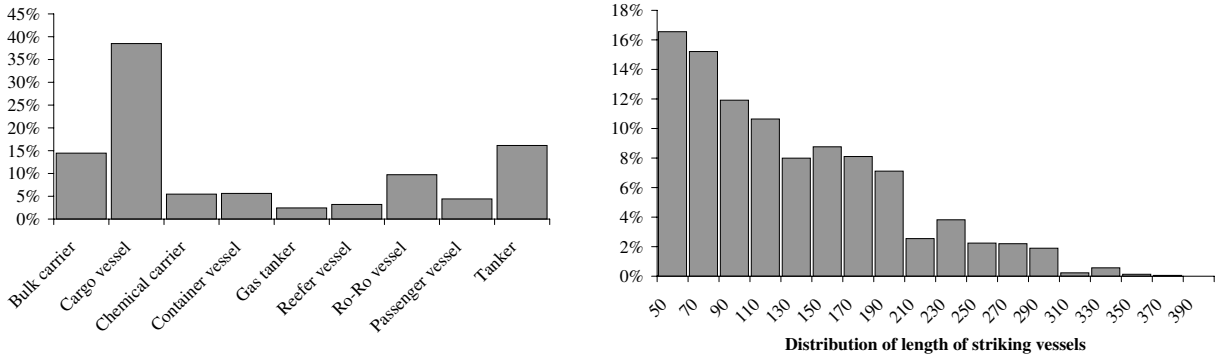


Figure 6.11: *Left: Percentage distribution of ship types. Right: Percentage distribution of lengths of all vessels.*

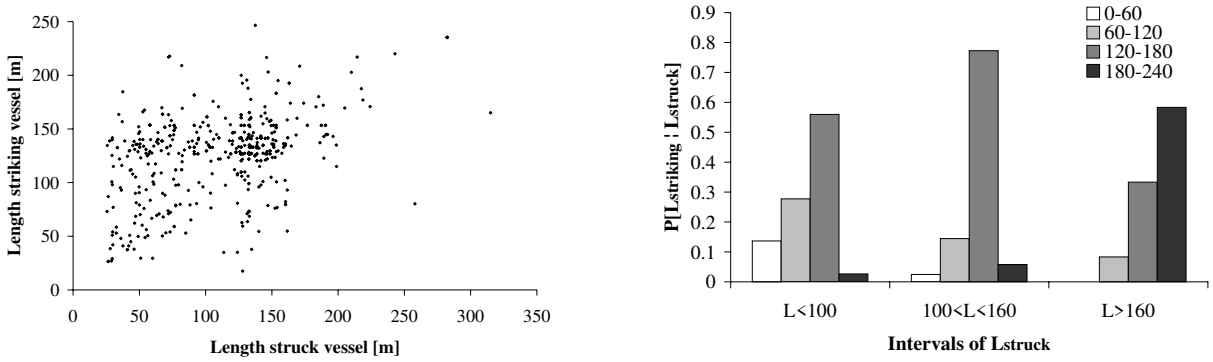


Figure 6.12: *Left: Relation between length of struck and striking vessels. Right: The distribution of the length of the striking vessel is shown for a given length of the struck vessel.*

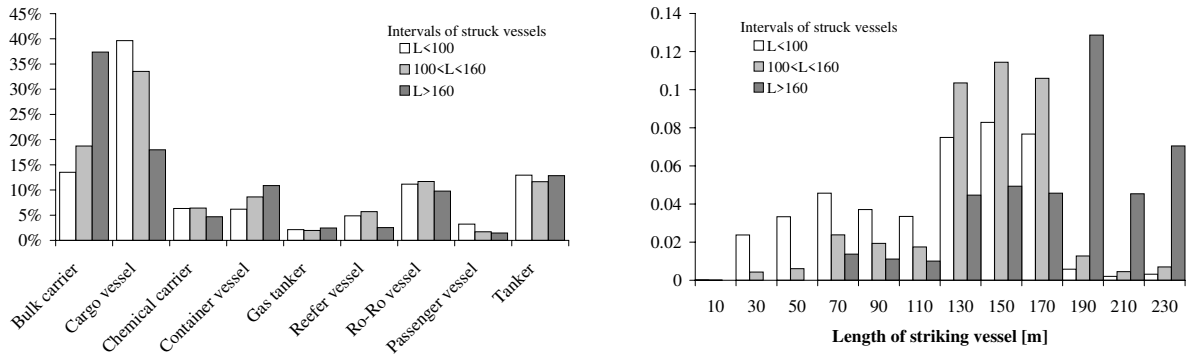


Figure 6.13: *Left: Percentage distribution of ship types for the three intervals of struck ship lengths. Right: Distribution of lengths of all types of vessels for the three intervals of struck ship's lengths.*

**Bow heights**

Unfortunately, the database (LMIS) contains no information about bow heights, but it is here assumed that half of the world fleet of large ships has a raised forecastles deck with an average height of 3m, see Herbert Engineering (2001). This is modelled by adding an equivalent height of 1.5m to the depth of all vessels.

Another proposal for the bow heights could be to add 3m to all vessels commonly designed with forecastle, but disregard it for all vessels commonly not built with forecastle.

**Loading Condition**

Information about the loading condition of the striking vessel is not available in the database. Therefore some assumptions have been made. Three different loading conditions have been defined, fully loaded, partially loaded and a ballast condition. The draughts for these loading conditions are:

- Full load:
  Maximum load line draught $T_{max}$
- Ballast:
  The ballast draught for all vessels is taken to be the minimum operational draught specified by MARPOL $T_{min} = 2.0m + 0.025 \cdot L$, where $L$ is the length of the striking vessel
- Partial draught:
  $T_{part} = T_{min} + 0.6(T_{max} - T_{min})$

The assumptions for the distribution between the different draughts for specific ship types are:

| | Full | Partly | Ballast |
|---|---|---|---|
| Tankers, bulk carriers | 50% | 0% | 50% |
| Cargo vessels, reefer vessels | 40% | 40% | 20% |
| Ro-Ro vessels, container vessels | 75% | 25% | 0% |
| Passenger vessels | 100% | 0% | 0% |

Furthermore, the vessel is assumed to have no trim.

## 6.4 Probability Distributions Describing the Collision Scenarios

Four distributions must be established for description of the collision scenarios. The striking location on the struck vessel, the velocity of both the struck and the striking vessel and finally the collision angle between the two vessels.

In this section reference will be made to a damage database handled in Section 7.1.

**Striking Location**
As the non-dimensional longitudinal damage location cannot be determined by simulation, the damage database or another assumption must be used to establish the probability density function.

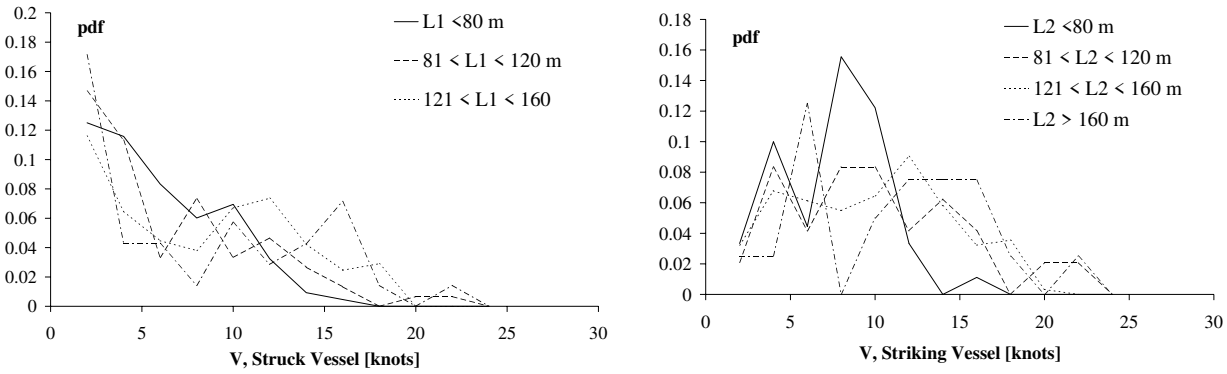


Figure 6.14: *Probability density functions for velocity of struck and striking vessel, struck vessel to the left, striking vessel to the right.*

**Velocity of Struck and Striking Vessel**
Figure 6.14 shows the probability density function (pdf) for the velocity of the struck and the striking vessel. All the data is taken from the damage database described in more detail in Section 7.1. It has been found that the velocity of the struck vessel can be approximated by a triangular distribution with a most likely value equal to zero speed. The probability density function for the velocity of the striking vessel is also given for various lengths of vessels. The pdf for the velocity is here modelled by a uniform distribution for velocities between zero and 75% of the service speed, then triangularly decreasing to zero for the service speed of the vessel.

**Collision Angle**
The collision angle is assumed to be uniformly distributed between $10^o$ and $170^o$. For a given route the collision angle may be taken to be triangular with a most likely value equal to a crossing angle between the two routes.

## 6.5 Probabilistic Simulation Analysis

The numerical Monte Carlo based simulation described earlier in this chapter will be used to analyse the damage to the struck vessels. Fifteen different struck vessels have been analysed, the main particulars of these vessels are given in Section 6.5.1. The distribution of striking vessels and collision scenarios has been described in Sections 6.3 and 6.4.

The analysis is separated into two different cases. The first case includes striking vessels of a length greater than 50 m (analysis 1), whereas the second case concerns all lengths of striking vessels but includes a relation between the struck and the striking vessel (analysis 2), see Section 6.3.

The outcome of the analysis is here the non-dimensional damage length, the non-dimensional penetration and the relation between these two parameters. A comparison of damages to dry cargo vessels and tankers is also included in analysis 1.

The damage calculations are performed in three positions along the length of the vessel; these non-dimensional striking positions are 0.25, 0.50 and 0.75. All damage results are given in output files as functions of these positions. For the analyses in this section it is assumed that the striking location is uniformly distributed along the length of the struck vessel and that the structure is the same in all three positions.

### 6.5.1 Struck Vessels

The numerical simulation will be carried out for the struck vessels defined in this section. The vessels are of different types and sizes.

| | | | |
|---|---|---|---|
| **CC** | Car carrier | **GC** | General cargo |
| **COC** | Crude oil carrier | **PCLS** | Passenger cruse liner |
| **DCBC** | Dry cargo, bulk carrier | **PRR** | Passenger Ro-Ro |
| **DCCS** | Dry cargo, container ship | **PC** | Product carrier, chemical carrier |
| **DCRR** | Dry cargo, Ro-Ro | **CT** | Chemical carrier |

| Type | No. | Displacement | Length | Depth | Breadth | Draught | Velocity | Double hull |
|---|---|---|---|---|---|---|---|---|
| CC | 01 | 32,775 | 190 | 32.6 | 32.3 | 9.0 | 20.0 | |
| COC | 01 | 111,000 | 234 | 21.0 | 42.0 | 13.6 | 14.5 | X |
| DCBC | 01 | 72,700 | 216 | 19.1 | 32.2 | 12.2 | 15.0 | |
| DCCS | 02 | 73,700 | 285 | 21.5 | 32.2 | 12.2 | 25.0 | X |
| DCCS | 03 | 28,430 | 180 | 15.2 | 27.8 | 8.3 | 19.0 | X |
| DSRR | 01 | 11,000 | 111 | 14.5 | 21.0 | 6.7 | 14.5 | |
| GC | 01 | 5,270 | 85 | 7.2 | 13.6 | 5.7 | 12.2 | X |
| PCLS | 01 | 39,300 | 237 | 21.8 | 32.2 | 7.6 | 22.0 | |
| PRR | 01 | 17,300 | 170 | 23.6 | 27.8 | 6.3 | 21.0 | |
| PRR | 02 | 17,300 | 176 | 20.0 | 25.0 | 6.4 | 26.6 | |
| PRR | 03 | 2,012 | 65 | 12.4 | 14.8 | 3.2 | 14.5 | |
| PC | 01 | 32,775 | 175 | 17.6 | 27.4 | 9.8 | 15.0 | X |
| PC | 02 | 30,000 | 158 | 15.6 | 27.4 | 10.5 | 15.0 | |
| CT | 01 | 3,145 | 78 | 6.6 | 13.5 | 5.5 | 11.5 | X |
| COC | 02 | 301,580 | 328 | 30.4 | 56.4 | 21.8 | 15.0 | X |

### 6.5.2 Results from Simulation, Analysis 1, Striking Vessels Longer than 50 m

**The non-dimensional damage length, $\overline{y} = \frac{y}{L}$**
For all analysed vessels the probability density distribution and the cumulative density distribution for the non-dimensional damage length are shown in Figure 6.15. All analyses show the same tendency of many small damage lengths but the figures also show a large variation in the mean value and a large deviation for the different struck vessels.

Figure 6.16 displays the 25-, 50- and 75-percentile values for the non-dimensional damage length versus the length of the struck vessel. Regression lines for the three percentile values are also seen. The figure shows that the non-dimensional damage length is not independent of the length of the struck vessel. A decrease is observed for increasing length of the struck vessel, the decrease is most distinct for the 75-percentile value, less for the 25-percentile value.

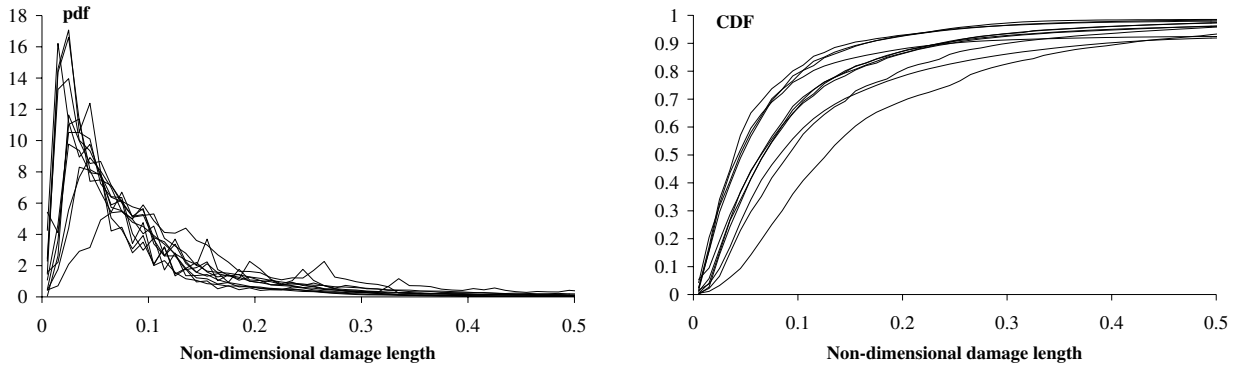


Figure 6.15: *Left: The probability density distribution for the non-dimensional damage length, $\overline{y}$. Right: The cumulative density distribution for the non-dimensional damage length. All analysed vessels are shown in the diagrams.*

The non-dimensional damage lengths for the three striking locations are depicted in Figure 6.17. The diagram shows the 50-percentile value for the non-dimensional damage length. The vessels in the diagrams are sorted by increasing length. For larger vessels the non-dimensional damage length seems nearly independent of the striking location, but for smaller vessels a difference in the damage length for the three positions is seen, which is due to the external dynamics.

**The Non-Dimensional Penetration, $\overline{z} = \frac{z}{B}$**
For all analysed vessels the probability density distribution and the cumulative density distribution for the non-dimensional penetration are seen in Figure 6.18. All analyses show the same tendency of many small penetrations but the figures also show that there is a large variation in the mean value for the different struck vessels.

Figure 6.19 presents the 25-, 50- and 75-percentile values for the non-dimensional penetration versus the length (left) and versus the breadth (right) of the struck vessel. Regression lines

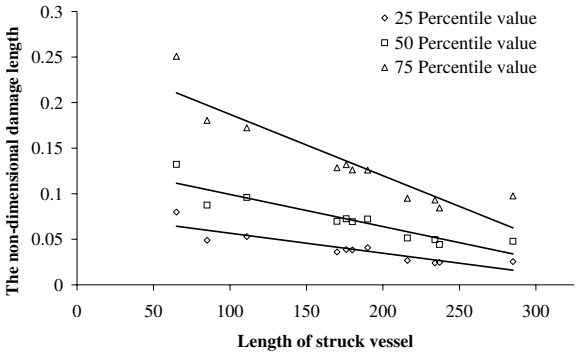


Figure 6.16: *The 25-, 50- and 75-percentile values for the non-dimensional damage length, $\overline{y}$, versus the length, $L$, of the struck vessel. Regression lines for the three percentile values are shown.*

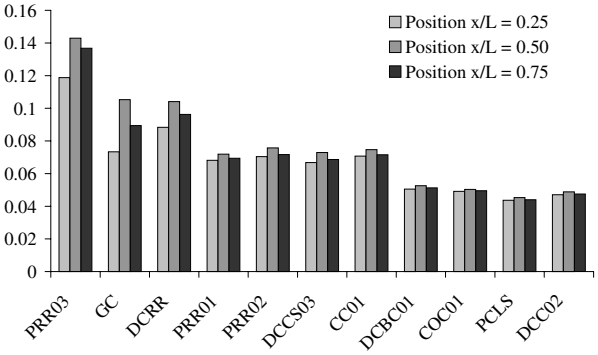


Figure 6.17: *The 50- percentile value for the non-dimensional damage length, $\overline{y}$, for the three striking locations 0.25, 0.50 and 0.75. The vessels are sorted by increasing length.*

for the three percentile values are also seen. The figures prove that the non-dimensional penetration is not independent either of the length or the breadth of the struck vessel. A decrease is seen for increasing length and breadth of the struck vessel.

The non-dimensional penetration for the three striking locations is shown in Figure 6.20. The diagram shows the 50-percentile value for the non-dimensional penetration. The vessels are placed in the diagrams after increasing length. The analyses reveal the same tendency which is due to the external dynamics; a small increase in the penetration for striking locations amidships, which is more significant for smaller vessels.

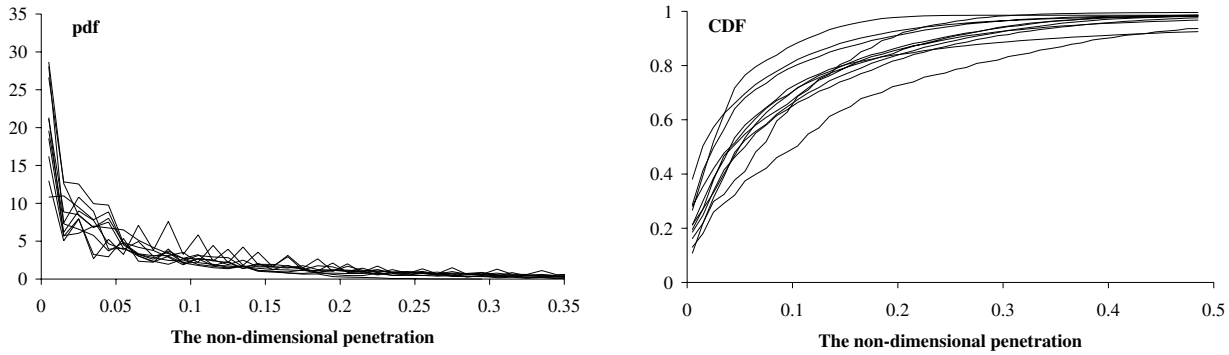


Figure 6.18: *Left: The probability density distribution for the non-dimensional penetration, $\overline{z}$. Right: The cumulative density distribution for the non-dimensional penetration. All analysed vessels are shown in the diagrams.*

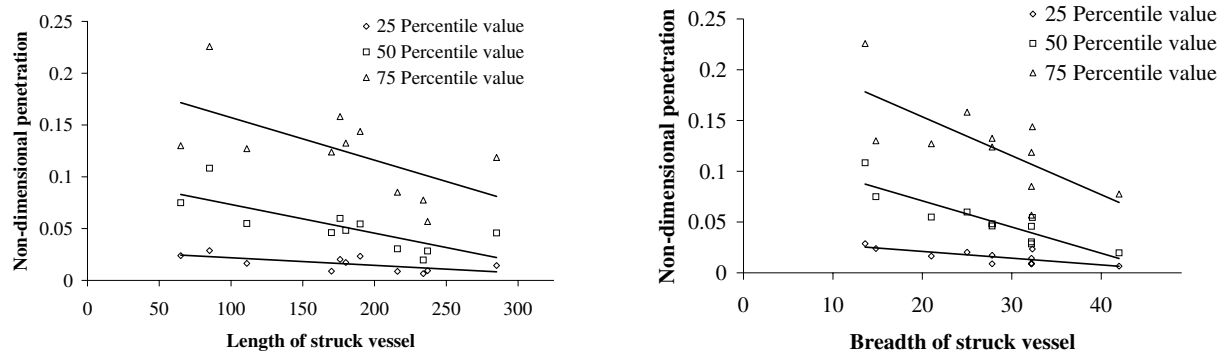


Figure 6.19: *Left: The 25-, 50- and 75 percentile value for the non-dimensional penetration, $\overline{z}$, versus the length, $L$, of the struck vessel. Right: The 25-, 50- and 75-percentile values for the non-dimensional penetration, $\overline{z}$, versus the breadth, $B$, of the struck vessel. Regression lines for the three percentile values are shown in both diagrams.*

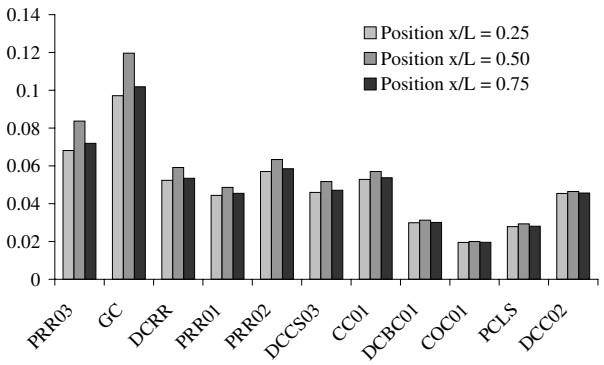


Figure 6.20: *The 50-percentile value for the non-dimensional penetration for the three striking locations 0.25, 0.50 and 0.75. The vessels are sorted by increasing length.*

**The Relation between the Non-Dimensional Damage Length and the Non-Dimensional Penetration**

For examination of the correlation between the non-dimensional damage length, $\overline{y}$, and the non-dimensional penetration, $\overline{z}$, the parameters $P[\overline{z_j}|\overline{y_i}]$ and $P[\overline{z_j}]$ are determined during the simulation. The non-dimensional damage length and the non-dimensional penetration are each separated into five intervals of the length 0.1. This gives a 5x5 matrix. During the simulation the number of observations in each cell is counted and from this the probabilities $P[\overline{y}]$, $P[\overline{z}]$ and the conditional probability $P[\overline{z}|\overline{y}]$ can be determined. Figure 6.21 shows the probabilities $P[\overline{z_j}|\overline{y_i}]$ and $P[\overline{z}]$ for vessels of different types and lengths, figures for all other analysed vessels are placed in Appendix D. A tendency towards $P[\overline{z_j}|\overline{y_i}] = P[\overline{z_j}]$ is seen for all vessels, from which it can be concluded that there is no dependency between the non-dimensional damage length and the non-dimensional penetration.

**Dry Cargo Vessels versus Tankers**

As the current regulations separate vessels into dry cargo vessels and tankers, a comparison of the damages to these two types of vessels is made.

The non-dimensional damage length

The probability density distribution and the cumulative density distribution for all analysed vessels are presented in Figure 6.22 where tankers are indicated by thicker lines. All analyses show the same tendency of many small penetrations but the figures also show a large variation in the mean value and considerable deviation for the different struck vessels. The tankers do not differ from this tendency, but there seems to be shorter damage lengths for tankers. The same can be seen in Figure 6.23 where the 25- and 75-percentile value of the non-dimensional damage length is shown.

The non-dimensional penetration

The probability density distribution and the cumulative density distribution for all analysed vessels are presented in Figure 6.24, where tankers are indicated by thicker lines. All analyses show the same tendency of many small penetrations but the figures also show a large variation in the mean value and the deviation for the different struck vessels. The tankers do not differ

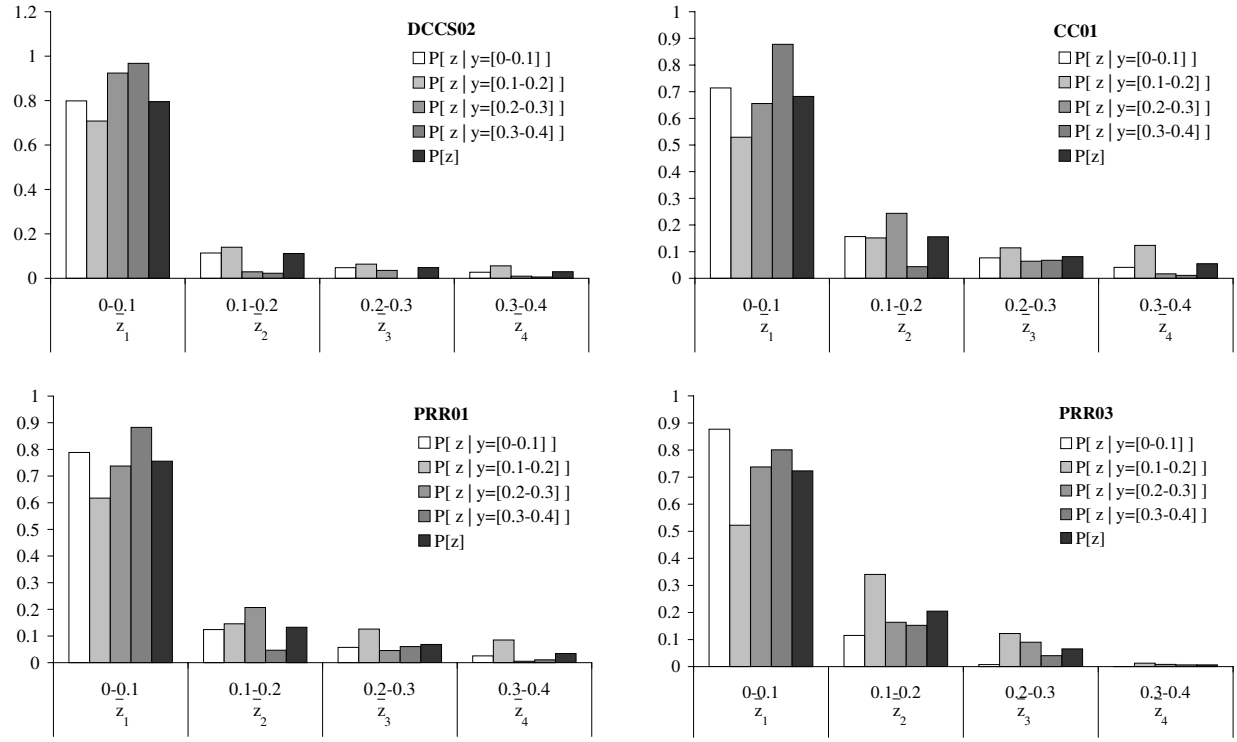


Figure 6.21: $P[\overline{z_j}|\overline{y_i}]$ *and* $P[\overline{z_j}]$ *for vessels of different types and sizes.*

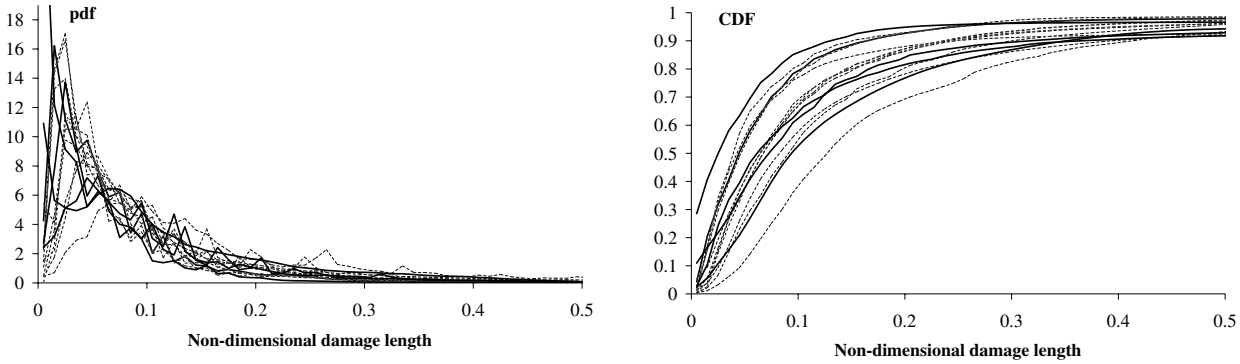


Figure 6.22: *Left: The probability density distribution for the non-dimensional damage length,* $\overline{y}$*. Right: The cumulative density distribution for the non-dimensional damage length. All analysed vessels are shown in the diagrams, tankers are indicated by thicker full lines.*

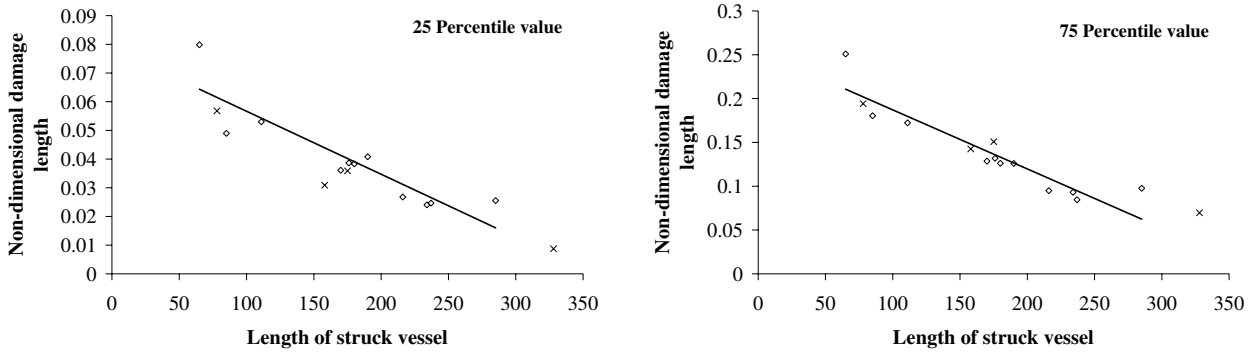


Figure 6.23: *Left: The 25-percentile value for the non-dimensional damage length, $\overline{y}$, versus the length of the struck vessel. Right: The-75 percentile value for the non-dimensional damage length versus the length of the struck vessel. Regression lines for the percentile values are shown in both diagrams and tankers are indicated by a cross.*

from this tendency. The same tendency can be observed in Figure 6.25 where the 25- and 75-percentile values of the non-dimensional penetration are displayed.

Conclusions

This analysis shows that the penetration into the tankers is of the same size as the penetration into dry cargo vessels, whereas the damage lengths for tankers are generally shorter. These results indicate that there is no difference in the structure, but the velocity of the tankers is lower.

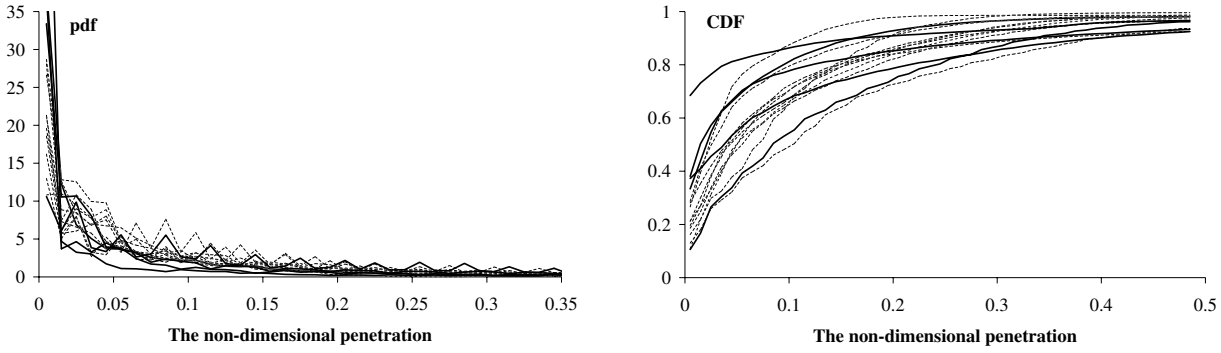


Figure 6.24: *Left: The probability density distribution for the non-dimensional penetration, $\overline{z}$. Right: The cumulative density distribution for the non-dimensional penetration. All analysed vessels are shown in the diagrams, tankers are indicated by thicker lines.*

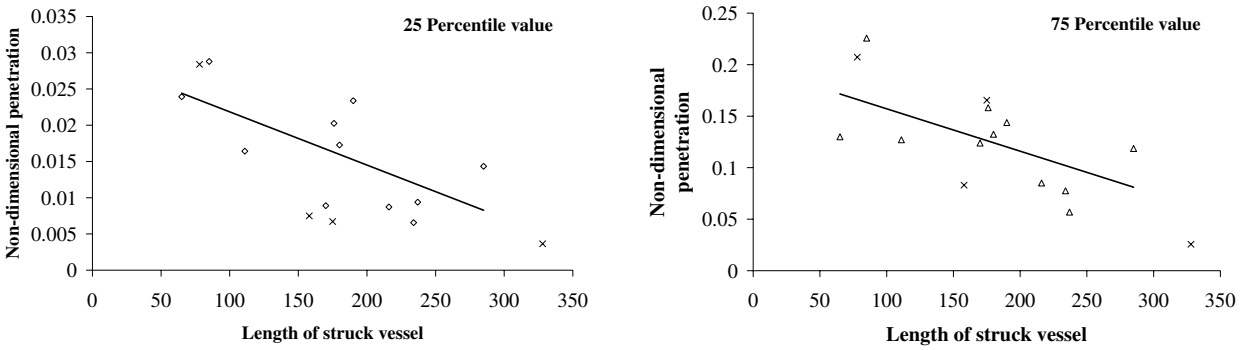


Figure 6.25: *Left: The 25-percentile value for the non-dimensional penetration, $\overline{z}$, versus the length of the struck vessel. Right: The 75-percentile value for the non-dimensional penetration versus the length of the struck vessel. Regression lines for the percentile values are shown in both diagrams and tankers are indicated by a cross.*

### 6.5.3 Results from Simulation, Analysis 2, Relation between struck and Striking Vessels

The struck vessels are here separated into three groups depending on size:
Group size $L \leq 100$ , $100 < L \leq 160$ and $L > 160$

**The Non-Dimensional Damage Length**
The probability density distribution and the cumulative density distribution for all analysed vessels are presented in Figure 6.26. All analyses show the same tendency of many small damages but the figures also show a large variation in the mean value and a large variation for the different struck vessels.

Figure 6.27 (left) presents the 25-, 50- and 75-percentile values for the non-dimensional damage length versus the length of the struck vessel. Regression lines for the three percentile values are also shown. In the left figure all analysed vessels are included, this figure proves that the non-dimensional damage length depends slightly on the length of the struck vessel. A decrease is seen for increasing length of the struck vessel, the decrease is most distinct for the 75-percentile value, less for the 25-percentile value. Two vessels are then omitted from the analysis as their deformation pattern differs from that of the other vessels. The first is a passenger cruse liner, PCLS01, which is very long compared to the displacement. The second omitted ship is a general cargo vessel, GC01, with a very low freeboard. Figure 6.27 (right) shows the 25-, 50- and 75-percentile values for the non-dimensional damage length versus the length of the struck vessel, after omitting PCLS01 and GC01. It is seen from the figure that now the non-dimensional damage length is nearly independent of the length of the struck vessel.

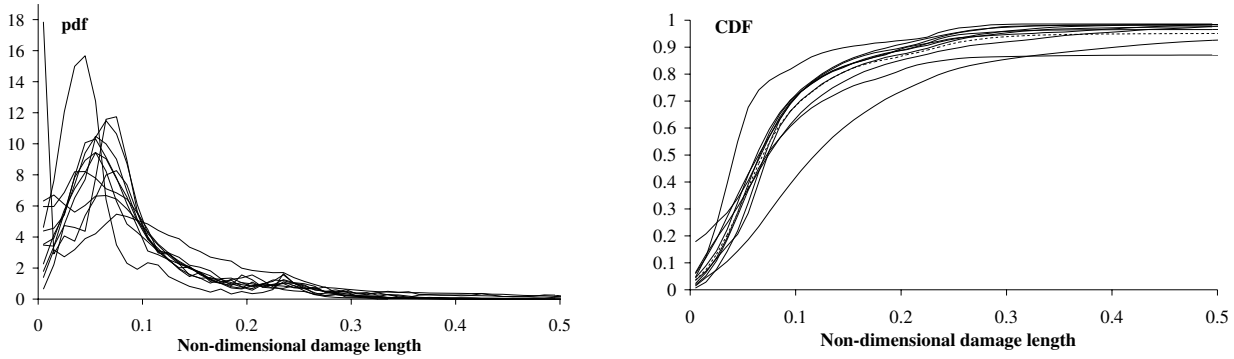


Figure 6.26: *Left: The probability density distribution for the non-dimensional damage length, $\overline{y}$. Right: The cumulative density distribution for the non-dimensional damage length. All analysed vessels are shown in the diagrams.*

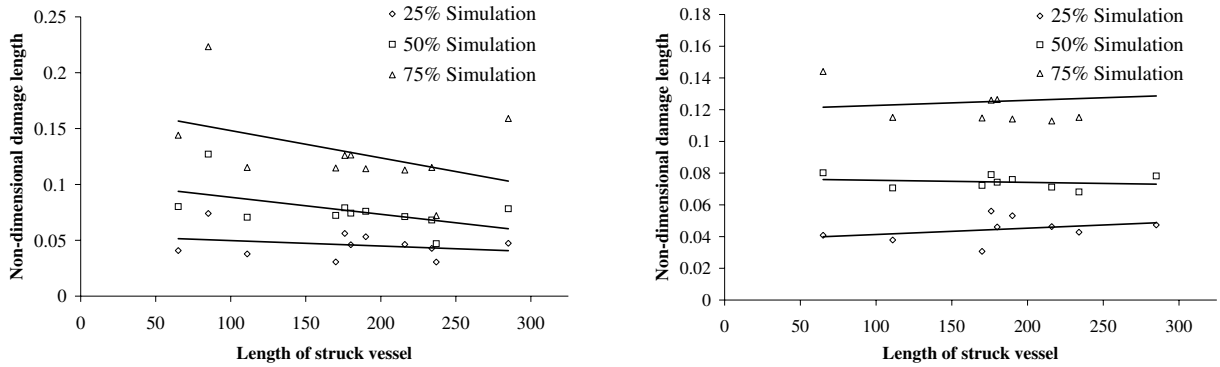


Figure 6.27: *The 25-, 50- and 75-percentile values for the non-dimensional penetration, $\overline{z}$, versus the length of the struck vessel, including tendency lines. Left: All struck vessels. Right: PCLS01 and GC01 omitted.*

### The Non-Dimensional Penetration

The probability density distribution and the cumulative density distribution for the non-dimensional penetration for all analysed vessels are shown in Figure 6.28. All analyses reveal the same tendency of many small penetrations.

Figure 6.29 shows the 25-, 50- and 75-percentile values for the non-dimensional penetration versus the length (left) and versus the breadth (right) of the struck vessel. Regression lines for the three percentile values are also seen. The figures show no systematic dependency on the non-dimensional penetration and the length or the breadth of the struck vessel.

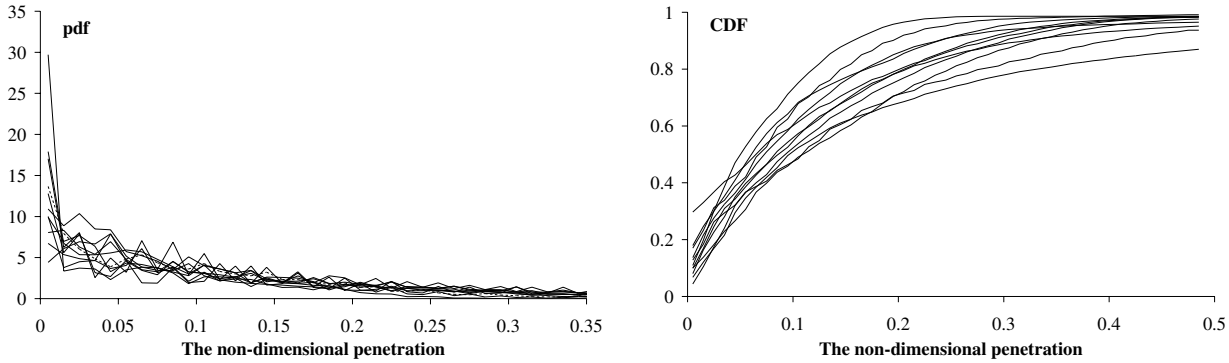


Figure 6.28: *Left: The probability density distribution for the non-dimensional penetration, $\overline{z}$. Right: The cumulative density distribution for the non-dimensional penetration. All analysed vessels are shown in the diagrams.*

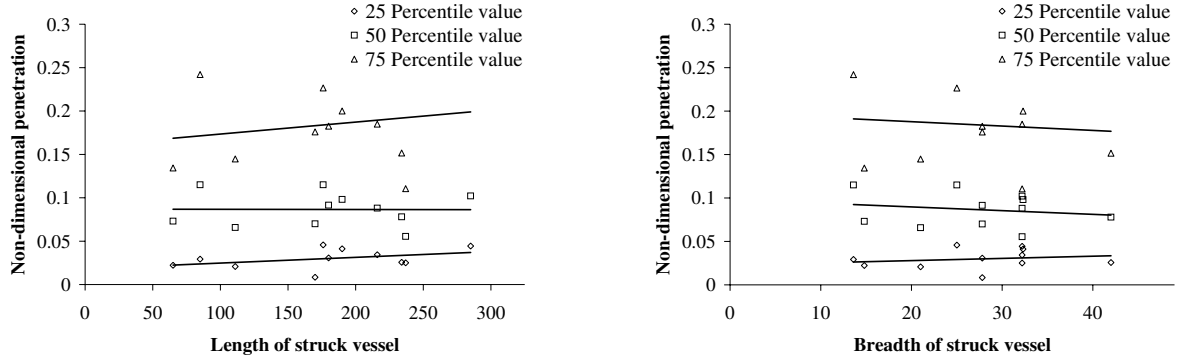


Figure 6.29: *Left: The 25-, 50- and 75-percentile values for the non-dimensional penetration, $\overline{z}$, versus the breadth of the struck vessel. Right: The 25-, 50- and 75-percentile values for the non-dimensional penetration versus the length of the struck vessel. Regression lines for the three percentile values are shown in both diagrams.*

### The Relation between the Non-Dimensional Damage Length and the Non-Dimensional Penetration

For examination of the correlation between the non-dimensional damage length $\overline{y}$ and the non-dimensional penetration $\overline{z}$, the parameters $P[\overline{z_j}|\overline{y_i}]$ and $P[\overline{z_j}]$ are determined during the

simulation. Figure 6.30 shows the probabilities $P[\overline{z_j}|\overline{y_i}]$ and $P[\overline{z}]$ for vessels of different types and lengths, figures for all other analysed vessels are placed in Appendix D. A tendency towards $P[\overline{z_j}|\overline{y_i}] = P[\overline{z_j}]$ is seen for all vessels. From this it can be concluded that there is no dependency between the non-dimensional damage length and the non-dimensional penetration.

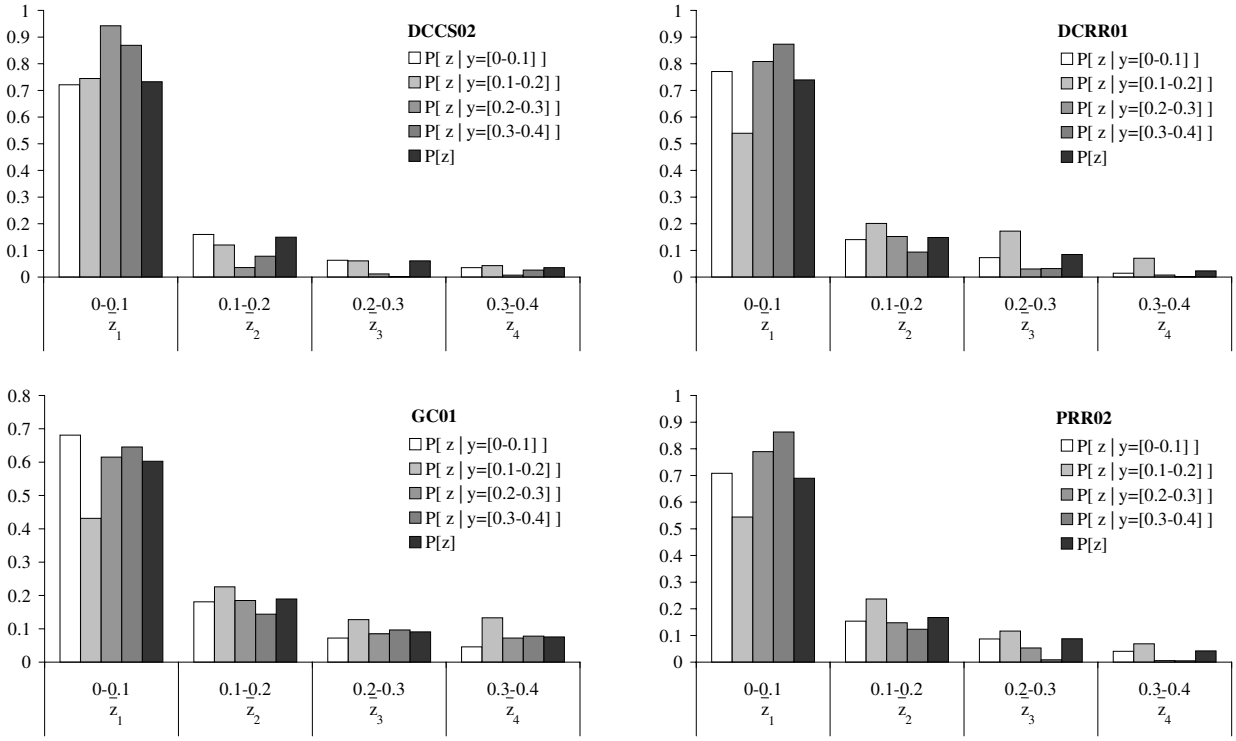


Figure 6.30: $P[\overline{z_j}|\overline{y_i}]$ *and* $P[\overline{z_j}]$ *for vessels of different types and sizes.*

## 6.6 Distribution of Energy to Be Absorbed in Struck Vessel - Energy Dissipation Values

Instead of describing a particular area or route by the distribution of vessels, the area may be related to collision energy. With a knowledge of the distribution of vessels and collision scenarios in a particular area, the present Monte Carlo simulation will here be used to determine probability distributions of energy levels released for crushing of the ship's structures, see Figure 6.31. The energy distribution will be given as a function of the displacement of the struck vessel and the striking location and as percentile value of the energy to be absorbed in the ship's structure.

Five cases have been investigated, namely vessels in worldwide trade, the Straits of Dover and Gibraltar and the eastern and western routes through the Great Belt (Denmark).

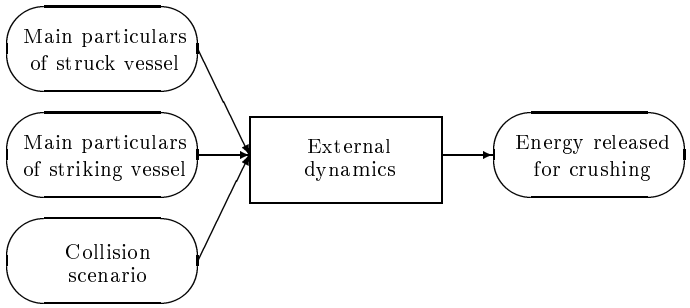


Figure 6.31: *Determination of energy released for crushing.*

### 6.6.1 Worldwide Trade

The 25-, 50-, 75- and 90-percentile values of the energy to be absorbed by vessels in worldwide trade are shown in Figure 6.32 for various types of struck vessels. The energy values are all calculated for a striking location in the middle of the struck vessel.

It has been found that the energy levels or the energy to be absorbed can be approximated by an exponential function:

$$E_x = b\left(1 - e^{\sqrt{\frac{\Delta}{a}}}\right) \tag{6.4}$$

where $\Delta$ is the displacement of the struck vessel and the parameters $a$ and $b$ can be described by the values in Table 6.6.

Table 6.6: Parameters $a$ and $b$ for the energy exponential function, Eq. (6.4), for vessels in worldwide trade.

| | 25-percentile value | 50-percentile value | 75-percentile value | 90-percentile value |
|---|---|---|---|---|
| a | 2000 | 4000 | 10000 | 30000 |
| b | 0.65 | 4.05 | 32.5 | 237 |

### 6.6.2 Specific European Shipping Routes

Energy reference values for vessels in worldwide trade and vessels on four different routes, the Straits of Dover and Gibraltar and the eastern and western routes through the Great Belt, have been compared. The 25- and 90-percentile values for the energy to be absorbed for the different areas are shown in Figure 6.33 as functions of the displacement of the struck vessel. The energy reference values have been estimated by means of Eq. (6.4) and values from Table 6.7. A comparison of the results with the probability density function for length

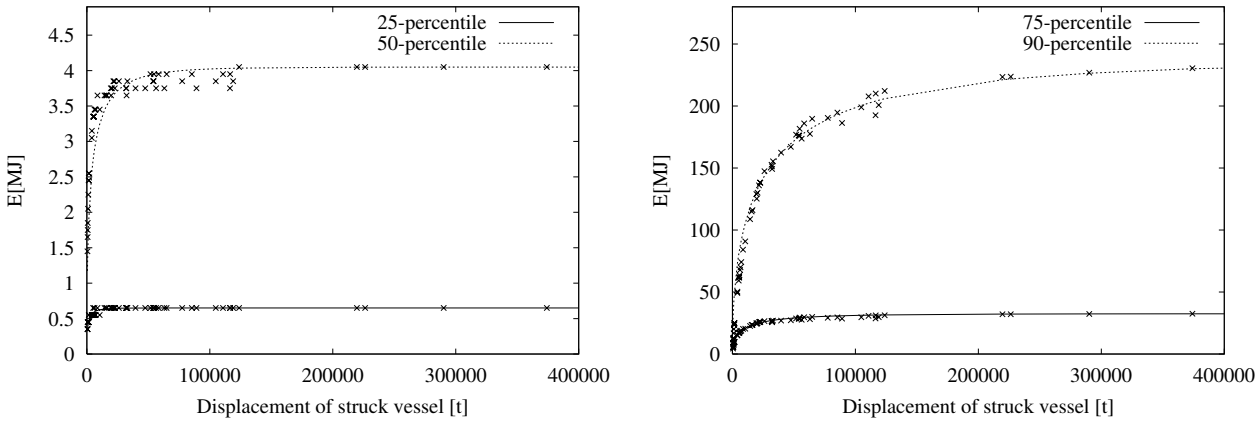


Figure 6.32: *Vessels in the worldwide trade. Left: The 25- and 50-percentile values for energy to be absorbed amidships versus displacement of the struck vessel. Right: The 75- and the 90 percentile value for energy to be absorbed amidships versus displacement of the struck vessel.*

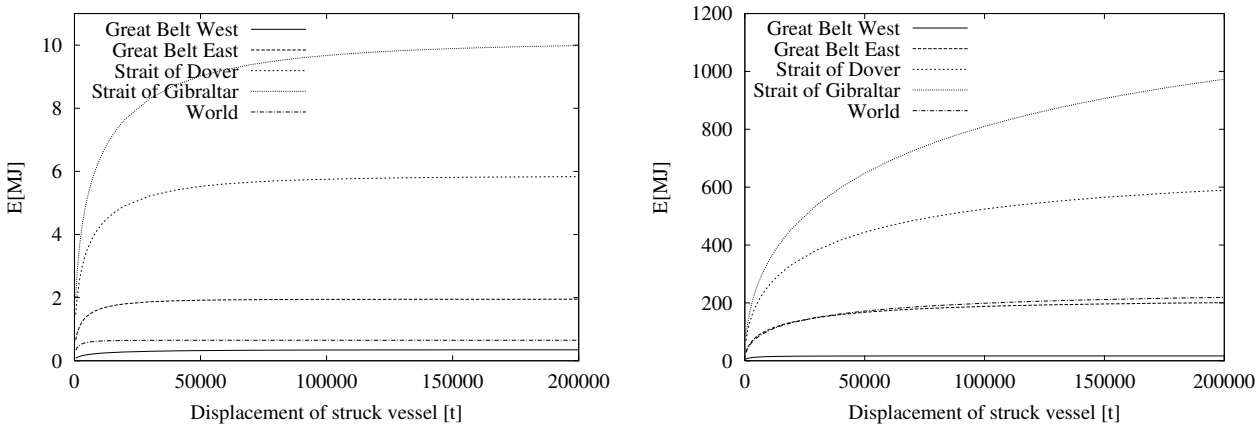


Figure 6.33: *Left: The 25-percentile value for energy to be absorbed amidships versus displacement of the struck vessel for various European routes. Right: The 90-percentile value for energy to be absorbed amidships versus displacement of the struck vessel for various European routes.*

in Figure 6.5 shows good agreement between the lengths of the vessels passing the area and the energy to be absorbed.

Table 6.7: Parameters $a$ and $b$ for the energy exponential function, Eq. (6.4), for various European shipping routes.

| | | 25-percentile value | 50-percentile value | 75-percentile value | 90-percentile value |
|---|---|---|---|---|---|
| Great Belt W | a | 8000 | 200 | 2000 | 2500 |
| | b | 0.35 | 1.35 | 5.25 | 16.65 |
| Great Belt E | a | 3000 | 7000 | 9000 | 19000 |
| | b | 1.95 | 12.05 | 55.90 | 208.90 |
| Strait of Dover | a | 6000 | 10000 | 20000 | 40000 |
| | b | 5.85 | 30.35 | 148.00 | 660.00 |
| Strait of Gibraltar | a | 10000 | 16000 | 28000 | 105000 |
| | b | 10.10 | 57.30 | 285.00 | 1300.00 |

This page is intentionally left blank.

# Chapter 7

# Probabilistic Analysis of Collision Damages, Damage Statistics

Damage stability regulations are either based on traditional deterministic methods or on the more modern probabilistic approach. The first international probabilistic concept for damage stability regulation, Resolution A.265, IMO (1971), was adopted by IMO in 1971. The probabilistic rules were an optional alternative to the deterministic passenger regulation in the SOLAS Convention and were developed for passenger vessels only. The passenger vessel regulation was in 1990 followed by the adoption of subdivision and damage stability rules for dry cargo vessels, SOLAS (1990), also based on the probabilistic concept. While the probabilistic rules for cargo vessels are generally based on the same overall principles and damage statistics as the passenger vessel rules, there are some differences, specially the treatment of the vertical extent of damage.

The damage statistics for the passenger regulation A.265 is based on data collected for casualties occurring in the 1950's and 1960's. Even though the shortcomings of the statistics were well known, the same statistics was used for the dry cargo regulation in 1990. The shortcomings mainly arise from lack of updating the statistics, but it is also important that the statistics is based on 296 ship collisions only. In order to overcome these problems, and in parallel with the activity within IMO, a European research programme entitled HARDER "Harmonization of Rules and Design Rationale" was initiated. The project, which began in 2000, is currently working to investigate systematically the validity, robustness, consistency, and impact of all aspects of the harmonised probabilistic damage stability regulations. Through this project a new updated damage database has been established.

This chapter starts with a short description of the new updated damage database. In the following sections the database is analysed with regard to collision type, the relation between the struck and the striking vessel and the relation between damage parameters and the main particulars of the struck vessel.

## 7.1 Damage Database

The new updated damage database from the European project HARDER consists of damage data files from:

- The old IMO damage database
- Updated IMO damage statistics
- Data from the classification societies
  - Det Norske Veritas
  - Germanischer Lloyd
  - Lloyd's Register of Ship Repair Statistics
  - Hellenic Register of Shipping
- Data collected by the former East German authorities (DSRK)

Presently, the updated damage database contains 2946 reports of eight different casualty types.

| | | | |
|---|---|---|---|
| Capsizing | 3 | Heavy weather | 9 |
| Collision | 1851 | Loss | 5 |
| Fire/explosion | 6 | Other | 139 |
| Grounding | 930 | Struck | 3 |

For use in the damage analysis the following is required when the data from the database is applied:

- The casualty must be a collision
- The collision must be between two ships, see Section 7.2.1
- The damage location must be aft of the collision bulkhead, see Section 7.2.2

The present damage stability regulations separate vessels into passenger vessels, dry cargo vessels and tankers. In Section 7.2.3 a comparison between tankers and dry cargo vessels is presented. Both data from the database and the functions representing the present regulation have been compared.

## 7.2 Analysis of Damage Database

### 7.2.1 Ship-Ship Collisions versus Other Collisions

In this section a comparison is made between ship-ship collisions with a damage location behind the collision bulkhead and other collisions than ship-ship collisions with no restriction in damage position. Other collisions might be collisions with floating objects or key contacts during berthing manoeuvres.

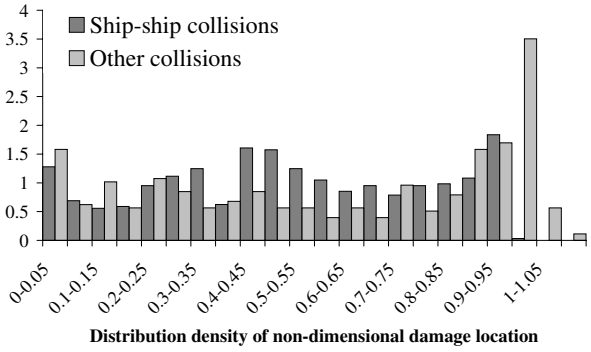


Figure 7.1: *Distribution density for the non-dimensional damage location, $\overline{x}$, for ship-ship collisions and other collisions.*

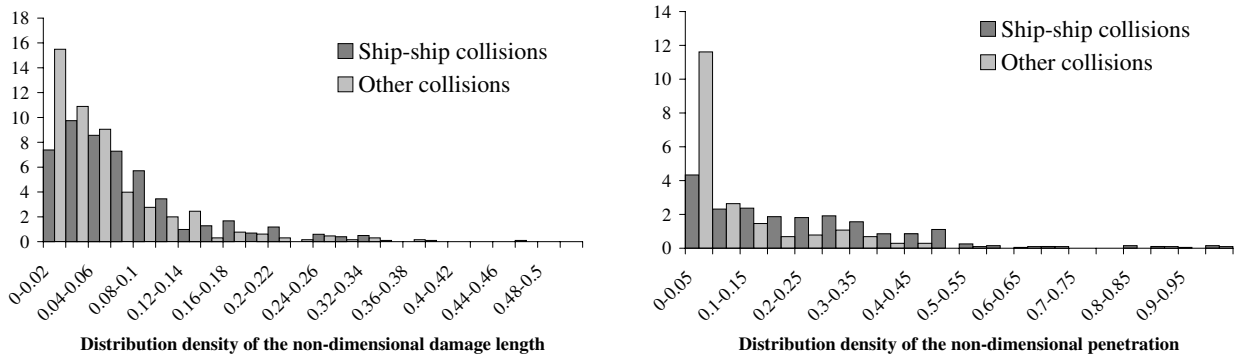


Figure 7.2: *Distribution density functions for the non-dimensional damage length, $\overline{y}$, (left) and the non-dimensional penetration, $\overline{z}$, (right).*

From Figure 7.1 illustrating the distribution density for the non-dimensional damage location, $\overline{x}$, for both ship-ship collisions and other collisions, it is seen that the damage location for other collisions than ship-ship collisions is situated more fore and aft than that of damage from ship-ship collisions. This may be a result of berthing damages resulting from harbour

manoeuvres. Collisions in the forward part of the vessel may come from impacts with floating objects.

Figure 7.2 shows that both the non-dimensional damage length, $\overline{y}$, and the non-dimensional penetration, $\overline{z}$, are smaller for other collisions than ship-ship collisions.

### 7.2.2 Collisions Aft of the Collision Bulkhead

If all damages are included, both forward and aft of the collision bulkhead, the dataset consists of 831 data points. When all collisions forward of the collision bulkhead are neglected the number is 610 data points. The difference between the two datasets and the reason for neglecting data will be explained in this section.

The distance from the forward perpendicular to the collision bulkhead is between 5% and 8% of the length of the vessel. For vessels of a length exceeding 200 m the distance between the forward perpendicular and the collision bulkhead need not be greater than 10m. In this analysis a distance of 5% of the length is used for all vessels of a length below 200m and 10m is used for all vessels of a length exceeding 200m.

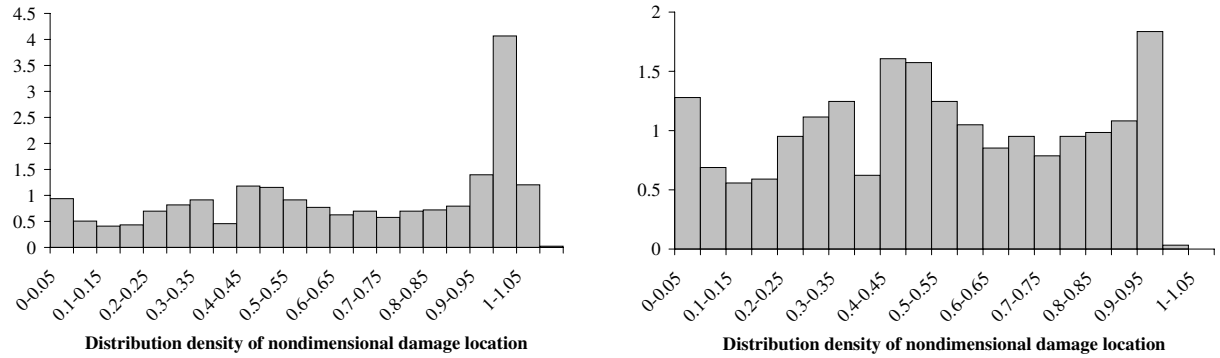


Figure 7.3: *The distribution density for the non-dimensional damage location, $\overline{x}$. Left: All collisions. Right: Collision aft of collision bulkhead.*

In Figure 7.3 the distribution density for the non-dimensional damage location is shown. To the left is the diagram for all collisions presented. The large peak in the fore part of the vessel is considered to arise from lack of information whether the considered vessel is a struck or a striking vessel. In order to eliminate striking vessels from the dataset all cases with collisions forward of the collision bulkhead are neglected. The result is a distribution density of considered collisions as shown in Figure 7.3 (right).

### 7.2.3 Tankers versus All Vessels

The data for tankers is separated from the damage database. To analyse the difference between collision damages to tankers and damages to dry cargo vessels, the non-dimensional damage length, the non-dimensional penetration and the longitudinal damage location have been compared.

Data from the database and the damage functions representing the present regulations SOLAS (1990) and IMO (1995) have been compared. The datasets show no significant difference between the damage dimensions for the different types of vessels, whereas the case of the regulations of MARPOL and SOLAS is different. See Figures 7.4 - 7.6. A function for the non-dimensional penetration is not present in the SOLAS regulation as the penetration is presented by a probability factor denoted $r$ in the regulation.

**The Damage Location**, Figure 7.4
Data from database: All vessels 610 data points, tankers 107 data points

**The Damage Length**, Figure 7.5
Data from database: All vessels 508 data points, tankers 107 data points

**The Damage Penetration**, Figure 7.6
Data from database: All vessels 398 data points, tankers 79 data points

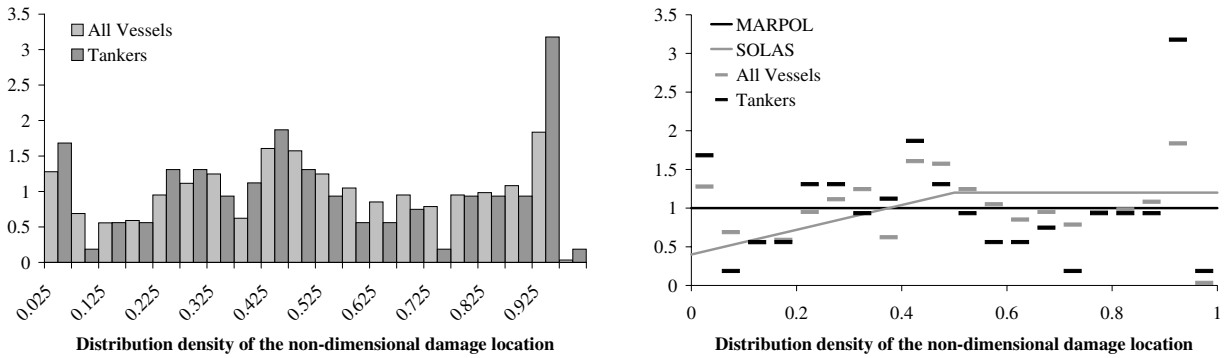


Figure 7.4: *The distribution density for the non-dimensional damage location, $\overline{x}$. Both the data and the regulations are compared for tankers and all vessels.*

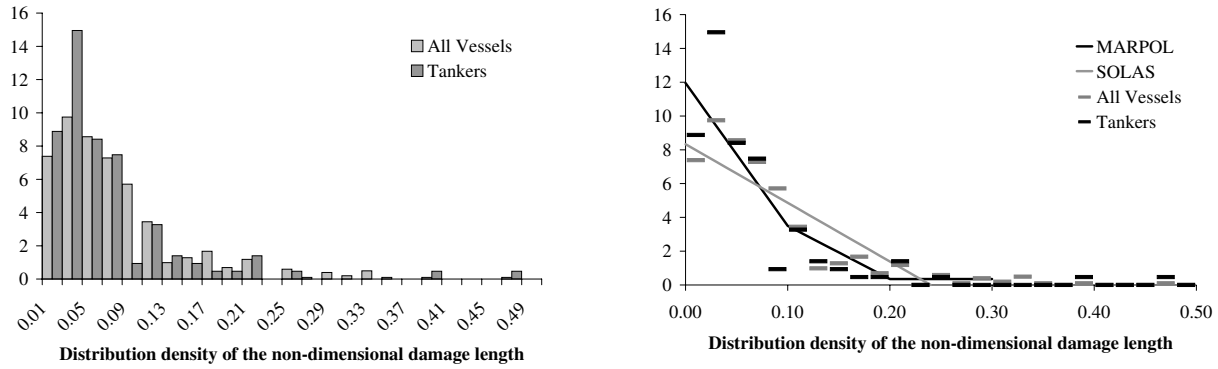


Figure 7.5: *The distribution density for the non-dimensional damage length, $\overline{y}$. Both the data and the regulations are compared for tankers and all vessels.*

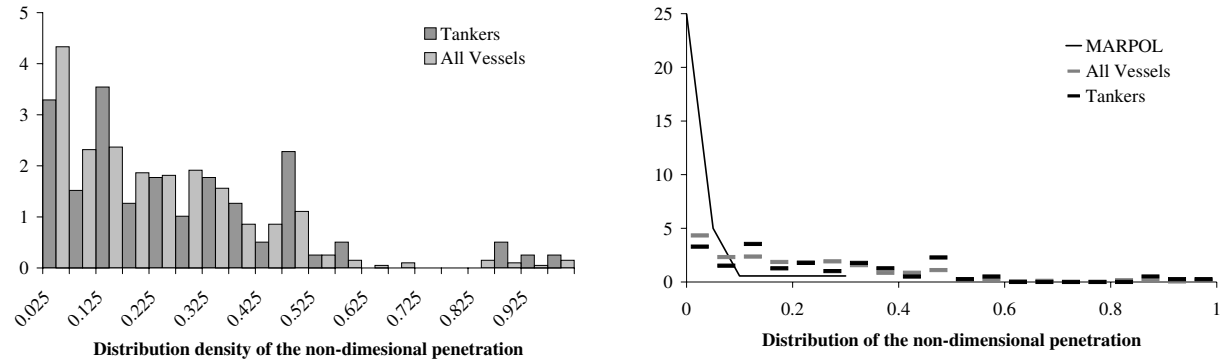


Figure 7.6: *The distribution density for the non-dimensional penetration, $\overline{z}$. Both the data and the regulations are compared for tankers and all vessels.*

### 7.2.4 Relation between the Struck and the Striking Vessel

**Correlation of Types of the Struck and the Striking Vessel**
As the type of the striking vessel is not given in the damage database, it is assumed that there is no correlation between the type of the struck and the striking vessel.

**Correlation of Lengths of the Struck and the Striking Vessel**
The relation between the length of the struck and the striking vessel is examined by use of the updated damage database. Data is shown in Figure 7.7 left. The correlation is calculated to be 0.427, which is high but not high enough to conclude that there is a correlation between the lengths. The figure shows a wide scatter, but the tendency is that small vessels are struck by other small vessels and larger vessels by larger vessels. If the lengths of the struck vessels are separated into three intervals, ($L \leq 100, 100 < L \leq 160$ and $L > 160$), the tendency is becomes clearer, see Figure 7.7 right. Here the probability of the lengths of the striking vessel given an interval of length of the struck vessel $P[L_{striking}|L_{struck}]$ is shown.

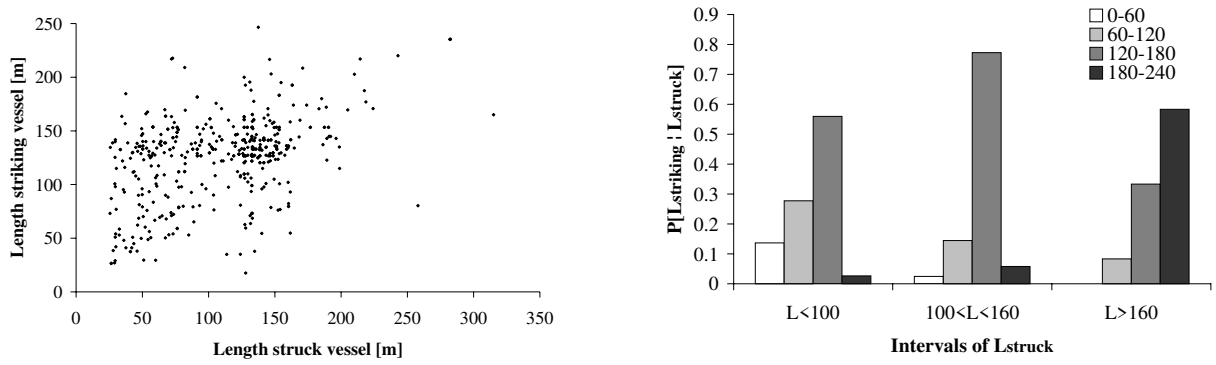


Figure 7.7: *Left: Length of struck vessel versus length of striking vessel. Right: The probability of length of the striking vessel given the length of the struck vessel.*

### Correlation between the Velocity of the Struck and the Striking Vessel

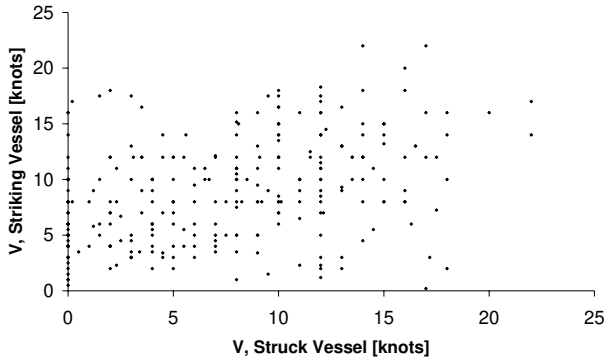


Figure 7.8: *Velocity of struck vessel versus velocity of striking vessel.*

The data from the damage database is used to determine a correlation between the velocities of the struck and the striking vessel in a collision event. The correlation is calculated to be 0.399, which is high but not high enough to conclude that there is a correlation between the velocities. This is also seen in Figure 7.8.

### 7.2.5 Relation between Damage Parameters and the Main Particulars of the Struck Vessel

**The examined relations are:**

- The length of the struck vessel, $L$, versus the non-dimensional damage length, $\overline{y} = \frac{y}{L}$
- The length of the struck vessel, $L$, versus the non-dimensional damage location, $\overline{x} = \frac{x}{L}$
- The non-dimensional damage location, $\overline{x}$, versus the non-dimensional damage length, $\overline{y}$
- The length of the struck vessel, $L$, versus the non-dimensional penetration, $\overline{z} = \frac{z}{B}$
- The breadth of the struck vessel, $B$, versus the non-dimensional penetration, $\overline{z}$
- The non-dimensional damage location, $\overline{x}$, versus the non-dimensional penetration, $\overline{z}$
- The non-dimensional damage length, $\overline{y}$, versus the non-dimensional penetration, $\overline{z}$

**The Length of Struck vessel, $L$, versus the Non-Dimensional Damage Length, $\overline{y}$**
Data points: 508
Correlation: 0.0058

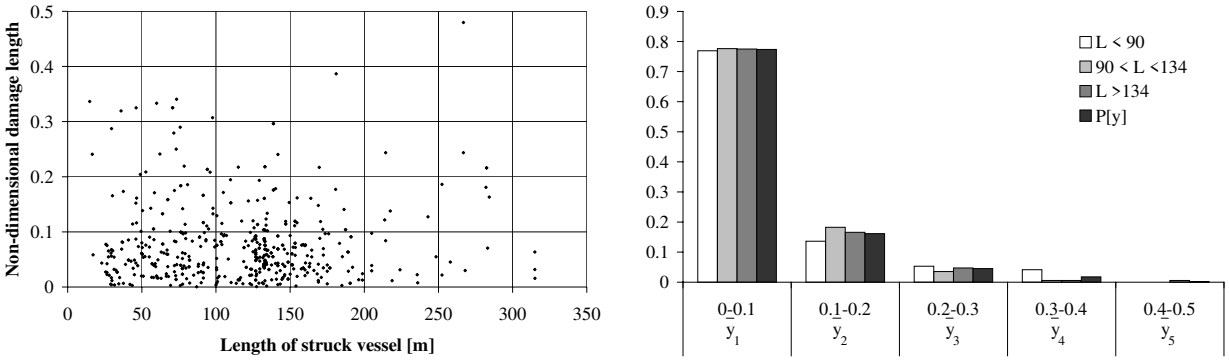


Figure 7.9: *Left: Length of struck vessel versus non-dimensional damage length, $\overline{y}$. Right: $P[\overline{y_j}|L_i]$ and $P[\overline{y_j}]$ as functions of length intervals.*

Figure 7.9 (left) shows the length of struck vessel versus the non-dimensional damage length, $\overline{y}$. As the correlation is very weak, it may be concluded that the non-dimensional damage length is independent of the length of the struck vessel. To prove that this is also the case for all intervals of lengths, the struck vessels are separated into three groups with an equal number of data points. The three intervals are $(L_1, L_2, L_3)$=$(L \leq 90m, 90m < L \leq 134m, L > 134m)$. The non-dimensional damage length is separated into five equal-sized intervals each of the length 0.1. Table 7.1 and Figure 7.9 (right) prove that $P[\overline{y_j}|L_i] = P[\overline{y_j}]$. For higher values of the non-dimensional damage length, $\overline{y}$, the number of observations is sparse, which results in uncertainties, but for the lower values it can be concluded that $L$

and $\overline{y}$ are independent. The same is seen in Figure 7.10 where the CDF and the pdf for the three intervals of lengths are shown.

Table 7.1: *Table with numbers for examining the dependency/independency of $L$ and $\overline{y}$.*

| | Number of observations | | | $P[\overline{y_j}\|L_i]$ | | | $P[\overline{y_j}]$ |
|---|---|---|---|---|---|---|---|
| $\overline{y_5}$ $(0.4-0.5)$ | 0 | 0 | 1 | 0.00000 | 0.00000 | 0.00592 | 0.00197 |
| $\overline{y_4}$ $(0.3-0.4)$ | 7 | 1 | 1 | 0.04142 | 0.00588 | 0.00592 | 0.01772 |
| $\overline{y_3}$ $(0.2-0.3)$ | 9 | 6 | 8 | 0.05325 | 0.03529 | 0.04734 | 0.04528 |
| $\overline{y_2}$ $(0.1-0.2)$ | 23 | 31 | 28 | 0.13609 | 0.18235 | 0.16568 | 0.16142 |
| $\overline{y_1}$ $(0.0-0.1)$ | 130 | 132 | 131 | 0.76923 | 0.77647 | 0.77515 | 0.77362 |
| | $L_1$ | $L_2$ | $L_3$ | $L_1$ | $L_2$ | $L_3$ | |

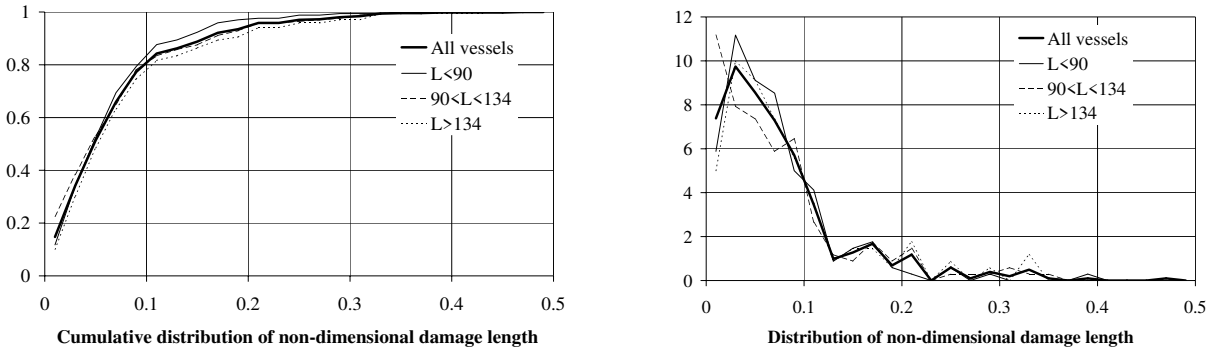


Figure 7.10: *Distribution of non-dimensional damage length, $\overline{y}$, for various lengths of struck vessel. Left: CDF. Right: pdf.*

**The Length of the Struck Vessel, $L$, Versus the Non-dimensional Damage Location, $\overline{x}$**

Data points: 508
Correlation: -0.0179

The length of the struck vessel versus the non-dimensional damage location, $\overline{x}$, is shown in Figure 7.11(left). The correlation is weak, and the sign of the correlation changes from -0.0179 to +0.0276 if the sparse data for vessels of a length larger than 200m is neglected (27 data points, approx. 5%), which also indicates independency of $L$ and $\overline{x}$.

To prove that this is also the case for all intervals of lengths, the struck vessels are separated into three groups with an equal number of data points, $(L_1, L_2, L_3)$=$(L \leq 90m, 90m < L \leq 134m, L > 134m)$. The non-dimensional damage location is separated into five equal-sized intervals each of the length 0.2. Table 7.2 and Figure 7.11 (right) show $P[\overline{x_j}|L_i]$ and $P[\overline{x_j}]$. The agreement is not perfect, but a tendency towards $P[\overline{x_j}|L_i] = P[\overline{x_j}]$ is seen, which indicates that $\overline{x}$ and $L$ are independent.

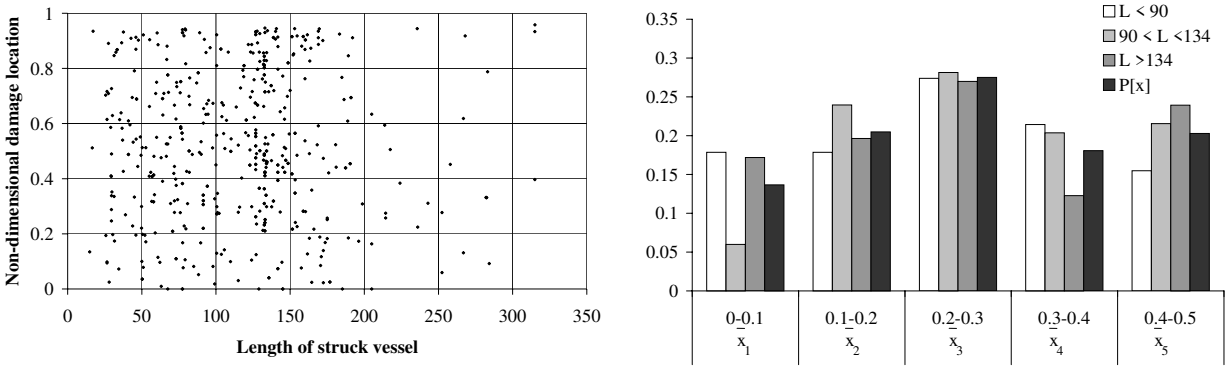


Figure 7.11: *Left: Length of struck vessel versus non-dimensional damage location, $\overline{x}$. Right: $P[\overline{x_j}|L_i]$ and $P[\overline{x_j}]$ as functions of length intervals.*

Table 7.2: *Table with numbers for examining the dependency/independency of $\overline{x}$ and $L$.*

| | Number of observations | | | $P[\overline{x_j}\|L_i]$ | | | $P[\overline{x_j}]$ |
|---|---|---|---|---|---|---|---|
| $\overline{x_5}$ $(0.8-1.0)$ | 26 | 36 | 39 | 0.15476 | 0.21557 | 0.23926 | 0.20281 |
| $\overline{x_4}$ $(0.6-0.8)$ | 36 | 34 | 20 | 0.21429 | 0.20359 | 0.12270 | 0.18072 |
| $\overline{x_3}$ $(0.4-0.6)$ | 46 | 47 | 44 | 0.27381 | 0.28144 | 0.26994 | 0.27510 |
| $\overline{x_2}$ $(0.2-0.4)$ | 30 | 40 | 32 | 0.17857 | 0.23952 | 0.19632 | 0.20482 |
| $\overline{x_1}$ $(0.0-0.2)$ | 30 | 10 | 28 | 0.17857 | 0.05988 | 0.17178 | 0.13655 |
| | $L_1$ | $L_2$ | $L_3$ | $L_1$ | $L_2$ | $L_3$ | |

**The Non-Dimensional Damage Location, $\overline{x}$, versus the Non-Dimensional Damage Length, $\overline{y}$**

Data points: 508
Correlation: 0.0688

Figure 7.12 (left) shows the non-dimensional damage location, $\overline{x}$, versus the non-dimensional damage length, $\overline{y}$. As the correlation is weak, it may be concluded that the non-dimensional damage location is independent of the non-dimensional damage length.

Table 7.3: *Table with numbers for examining the dependency/independency of $\overline{x}$ and $\overline{y}$.*

| | Number of observations | | | $P[\overline{y_j}\|\overline{x_i}]$ | | | $P[\overline{y_j}]$ |
|---|---|---|---|---|---|---|---|
| $\overline{y_5}$ $(0.4-0.5)$ | 0 | 1 | 0 | 0.00000 | 0.00588 | 0.00000 | 0.00197 |
| $\overline{y_4}$ $(0.3-0.4)$ | 3 | 5 | 1 | 0.01775 | 0.02941 | 0.00592 | 0.01772 |
| $\overline{y_3}$ $(0.2-0.3)$ | 9 | 8 | 6 | 0.05325 | 0.04706 | 0.03550 | 0.04528 |
| $\overline{y_2}$ $(0.1-0.2)$ | 21 | 28 | 33 | 0.12426 | 0.16471 | 0.19527 | 0.16142 |
| $\overline{y_1}$ $(0.0-0.1)$ | 136 | 128 | 129 | 0.80473 | 0.75294 | 0.76331 | 0.77362 |
| | $\overline{x_1}$ | $\overline{x_2}$ | $\overline{x_3}$ | $\overline{x_1}$ | $\overline{x_2}$ | $\overline{x_3}$ | |

To prove that this is also the case for all intervals of the non-dimensional damage location, the data points are separated into three groups with an equal number of data: $(\overline{x_1}, \overline{x_2}, \overline{x_3})$=$(\overline{x} \leq 0.37, 0.37 < \overline{x} \leq 0.66, \overline{x} > 0.66)$. The non-dimensional damage length is separated into five

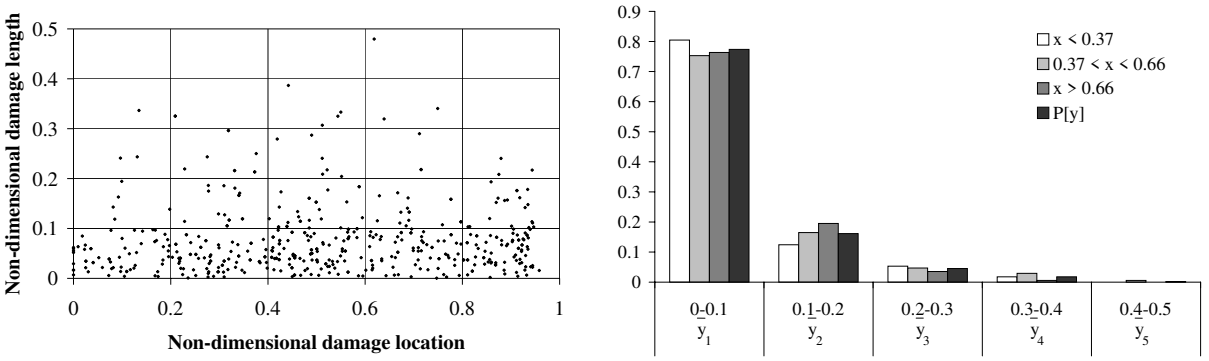


Figure 7.12: *Left: Non-dimensional damage location, $\overline{x}$, versus non-dimensional damage length, $\overline{y}$. Right: $P[\overline{y_j}|\overline{x_i}]$ and $P[\overline{y_j}]$ as functions of intervals of $\overline{x}$.*

equal sized intervals each of the length 0.1. Table 7.3 and Figure 7.12 (right) prove that $P[\overline{y_j}|\overline{x_i}] = P[\overline{y_j}]$. For higher values of $\overline{y}$ the number of observations is sparse, which results in uncertainties, but for the lower values it can be concluded that $\overline{x}$ and $\overline{y}$ are independent.

**The Length of the Struck Vessel, $L$, versus the Non-Dimensional Penetration, $\overline{z}$**
Data points: 397
Correlation: -0.088

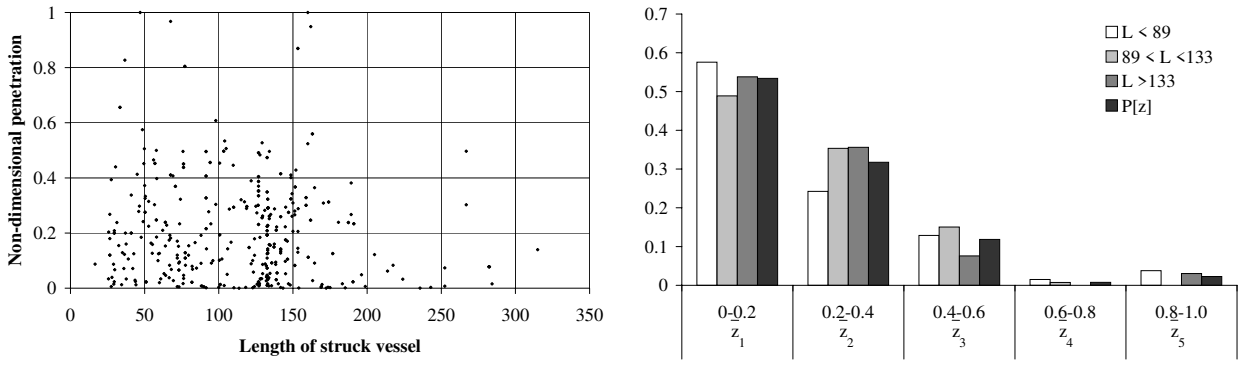


Figure 7.13: *Left: Length of struck vessel versus non-dimensional penetration, $\overline{z}$. Right: $P[\overline{z_j}|L_i]$ and $P[\overline{z_j}]$ as functions of length intervals.*

The length of the struck vessel versus the non-dimensional penetration, $\overline{z}$, is shown in Figure 7.13 (left). As the correlation is weak, it may be concluded that the non-dimensional penetration is independent of the length of the struck vessel. To prove that this is also the case for all intervals of the non-dimensional penetration, the struck vessels are separated into three groups with an equal number of data points: $(L_1, L_2, L_3)$=$(L \leq 89m, 89m < L \leq 133m, L > 133m)$. The non-dimensional penetration is separated into five equal-sized intervals each of the length 0.2. Table 7.4 and Figure 7.13 (right) prove that $P[\overline{z_j}|L_i] = P[\overline{z_j}]$. For higher values of $\overline{z}$ the number of observations is sparse, which results in uncertainties, but for the

lower values it can be concluded, also with the knowledge of the size of the correlation, that $L$ and $\overline{z}$ are independent parameters.

Table 7.4: *Table with numbers for examining the dependency/independency of* $\overline{z}$ *and* $L$.

| | Number of observations | | | $P[\overline{z_j}\|L_i]$ | | | $P[\overline{z_j}]$ |
|---|---|---|---|---|---|---|---|
| $\overline{z_5}$ $(0.8-1.0)$ | 5 | 0 | 4 | 0.03788 | 0.00000 | 0.03030 | 0.02267 |
| $\overline{z_4}$ $(0.6-0.8)$ | 2 | 1 | 0 | 0.01515 | 0.00752 | 0.00000 | 0.00756 |
| $\overline{z_3}$ $(0.4-0.6)$ | 17 | 20 | 10 | 0.12879 | 0.15038 | 0.07576 | 0.01184 |
| $\overline{z_2}$ $(0.2-0.4)$ | 32 | 47 | 47 | 0.24242 | 0.35338 | 0.35606 | 0.31738 |
| $\overline{z_1}$ $(0.0-0.2)$ | 76 | 65 | 71 | 0.57576 | 0.48872 | 0.53788 | 0.53401 |
| | $L_1$ | $L_2$ | $L_3$ | $L_1$ | $L_2$ | $L_3$ | |

**The Breadth of the Struck Vessel, $B$, versus the Non-Dimensional Penetration, $\overline{z}$**

Data points: 397

Correlation: -0.102

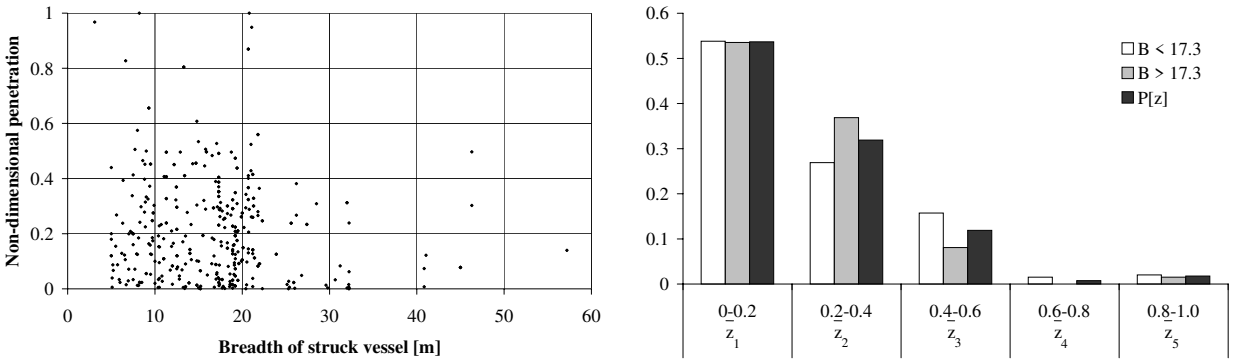


Figure 7.14: *Left: Breadth of struck vessel versus the non-dimensional penetration,* $\overline{z}$*. Right:* $P[\overline{z_j}|B_i]$ *and* $P[z_j]$ *as functions of breadth intervals.*

Table 7.5: *Table with numbers for examining the dependency/independency of* $\overline{z}$ *and* $B$.

| | Number of observations | | $P[\overline{z_j}\|B_i]$ | | $P[\overline{z_j}]$ |
|---|---|---|---|---|---|
| $\overline{z_5}$ $(0.8-1.0)$ | 4 | 3 | 0.02030 | 0.01515 | 0.01772 |
| $\overline{z_4}$ $(0.6-0.8)$ | 3 | 0 | 0.01523 | 0.00000 | 0.00759 |
| $\overline{z_3}$ $(0.4-0.6)$ | 31 | 16 | 0.15736 | 0.08081 | 0.11899 |
| $\overline{z_2}$ $(0.2-0.4)$ | 53 | 73 | 0.26904 | 0.36869 | 0.31899 |
| $\overline{z_1}$ $(0.0-0.2)$ | 106 | 106 | 0.53807 | 0.53535 | 0.53671 |
| | $B_1$ | $B_2$ | $B_1$ | $B_2$ | |

The breadth of the struck vessel versus the non-dimensional penetration, $\overline{z}$, is shown in Figure 7.14 (left). As the correlation is weak, it may be concluded that the non-dimensional penetration is independent of the breadth of the struck vessel. To prove that this is also the case for all intervals of the breadth, the struck vessels are separated into two groups with

an equal number of data points. The intervals are $(B_1, B_2)$=$(B \leq 17.3m, B > 17.3m)$. The non-dimensional penetration is separated into five equal-sized intervals each of the length 0.2. Table 7.5 and Figure 7.14 (right) prove that $P[\overline{z_j}|B_i] = P[\overline{z_j}]$. For higher values of $\overline{z}$ the number of observations is sparse, which results in uncertainties, but for the lower values it can be concluded that $B$ and $\overline{z}$ are independent. The same can be seen in Figure 7.15 where the CDF and the pdf for the two intervals of breadth are shown.

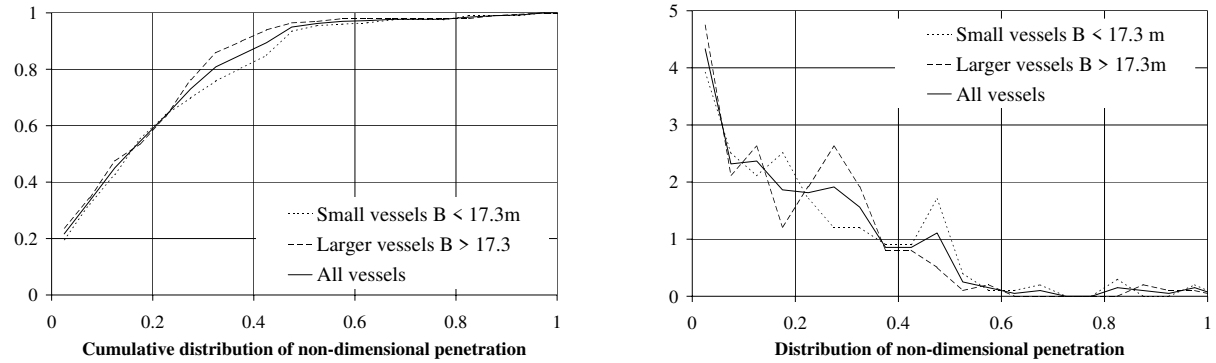


Figure 7.15: *Distribution of non-dimensional penetration for various breadths of struck vessel. Left: CDF. Right: pdf.*

**The Non-Dimensional Damage Location, $\overline{x}$, versus the Non-Dimensional Penetration, $\overline{z}$**
Data points: 397
Correlation: 0.117

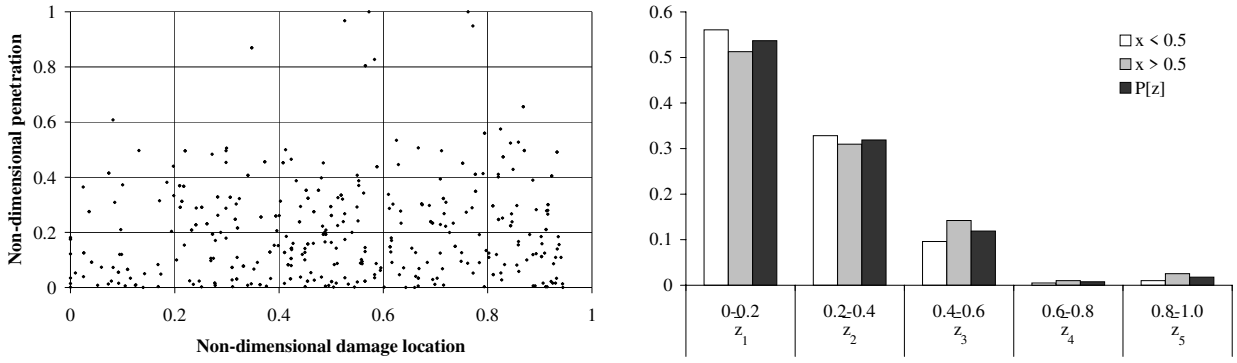


Figure 7.16: *Left: The non-dimensional damage location, $\overline{x}$, versus the non-dimensional penetration, $\overline{z}$. Right: $P[\overline{z_j}|\overline{x}_i]$ and $P[\overline{z_j}]$ as functions of non-dimensional damage location intervals.*

The non-dimensional damage location, $\overline{x}$, versus the non-dimensional penetration, $\overline{z}$, is shown in Figure 7.16 (left). As the correlation is weak, it may be concluded that the two parameters are independent. To prove that this is also the case for all intervals of the non-dimensional damage location, the data points are separated into two groups with an equal

Table 7.6: *Table with numbers for examining the dependency/independency of $\overline{x}$ and $\overline{z}$.*

| | Number of observations | | $P[\overline{z_j}\|\overline{x_i}]$ | | $P[\overline{z_j}]$ |
|---|---|---|---|---|---|
| $\overline{z_5}$ $(0.8-1.0)$ | 2 | 5 | 0.01010 | 0.02538 | 0.01772 |
| $\overline{z_4}$ $(0.6-0.8)$ | 1 | 2 | 0.00505 | 0.01015 | 0.00759 |
| $\overline{z_3}$ $(0.4-0.6)$ | 19 | 28 | 0.09596 | 0.14213 | 0.11899 |
| $\overline{z_2}$ $(0.2-0.4)$ | 65 | 61 | 0.32828 | 0.30964 | 0.31899 |
| $\overline{z_1}$ $(0.0-0.2)$ | 111 | 101 | 0.56061 | 0.51269 | 0.53671 |
| | $\overline{x_1}$ | $\overline{x_2}$ | $\overline{x_1}$ | $\overline{x_2}$ | |

number of data: $(\overline{x_1}, \overline{x_2})$=$(\overline{x} \leq 0.5, \overline{x} > 0.5)$. The non-dimensional penetration is separated into five equal sized intervals each of length 0.2. Table 7.6 and Figure 7.16 (right) prove that $P[\overline{z_j}|\overline{x}_i] = P[\overline{z_j}]$. For higher values of $\overline{z}$ the number of observations is sparse, which results in uncertainties, but for the lower values it can be concluded that $\overline{z}$ and $\overline{x}$ are independent.

**The Non-Dimensional Damage Length, $\overline{y}$, versus the Non-Dimensional Penetration, $\overline{z}$**

Data points: 378
Correlation: 0.214

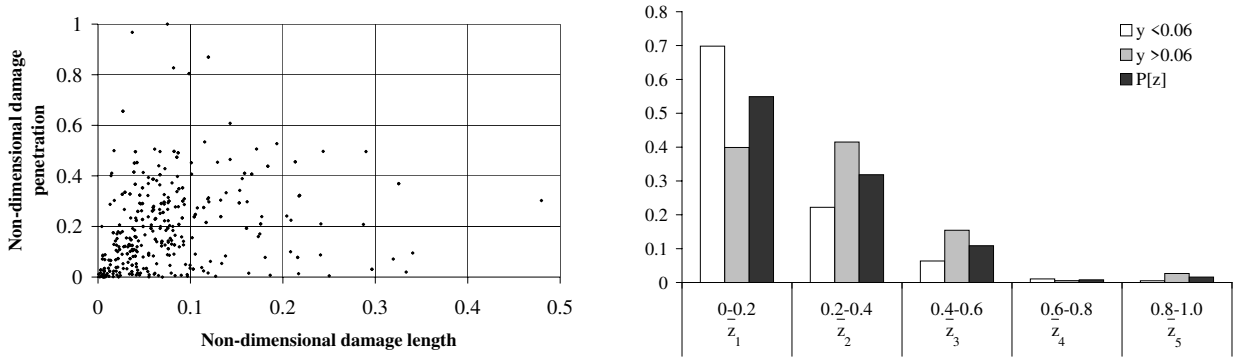


Figure 7.17: *Left: The non-dimensional damage length, $\overline{y}$, versus the non-dimensional penetration, $\overline{z}$. Right: $P[\overline{z_j}|\overline{y}_i]$ and $P[\overline{z_j}]$ as functions of non-dimensional damage length intervals.*

The non-dimensional damage length, $\overline{y}$, versus the non-dimensional penetration, $\overline{z}$, is shown in Figure 7.17 (left). The relatively strong correlation indicates that the relation between $\overline{y}$ and $\overline{z}$ must be examined in more detail. Figure 7.17 (right) where the relation between $P[\overline{z_j}|\overline{y}_i]$ and $P[\overline{z_j}]$ is examined shows only a small relation between the two parameters.

As the data is sparse for deep penetrations and long damages the considered area is reduced as follows:

- Data with a non-dimensional damage length, $\overline{y}$, larger than 0.25 is excluded (less than 3% of the data)

- Data with a non-dimensional penetration, $\overline{z}$, larger than 0.5 is excluded (less than 5% of the data)

The non-dimensional damage length, $\overline{y}$, is divided into two intervals ($\overline{y} \leq 0.033, \overline{y} > 0.033$), which are examined separately.

Non-dimensional damage length larger than 0.033
Data points: 266
Correlation: 0.148

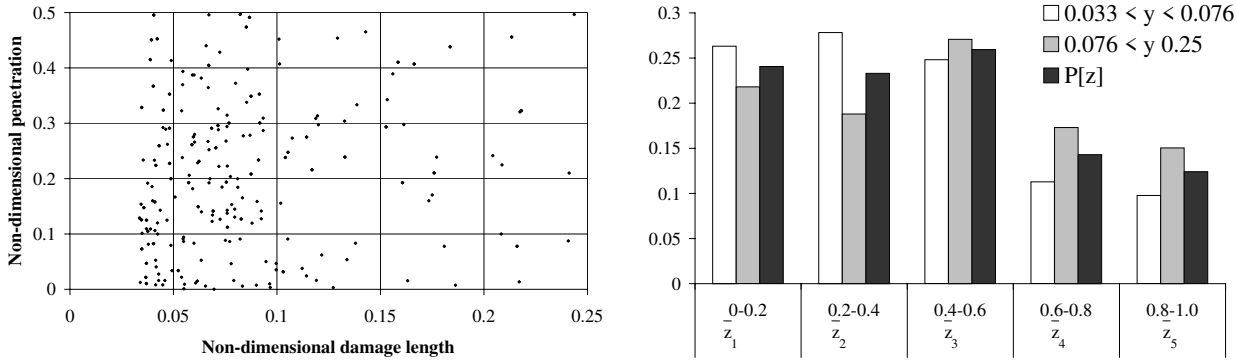


Figure 7.18: *Left: The non-dimensional damage length, $\overline{y}$, versus the non-dimensional penetration, $\overline{z}$. Right: $P[\overline{z_j}|\overline{y}_i]$ and $P[\overline{z_j}]$ as functions of non-dimensional damage length intervals.*

The non-dimensional damage length versus the non-dimensional penetration is shown in Figure 7.18 (left). As the correlation is weak, it may be concluded that the non-dimensional damage location is independent of the non-dimensional penetration. To prove that this is also the case for all intervals of the non-dimensional damage length the struck vessels are separated into two groups with an equal number of data points. The intervals are $(\overline{y_1}, \overline{y_2})$=$(0.033 < \overline{y} \leq 0.076, 0.076 < \overline{y} \leq 0.25)$. The non-dimensional penetration is separated into five equal-sized intervals each of the length 0.1. Table 7.7 and Figure 7.18 (right) show $P[\overline{z_j}|\overline{y}_i]$ and $P[\overline{z_j}]$. The agreement is not perfect, but a tendency towards $P[\overline{z_j}|\overline{y}_i] = P[\overline{z_j}]$ is seen.

Table 7.7: *Table with numbers for examining the dependency/independency of $\overline{y}$ and $\overline{z}$.*

| | Number of observations | | $P[\overline{z_j}\|\overline{y_i}]$ | | $P[\overline{z_j}]$ |
|---|---|---|---|---|---|
| $\overline{z_5}$ $(0.4-0.5)$ | 10 | 19 | 0.09774 | 0.15038 | 0.12406 |
| $\overline{z_4}$ $(0.3-0.4)$ | 15 | 21 | 0.11278 | 0.17293 | 0.14286 |
| $\overline{z_3}$ $(0.2-0.3)$ | 38 | 30 | 0.24812 | 0.27068 | 0.25940 |
| $\overline{z_2}$ $(0.1-0.2)$ | 27 | 18 | 0.27820 | 0.18797 | 0.23308 |
| $\overline{z_1}$ $(0.0-0.1)$ | 26 | 28 | 0.26316 | 0.21805 | 0.24060 |
| | $\overline{y_1}$ | $\overline{y_2}$ | $\overline{y_1}$ | $\overline{y_2}$ | |

Non-dimensional damage length less than 0.033
Data points: 89
Correlation: 0.374

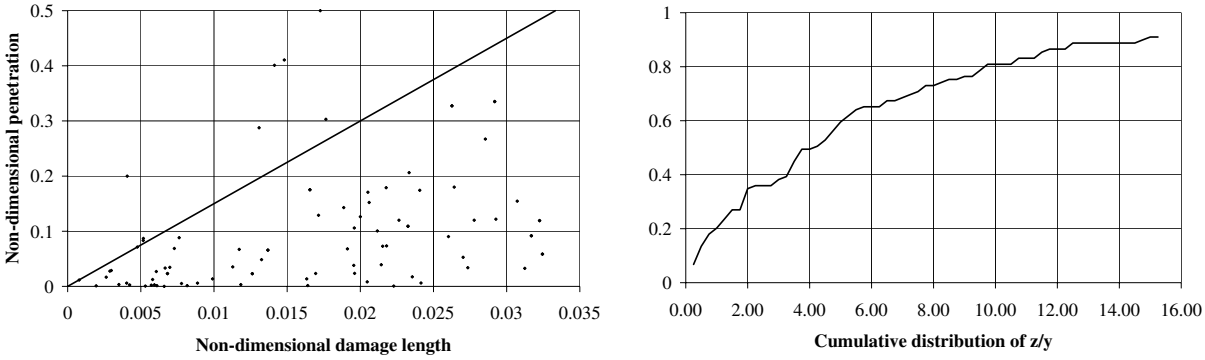


Figure 7.19: *Left: The non-dimensional damage length, $\overline{y}$, versus the non-dimensional penetration, $\overline{z}$. Right: The cumulative distribution for the relation $\overline{z}/\overline{y}$.*

The non-dimensional damage length versus the non-dimensional penetration is shown in Figure 7.19 (left) for non-dimensional damage lengths, $\overline{y}$, less than 0.033. A line: $\overline{z} = 15\overline{y}$ is also shown in the figure. Figure 7.19 (right) presents the cumulative distribution for the relation $\overline{z}/\overline{y}$. The two figures show that for a given non-dimensional damage length, $\overline{y}$, the non-dimensional penetration is less than $\overline{z} = 15\overline{y}$ in more than 90% of all cases.

Non-dimensional penetrations greater than $\overline{z} = 15\overline{y}$ are now neglected. The correlation between the non-dimensional damage length and the non-dimensional penetration then changes to 0.572, a relatively high correlation. A diagram for the data and the corresponding linear regression line is shown in Figure 7.20 (left). The figure shows that although there is an upward linear tendency, the spread of the responses appears to increase as the non-dimensional damage length increases. The residual between observed data and the linear regression is shown in Figure 7.20 (right). The residual plot shows a random scatter about zero with the spread of the points increasing for increasing $\overline{y}$.

### 7.2.6 Summary of the Analyses

The analyses of the database for ship-ship collisions can be summarised as:

i. The non-dimensional penetration, $\overline{z}$, is uncorrelated with the non-dimensional damage location, $\overline{x}$

ii. The non-dimensional damage length, $\overline{y}$, is uncorrelated with the non-dimensional damage location, $\overline{x}$

iii. Only 5% of the penetrations are greater than $0.5 \cdot B$

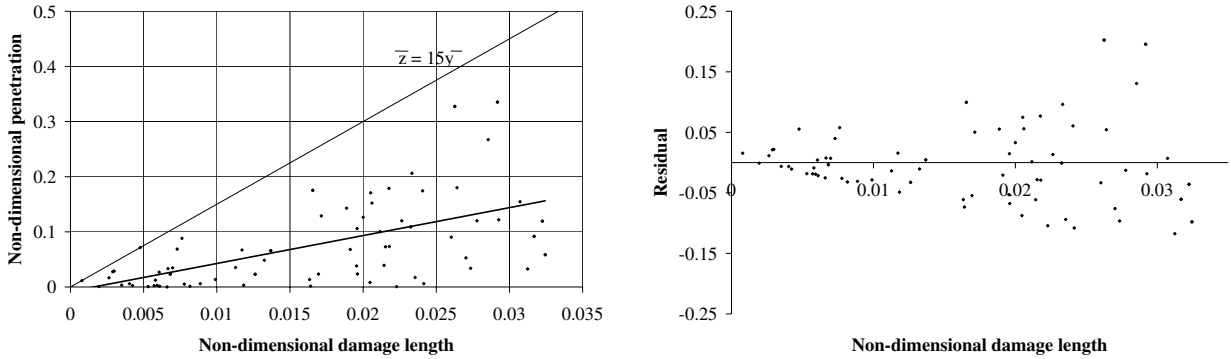


Figure 7.20: *Left: The non-dimensional damage length, $\overline{y}$, versus the non-dimensional penetration, $\overline{z}$, and the linear regression line. Right: The residual between observed data and the linear regression.*

iv. The largest damage length is observed to be $0.48 \cdot L$

v. The relation between the non-dimensional penetration, $\overline{z}$, and the non-dimensional damage length, $\overline{y}$, when the non-dimensional damage length is less than 0.033:
For a given non-dimensional damage length, $\overline{y}$, the non-dimensional penetration, $\overline{z}$, is less than $\overline{z} = 15\overline{y}$ in more than 90% of all cases. The analysis shows that although there is an increasing linear tendency between $\overline{z}$ and $\overline{y}$, the spread of the responses appears to increase as the non-dimensional damage length increases. As the scatter is spreading, it is not possible to determine a function, but just to indicate that the probability that the penetration is less than a given breadth $b$ becomes an increasing function of the relation between $b$ and the breadth of the vessel, $B$

vi. The relation between the non-dimensional penetration, $\overline{z}$, and the non-dimensional damage length, $\overline{y}$, when the non-dimensional damage length is greater than 0.033:
The non-dimensional damage length $\overline{y}$ is uncorrelated with the non-dimensional penetration $\overline{z}$

This page is intentionally left blank.

# Chapter 8

# Comparison of Results from Simulation and Observations

In this chapter the results from the numerical simulations in Chapter 6, regarding distribution of damage sizes, are compared to distributions obtained from the damage statistics analysed in Chapter 7. The damage sizes are treated separately as both the database analysis and the simulation show that these parameters are independent.

Only the results from the numerical analysis number 2 are compared with results from the observations. Analysis 2 includes all vessels in the world distribution of vessels except fishing vessels. A relation between struck and striking vessels is included, see Section 6.3.

**The Non-Dimensional Damage Location**
The ship collision probability model described in Sections 2.1.2 and 2.1.3 predicts a uniform distribution of the damage location. This is in agreement with the observed findings in Chapter 7.

**The Non-Dimensional Penetration, $\overline{z}$**
The probability density distribution and the cumulative density distribution for all analysed vessels are shown in Figure 8.1, database results are indicated by thicker lines. The 25-, 50- and 75-percentile values for the non-dimensional penetration versus the breadth of the struck vessel are shown in Figure 8.2. The figure shows results from both the simulation and the damage database. The agreement between the simulated results and the observed data is poor. The observed penetrations are significantly larger than the simulated results. A reason for this difference might be that the analysed vessels of a more recent date are based on a structural layout which absorbs the energy better, so that the result is smaller penetration. However, the main reason for the difference is probably that minor damages are not reported to either the authorities or the classification societies and are therefore not present in the damage database.

The frequency for the non-dimensional penetration of observed data is shown in Figure 8.3, here the total number of observed data from the database is 397. To test the hypothesis that

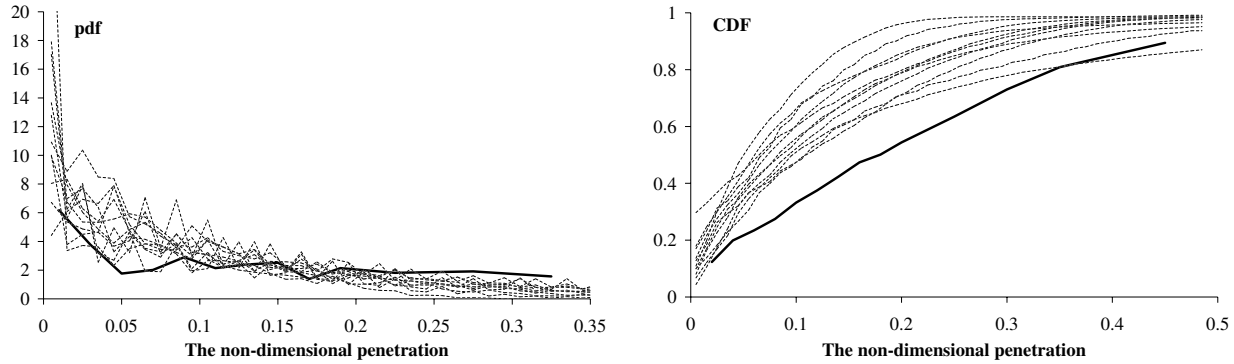


Figure 8.1: *Comparison of non-dimensional penetrations determined from simulation and observed data. Left: The probability density distribution. Right: The cumulative distribution. Simulation results are indicated by thin dotted lines.*

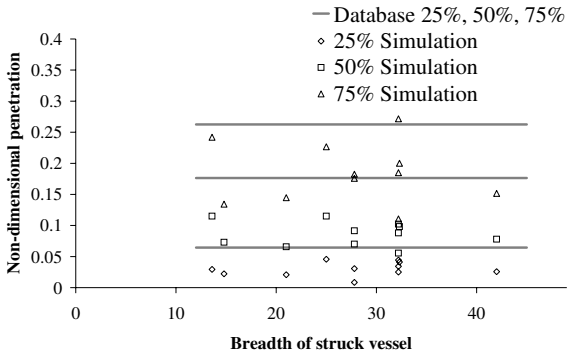


Figure 8.2: *The 25-, 50- and 75-percentile values for the non-dimensional penetration versus the breadth of the struck vessel. Regression lines for the three percentile values are shown.*

some smaller damages are not reported, the observed data can be augmented by inclusion of more minor damages to see if a fit to the simulated results can be achieved. It is here assumed that only non-dimensional penetrations smaller than 0.1 are not reported. The frequency for the penetrations smaller than $0.1B$ is now fitted to the average of the simulated data by a least-squared error method based on the cumulative distribution function. Figure 8.4 (left) shows the CDF for the non-dimensional penetration, simulated data represented by thin dotted lines, observed data by the thick dotted line and 'corrected' observed data by the full thick line. Figure 8.4 (right) shows the 25-, 50- and 75-percentile value for the non-dimensional penetration versus the breadth of the struck vessel. Regression lines for the three percentile values are shown by dotted lines, while the 'corrected' data from the database is shown by full lines. It is found from this analysis that, if the simulated results are right, only approx. 1/3 of the smaller penetration below $0.1B$ is reported and present in the database. This does not seem to be an unrealistic assumption.

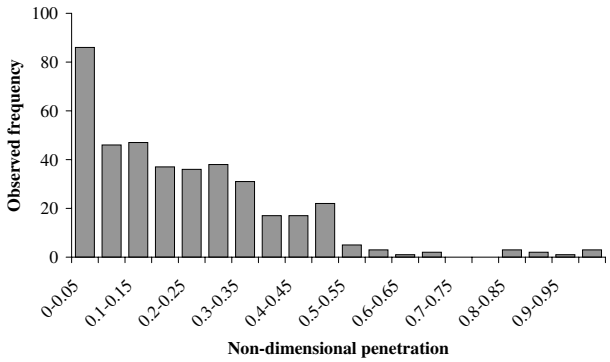


Figure 8.3: *The frequency of observed data for the non-dimensional penetration.*

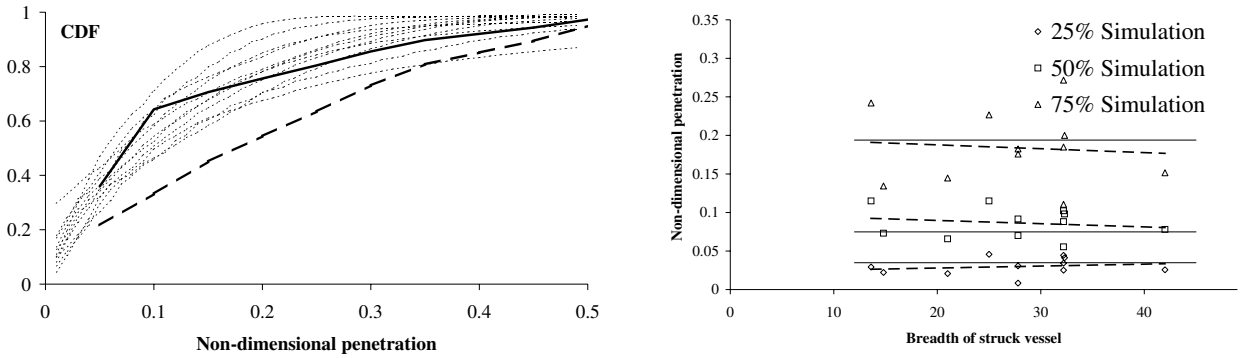


Figure 8.4: *Left: The CDF for the non-dimensional penetration, simulated data represented by thin dotted lines, observed data represented by the thick dotted line and 'corrected' observed data by the full thick line. Right: The 25-, 50- and 75-percentile values for the non-dimensional penetration versus the breadth of the struck vessel. Regression lines for the three percentile values are shown by dotted lines, the 'corrected' data from the database by full lines.*

**Non-Dimensional Damage Length, $\overline{y}$**

The probability density distribution and the cumulative density distribution for all analysed vessels are given in Figure 8.5, the Monte Carlo simulation results are represented by thin dotted lines. The 25-, 50- and 75-percentile values for the non-dimensional damage length versus the length of the struck vessel are shown in Figure 8.6,which gives results from both the simulation and the damage database. Figures 8.5 - 8.6 show good agreement between simulated results and observed data, but it should be noted that the simulated damage lengths are a little longer than the damage lengths obtained from the database analysis. The main reason for this difference is probably that the analysed vessels of more recent date have a higher velocity, which results in longer damages. The same difference can be seen in comparisons of damage lengths of tankers and other vessels. As the tankers are normally low velocity vessels the damage lengths are also smaller, see Section 7.2.3.

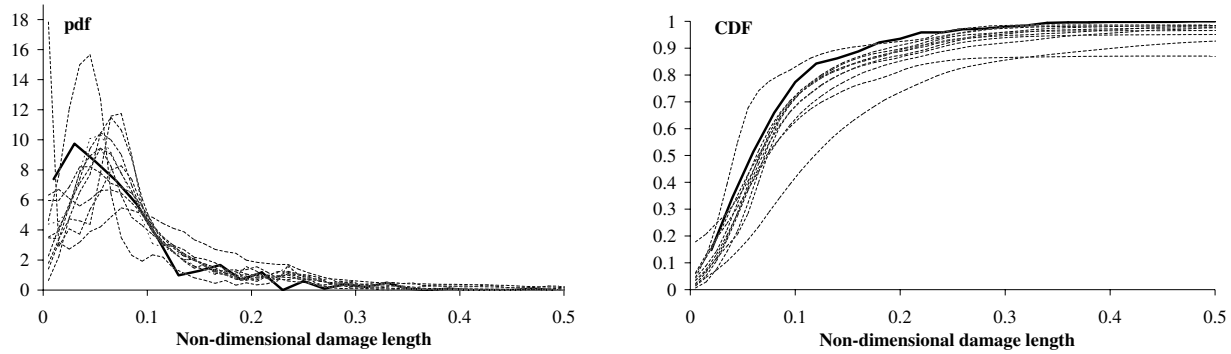


Figure 8.5: *Comparison of non-dimensional damage lengths determined from simulation and observed data. Left: The probability density distribution. Right: The cumulative distribution. Simulation results are indicated by thin dotted lines.*

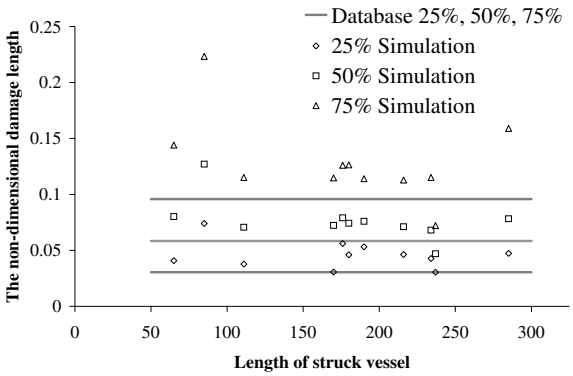


Figure 8.6: *The 25-, 50- and 75-percentile values for the non-dimensional damage length versus the length of the struck vessel. Results from both simulation and damage database. Regression lines for the three percentile values determined by simulation are shown.*

# Chapter 9

# Probabilistic Damage Stability Regulations

The International Maritime Organisation (IMO) is currently seeking to harmonise the damage stability regulation for all types of vessels using the probabilistic damage stability concept. Following the introduction of the probabilistic damage stability requirements of dry cargo ships, SOLAS Part B-1, IMO put on their work programme for harmonisation of all damage stability requirements in SOLAS using a probabilistic concept of survival. The main framework of these new harmonised regulations should follow the concept of SOLAS Part B-1, but include the main features of IMO Res. A.265 and the current deterministic regulations of SOLAS Chapter 8, also referred to as SOLAS 90.

The main concept of the current probabilistic damage stability regulations is the determination of a subdivision index, denoted $A$. The expression for $A$ consists of two parts, one describing the probability of damaging a particular section of the vessel, the other accounting for the probability of survival after flooding of the section. In general, the overall methodology and theory in the concept for Resolution A.264, is primarily based on the work performed by Wendel (1960) and Denis (1962).

This chapter will focus on the probability of damaging a particular section of the vessel. This can be separated into three individual factors $p$, $v$ and $r$. The factor $p$ accounts for the probability that only one compartment or a group of compartments is flooded, disregarding the horizontal and the longitudinal subdivision, $v$ concerns the horizontal subdivision and $r$ the longitudinal subdivision.

The chapter starts with a short introduction to the probabilistic damage stability calculation, including a list of the commonest terms and symbols.

In Section 9.2 a proposal for the $p-$factor is given. The current method for determination of $p$ is validated on the basis of the damage statistics analysed in Chapter 7. The damage

statistics, and not the simulation, is chosen for validation as the Monte Carlo based simulation presented in Chapter 6 shows a large variation in the results for different struck vessels. It is also decided to use the database with the reported data as it is, and not to include more minor damages. If these minor damages are not reported, they are assumed to be of less importance.

New functions to describe the non-dimensional damage location and the non-dimensional damage length are introduced and compared with functions used for current regulation and earlier international proposals. The section ends with a final proposal for the $p-$factor. Then a section on the $r-$factor follows. The theory for the $r-$factor approach is described in detail. In the following section the new proposals for the $p-$ and $r-$factors will be compared with current regulation by use of a small number of application examples. Determination of the factors $p$ and $r$ is based on methods described by Pawlowski (1996) and Jensen (2000). Section 9.5 deals with determination of the $v-$factor. Two proposals are presented. The first is based on analysis of the damage statistics, the second on the bow-height statistics.

In the last section a wide range of application examples is presented. The first example deals with the IMO-boxes, 11 different boxes with six different subdivisions are examined in detail regarding the $p$-, $r$-, and $v$-factors and the total attained subdivision index. Then three examples follow illustrating the attained index for two different vessels, a Ro-Ro ferry of a length of 64 m and a container vessel of a length of 190 m.

## 9.1 Introduction to Probabilistic Damage Stability

The philosophy behind the probabilistic damage stability concept is that two different ships with the same index of subdivision are of equally safe.

In order to develop the probabilistic concept of subdivision, it is assumed that the ship is damaged. Since the location and the size of the damage is random, it is not possible to state which part of the ship is flooded. However, the probability of flooding a space can be determined if the probability of occurrence of certain damages is known. The probability of flooding a space is equal to the probability of occurrence of all such damages, which just open the considered space. A space is a part of the volume of the ship which is bounded by undamaged watertight structural divisions.

Next, it is assumed that a particular space is flooded. In addition to some inherent geometrical characteristics of the ship, various other factors influence whether the ship can survive such flooding. They include the initial draught and GM, the permeability of the space and the weather conditions, all of which are random at the time the ship is damaged. Provided that the limiting combinations of the aforementioned variables and the probability of their occurrence are known, the probability that the ship will not capsize or sink, with the considered space flooded, can be determined.

The main concept of the current probabilistic damage stability regulations is the determination of a subdivision index $A$ expressed by the formula

$$A = \sum p_i \cdot s_i \cdot v_i$$

where

$i$ represents each compartment or group of compartments under consideration

$p_i$ accounts for the probability that only one compartment or a group of compartments is flooded, disregarding the horizontal subdivision

$s_i$ accounts for the probability of survival after flooding the compartment or group of compartments under consideration

$v_i$ is the probability that the space above a horizontal subdivision will not be flooded

If wing compartments are fitted, the $p$-factor shall be obtained by multiplying by a factor $r$ for a wing compartment and multiplying by $(1 - r)$ for simultaneous flooding of the wing tank and adjacent inboard compartment.

The attained index $A$ shall not be taken less than a required index $R$. For dry cargo vessels the required index is today only a function of the length of the struck vessel, whereas the index for passenger vessels is a function of the length of the vessel, the number of persons whom the vessel is permitted to carry and the number of persons for whom lifeboats are provided.

$$A = \sum p_i \cdot s_i \cdot v_i > R$$

In order to prepare the calculation of the index $A$ the length of the ship is divided into a fixed discrete number of damage zones. The triangle in Figure 9.1 illustrates the possible single- and multiple zone damages in a ship with watertight arrangement suitable for a seven zone division. The triangles at the bottom line indicate single zone damages and the parallelograms indicate combinations of adjacent damages.

**List of Symbols Used in This Chapter**

$\overline{x}$ The non-dimensional damage location, $\overline{x} = \frac{x}{L}$, where $x$ is the longitudinal position and $L$ the length of the vessel

$\overline{y}$ The non-dimensional damage length, $\overline{y} = \frac{y}{L}$, where $y$ is the damage length and $L$ the length of the vessel

$\overline{z}$ The non-dimensional penetration, $\overline{z} = \frac{z}{B}$, where $z$ is the penetration and $B$ the breadth of the vessel

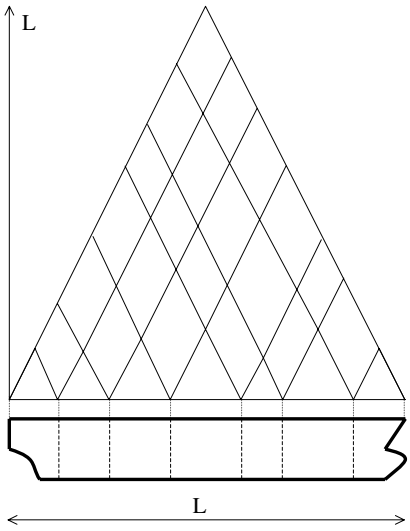


Figure 9.1: *Figure illustrating the possible single and multiple zone damages.*

$\overline{x_1}$ The non-dimensional distance from the aft terminal of $L$ to the aftermost position of the compartment being considered

$\overline{x_2}$ The non-dimensional distance from the aft terminal of $L$ to the foremost position of the compartment being considered

$J$ The non-dimensional length of the considered compartment or compartments ($J = \overline{x_2} - \overline{x_1}$)

## 9.2 Determination of the $p$-Factor

The factor $p$, which accounts for the probability that only the compartment or group of compartments under consideration is flooded, can be determined as

$$p = \int f(\overline{x}, \overline{y}) d\overline{x} d\overline{y}$$

where $f(\overline{x}, \overline{y})$ is the joint probability density function of the non-dimensional damage location and the non-dimensional damage length. In the analyses in Sections 6 and 7 it was found that the non-dimensional damage location, $\overline{x}$, and the non-dimensional damage length, $\overline{y}$, can be considered as independent parameters. Therefore, the joint probability density function $f(\overline{x}, \overline{y})$ can be written

$$f(\overline{x}, \overline{y}) = a(\overline{x}) b(\overline{y})$$

In the following, the non-dimensional damage location and the non-dimensional damage length are analysed. Functions from existing regulations and earlier proposals are shown together with the analysed data.

Proposals for the damage distributions are based on data from the updated database described in Section 7. When functions are fitted to the discrete distributions for the non-dimensional damage location and the non-dimensional damage length, some considerations must be made. In general, the distribution functions can be separated into two main categories: a) general statistical distributions, e.g. a log-normal distribution or b) very simple linear or piecewise linear distributions. The advantage of the general statistical distributions is that the functions are normally easy to fit to the discrete distributions, but truncation problems make the calculation more difficult. The linear distribution is the simple solution used in the present damage stability regulation. This distribution is easy to use in calculations and due to the statistical uncertainty of the data from the damage database, it seems reasonable to choose the simple functions even though the accuracy may be smaller. Examples and comparison of both methods will be presented in this section.

**The Non-Dimensional Damage Location** $a(\overline{x})$
Collisions forward of the collision bulkhead are neglected, see Section 7.1.
Data points 610

Data from the old database and the updated database is shown in Figure 9.2 (left). The distribution from SOLAS part B-1 and a proposal from SLF 43/3/2 are also shown.

$$\text{SOLAS B1:} \quad a(\overline{x}) = \begin{cases} 0.4 + 1.6 \cdot \overline{x} & \text{for} \quad \overline{x} \leq 0.5 \\ 1.2 & \text{for} \quad \overline{x} > 0.5 \end{cases}$$

$$\text{SLF 43/3/2:} \quad a(\overline{x}) = 0.6 + 0.8 \cdot \overline{x}$$

The distribution for damage location used for tankers, described in MARPOL IMO (1995), is a uniform distribution along the length of the struck vessel: $a(\overline{x}) = 1$. This function is not shown in the diagram.

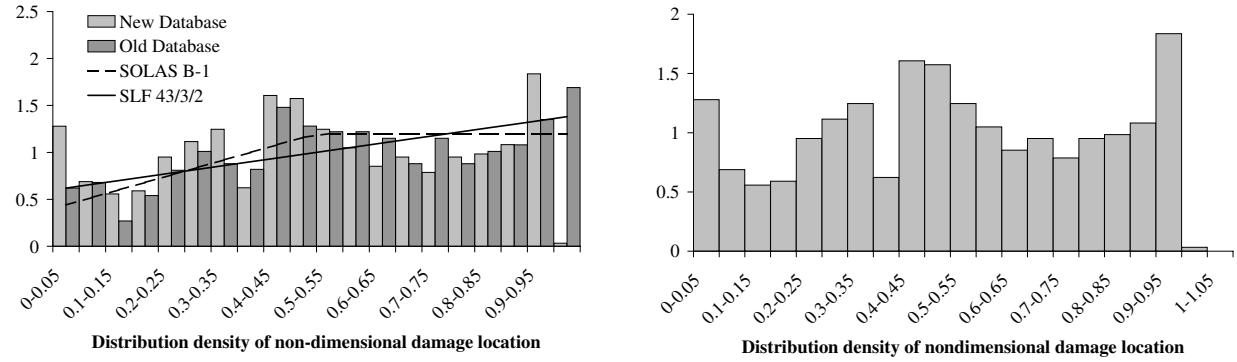


Figure 9.2: *Distribution density of the non-dimensional damage location, $\overline{x}$. Only data from the new damage database is shown in the right diagram.*

In Figure 9.2 (right) the distribution density of the non-dimensional damage location is shown for data from the new database only. The tendency from both the regulations and

the proposal from SLF 43/3/2 where the likelihood of damage seems to be greater towards the forward half of the vessel is not seen for the updated database. Many collisions seem to occur in the middle of the struck vessel but also stern and bow collisions are seen.

Different functions have been used to describe the non-dimensional damage location. In Figure 9.3 the observed results from the database are shown together with two proposals, a piecewise-linear function and a Weibull distribution. Figure 9.3 also shows the distributions for a uniform distribution and the current SOLAS regulations. The proposals are fitted to the data by a least squared error method based on the cumulative distribution function.

The different functions may be compared by summation of the relative errors:

$$error = \sum \frac{|F(\overline{x}) - D(\overline{x})|}{D(\overline{x})}$$

where $F$ is the current function and $D$ results observed from the database.

| | Bi-linear | Linear | Weibull | SOLAS | Uniform |
|---|---|---|---|---|---|
| *error* | 1.11 | 1.51 | 2.80 | 4.08 | 1.59 |

The table shows that the best fit is the bi-linear function, but as the difference in the relative error for the bi-linear function and the linear function is small, it is decided to make two proposals, one using the bi-linear and the other the linear function. The linear function is by optimisation found to be: $a(\overline{x}) = 0.065 \cdot \overline{x} + 0.968$, which is very close to a uniform distribution. A uniform distribution is therefore chosen for the linear proposal as this makes the rules easier to implement later on.

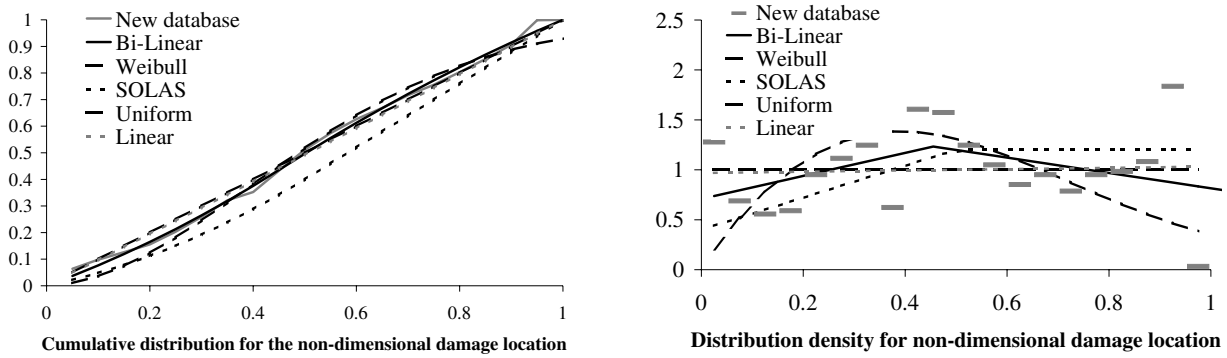


Figure 9.3: *Cumulative and density distributions of the non-dimensional damage location, $\overline{x}$, for various functions.*

**The Non-Dimensional Damage Length $b(\overline{y})$**
Data points: 508

Data from the old database and the updated database is presented in Figure 9.4 where also the distribution from SOLAS part B-1 is included. The diagram shows that neither the old

dataset nor the new dataset is described well by the regulation in SOLAS.

SOLAS part B-1: $b(\overline{y}) = \frac{2}{J_m}\left(1 - \frac{\overline{y}}{J_m}\right)$ where $J_m$ is the maximum non-dimensional damage length: $J_m = \frac{48}{L}$, but not greater than 0.24

This means that the distribution described in SOLAS depends on the length of the struck vessel, which is in contrast to the findings in Section 7.

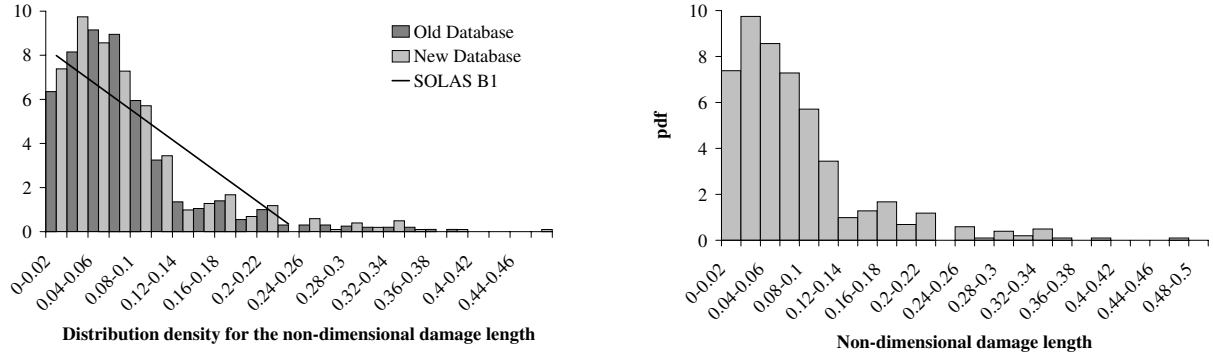


Figure 9.4: *Distribution density for the non-dimensional damage length, $\overline{y}$. Right diagram shows new data only.*

Different functions have been used to describe the non-dimensional damage length. In Figure 9.5 the observed results from the database are shown together with two proposals, one using a bi-linear function and one the Weibull distribution. The distributions from the current SOLAS regulations are also shown in Figure 9.5. The proposals are fitted to the data by a least squared error method based on the cumulative distribution function.

The different functions are compared by summation of the relative errors:

| | Bi-linear | Weibull | SOLAS | Bi-linear* |
|---|---|---|---|---|
| *error* | 0.62 | 0.51 | 1.05 | 0.67 |

Two bi-linear functions are included in the table. The bi-linear* function is, as the other functions, optimised by a least-squared error method, but with the constraints that the parameters must be described by fractions and that the integrated function must be exactly equal to one. The table shows that the best fit is the Weibull distribution, but it is not significantly better than the bi-linear functions. It is here decided to use the bi-linear function, as this will be easy to implement in a proposal for new regulations. The bi-linear and not a one-piece linear function is chosen as it is assumed to be important to keep track of the larger damages.

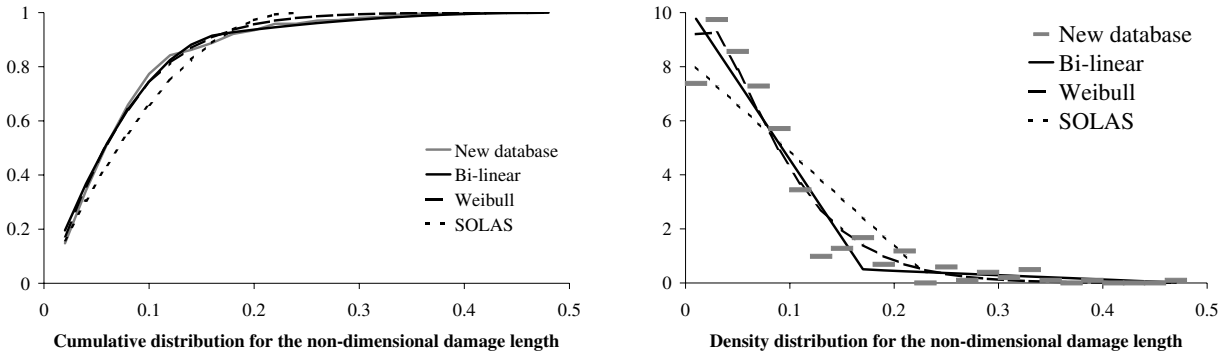


Figure 9.5: *Cumulative and density distributions of the non-dimensional damage length, $\overline{y}$, for various functions.*

### 9.2.1 New Proposals for Parameters Describing the $p$–Factor

Two proposals for determination of the factor $p$, which accounts for the probability that only the compartment or group of compartments under consideration may be flooded, will in the following be presented.

1. The non-dimensional damage length and the non-dimensional damage location are both given as bi-linear functions
2. The non-dimensional damage length is given as a bi-linear function, whereas the non-dimensional damage location is assumed to be uniformly distributed along the length of the struck vessel

The function for the non-dimensional damage location $a(\overline{x})$ is taken to be

$$a(\overline{x}) = \begin{cases} a_1(\overline{x}) = a_{11} \cdot \overline{x} + a_{12} & \text{for} \quad \overline{x} \leq \overline{x_k} \\ a_2(\overline{x}) = a_{21} \cdot \overline{x} + a_{22} & \text{for} \quad \overline{x} > \overline{x_k} \end{cases}$$

where $\overline{x_k}$ is the knuckle point between $a_1(\overline{x})$ and $a_2(\overline{x})$. The parameters $a_{11}$, $a_{12}$, $a_{21}$ and $a_{22}$ must satisfy the conditions that the function is continuous over $\overline{x_k}$ and that the integration along the length of the vessel equals one.

$$\int_0^1 a(\overline{x}) dx = 1$$

In analogy to the definition of $a(\overline{x})$ the function for the distribution of the non-dimensional damage length $b(\overline{y})$ is taken to be

$$b(\overline{y}) = \begin{cases} b_1(\overline{y}) = b_{11} \cdot \overline{y} + b_{12} & \text{for} \quad \overline{y} \leq J_k \\ b_2(\overline{y}) = b_{21} \cdot \overline{y} + b_{22} & \text{for} \quad \overline{y} > J_k \end{cases}$$

where $J_k$ is the knuckle point between $b_1(\overline{y})$ and $b_2(\overline{y})$. The parameters $b_{11}$, $b_{12}$, $b_{21}$ and $b_{22}$ must satisfy the condition that the function is continuous over $J_k$. Furthermore, the integration from zero to the maximum non-dimensional damage length to be expected, $J_m$, must be equal to one.

$$\int_0^{J_m} b(\overline{y})dy = 1$$

The parameters for the non-dimensional damage location, $a(\overline{x})$, are by optimisation determined as

| | $\overline{x_k}$ | $a_{11}$ | $a_{12}$ | $a_{21}$ | $a_{22}$ |
|---|---|---|---|---|---|
| Proposal 1 | 0.455 | 1.154 | 0.708 | -0.768 | 1.583 |
| Proposal 2 | 1 | 0 | 1 | 0 | 0 |

The parameters for the non-dimensional damage length, $b(\overline{y})$, are by optimisation determined as

| | $J_k$ | $J_m$ | $b_{11}$ | $b_{12}$ | $b_{21}$ | $b_{22}$ |
|---|---|---|---|---|---|---|
| Bi-linear | 0.170 | 0.48 | -57.894 | 10.350 | -1.602 | 0.769 |
| Bi-linear* | $\frac{1}{6}$ | $\frac{1}{2}$ | $-\frac{60}{1}$ | $\frac{21}{2}$ | $-\frac{3}{2}$ | $\frac{3}{4}$ |

Integration of $b(\overline{y})$ using the bi-linear function from zero to $J_m$ will result in a small error of the size +1.3% due to rounding numbers during the optimisation, whereas integration of the bi-linear* function exactly equals one.

### 9.2.2 Integrations for Determination of the $p$-factor

From the joint probability function $f(\overline{x},\overline{y}) = a(\overline{x})b(\overline{y})$, the probability $p$ that only the compartment or the compartments bounded by $\overline{x_1}$ and $\overline{x_2}$ ($\overline{x_1} < \overline{x_2}$) are damaged can be taken to be

$$p = \int b(\overline{y}) \int a(\overline{x})d\overline{x}d\overline{y}$$

For calculation of the $p$-factor it is chosen to treat forward, aft and inside compartments by separate procedures. The probability of only damaging the forward or the aft compartment will be calculated by use of Figures 9.7 and 9.8, whereas all inside compartments are treated according to Figure 9.6. The advantage of this model is that the probability of damaging the compartment in a single-compartment vessel becomes one. But using this model or using the same methods for all compartments is of less importance as the compartments fore and aft are normally very small.

**Inside Compartments**

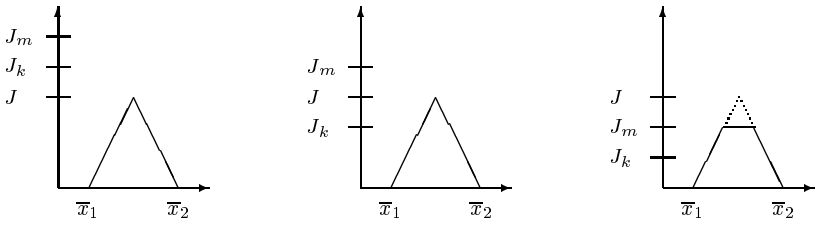


Figure 9.6: *Area of integration to obtain the probability p that only one inside compartment is damaged.*

The area of integration to obtain the probability $p$ for the inside compartments is illustrated in Figure 9.6. The left diagram illustrates the situation where the considered length, $J = \overline{x_2} - \overline{x_1}$, is smaller than both the knuckle point, $J_k$, and the maximum non-dimensional damage length to be expected, $J_m$. The middle diagram illustrates a length between $J_k$ and $J_m$ and the right diagram a situation of a length greater than both $J_k$ and $J_m$. The boundaries for the integration are between $\overline{x_1}$ and $\overline{x_2}$ and the minimum value of $J$ and $J_m$.

Proposal 1 (Two bi-linear functions)
Three different cases for the location of damage and the placement of the knuckle points, $\overline{x_k}$ and $J_k$, must be considered. The cases can be described by the matrix in Table 9.1. The midpoint of the compartment is denoted $\overline{x_m}$.

Table 9.1: *Integration overview for inside compartments.*

| | Aft part of vessel $\overline{x_2} \leq \overline{x_k}$ | Damage over mid-length of vessel $\overline{x_1} \leq \overline{x_k} < \overline{x_2}$ | | Forward part of vessel $\overline{x_1} > \overline{x_k}$ |
|---|---|---|---|---|
| | | $\overline{x_k} \leq \overline{x_m}$ $J' = 2(\overline{x_k} - \overline{x_1})$ | $\overline{x_k} > \overline{x_m}$ $J' = 2(\overline{x_2} - \overline{x_k})$ | |
| $J \leq J_k$ | $i1)$ | $i5)$ | $i8)$ | $i3)$ |
| $J > J_k$ $J' \leq J_k$ | $i2)$ | $i6)$ | $i9)$ | $i4)$ |
| $J > J_k$ $J' > J_k$ | | $i7)$ | $i10)$ | |

The expressions for the cases $i1) - i10)$ in Table 9.1 can be seen in Appendix E.

Proposal 2 (One bi-linear and one linear function)
The problem is separated into two: the length of the damaged room, $J$, less than or longer than $J_k$:

$$J \leq J_k \qquad p = \int_0^J b_1 \int_{\overline{x_1}+\frac{\overline{y}}{2}}^{\overline{x_2}-\frac{\overline{y}}{2}} a \; d\overline{x}d\overline{y}$$

$$J > J_k \qquad p = \int_0^{J_k} b_1 \int_{\overline{x_1}+\frac{\overline{y}}{2}}^{\overline{x_2}-\frac{\overline{y}}{2}} a \; d\overline{x}d\overline{y} + \int_{J_k}^{\min(J,J_m)} b_2 \int_{\overline{x_1}+\frac{\overline{y}}{2}}^{\overline{x_2}-\frac{\overline{y}}{2}} a \; d\overline{x}d\overline{y}$$

**Forward Compartment**

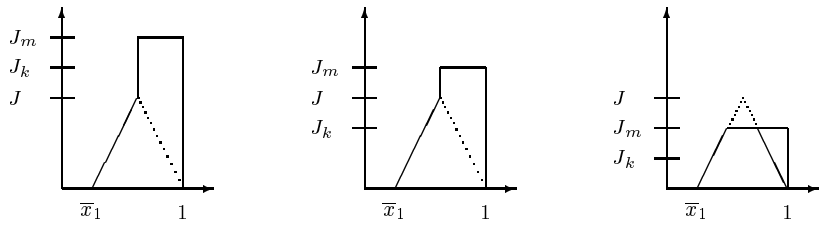


Figure 9.7: *Area of integration to obtain the probability p that only the forward compartment is damaged.*

The area of integration to obtain the probability $p$ is illustrated in Figure 9.7. The boundaries for the forward compartment are given by $\overline{x_2} = 1$, $\overline{x_1} = 1 - J$ and the minimum value of $J$ and $J_m$.

Proposal 1 (Two bi-linear functions)
Two different cases for location of damage and placement of the knuckle points $\overline{x_k}$ and $J_k$ must be considered. The cases can be described by the matrix in Table 9.2. The midpoint of the compartment has the position $1 - J/2$.

Table 9.2: *Integration overview for forward compartments.*

| | Forward of knuckle point $\overline{x_1} > \overline{x_k}$ | Knuckle point in compartment $\overline{x_1} \leq \overline{x_k}$ | |
|---|---|---|---|
| | | $\overline{x_k} \leq 1 - J/2$ | $\overline{x_k} > 1 - J/2$ |
| $J \leq J_k$ | $f1)$ | $f3)$ | $f6)$ |
| $J > J_k$ $2(\overline{x_k} - \overline{x_1}) \leq J_k$ | $f2)$ | $f4)$ | $f7)$ |
| $J > J_k$ $2(\overline{x_k} - \overline{x_1}) > J_k$ | | $f5)$ | |

The expressions for the cases $f1) - f7)$ in Table 9.2 can be seen in Appendix E.

Proposal 2 (One bi-linear and one linear function)
The problem is separated into two: the length of the damaged room, $J$, less than or longer than $J_k$:

$$J \leq J_k \quad p = \int_0^J b_1 \int_{\overline{x_1}+\frac{\overline{y}}{2}}^1 a \; d\overline{x}d\overline{y} + \int_J^{J_k} b_1 \int_{1-\frac{J}{2}}^1 a \; d\overline{x}d\overline{y} + \int_{J_k}^{J_m} b_2 \int_{1-\frac{J}{2}}^1 a \; d\overline{x}d\overline{y}$$

$$J > J_k \quad p = \int_0^{J_k} b_1 \int_{\overline{x_1}+\frac{\overline{y}}{2}}^1 a \; d\overline{x}d\overline{y} + \int_{J_k}^{\min(J,J_m)} b_2 \int_{\overline{x_1}+\frac{J}{2}}^{1-\frac{J}{2}} a \; d\overline{x}d\overline{y} + \int_{J_k}^{J_m} b_2 \int_{1-\frac{J}{2}}^1 a \; d\overline{x}d\overline{y}$$

**Aft Compartment**

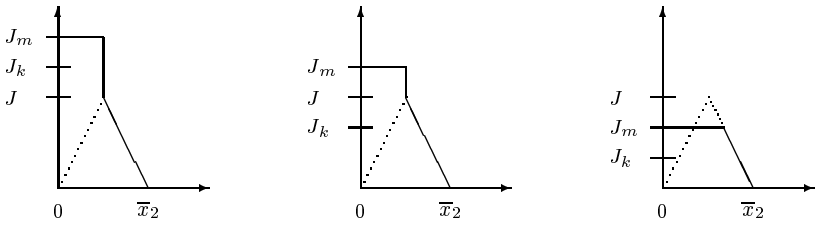


Figure 9.8: *Area of integration to obtain the probability p that only the aft compartment is damaged.*

The area of integration to obtain the probability $p$ is illustrated in Figure 9.8. The boundaries for the aft compartment are given by $\overline{x_2} = J$, $\overline{x_1} = 0$ and the minimum value of $J$ and $J_m$.

Proposal 1 (Two bi-linear functions)
Two different cases for location of damage related to the knuckle points $\overline{x_k}$ and $J_k$ must be considered. The cases can be described by the matrix in Table 9.3. The midpoint of the compartment has the position $J/2$.

Table 9.3: *Integration overview for aft compartments.*

| | Aft of knuckle point $\overline{x_k} > \overline{x_2}$ | Knuckle point in compartment $\overline{x_2} \geq \overline{x_k}$ | |
|---|---|---|---|
| | | $\overline{x_k} \leq J/2$ | $\overline{x_k} > J/2$ |
| $J \leq J_k$ | $a1)$ | $a3)$ | $a5)$ |
| $J > J_k$ $2(J - \overline{x_k}) \leq J_k$ | $a2)$ | $a4)$ | $a6)$ |
| $J > J_k$ $2(J - \overline{x_k}) > J_k$ | | | $a7)$ |

The expressions for the cases $a1) - a7)$ in Table 9.2 can be seen in Appendix E.

Proposal 2 (One bi-linear and one linear function)
The problem is separated into two: the length of the damaged room, $J$, less than or longer than $J_k$:

$$J \leq J_k \qquad p = \int_0^J b_1 \int_0^{J-\frac{\overline{y}}{2}} a \; d\overline{x}d\overline{y} + \int_J^{J_k} b_1 \int_0^{\frac{J}{2}} a \; d\overline{x}d\overline{y} + \int_{J_k}^{J_m} b_2 \int_0^{\frac{J}{2}} a \; d\overline{x}d\overline{y}$$

$$J > J_k \qquad p = \int_0^{J_k} b_1 \int_0^{J-\frac{\overline{y}}{2}} a \; d\overline{x}d\overline{y} + \int_{J_k}^{\min(J,J_m)} b_2 \int_{\frac{J}{2}}^{J-\frac{\overline{y}}{2}} a \; d\overline{x}d\overline{y} + \int_{J_k}^{J_m} b_2 \int_0^{\frac{J}{2}} a \; d\overline{x}d\overline{y}$$

**Vessel with Only One Compartment**
The probability $p$ that the compartment is damaged is equal to one.

### 9.2.3 The Final Proposal for the $p$-Factor

It is decided, for the final proposal for the $p$-factor, to describe the non-dimensional damage location by a uniform distribution along the length of the struck vessel. The formulation for $p$ is therefore also identical for compartments where the limit of the compartment coincides with either the forward terminal or with the aft terminal. The bi-linear* function is chosen for the non-dimensional damage length:

$$a(\overline{x}) = 1$$

$$b(\overline{y}) = \begin{cases} b_1(\overline{y}) = \frac{1}{2}(-120 \cdot \overline{y} + 21) & \text{for} \quad \overline{y} \leq \frac{1}{6} \\ b_2(\overline{y}) = \frac{1}{4}(-6 \cdot \overline{y} + 3) & \text{for} \quad \frac{1}{6} < \overline{y} \leq \frac{1}{2} \end{cases}$$

The probability $p$ for cases where limits of neither compartment nor group of compartments under consideration coincide with the aft or the forward terminals:

$$J \leq \left(J_k = \frac{1}{6}\right) \qquad p_{i1} = \frac{1}{6}J^2(b_{11}J + 3b_{12})$$

$$= -10 \cdot J^3 + \frac{21}{4} \cdot J^2$$

$$J > \left(J_k = \frac{1}{6}\right) \qquad p_{i2} = -\frac{1}{3}b_{11}J_k^3 + \frac{1}{2}(b_{11}J - b_{12})J_k^2 + Jb_{12}J_k - \frac{1}{3}b_{21}(J_n^3 - J_k^3)$$

$$+ \frac{1}{2}(b_{12}J - b_{22})(J_n^2 - J_k^2) + b_{22}J(J_n - J_k)$$

$$= -\frac{13}{288} + \frac{13}{16} \cdot J + \frac{1}{2} \cdot J_n^3 - \frac{3}{4} \cdot J \cdot J_n^2 - \frac{3}{8} \cdot J_n^2 + \frac{3}{4} \cdot J \cdot J_n$$

The probability $p$ for cases where the forward limit of the compartment or group of compartments under consideration coincides with the forward terminal - or - where the aft limit of the compartment or group of compartments under consideration coincides with the aft

terminal:

$$J \leq \left(J_k = \frac{1}{6}\right) \quad p_{af} = -\frac{1}{6}b_{11}J^3 + \frac{1}{4}(2b_{11}J - b_{12})J^2 - \frac{1}{4}b_{11}J(J^2 - J_k^2)$$
$$- \frac{1}{2}b_{12}J(J - J_k) + \frac{1}{4}b_{21}J(J_m^2 - J_k^2) + \frac{1}{2}b_{22}J(J_m - J_k)$$
$$= \frac{1}{2}(p_{i1} + J)$$

$$J > \left(J_k = \frac{1}{6}\right) \quad p_{af} = -\frac{1}{6}b_{11}J_k^3 + \frac{1}{4}(2b_{11}J - b_{12})J_k^2 + Jb_{12}J_k - \frac{1}{6}b_{21}(J_n^3 - J_k^3)$$
$$+ \frac{1}{4}(b_{12}J - b_{22})(J_n^2 - J_k^2) + \frac{1}{2}b_{22}J(J_n - J_k) + \frac{1}{4}b_{21}J(J_m^2 - J_k^2)$$
$$+ \frac{1}{2}b_{22}J(J_m - J_k)$$
$$= \frac{1}{2}(p_{i2} + J)$$

Where the compartment considered extends over the entire ship's length:

$$p = 1$$

For all the above expressions are $J_n$ defined as $\min(J, J_m)$, where $J$ is the length of the considered compartment ($J = \overline{x_2} - \overline{x_1}$) and $J_m$ is the largest expected non-dimensional damage length ($J_m = \frac{1}{2}$).

## 9.3 Determination of the $r$-Factor

When combined subdivision is dealt with, the main problem is determination of the probability $r$ that a penetration is less than a given transverse breadth $b$. This factor can be determined as

$$r = \int f(\overline{x}, \overline{y}, \overline{z}) d\overline{x} d\overline{y} d\overline{z}$$

where $f = f(\overline{x}, \overline{y}, \overline{z})$ is the joint probability function of the non-dimensional damage location, the non-dimensional damage length and the non-dimensional penetration.

The observations described in paragraph (v) in Section 7.2.6 imply that, given a transverse breadth $b$ of the compartment, the probability $r$ that the penetration is less than $b$ becomes an increasing function of $b/B$ for non-dimensional damage lengths less than 0.033:

$$r = r\left(\frac{b}{B}\right) \qquad \text{and} \qquad \frac{\partial r}{\partial\left(\frac{b}{B}\right)} > 0$$

Furthermore, it must be required for the factor $r$ that

$r \rightarrow 0$ for $b/B \rightarrow 0$ and $0 \leq r \leq 1$

Damage penetrations through the centre line are very unlikely see paragraph (iii) in Section 7.2.6. As a result of this and since the vessel is assumed to be symmetrical it should be expected that

$$r = r\left(\frac{b}{B} = \frac{1}{2}\right) = 1 \qquad \text{and} \qquad \frac{b}{B} \in \left[0; \frac{1}{2}\right]$$

by use of the observations from the analyses in Sections 7.2.5 and 7.2.6, the probability of damaging only a wing tank of the breadth $b$, $p \cdot r$ can be written as

$$p \cdot r = \int b(\overline{y}) \int a(\overline{x}) \int_0^{J_b} c(\overline{z}|\overline{y}) d\overline{z} d\overline{x} d\overline{y}$$

where $J_b$ is equal to $\frac{b}{15B}$ and $c(\overline{z}|\overline{y})$ is the conditional probability function of the non-dimensional penetration, $\overline{z}$, given the non-dimensional damage length, $\overline{y}$. The corresponding conditional probability distribution function is defined by

$$C(\overline{z}|\overline{y}) = \int_0^{\overline{z}} c(\overline{z}|\overline{y}) d\overline{z}$$

From the paragraphs (v) and (vi) in Section 7.2.6, it can be concluded that the function $C(\overline{z}|\overline{y})$ must depend on $\overline{y}$ so that

$$C(\overline{z}|\overline{y}) = \begin{cases} 1 & \text{for} \quad \overline{y} \leq \frac{\overline{z}}{15} \\ C(\overline{z}) & \text{for} \quad \overline{y} > \frac{\overline{z}}{15} \end{cases}$$

The expression for $p \cdot r$ can now be written

$$p \cdot r = \int_0^{J_b} b(\overline{y}) \int a(\overline{x}) d\overline{x} d\overline{y} + C\left(\frac{b}{B}\right) \int_{J_b} b(\overline{y}) \int a(\overline{x}) d\overline{x} d\overline{y}$$

and the probability $r$ that the penetration is less than the breadth of the wing tank $b$ can be written as

$$r = \frac{p \cdot r}{p} = 1 - \left[1 - C\left(\frac{b}{B}\right)\right] \cdot \left[1 - \frac{G}{p}\right]$$

where $G$ is defined by

$$G = \int_0^{J_b} b(\overline{y}) \int a(\overline{x}) d\overline{x} d\overline{y}$$

The factor $p$ is the probability that this particular compartment, disregarding the longitudinal subdivision, is damaged (see Section 9.2).

When the integration is carried out, the position of the knuckle point, $J_k$, in the expression for the non-dimensional damage length must be considered. The $G$ function can be expressed as

$$J_b \leq J_k \qquad G = \int_0^{J_o} b_1(\overline{y}) \int a(\overline{x}) d\overline{x} d\overline{y}$$

$$J_b > J_k \qquad G = \int_0^{J_k} b_1(\overline{y}) \int a(\overline{x}) d\overline{x} d\overline{y} + \int_{J_k}^{J_o} b_2(\overline{y}) \int a(\overline{x}) d\overline{x} d\overline{y}$$

where $J_o$ is $\min(J_b, J)$.
The integration of the non-dimensional damage location $a(\overline{x})$ must be considered as in Section 9.2.

If the non-dimensional damage location is described by a uniform distribution along the length of the struck vessel and the non-dimensional damage length as a bi-linear function like proposal 2 from Section 9.2, the $G$-function can be described as:

**Inside Compartment**

$$J_b \leq J_k \qquad G = \int_0^{\min(J_b, J)} b_1 \int_{\overline{x_1}+\frac{\overline{y}}{2}}^{\overline{x_2}-\frac{\overline{y}}{2}} a \; d\overline{x} d\overline{y}$$

$$J_b > J_k \qquad G = \int_0^{J_k} b_1 \int_{\overline{x_1}+\frac{\overline{y}}{2}}^{\overline{x_2}-\frac{\overline{y}}{2}} a \; d\overline{x} d\overline{y} + \int_{J_k}^{\min(J_b, J, J_m)} b_2 \int_{\overline{x_1}+\frac{\overline{y}}{2}}^{\overline{x_2}-\frac{\overline{y}}{2}} a \; d\overline{x} d\overline{y}$$

**Forward or Aft Compartments**
As the non-dimensional damage location is assumed to be uniformly distributed along the length of the vessels, the formulation of the function $G$ must be identical for forward and aft compartments. Therefore only the formulation for the aft compartment is given:

$$J_b \leq J_k \qquad G = \int_0^{\min(J_b, J)} b_1 \int_0^{J-\frac{\overline{y}}{2}} a \; d\overline{x} d\overline{y} + \int_{\min(J_b, J)}^{J_b} b_1 \int_0^{\frac{J}{2}} a \; d\overline{x} d\overline{y}$$

$$J_b > J_k \qquad G = \int_0^{J_k} b_1 \int_0^{J-\frac{\overline{y}}{2}} a \; d\overline{x} d\overline{y} + \int_{J_k}^{\min(J_b, J, J_m)} b_2 \int_{\frac{J}{2}}^{J-\frac{\overline{y}}{2}} a \; d\overline{x} d\overline{y}$$
$$+ \int_{J_k}^{\min(J_b, J_m)} b_2 \int_0^{\frac{J}{2}} a \; d\overline{x} d\overline{y}$$

**The Compartment Extending over the Entire Ship's Length**

$$J_b \leq J_k \qquad G = \int_0^{J_b} b_1 \int_0^1 a \; d\overline{x} d\overline{y}$$

$$J_b > J_k \qquad G = \int_0^{J_k} b_1 \int_0^1 a \; d\overline{x} d\overline{y} + \int_{J_k}^{J_b} b_2 \int_0^1 a \; d\overline{x} d\overline{y}$$

### 9.3.1 Final Proposal for the $G$-Function

With respect to the final proposal for the $G-$function, the non-dimensional damage location is described by a uniform distribution along the length of the struck vessel. The formulation for $p$ is therefore also identical for compartments where the limit of the compartment coincides with either the forward terminal or the aft terminal. The bi-linear* function is chosen for the non-dimensional damage length, see Section 9.2.3.

The function $G$ must be examined in more detail. The upper limit of $J_b$ has a maximum of 0.033 as $b/B$ is always less than 0.5. The maximum value for the non-dimensional damage length $J_m$ is larger: 0.24 for the current regulation and 0.5 for the new proposal, therefore it will here be assumed that $J_m$ is always larger than $J_b$. Thus $\min(J, J_b, J_m)$=$\min(J, J_b)$. Furthermore, the factor $r$ will for $J$ greater than $J_b$ be equal to one, see the analysis on the non-dimensional damage length versus the non-dimensional penetration in Section 7.2.5, which means that $\min(J, J_b)$ can be taken as $J_b$ in the formulation for $r$.

The knuckle point $J_k$ is in the new proposal defined to be equal to $\frac{1}{6}$, i.e. $J_b$ will always be smaller than $J_k$. The expressions for the function $G$ can now be simplified.

The function $G$ for cases where the compartment considered extends over the entire ship's length is determined as

$$\begin{aligned} G_t &= \frac{1}{2}b_{11}J_b^2 + b_{12}J_b \\ &= -30 \cdot J_b^2 + \frac{21}{2} \cdot J_b \end{aligned}$$

The function $G$ for cases where limits of neither compartment nor group of compartments under consideration coincide with the aft or the forward terminals:

$$\begin{aligned} G_i &= -\frac{1}{3}b_{11}J_b^3 + \frac{1}{2}(b_{11}J - b_{12})J_b^2 + b_{12}JJ_b \\ &= 20 \cdot J_b^3 - \frac{21}{4} \cdot J_b^2 + G_t \cdot J \end{aligned}$$

The function $G$ for cases where the forward limit of the compartment or group of compartments under consideration coincides with the forward terminal - or - where the aft limit of the compartment or group of compartments under consideration coincides with the aft terminal is determined as

$$\begin{aligned} G &= -\frac{1}{6}b_{11}J_b^3 + \frac{1}{4}(2b_{11}J - b_{12})J_b^2 + Jb_{12}J_b + \frac{1}{4}b_{11}J(J_b^2 - J_b^2) + \frac{1}{2}b_{12}J(J_b - J_b) \\ &= \frac{1}{2}(G_i + G_t \cdot J) \end{aligned}$$

### 9.3.2 Proposal for the $C(\overline{z})$-Function

**The Non-Dimensional Penetration**
Data points: 398

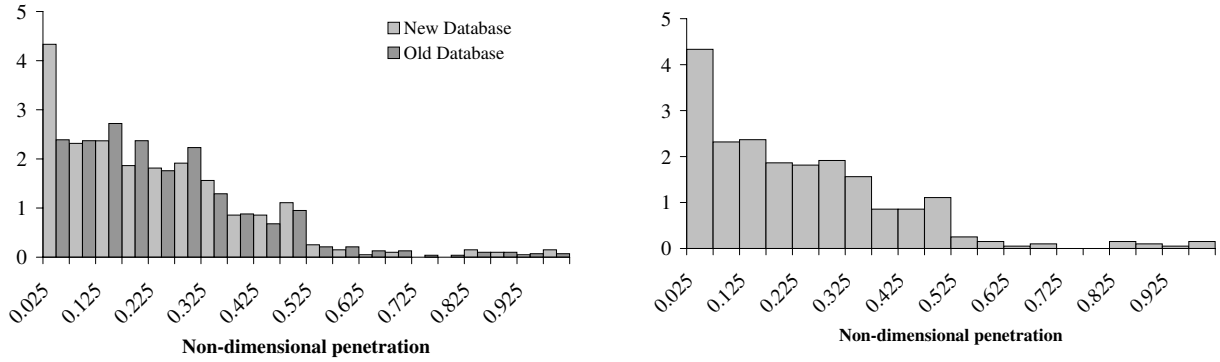


Figure 9.9: *Distribution density for the non-dimensional penetration, $\overline{z}$. Right diagram shows new data only.*

Data from the old database and the updated database is shown in Figure 9.9.

A linear function has been used for describing the non-dimensional penetration or the $c(\overline{z})$ function. As only 5% of the non-dimensional penetrations are greater than 0.5, the maximum value will be taken as 0.5. The proposal is fitted to the data by the least-squared error method for the cumulative distribution function requiring that all parameters must be described by fractions. The function of $c(\overline{z})$ can thus be determined as

$$c(\overline{z}) = \frac{1}{5}(-24 \cdot \overline{z} + 16) \qquad \text{for} \quad 0 \leq \overline{z} \leq 0.5$$

and the corresponding probability distribution function as

$$C(\overline{z}) = \frac{1}{5}(-12 \cdot \overline{z}^2 + 16 \cdot \overline{z}) \qquad \text{for} \quad 0 \leq \overline{z} \leq 0.5$$

The functions $c(\overline{z})$ and $C(\overline{z})$ can be seen in Figure 9.10 together with the results from the database.

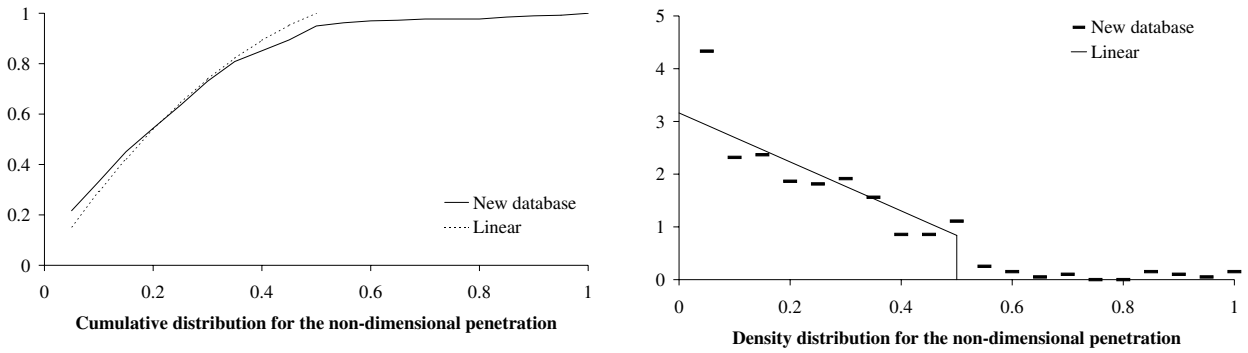


Figure 9.10: *Cumulative and density distributions of the non-dimensional penetration, $\overline{z}$, for data from the updated database and a linear function proposal.*

## 9.4 Comparison and Examples Using the New Proposal and Current Regulations

### Current Regulations (SOLAS B-1)

Non-dimensional damage location:

$$a(\overline{x}) = \begin{cases} 0.4 + 1.6 \cdot \overline{x} & \text{for} \quad \overline{x} \leq 0.5 \\ 1.2 & \text{for} \quad \overline{x} > 0.5 \end{cases}$$

Non-dimensional damage length:

$b(\overline{y}) = \dfrac{1}{J_m}\left(1 - \dfrac{\overline{y}}{J_m}\right)$ where $J_m$ is the maximum non-dimensional damage length: $J_m = 48/L$, but not more than 0.24

The reduction factor $r$ shall be determined by the following formulas:

$$r = \begin{cases} \frac{b}{B} \cdot \left[2.3 + \frac{0.08}{J+0.03}\right] + 0.1 & \text{for} \quad \frac{b}{B} \leq 0.2 \\ \frac{0.016}{J+0.03} + \frac{b}{B} + 0.36 & \text{for} \quad \frac{b}{B} > 0.2 \end{cases}$$

For $J < 0.2\frac{b}{B}$ the reduction factor is calculated by linear interpolation between $r = 1$ for $J = 0$, and $r$ is equal to the value calculated by the above formula for $J = 0.2\frac{b}{B}$.

### New Proposal

The non-dimensional damage location:

$a(\overline{x}) = 1$

The non-dimensional damage length:

$$b(\overline{y}) = \begin{cases} b_1(\overline{y}) = \frac{1}{2}(-120 \cdot \overline{y} + 21) & \text{for} \quad \overline{y} \leq \frac{1}{6} \\ b_2(\overline{y}) = \frac{1}{4}(-6 \cdot \overline{y} + 3) & \text{for} \quad \frac{1}{6} < \overline{y} \leq \frac{1}{2} \end{cases}$$

The non-dimensional penetration:

$$c(\overline{z}) = \frac{1}{5}(-24 \cdot \overline{z} + 16) \qquad \text{for} \quad 0 \leq \overline{z} \leq 0.5$$

The reduction factor $r$ shall be determined by the following formulas:

$$r = \frac{p \cdot r}{p} = 1 - \left[1 - C\left(\frac{b}{B}\right)\right] \cdot \left[1 - \frac{G}{p}\right]$$

where the functions for $p$, $G$ and $C$ are defined in Sections 9.2.3, 9.3.1 and 9.3.2.

### 9.4.1 Application Examples for the $p$-Factor

Two examples will be used for comparison of the two different approaches, here the current regulation and the new proposal, to determination of the probability of damaging only one compartment, $p$.

The first example, see Figure 9.11, deals with a vessel divided into two compartments. The probability of damaging either the aft or the forward compartment is calculated for varying positions of the transverse bulkhead. Figure 9.11 (right) shows $p$ as a function of the length of the compartment $J$. The current regulation shows a higher probability of damaging the forward compartment, whereas the new proposal is symmetrical regarding the damage location and it is therefore presented by one line only.

In the second example, see Figure 9.12, the probability $p$ is calculated for vessels with equal sized compartments. Three different vessels have been examined, each with respectively 2, 3 and 4 compartments. The figures show that the probability is more evenly distributed throughout the length of the vessel for the new proposal.

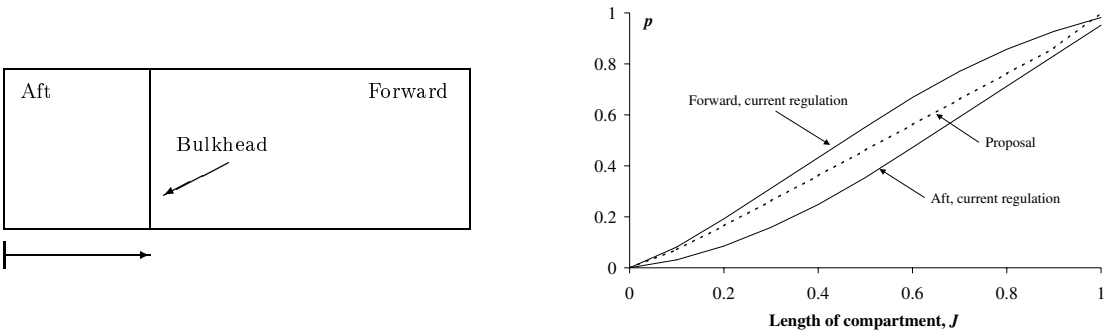


Figure 9.11: *Two-compartment vessel with moving bulkhead. Left: Drawing of the vessel. Right: The probability of damaging one particular compartment, p, as a function of the compartment length.*

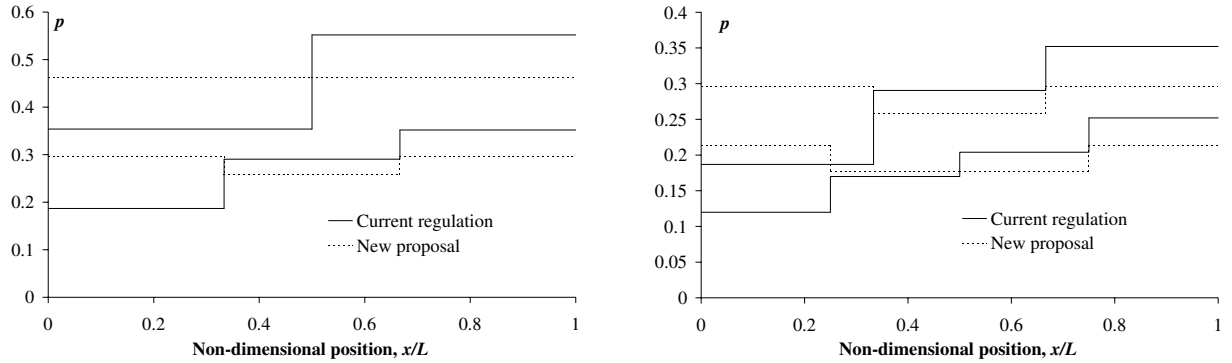


Figure 9.12: *The probability of damaging one particular compartment, p, as a function of number of equal-sized compartments and their position. Left: two and three compartments. Right: three and four compartments.*

### 9.4.2 Application Examples for the $r$-Factor

The first example deals with a vessel without transverse bulkheads. The probability $r$ that the penetration is less than the breadth of a wing tank $b$ will in this case be calculated using both the current regulation and the new proposal.

The $r$-factor for the current regulation, see Section 9.4, is only a function of the relation between the wing tank breadth and the breadth of the vessel as the compartment length, $J$, is equal to one. In Figure 9.13 the $r$-factor is shown as a function of the relation $b/B$ for both the current regulation and the new proposal. The figure shows that the new proposal is equal to zero for no wing tank, $\frac{b}{B} = 0$, and equal one for $\frac{b}{B} = \frac{1}{2}$.

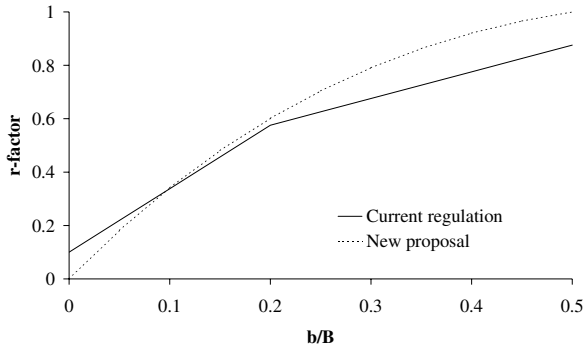


Figure 9.13: *Comparison of the r-factors for the current regulation and the new proposal.*

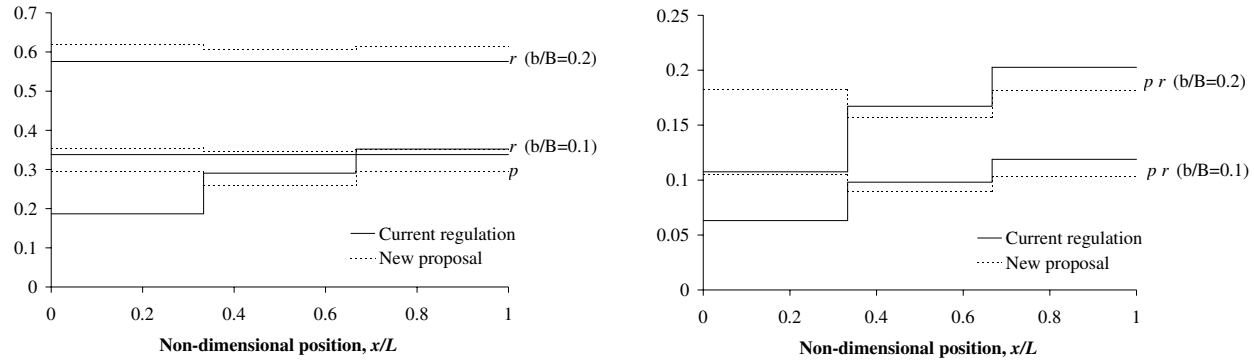


Figure 9.14: *Three equal sized compartments. Left: $p$- and $r$-factors for the current regulation and the new proposal. Right: $(p \cdot r)$ for the current regulation and the new proposal. $p$, $r$ and $(p \cdot r)$ are shown as functions of the non-dimensional longitudinal position and for values of $b/B$ equal to 0.1 and 0.2 in both figures.*

The second example deals with vessels having two transverse and two longitudinal bulkheads. The transverse bulkheads are placed to establish three equal sized compartments. The position of the longitudinal bulkheads is variable. The probability of damaging the aft, the middle and the forward compartment is calculated to be 0.2930, 0.3655 and 0.2930 respectively. The probability, $p$, and the $r$-factor for the three compartments are shown in Figure 9.14 (left) for the current regulation and the new proposal. The probability $(p \cdot r)$ for the current regulation and the new proposal is shown in Figure 9.14 (right). Both $p$, $r$ and $(p \cdot r)$ are shown as functions of the non-dimensional longitudinal position and for values of $b/B$ equal to 0.1 and 0.2 in the figures.

## 9.5 The $v$-Factor

The $v$-factor is defined as the probability that the damage will not exceed a given height above the water line. This factor can be determined in two ways:

- Use of damage statistics to make a distribution for possible damage heights above the water line
- Use of the information on the distribution of striking vessels to define statistics on bow heights. This will together with the assumptions about loading condition give a distribution for the highest point of damage above the water line

### 9.5.1 Damage Statistics

The following three requirements are here used as regards the damage statistics:

- The casualty must be a collision
- The collision must be between two ships
- The damage location must be aft of the collision bulkhead

See also Section 7.1.

This section makes use of the following vessel parameters:

| | |
|---|---|
| $D$ | The depth of the struck vessel |
| $T$ | The draught of the struck vessel |
| $Z$ | The vertical distance from the baseline to the lowest point of damage |
| $h$ | The maximum vertical damage height measured from $Z$ |
| $D_2$ | The depth of the striking vessel |
| $T_2$ | The draught of the striking vessel |

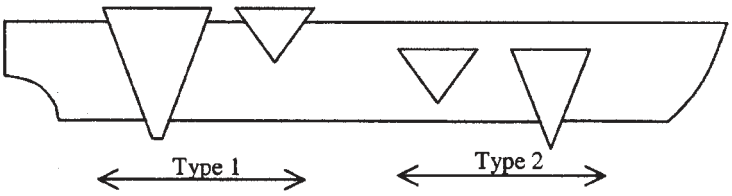


Figure 9.15: *Damage types.*

The damages are separated into two types, see Figure 9.15. The complete distribution of the upper limit of the vertical damage extent is known directly for damage type 2 only. For type 1 damages, nothing can be deduced about the upper limit, however, if it is assumed that the damage may extend up to the bow of the striking vessel, the upper limit can be calculated. It is here assumed that half of the world fleet of large ships has raised forecastle deck of an average height of 3m. This is modelled by adding an equivalent height of 1.5m to the depth of all vessels, see Herbert Engineering (2001) and Tagg et al. (2001).

**Type 1**

| | |
|---|---|
| Requirement: | $D - (Z + h) < 0$ |
| Upper limit of damage: | $D_2 - T_2 + 1.5$ |
| Data: | 99 |

**Type 2**

| | |
|---|---|
| Requirement: | $D - (Z + h) \geq 0$ |
| Upper limit of damage: | $Z + h - T$ |
| Data: | 114 |

If all collisions are included in the analysis the number of observed data of type 2 is increased to 237.

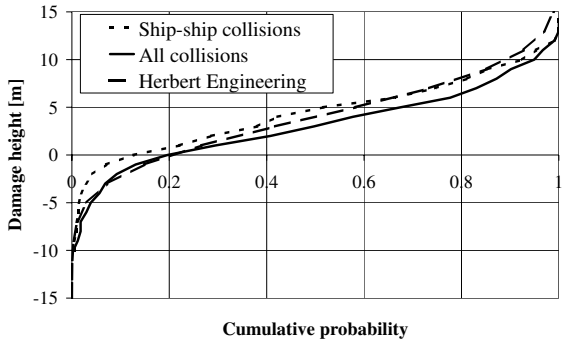


Figure 9.16: *The cumulative probability of damage heights. Damage statistics using all collisions, damage statistics using ship-ship collisions only and an analysis performed by Herbert Engineering (2001).*

Figure 9.16 display the cumulative probability of damage heights. Three graphs are shown in the diagram. Damage statistics using ship-ship collisions only, damage statistics using all collisions, and results from an analysis of the vertical extent of damage performed by Herbert Engineering (2001). As expected the ship-ship collisions do not have so many low damages as the other two analyses. The figure also shows that the analysis performed by Herbert Engineering has a large range between the lowest and the highest damage.

The damage statistics including the ship-ship collisions only is used for the $v$-factor proposal. No distinction is made between different sizes of vessels as the correlation between the length and the damage height is calculated to be 0.045.

Two proposals using the damage statistics will be presented. In the first proposal are damages below the waterline not included; in the second proposal are all damages included to describe the $v$-factor.

**Proposal for the $v$-Factor based on Damage Statistics, no Damages below Waterline**

Even though the statistics shows damages below the water line, which probably is a result of a bulb penetrating the side of the struck vessel, the factor for 0% is taken to be equal to 0 as no damages below the water line are desirable. The v-factor for the cumulative probability of 80% is taken directly from the statistics. The factor for 100% is found by fitting a bi-linear function to the data by a least squared error method. See Figure 9.17.

The function is bi-linear with the knuckle point $v = 0.8$

$v = 0.0 \qquad (H - T) = 0.0$

$v = 0.8 \qquad (H - T) = 7.8$

$v = 1.0 \qquad (H - T) = 12.5$

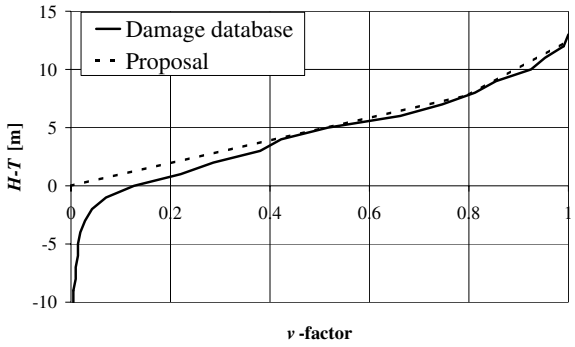


Figure 9.17: *The cumulative probability of damage heights. v-factor based on the damage statistics from the damage database using ship-ship collisions only and no damages below the waterline.*

**Proposal for the $v$-Factor based on Damage Statistics, including Damages below Waterline**

The $v$-factor is independent of the length of the vessel. The function is described by a Weibull distribution:

$$v = 1 - e^{-\left(\frac{(H-T)+10}{16}\right)^4}$$

See also Figure 9.18.

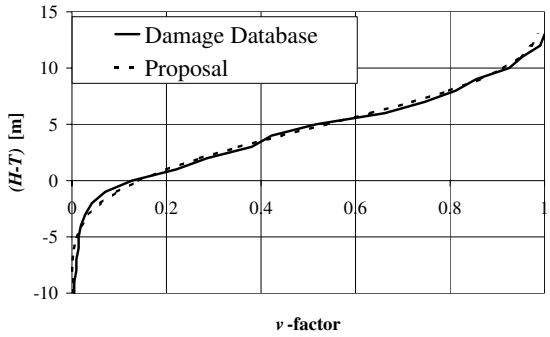


Figure 9.18: *The cumulative probability of damage heights. v-factor based on the damage statistics from the damage database using ship-ship collisions only, including damages below the waterline.*

### 9.5.2 Analysis of Bow Heights of Striking Vessels

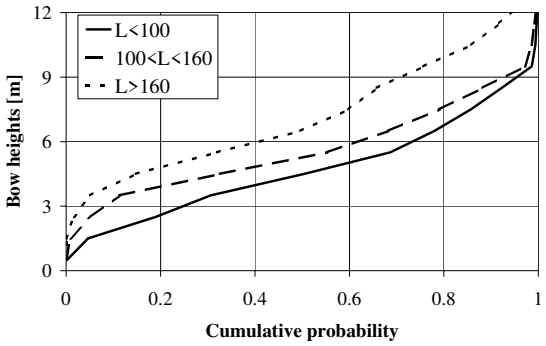


Figure 9.19: *The cumulative distribution of bow heights of striking vessels. The bow heights are separated into intervals for lengths of struck vessels.*

The bow heights have been analysed by use of the assumption about striking vessels from Section 6.3, regarding numerical simulation. Here the struck vessels are separated into three intervals, $L \leq 100$, $100 < L \leq 160$ and $L > 160$, the type and length assumptions are according to analysis 2 in Section 6.3. Analysis 2 includes the relation between the sizes of the struck and the striking vessel. Also assumptions about loading conditions and the height of the raised forecastle are taken directly from the description of the striking vessels used for the numerical simulation. Figure 9.19 shows the cumulative distribution of the bow heights of the striking vessels for the three intervals of struck vessels.

**Proposal for the $v$-Factor**

The $v$-factor for the cumulative probability of 50% or $v$=0.5 is taken directly from the bow height distributions. The factors for 0 and 100% are found by fitting a bi-linear function to the data by a least squared error method. Table 9.4 shows the values for the deck height above the water line $(H-T)$ for the intervals of struck vessels, $L \leq 100, 100 < L \leq 160$ and $L > 160$.

It is decided to keep the values for the small vessels as minimum values and the values for the large vessels as maximum values. To obtain the $v$-factor for medium-sized vessels, the $v$-factor can be found by interpolation, see also Table 9.5.

Table 9.4: *Deck height above the water line $(H-T)$, fitted to the distributions.*

| | $L \leq 100m$ | $100m < L \leq 160m$ | $L > 160m$ |
|---|---|---|---|
| $v = 0.0$ | $(H-T)$ =1.0 | $(H-T)$ =1.7 | $(H-T)$ =2.1 |
| $v = 0.5$ | $(H-T)$ =4.5 | $(H-T)$ =5.3 | $(H-T)$ =6.5 |
| $v = 1.0$ | $(H-T)$ =9.0 | $(H-T)$ =9.9 | $(H-T)$ =13.2 |

**Comparison of $v$-Factor Proposal with Damage Statistics**

For comparison of the statistics and the bow height distribution, only ship-ship collisions from the damage statistics are used.

Table 9.5: *Deck height above the water line* $(H-T)$*. Interpolation for medium-sized vessels.*

| | $L \leq 100m$ | $100m < L \leq 160m$ | $L > 160m$ |
|---|---|---|---|
| $v = 0.0$ | $(H-T)$ =1.0 | $(H-T) = 1.0 + \frac{1.1}{60} \cdot (L-100)$ | $(H-T)$ =2.1 |
| $v = 0.5$ | $(H-T)$ =4.5 | $(H-T) = 4.5 + \frac{2.0}{60} \cdot (L-100)$ | $(H-T)$ =6.5 |
| $v = 1.0$ | $(H-T)$ =9.0 | $(H-T) = 9.0 + \frac{4.2}{60} \cdot (L-100)$ | $(H-T)$ =13.2 |

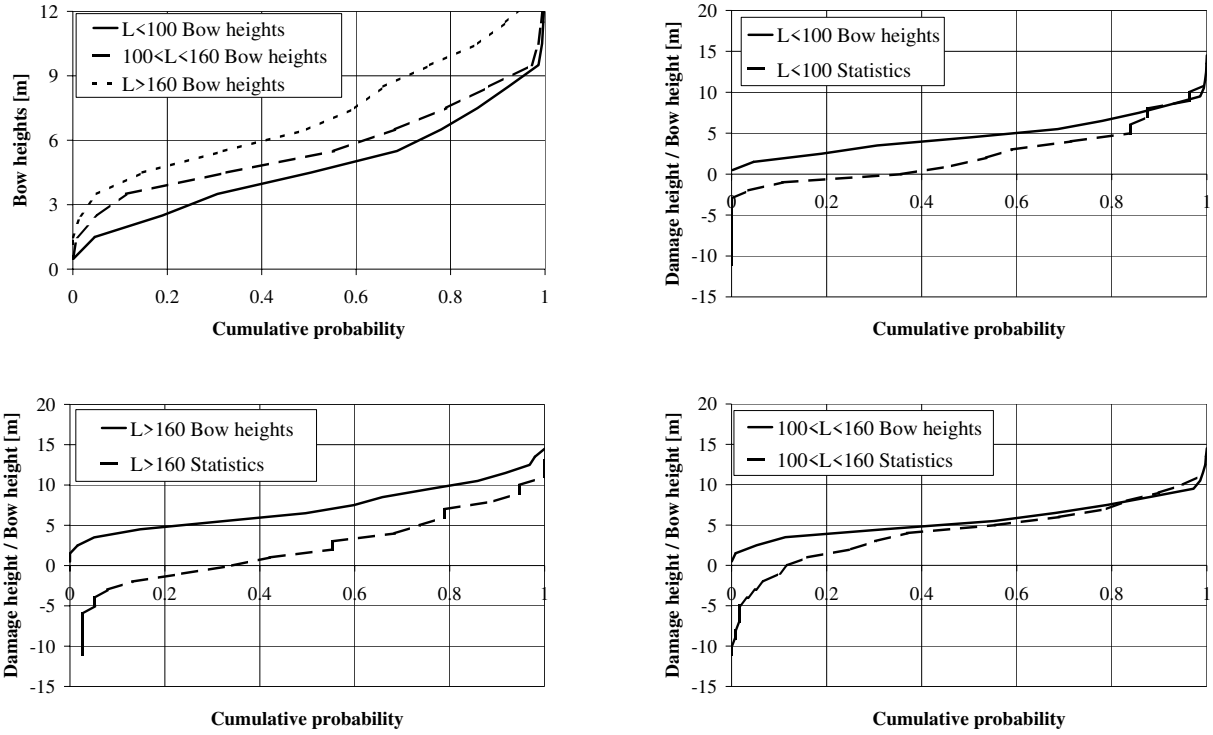


Figure 9.20: *Comparison of data from the damage statistics and the bow height distribution.* $L \leq 100$ *(56 data),* $100 < L \leq 160$ *(119 data),* $L > 160$ *(38 data).*

Figure 9.20 shows diagrams for comparison of data from the damage statistics and the bow height distribution. The first diagram (top, left) shows the results from the small struck vessels of a length below 100 m. In this case the mean value for the length of the striking vessels is approx. 124 m, which means that the striking vessels in many cases are larger than the struck ones. The large number of observed damages below the water line may be a result of the difference between struck and striking vessel, as the vessel in many cases will only be hit by the bulb of the striking vessel, whereas the top of the bow is above the upper deck. For medium-sized struck vessels between 100 m and 160 m the mean value for the length of striking vessels is approx. 143 m, about the same size as the struck vessels. The figure (top, right) shows good agreement between statistics and bow heights. The small amount of damages below the water line may be a result of soft bows with rigid bulbs. The diagram for the larger struck vessels of a length above 160 m (bottom figure) shows a large difference between the data from the statistics and the bow heights. In this case the mean value for

the length of striking vessels is approx. 177 m. The difference is probably a result of the sparse dataset in this interval.

### 9.5.3 Comparison of the Present Proposals, SOLAS Part B-1 and the Proposal from SLF 43/3/2

SOLAS Part B-1

$v = 0 \quad (H - T) = 0.0$
$v = 1 \quad (H - T) = 0.056 \cdot L \cdot \left(1 - \frac{L}{500}\right) \quad$ max. 7 m

SLF 43/3/2

$v = 0 \quad (H - T) = 0.012 \cdot L \quad$ max. 3 m
$v = 1 \quad (H - T) = 0.032 \cdot L + 3 \quad$ max. 11 m

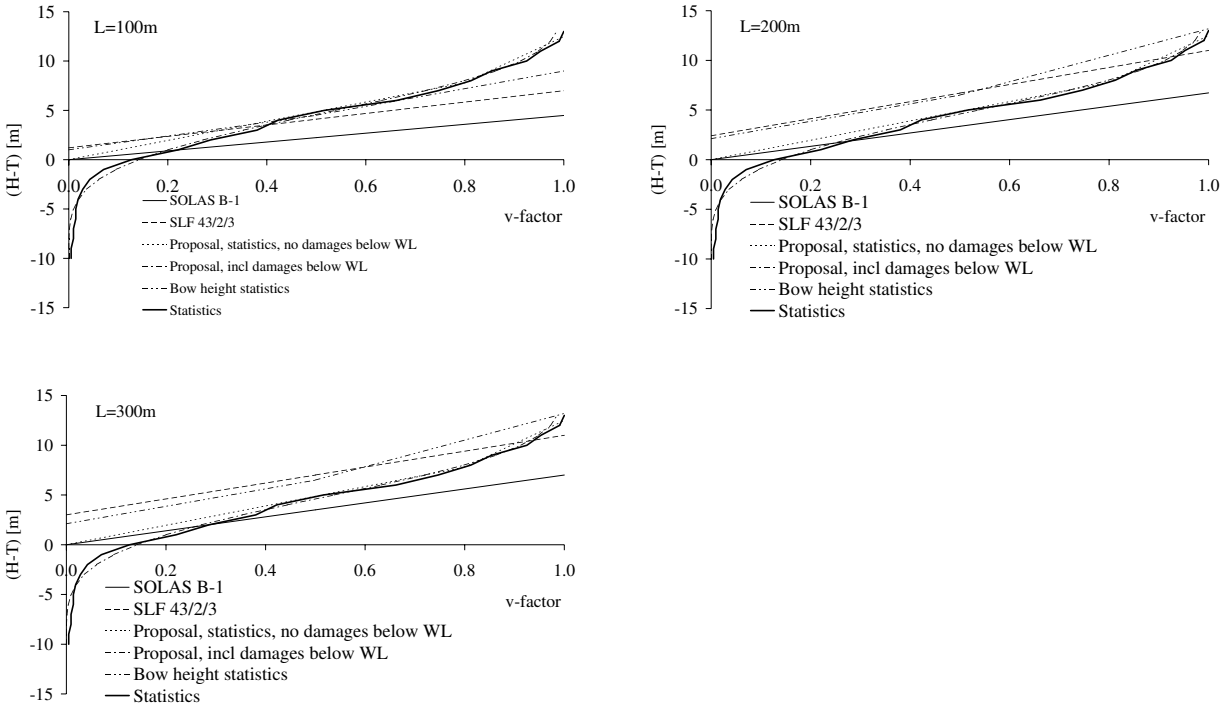


Figure 9.21: *Comparison of v-factors. Vessels of a length of 100m, 200m and 300m.*

Figure 9.21 shows a comparison of the $v$-factor calculated by use of the current regulation SOLAS Part B-1, a proposal from SLF (SLF 43/3/2) and the present proposals. The diagrams are for vessels of a length of 100m, 200m and 300m. The current regulation results are for all vessels in the lowest damage height above the water line. For smaller heights the

proposal from SLF and the bow height proposal are nearly identical, whereas the bow height proposal also includes higher damages. The damage statistics proposal shows a different pattern. The proposal including damages below the water line follows the damage statistics, whereas the proposal excluding the damages below the water line starts at zero but include also higher damages.

## 9.6 Application Examples

This section includes application examples for calculation of the attained subdivision index using the new proposals for the $p$-, $r$-, and $v$-factors. The new proposals are implemented in an existing software package, I-ship, for probabilistic damage stability calculation. The software package is developed at the Technical University of Denmark.

Three examples will be used for comparison of the different approaches to determination of the attained subdivision. The calculations are performed using IMO resolution MSC19(58), the proposal SLF 43/3/2 and the new proposals. An overview of the SLF 43/3/2 proposal is found in Appendix F.

The first example deals with the IMO-boxes, 11 different boxes with six different subdivisions are examined in detail regarding the $p$-, $r$-, and $v$-factors and the total attained subdivision index. The following examples illustrate the attained index for two different vessels, a Ro-Ro ferry of a length of 64 m and a container vessel of a length of 190 m.

Three loading conditions are considered when the attained subdivision index is calculated, namely lightweight, partially loaded and fully loaded condition. The attained index for these loading conditions is weighted by 20%, 40% and 40%, respectively, giving:

$$A = 0.2 \cdot A_l + 0.4 \cdot A_p + 0.4 \cdot A_s$$

For the two examples regarding the vessels, the survivability index, $s$, is, except for the current regulation, calculated according to the SLF 43/3/2 proposal.

### 9.6.1 IMO-Boxes

**Boxes and Subdivision Sets**

| Ship no. | $L$ [m] | $B$ [m] | $D$ [m] | $T_s$ [m] | $T_p$ [m] | $T_l$ [m] |
|---|---|---|---|---|---|---|
| 1 | 100 | 20 | 12 | 6 | 4.8 | 3 |
| 2 | 200 | 40 | 24 | 12 | 9.6 | 6 |
| 3 | 300 | 60 | 36 | 18 | 14.4 | 9 |

| Box no. | Set | Ship no. | Internal subdivision | Examined parameters |
|---|---|---|---|---|
| 1 | A | 1 | T | $p$ |
| 2 | | 2 | T | $p$, $r$ |
| 3 | | 3 | T | $p$, $r$ |
| 6 | B | 3 | T,L | $p$, $r$ |
| 7 | C | 1 | T,L | $p$, $r$ |
| 8 | D | 1 | T,L | $p$, $r$ |
| 9 | | 1 | T,L | $p$, $r$ |
| 13 | F | 1 | T,H | $p$, $v$ |
| 14 | | 2 | T,H | $p$, $v$ |
| 15 | | 3 | T,H | $p$, $v$ |
| 16 | G | 1 | T,L,H | $p$, $v$ |

**Set A, Box-Forms 1, 2 and 3**

Subdivision in Set A: Transverse only. The boxes are seen in Figure 9.22.

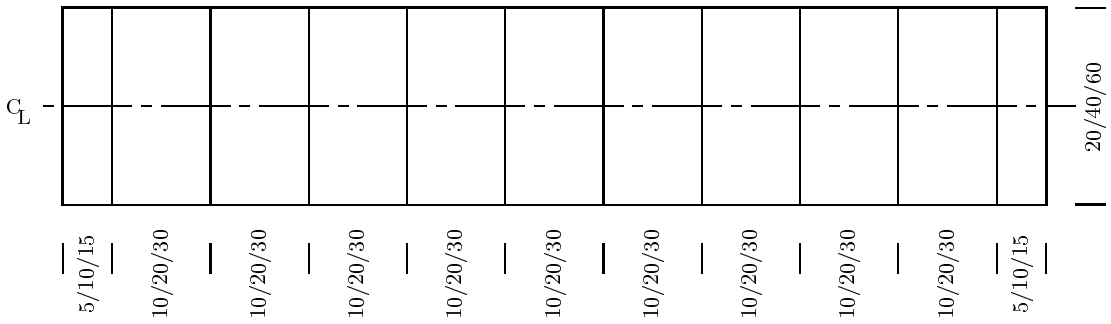


Figure 9.22: *Set A, box-forms 1, 2 and 3.*

As the boxes are transversely stiffened only, there will be no contributions from the $r$- and the $v$-factor. Thus the subdivision index will reflect the $p$-factor.

The attained index is calculated according to resolution MSC 19(58), the proposal SLF 43/3/2 and the present proposal.

Both the regulations from MSC 19(58) and the proposal SLF 43/3/2 include length dependency for vessels of a length above 200 m, see the description of the distribution for non-dimensional damage length, $b$, where $J_m$ is a function of $L$. The present proposal includes no length dependency. Because of the above mentioned length dependency, the boxes are here separated into two groups, 1+2 and 3 as box no. 3 is above 200 m.

Figure 9.23 shows the probability of damaging one particular compartment. The figure shows that the current regulation MSC 19(58) and the proposal SLF 43/3/2 have a higher probability of damaging the forward compartments, whereas the new proposal is symmetrical regarding the damage location and more evenly distributed throughout the length of the vessel.

Figure 9.24 shows the subdivision index as a function of number of damaged zones for all three methods of calculation. The MSC 19(58) and the SLF 43/3/2 calculations are nearly identical, whereas the new proposal is a little higher for the smaller vessels and lower for the larger vessels. The numbers for the attained index are all given in Tables 9.6 and 9.7.

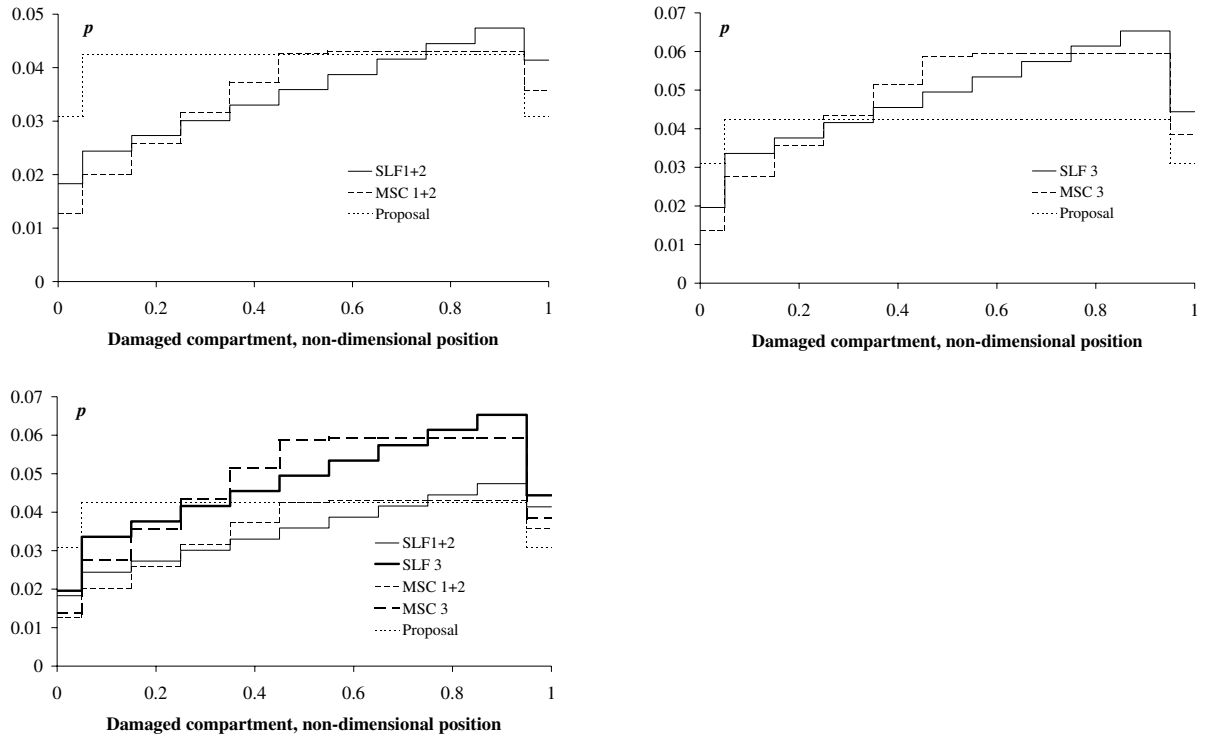


Figure 9.23: *Probability of damaging one particular compartment, box-forms 1, 2 and 3.*

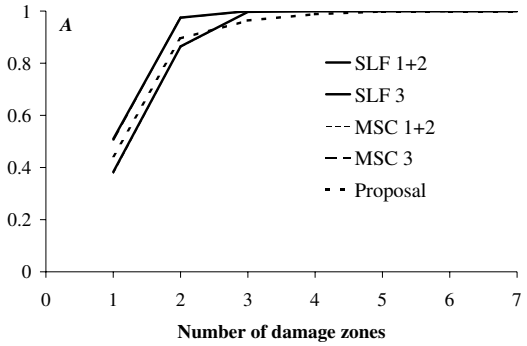


Figure 9.24: *Attained subdivision index as a function of number of damage zones.*

Table 9.6: *Attained subdivision index, cumulative number of damage zones, Set A.*

| Box no. | Formulation | 1 cmpt. | 2 cmpt. | 3 cmpt. | 4 cmpt. | 5 cmpt. | 6 cmpt. | 7 cmpt. |
|---|---|---|---|---|---|---|---|---|
| 1 | MSC | 0.3781 | 0.8608 | 0.9969 | 1 | 1 | 1 | 1 |
| 1 | SLF | 0.3826 | 0.8643 | 0.9970 | 1 | 1 | 1 | 1 |
| 1 | Proposal | 0.4444 | 0.8948 | 0.9639 | 0.9883 | 0.9985 | 1 | 1 |
| 2 | MSC | 0.3781 | 0.8608 | 0.9969 | 1 | 1 | 1 | 1 |
| 2 | SLF | 0.3826 | 0.8643 | 0.9970 | 1 | 1 | 1 | 1 |
| 2 | Proposal | 0.4444 | 0.8948 | 0.9639 | 0.9883 | 0.9985 | 1 | 1 |
| 3 | MSC | 0.5066 | 0.9742 | 1 | 1 | 1 | 1 | 1 |
| 3 | SLF | 0.5093 | 0.9747 | 1 | 1 | 1 | 1 | 1 |
| 3 | Proposal | 0.4444 | 0.8948 | 0.9639 | 0.9883 | 0.9985 | 1 | 1 |

Table 9.7: *Attained subdivision index, contributions from individual number of damage zones, Set A.*

| Box no. | Formulation | 1 cmpt. | 2 cmpt. | 3 cmpt. | 4 cmpt. | 5 cmpt. | 6 cmpt. | 7 cmpt. |
|---|---|---|---|---|---|---|---|---|
| 1 | MSC | 0.3781 | 0.4827 | 0.1361 | 0 | 0 | 0 | 0 |
| 1 | SLF | 0.3826 | 0.4817 | 0.1327 | 0.0030 | 0 | 0 | 0 |
| 1 | Proposal | 0.4444 | 0.4504 | 0.0691 | 0.0244 | 0.0102 | 0.0015 | 0 |
| 2 | MSC | 0.3781 | 0.4827 | 0.1361 | 0 | 0 | 0 | 0 |
| 2 | SLF | 0.3826 | 0.4817 | 0.1327 | 0.0030 | 0 | 0 | 0 |
| 2 | Proposal | 0.4444 | 0.4504 | 0.0691 | 0.0244 | 0.0102 | 0.0015 | 0 |
| 3 | MSC | 0.5066 | 0.4676 | 0.0258 | 0 | 0 | 0 | 0 |
| 3 | SLF | 0.5093 | 0.4654 | 0.0253 | 0 | 0 | 0 | 0 |
| 3 | Proposal | 0.4444 | 0.4504 | 0.0691 | 0.0244 | 0.0102 | 0.0015 | 0 |

**Set B, Box-Form 6**

Subdivision in Set B: Transverse and longitudinal. See Figure 9.25.

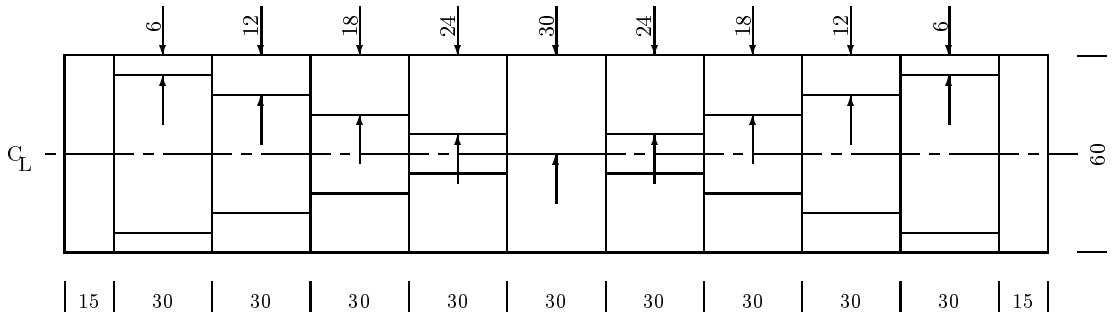


Figure 9.25: *Set B, box-form 6.*

As the box is transversely and longitudinally stiffened, there will be contributions from both the $p$- and the $r$-factor.

The attained index is calculated according to the proposal SLF 43/3/2 and the present proposal. Only the large vessel of a length of 300 m is considered.

Figure 9.26 shows the probability of damaging one particular outer compartment. Three diagrams are given, the upper left is the $p$- and the $(p \cdot r)$-factors for the calculation performed by SLF 43/3/2, the upper right the same factors for the present proposal and the bottom diagram shows the $r$-factor for both methods of calculation. The forward and the aft compartments are taken as outer compartments but as these compartments have no longitudinal subdivision, the term $(p \cdot r)$ for these compartments equals $p$.

Figure 9.27 shows the subdivision index as a function of number of damaged zones for both methods of calculation, the agreement is good. The numbers for the attained index are all given in Tables 9.8 and 9.9.

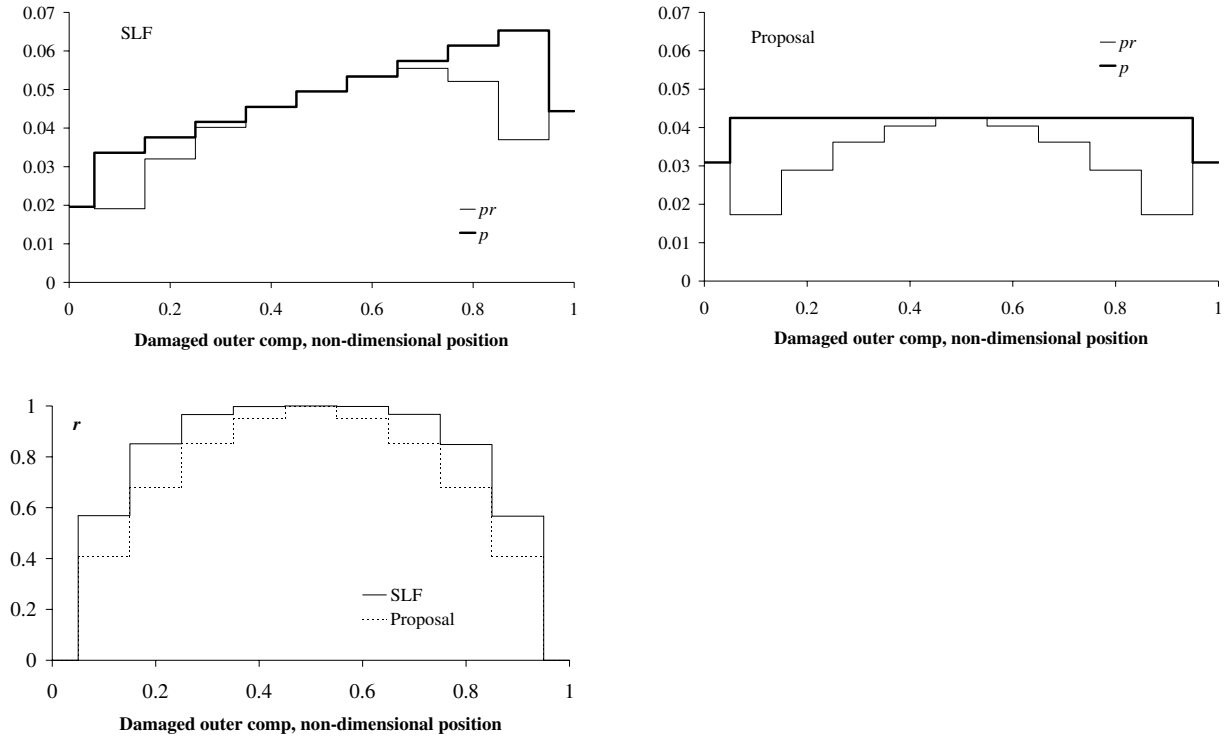


Figure 9.26: *Probability of damaging one particular outer compartment. The contributions from $p$, $r$ and $p \cdot r$ are shown.*

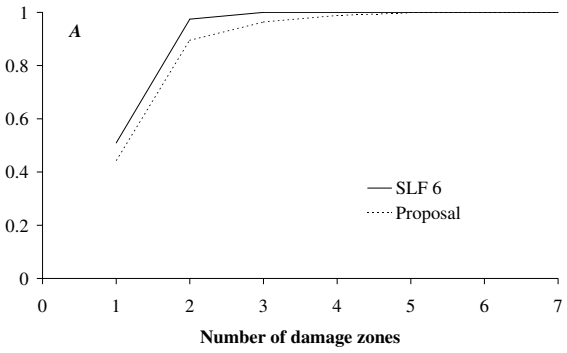


Figure 9.27: *Attained subdivision index as a function of number of damage zones.*

Table 9.8: *Attained subdivision index, cumulative number of damage zones, Set B.*

| Box no. | Formulation | 1 cmpt. | 2 cmpt. | 3 cmpt. | 4 cmpt. | 5 cmpt. | 6 cmpt. | 7 cmpt. |
|---|---|---|---|---|---|---|---|---|
| 6 | SLF | 0.5093 | 0.9747 | 1 | 1 | 1 | 1 | 1 |
| 6 | Proposal | 0.4444 | 0.8948 | 0.9639 | 0.9883 | 0.9985 | 1 | 1 |

Table 9.9: *Attained subdivision index, contributions from individual number of damage zones, Set B.*

| Box no. | Formulation | 1 cmpt. | 2 cmpt. | 3 cmpt. | 4 cmpt. | 5 cmpt. | 6 cmpt. | 7 cmpt. |
|---|---|---|---|---|---|---|---|---|
| 6 | SLF | 0.5093 | 0.4654 | 0.0253 | 0 | 0 | 0 | 0 |
| 6 | Proposal | 0.4444 | 0.4504 | 0.0691 | 0.0244 | 0.0102 | 0.0015 | 0 |

**Set C, Box-Form 7**

Subdivision in Set C: Transverse and longitudinal. Both outer and inner longitudinal divisions. The centre compartments form part of an assumed flooding case where $s = 0$. The box is seen in Figure 9.28.

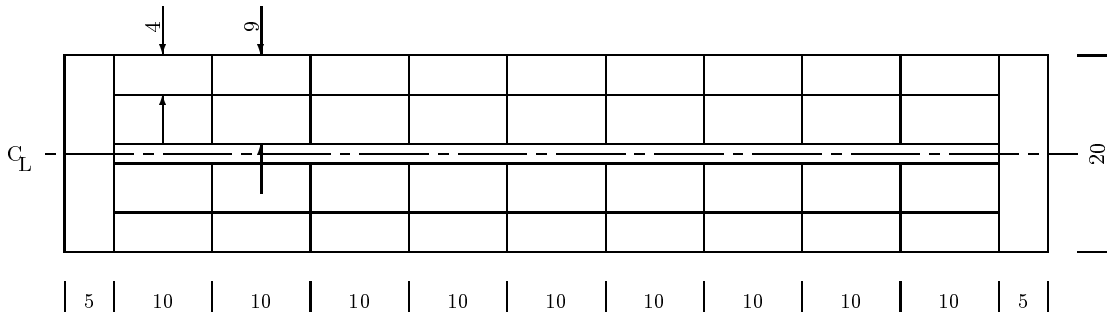


Figure 9.28: *Set C, box-form 7.*

As the box is transversely and longitudinally stiffened, there will be contributions from both the $p$- and the $r$-factor.

The attained index is calculated according to the proposal SLF 43/3/2 and the present proposal. Only the small vessel of a length of 100 m is considered.

Figure 9.29 presents the probability of damaging one particular outer compartment. The contributions from $p$ and $(p \cdot r)$ are seen. Two diagrams are shown, in the left diagram the $p$- and the $(p \cdot r)$-factors for the calculation performed by SLF 43/3/2 are given. In the right diagram the same factors are shown for the present proposal. The forward and the aft compartments are taken as outer compartments but as these compartments have no longitudinal subdivision, the term $(p \cdot r)$ for these compartments equals $p$.

Figure 9.30 shows the subdivision index as a function of number of damaged zones for both methods of calculation. The figure shows good agreement between the two methods of calculation. The numbers for the attained index are all given in Tables 9.10 and 9.11.

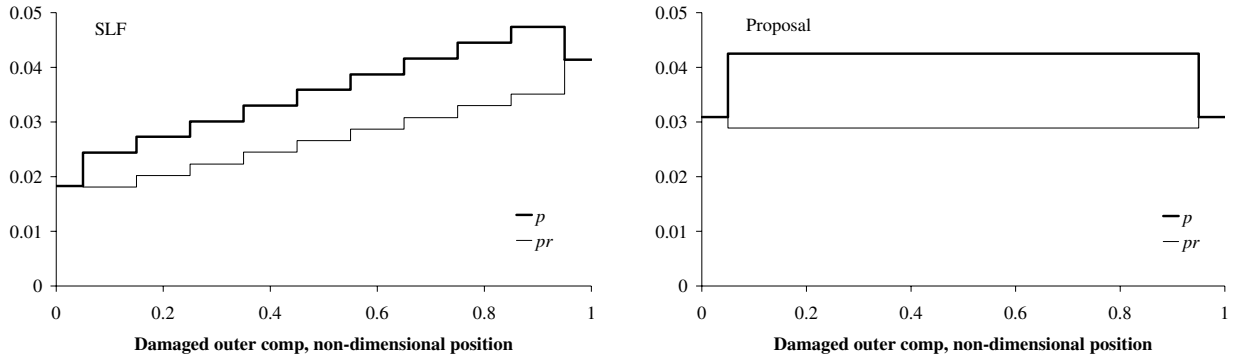


Figure 9.29: *Probability of damaging one particular outer compartment. The contributions from $p$ and $p \cdot r$ are shown.*

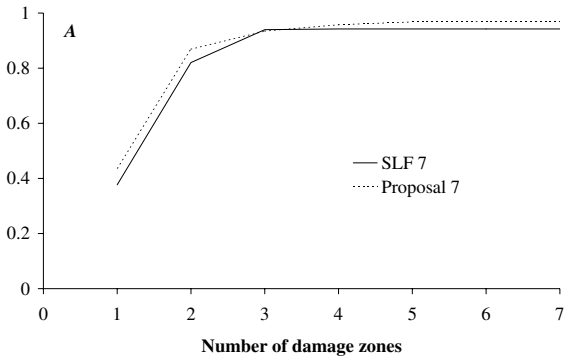


Figure 9.30: *Attained subdivision index as a function of number of damaged zones.*

Table 9.10: *Attained subdivision index, cumulative number of damage zones, Set C.*

| Box no. | Formulation | 1 cmpt. | 2 cmpt. | 3 cmpt. | 4 cmpt. | 5 cmpt. | 6 cmpt. | 7 cmpt. |
|---|---|---|---|---|---|---|---|---|
| 7 | SLF | 0.3769 | 0.8205 | 0.9398 | 0.9425 | 0.9425 | 0.9425 | 0.9425 |
| 7 | Proposal | 0.4370 | 0.8686 | 0.9345 | 0.9578 | 0.9676 | 0.9690 | 0.9690 |

Table 9.11: *Attained subdivision index, contributions from individual number of damage zones, Set C.*

| Box no. | Formulation | 1 cmpt. | 2 cmpt. | 3 cmpt. | 4 cmpt. | 5 cmpt. | 6 cmpt. | 7 cmpt. |
|---|---|---|---|---|---|---|---|---|
| 7 | SLF | 0.3769 | 0.4436 | 0.1193 | 0.0027 | 0 | 0 | 0 |
| 7 | Proposal | 0.4370 | 0.4316 | 0.0659 | 0.0233 | 0.0098 | 0.0014 | 0 |

**Set D, Box-Forms 8 and 9**

Subdivision in Set D: Transverse and longitudinal. For box-form 8 the centre compartments form part of an assumed flooding case where $s = 0$. The boxes are seen in Figure 9.31.

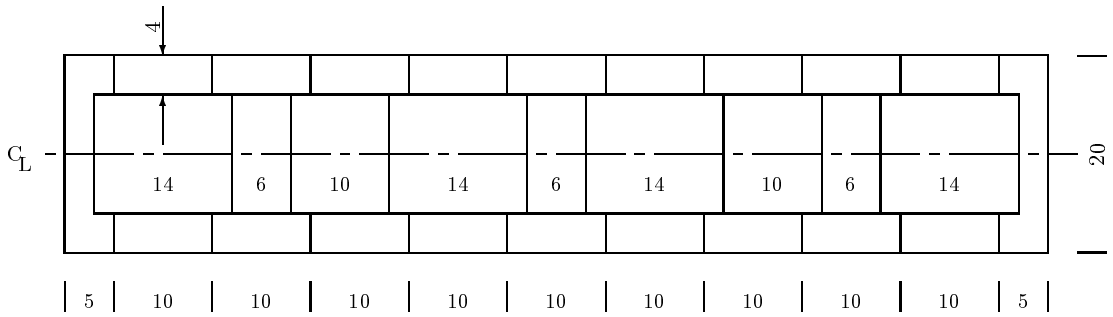


Figure 9.31: *Set D, box-forms 8 and 9.*

As the boxes are transversely and longitudinally stiffened, there will be contributions from both the $p$- and the $r$-factor.

The attained index is calculated according to the proposal SLF 43/3/2 and the present proposal. Only the small vessel of a length of 100 m is considered.

Figure 9.32 presents the subdivision index as a function of number of damaged zones for both methods of calculation. The numbers for the attained index are all shown in Tables 9.12 and 9.13. The effect of the survivability $s = 0$ for the centre compartments in the calculation of box-form 8 is significant for both methods of calculation.

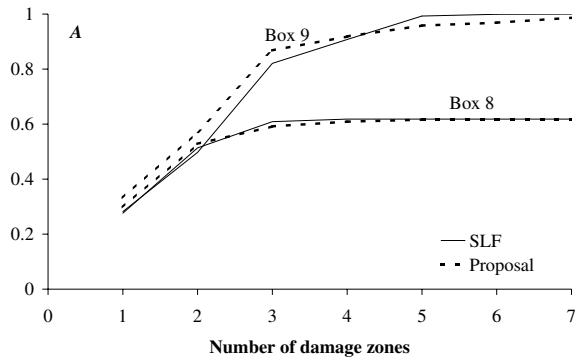


Figure 9.32: *Attained subdivision index as a function of number of damage zones.*

Table 9.12: *Attained subdivision index, cumulative number of damage zones, Set D.*

| Box no. | Formulation | 1 cmpt. | 2 cmpt. | 3 cmpt. | 4 cmpt. | 5 cmpt. | 6 cmpt. | 7 cmpt. |
|---|---|---|---|---|---|---|---|---|
| 8 | SLF | 0.2762 | 0.5137 | 0.6088 | 0.6184 | 0.6184 | 0.6184 | 0.6184 |
| 8 | Proposal | 0.2980 | 0.5280 | 0.5919 | 0.6088 | 0.6160 | 0.6177 | 0.6178 |
| 9 | SLF | 0.2820 | 0.4971 | 0.8209 | 0.9077 | 0.9928 | 0.9991 | 1 |
| 9 | Proposal | 0.3318 | 0.5719 | 0.8677 | 0.9183 | 0.9584 | 0.9686 | 0.9865 |

Table 9.13: *Attained subdivision index, contributions from individual number of damage zones, Set D.*

| Box no. | Formulation | 1 cmpt. | 2 cmpt. | 3 cmpt. | 4 cmpt. | 5 cmpt. | 6 cmpt. | 7 cmpt. |
|---|---|---|---|---|---|---|---|---|
| 8 | SLF | 0.2762 | 0.2375 | 0.0951 | 0.0096 | 0 | 0 | 0 |
| 8 | Proposal | 0.2980 | 0.2300 | 0.0639 | 0.0169 | 0.0072 | 0.0017 | 0.0001 |
| 9 | SLF | 0.2820 | 0.2151 | 0.3238 | 0.0868 | 0.0851 | 0.0063 | 0.0009 |
| 9 | Proposal | 0.3318 | 0.2401 | 0.2958 | 0.0506 | 0.0401 | 0.0102 | 0.0179 |

### Set F, Box-Forms 13, 14 and 15

Subdivision in Set F: Transverse and horizontal. Both lower and upper horizontal divisions. All upper compartments form part of an assumed flooding case where $s = 0$. The boxes are seen in Figure 9.33.

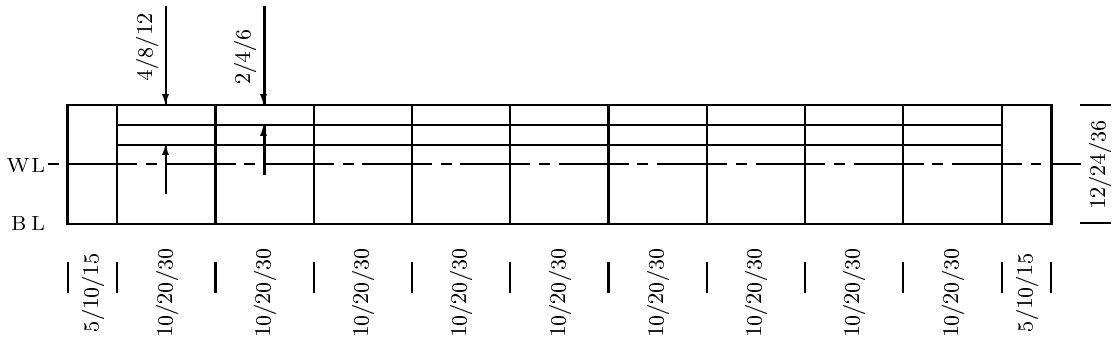


Figure 9.33: *Set F, box-forms 13, 14 and 15.*

As the boxes are transversely and horizontally stiffened, there will be contributions from both the $p$- and the $v$-factor.

The attained index is calculated according to the proposal SLF 43/3/2 and the present proposal using bow height statistics for the $v$-factor.

Minimum heights above the water line of the upper deck are 4, 8 and 12 m for box 13, 14 and 15, respectively.

SLF 43/3/2 The $p$-factor: Length dependency for vessels of a length above 200 m, see the distribution for non-dimensional damage length, $b$, where $J_m$ is a function of $L$. The $v$-factor: Minimum heights above the water line from the definition of $v$ for box 13, 14 and 15,

respectively: 1.2/2.4/3.0 m. These values are lower than the minimum height of the upper deck; the $v$-factor will then be greater than zero and thus depend on the length of the vessel.

Present proposal using bow height statistics: The $p$-factor: No length dependency. The $v$-factor: Minimum heights above the water line from the definition of $v$ for box 13, 14 and 15, respectively: 1.0/2.1/2.1 m. These values are lower than the minimum height of the upper deck; thus $v$ is greater than zero and depends on the length of the vessel.

Figure 9.34 shows the subdivision index as a function of number of damaged zones for both methods of calculation. The numbers for the attained index are all given in Tables 9.14 and 9.15. The difference between the methods of calculation is significant. The formulation of the $v$-factor for the new proposal results in a much lower attained index. The influence of the length of the vessel is seen in Figure 9.35.

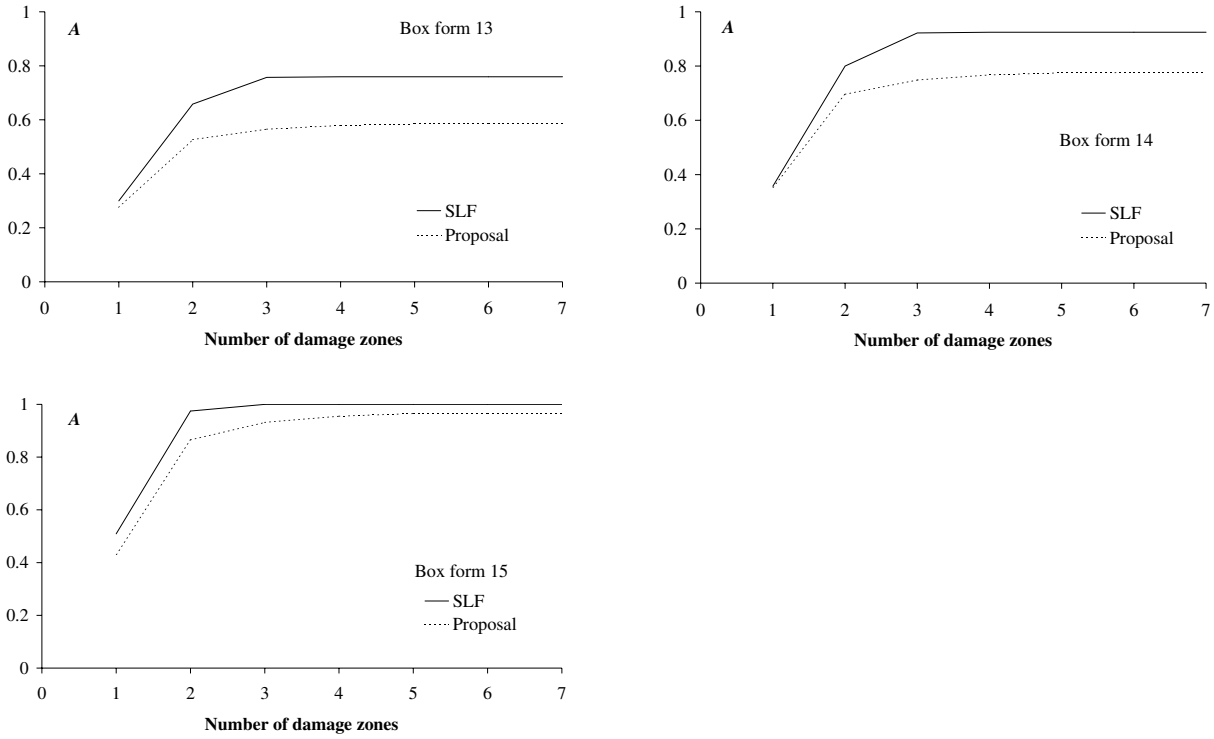


Figure 9.34: *Attained subdivision index as a function of number of damage zones, proposal refers to bow height statistics.*

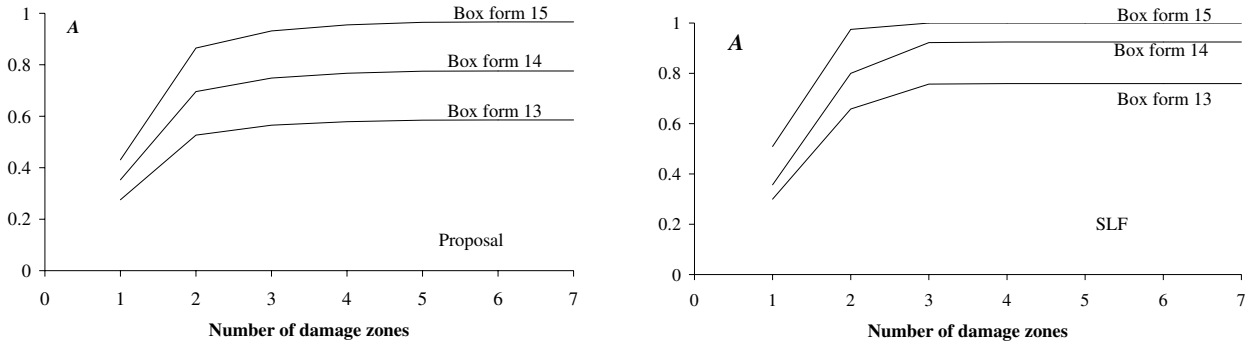


Figure 9.35: *Attained subdivision index as a function of number of damage zones, proposal refers to bow height statistics.*

Table 9.14: *Attained subdivision index, cumulative number of damage zones, Set F.*

| Box no. | Formulation | 1 cmpt. | 2 cmpt. | 3 cmpt. | 4 cmpt. | 5 cmpt. | 6 cmpt. | 7 cmpt. |
|---|---|---|---|---|---|---|---|---|
| 13 | SLF | 0.2999 | 0.6583 | 0.7571 | 0.7593 | 0.7593 | 0.7593 | 0.7593 |
| 13 | Proposal | 0.2753 | 0.5267 | 0.5653 | 0.5789 | 0.5846 | 0.5854 | 0.5854 |
| 14 | SLF | 0.3568 | 0.7999 | 0.9220 | 0.9248 | 0.9248 | 0.9248 | 0.9248 |
| 14 | Proposal | 0.3530 | 0.6959 | 0.7485 | 0.7671 | 0.7749 | 0.7760 | 0.7760 |
| 15 | SLF | 0.5093 | 0.9747 | 1 | 1 | 1 | 1 | 1 |
| 15 | Proposal | 0.4307 | 0.8649 | 0.9316 | 0.9552 | 0.9650 | 0.9664 | 0.9664 |

Table 9.15: *Attained subdivision index, contributions from individual number of damage zones, Set F.*

| Box no. | Formulation | 1 cmpt. | 2 cmpt. | 3 cmpt. | 4 cmpt. | 5 cmpt. | 6 cmpt. | 7 cmpt. |
|---|---|---|---|---|---|---|---|---|
| 13 | SLF | 0.2999 | 0.3584 | 0.0988 | 0.0022 | 0 | 0 | 0 |
| 13 | Proposal | 0.2753 | 0.2514 | 0.0386 | 0.0136 | 0.0057 | 0.0008 | 0 |
| 14 | SLF | 0.3568 | 0.4431 | 0.1221 | 0.0028 | 0 | 0 | 0 |
| 14 | Proposal | 0.3530 | 0.3429 | 0.0526 | 0.0186 | 0.0078 | 0.0011 | 0 |
| 15 | SLF | 0.5093 | 0.4654 | 0.0253 | 0 | 0 | 0 | 0 |
| 15 | Proposal | 0.4307 | 0.4342 | 0.0667 | 0.0236 | 0.0098 | 0.0014 | 0 |

**Set G, Box-Form 16**

Subdivision in Set G: Transverse, longitudinal and horizontal. Both lower and upper horizontal divisions. All upper compartments form part of an assumed flooding case where $s = 0$. The box is seen in Figure 9.36.

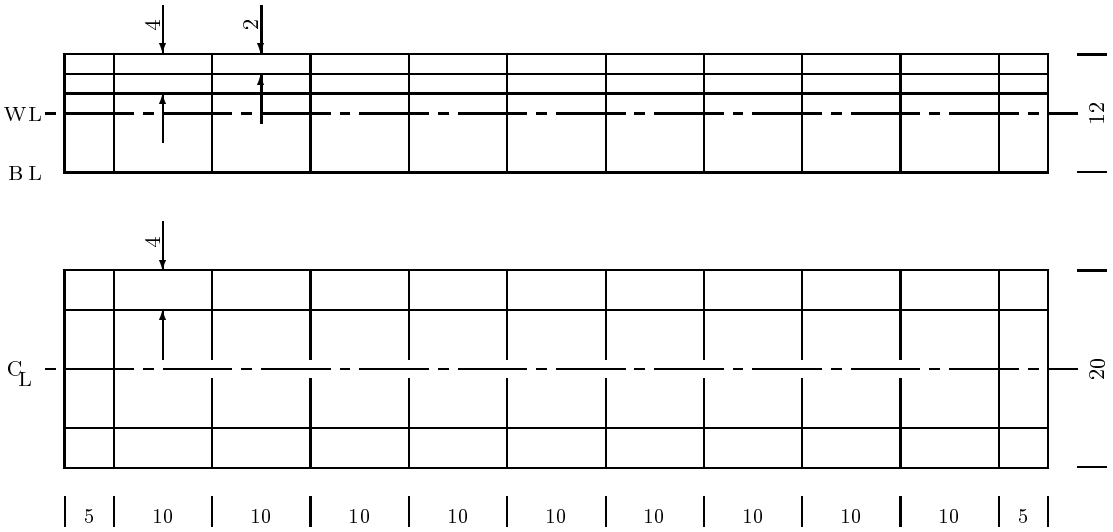


Figure 9.36: *Set G, box-form 16.*

The attained index is calculated according to resolution MSC 19(58), the proposal SLF 43/3/2 and the present proposals.

Figure 9.37 shows the subdivision index as a function of number of damaged zones for three methods of calculation, the resolution MSC 19(58), the proposal SLF 43/3/2 and the present proposal where the bow height statistics is used for describing the $v$-factor. The numbers for the attained index are all presented in Tables 9.16 and 9.17. The difference between the methods of calculation is significant. The formulation of the $v$-factor for the new proposal results in a much lower attained index.

Table 9.16: *Attained subdivision index, cumulative number of damage zones, Set G.*

| Box no. | Formulation | 1 cmpt. | 2 cmpt. | 3 cmpt. | 4 cmpt. | 5 cmpt. | 6 cmpt. | 7 cmpt. |
|---|---|---|---|---|---|---|---|---|
| 16 | MSC | 0.3579 | 0.8147 | 0.9435 | 0.9464 | 0.9464 | 0.9464 | 0.9464 |
| 16 | SLF | 0.2847 | 0.6430 | 0.7418 | 0.7440 | 0.7440 | 0.7440 | 0.7440 |
| 16 | Proposal | 0.2480 | 0.4994 | 0.5380 | 0.5516 | 0.5573 | 0.5581 | 0.5581 |

Table 9.17: *Attained subdivision index, contributions from individual number of damage zones, Set G.*

| Box no. | Formulation | 1 cmpt. | 2 cmpt. | 3 cmpt. | 4 cmpt. | 5 cmpt. | 6 cmpt. | 7 cmpt. |
|---|---|---|---|---|---|---|---|---|
| 16 | MSC | 0.3579 | 0.4568 | 0.1288 | 0.0029 | 0 | 0 | 0 |
| 16 | SLF | 0.2847 | 0.3583 | 0.0988 | 0.0022 | 0 | 0 | 0 |
| 16 | Proposal | 0.2480 | 0.2514 | 0.0386 | 0.0136 | 0.0057 | 0.0008 | 0 |

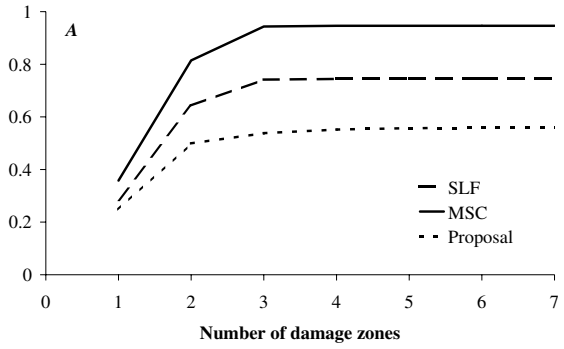


Figure 9.37: *Attained subdivision index as a function of number of damage zones, proposal refers to bow height statistics.*

The proposal based on the damage statistics is also used for calculation of the attained index in box 16. The results from the determination of the attained index are seen in Table 9.18. The difference in attained index for the proposals is not significant for this box.

Table 9.18: Attained subdivision index, Set G, box 16.

| Formulation | $A$ |
|---|---|
| MSC 19(58) | 0.9464 |
| SLF 43/3/2 | 0.7440 |
| Proposal, bow height statistics | 0.5581 |
| Proposal, damage statistics, no damages below water line | 0.5210 |
| Proposal, damage statistics, including damages below water line | 0.5444 |

### 9.6.2 Ro-Ro Ferry, $L$=65 m

The small Ro-Ro ferry is here divided into 27 compartments.

Main particulars:

| | |
|---|---|
| Length over all [m] | 68.83 |
| Length between perpendiculars [m ] | 64.60 |
| Subdivision length [m] | 68.73 |
| Breadth [m] | 14.80 |
| Depth to car deck [m] | 4.35 |
| Depth to top deck [m] | 9.50 |
| Full load draught [m] | 3.00 |
| Full load displacement [t] | 2041 |
| Partial load draught [m] | 2.84 |
| Partial load displacement [t] | 1907 |

Figure 9.39 shows the subdivision index as a function of number of damaged zones for the four methods of calculation: the resolution MSC 19(58), the proposal SLF 43/3/2 and two of

the present proposals, the bow height proposal and the damage statistics proposal excluding damages below the water line. The numbers for the attained index are all given in Tables 9.19 and 9.20. The figure reveals only a little difference in the calculated attained index for the different methods of calculation. The current regulation gives the highest attained index, the SLF proposal and the present bow height proposal are nearly identical and the present damage statistics proposal is in between.

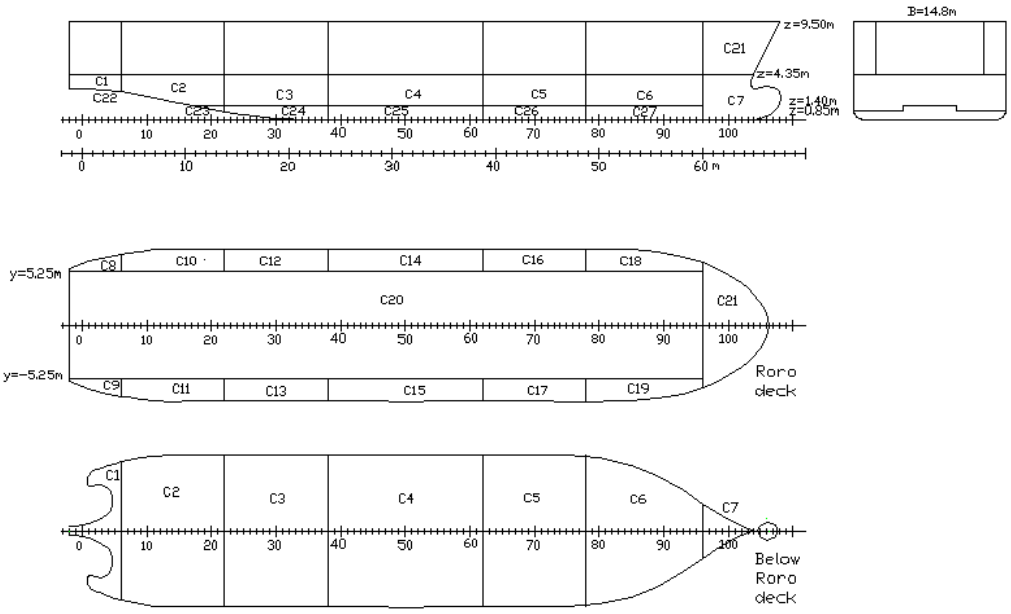


Figure 9.38: *A small Ro-Ro ferry.*

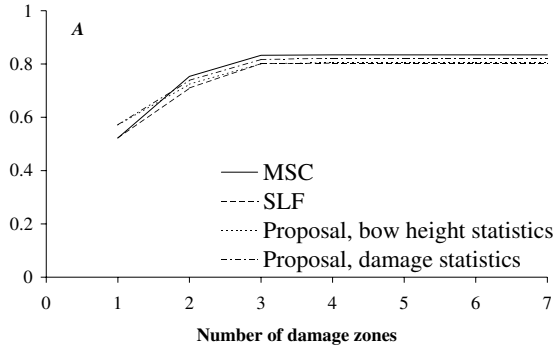


Figure 9.39: *Attained subdivision index as a function of number of damage zones.*

Table 9.19: *Attained subdivision index, cumulative number of damage zones, small Ro-Ro ferry.*

| Formulation | 1 cmpt. | 2 cmpt. | 3 cmpt. | 4 cmpt. | 5 cmpt. | 6 cmpt. | 7 cmpt. |
|---|---|---|---|---|---|---|---|
| MSC | 0.5225 | 0.7536 | 0.8328 | 0.8344 | 0.8344 | 0.8344 | 0.8344 |
| SLF | 0.5221 | 0.7099 | 0.8015 | 0.8031 | 0.8031 | 0.8031 | 0.8031 |
| Proposal, bow height statistics | 0.5710 | 0.7245 | 0.8013 | 0.8049 | 0.8052 | 0.8052 | 0.8052 |
| Proposal, damage statistics | 0.5716 | 0.7384 | 0.8171 | 0.8217 | 0.8221 | 0.8221 | 0.8221 |

Table 9.20: *Attained subdivision index, contributions from individual number of damage zones, small Ro-Ro ferry.*

| Formulation | 1 cmpt. | 2 cmpt. | 3 cmpt. | 4 cmpt. | 5 cmpt. | 6 cmpt. | 7 cmpt. |
|---|---|---|---|---|---|---|---|
| MSC | 0.5225 | 0.2311 | 0.0792 | 0.0016 | 0 | 0 | 0 |
| SLF | 0.5221 | 0.1878 | 0.0916 | 0.0016 | 0 | 0 | 0 |
| Proposal, bow height statistics | 0.5710 | 0.1535 | 0.0768 | 0.0036 | 0.0003 | 0 | 0 |
| Proposal, damage statistics | 0.5716 | 0.1668 | 0.0787 | 0.0046 | 0.0004 | 0 | 0 |

### 9.6.3 Container Vessel, $L$=190 m

The container vessel is here divided into 50 compartments.

Main particulars:

| | |
|---|---|
| Length over all [m] | 190.49 |
| Breadth [m] | 27.80 |
| Full load draught [m] | 8.25 |
| TEU | 1500 |

Figure 9.41 shows the subdivision index as a function of number of damaged zones for the four methods of calculation: the resolution MSC 19(58), the proposal SLF 43/3/2 and two of the present proposals, the bow height proposal and the damage statistics proposal excluding damages below the water line. The numbers for the attained index are all given in Tables 9.21 and 9.22. For this vessel the current regulation and the proposal from SLF are nearly identical. The bow height proposal starts with a higher attained index, $A$, if only few damage zones are included, but ends with an attained index close to the current regulation. The damage statistics proposal gives for this particular vessel a significantly higher attained index.

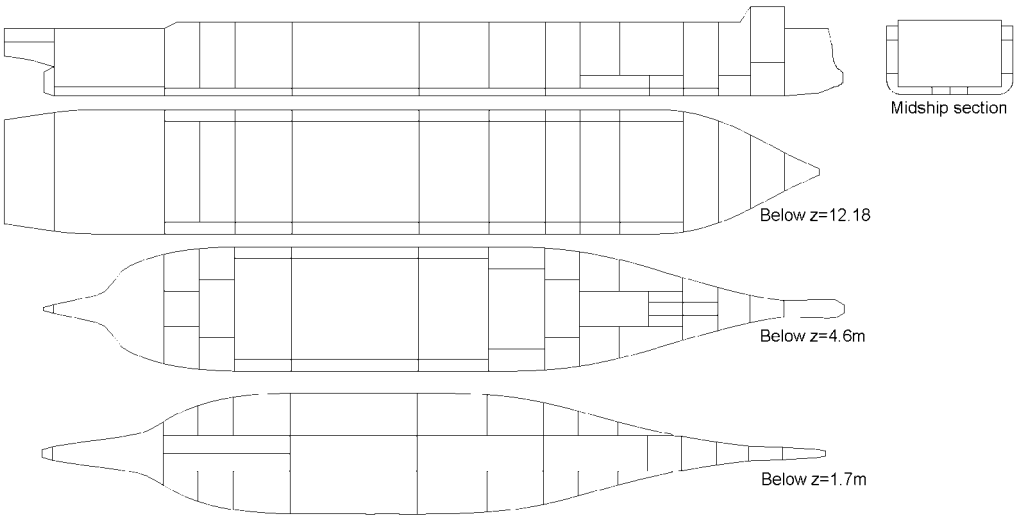


Figure 9.40: *A container vessel.*

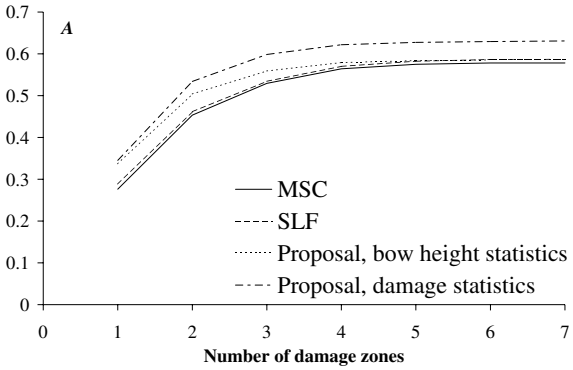


Figure 9.41: *Attained subdivision index as a function of number of damaged zones.*

Table 9.21: *Attained subdivision index, cumulative number of damage zones, container vessel.*

| Formulation | 1 cmpt. | 2 cmpt. | 3 cmpt. | 4 cmpt. | 5 cmpt. | 6 cmpt. | 7 cmpt. |
|---|---|---|---|---|---|---|---|
| MSC | 0.2763 | 0.4534 | 0.5294 | 0.5641 | 0.5751 | 0.5781 | 0.5781 |
| SLF | 0.2882 | 0.4615 | 0.5342 | 0.5700 | 0.5823 | 0.5864 | 0.5869 |
| Proposal, bow height statistics | 0.3367 | 0.5039 | 0.5590 | 0.5792 | 0.5838 | 0.5855 | 0.5866 |
| Proposal, damage statistics | 0.3451 | 0.5340 | 0.5985 | 0.6218 | 0.6274 | 0.6295 | 0.6308 |

Table 9.22: *Attained subdivision index, contributions from individual number of damage zones, container vessel.*

| Formulation | 1 cmpt. | 2 cmpt. | 3 cmpt. | 4 cmpt. | 5 cmpt. | 6 cmpt. | 7 cmpt. |
|---|---|---|---|---|---|---|---|
| MSC | 0.2763 | 0.1771 | 0.076 | 0.0347 | 0.0110 | 0.0030 | 0 |
| SLF | 0.2882 | 0.1733 | 0.0727 | 0.0358 | 0.0123 | 0.0041 | 0.0005 |
| Proposal, bow height statistics | 0.3367 | 0.1672 | 0.0551 | 0.0202 | 0.0046 | 0.0017 | 0.0011 |
| Proposal, damage statistics | 0.3451 | 0.1889 | 0.0645 | 0.0233 | 0.0056 | 0.0021 | 0.0013 |

## 9.7 Conclusions

The International Maritime Organization (IMO) is currently seeking to harmonise the damage stability regulations for all types of vessels using the probabilistic damage stability concept. It has been decided that the main framework of these new harmonised regulations should follow the concept of SOLAS Part B-1 and the proposal from SLF 39/3/2.

In this chapter a damage stability regulation proposal following the criteria laid down by IMO has been presented. The overall goal has been to develop a rational procedure for the probabilistic damage stability, addressing all types of ships and damage scenarios. The main approach was analyses of damage statistics giving distributions for damage locations and damage sizes. These distributions were used as a basis for a new proposal for determination of the probability of damaging a particular section of the vessel. The probability was, as in the current regulations, separated into three individual parameters: $p$, $v$ and $r$. The method for determination of these parameters was validated on the basis of the damage statistics analysed in Chapter 7.

A wide range of application examples was presented. Most of the examples end up giving nearly the same attained subdivision index as the current regulations, especially when the parameters with most influence are the $p$- and $r$- factors. If the vessel was designed with a large number of horizontal subdivisions or many decks around the water line, the influence from the new $v$-factor will lower the attained subdivision index significantly.

# Chapter 10

# Conclusions

The purpose of this thesis has been to develop a rational procedure for analysis of ship collisions, addressing all types of ships and damage scenarios.

The thesis can be separated into four main parts.

1. Deterministic analysis of ship collisions
2. Numerical Monte Carlo based simulations of ship collisions for estimation of distributions for the damage to the struck vessel and for the energy released for crushing
3. Analysis of damage statistics regarding ship collisions
4. A new proposal for damage stability regulation using the probabilistic approach

The parts will in the following be presented individually.

**1. Deterministic Analysis of Ship Collisions**
The present theoretical collision model is based on the principle of splitting the collision problem into an internal and an external analysis.

A model for the external dynamics, which deals with the movements of the two vessels and the interaction with the surrounding water during the collision, has been presented. The aim of the external dynamics is to estimate the fraction of the kinetic energy which is released for crushing of the structure. An analytical method for determination of the energy loss during ship collisions, developed by Pedersen and Zhang (1998), has been presented. This model has been used for all studies in the thesis regarding the external dynamics.

A simplified but rational model for determining the internal mechanics has been presented. The method is based on the super-element method, where the ship's structure is separated into its structural elements like plates, beams or plate intersections like X- and T-elements.

The procedure is validated by experiments on double-hull structures performed by Nagasawa and Tani (1977) and Amdahl and Kavlie (1992).

A model for estimating the bow geometry, given the main particulars of a vessel, has been presented; the bow can be either a conventional bow or a bulbous bow. The geometry of the two types of bows is idealised so the geometry can be described by few parameters, still covering with sufficient accuracy almost all existing bows. The geometry is based on a model presented by Scharrer (1996). When the bow geometry is known, the area of contact between the two vessels can be estimated.

A program for modelling the ship's structure has been developed. The method is based on the principle that the area of the struck ship which is affected by the collision is restricted to the area touched by the bow of the striking vessel. The structure within this area is divided into its structural components or super elements, and the total contact load between the two involved vessels can be determined by summing up the crushing forces of each super element. In order to allow fast input, or easy description of the structure, it is assumed that all elements can be located longitudinally, transversely or vertically only, and that the material is described by few parameters.

The results from the developed program have been compared to results from other programs for analysis of collisions. In all the analyses the bow of the striking vessel is assumed to be rigid, which means that only the side of the struck vessels will deform. Two series of comparisons are made.

- First a comparison of force and energy absorption as a function of the penetration for a collision between two Ro-Ro vessels. The comparison is made between calculation models developed by Hysing (1995), Scharrer (1996) and the present model. Considering the complexity of the problem, the comparisons indicate good agreement.
- Then the results from the present model are compared to results obtained by using three other collision models: DAMAGE developed in connection with the Joint MIT-Industry Program on Tanker Safety, ALPS/SCOL developed by Prof. Paik in Korea and SIMCOL, and the Simplified Collision Model developed by Prof. Brown from Virginia Tech. Three scenario test matrices are used in the comparison study, including varying velocity of striking vessel, collision angle and striking location. The results from the developed program are fully comparable with results from other collision programs.

In order to investigate the sensitivity of the collision analysis, the effect of changing the striking location has been analysed. Three analyses have been performed, the local striking location relative to the web framing, the global striking location along the hull girder and finally the vertical location, i.e. the influence of the loading condition on the involved vessels. Also the effect of changing the design has been analysed.

Two models for bow crushing have been presented, one dealing with longitudinally stiffened bows, the other with transversely stiffened bows. The bow strengths for the two differently

stiffened vessels have been compared. The two vessels are comparable in size and geometry, but the structural layout of the two bows is different. The first vessel is a longitudinally stiffened container vessel of a high ice class, the other vessel is a transversely stiffened bulk carrier. The result of the strength analysis shows a significantly lower resistance for a transversely stiffened bow.

Also a model for deformation of both the struck and the striking vessel has been developed. The calculation is here carried out in penetration steps. Only one of the involved vessels can be deformed in each step. By comparison of the crushing forces for respectively the bow and the side, it can be determined which vessel deforms during the considered step. A sensitivity analysis has been carried out using a series of computer simulations of collisions involving 11 different ships, five striking and six struck, in order to determine when the energy released for crushing is absorbed by the bow of the striking vessel or by the side structure of the struck vessel.

**2. Numerical Monte Carlo Based Simulations of Ship Collisions**

A probabilistic method for determination of damage distributions and energy distributions has been presented. The probabilistic program or calculation method is built around the deterministic program calculating the damage to the struck vessel. The probabilistic analysis is based on input distributions of striking vessels, velocities, striking locations and collision angles. This input for the calculation can be separated into three groups, the struck vessel, the striking vessels and the collision scenarios.

The striking vessels are analysed with respect to distribution of types and lengths within a particular area. Five cases have been investigated, namely vessels in worldwide trade, the Straits of Dover and Gibraltar and the eastern and western routes through the Great Belt. When type and length are given the rest of the main particulars for the striking vessels must be found. A database containing ship characteristics for the world fleet has been purchased from LMIS (2000). This data has been analysed to find simple linear relations for length versus breadth, draught, depth, displacement and service speed for each type of vessel. Also a neural network has been established, which can be used as a design tool for estimation of the main particulars of the striking vessel. To get a complete picture of the striking vessels some assumptions about the loading conditions have been made.

The probability distributions for parameters defining the collision scenarios are found. This input group consists of the velocity of the struck and the striking vessel, the collision angle and the striking location on struck vessel.

Fifteen different struck vessels have been subjected to the damage analysis giving distributions for the damage lengths and penetrations.

Distributions for energy to be absorbed have been calculated for vessels sailing in worldwide trade, the Straits of Dover and Gibraltar and the eastern and western routes through the Great Belt. It has been found that the energy distributions can be described by a geographical location and the displacement of the struck vessel only.

**3. Analysis of Damage Statistics regarding Ship Collisions**
A damage database, collected within the European research program HARDER, has been analysed with regard to collision type, the relation between the struck and the striking vessel and the relation between damage parameters and the main particulars of the struck vessel. The main findings from the analysis can be summarised as

- The non-dimensional penetration $\overline{z}$ is uncorrelated with the non-dimensional damage location $\overline{x}$
- The non-dimensional damage length $\overline{y}$ is uncorrelated with the non-dimensional damage location $\overline{x}$
- Only 5% of the penetrations are greater than $0.5 \cdot B$
- The largest damage length is observed to be $0.48 \cdot L$
- The relation between the non-dimensional penetration, $\overline{z}$, and the non-dimensional damage length, $\overline{y}$, when the non-dimensional damage length is less than 0.033:
  For a given non-dimensional damage length, $\overline{y}$, the non-dimensional penetration, $\overline{z}$, is less than $\overline{z} = 15\overline{y}$ in more than 90% of all cases. The analysis shows that although there is an increasing linear tendency between $\overline{z}$ and $\overline{y}$, the spread of the responses appears to increase as the non-dimensional damage length increases. As the scatter is spreading, it is not possible to determinine a function, but just indicate that the probability $r$ that the penetration is less than $b$ becomes an increasing function of the relation $b/B$.
- The relation between the non-dimensional penetration, $\overline{z}$, and the non-dimensional damage length, $\overline{y}$, when the non-dimensional damage length is greater than 0.033:
  The non-dimensional damage length $\overline{y}$ is uncorrelated with the non-dimensional penetration $\overline{z}$

The results from the statistics have been compared to the results obtained from the numerical Monte Carlo based simulation. The damage location, the damage length and the penetration are treated separately as both the damage database analyses and the simulation show that these parameters are independent.

The non-dimensional damage location
The ship collision probability model described in Sections 2.1.2 and 2.1.3 predicts a uniform distribution of the damage location. This is in agreement with the observed results.

Non-dimensional penetration
The agreement for the non-dimensional penetration obtained by simulation and analysis of the observed data is poor. The observed penetrations are significantly larger than the simulated results. A reason for this difference might be that the analysed vessels of a more recent date are based on a structural layout which absorbs the energy better, so that the

result is smaller penetration. However, the main reason for the difference is probably that minor damages are not reported to either the authorities or the classification societies and are therefore not present in the damage database. To test the hypothesis that some minor damages are not reported, the observed data has been augmented by inclusion of more minor damages to see if a fit to the simulated results can be achieved. It is here assumed that only non-dimensional penetrations smaller than 0.1 are not reported. This analysis shows that, if the simulated results are right, only approx. 1/3 of the smaller penetrations below $0.1B$ is reported and present in the damage database. This does not seem to be an unrealistic assumption.

Non-dimensional damage length

A good agreement between simulated results and observed data has been found, but it is seen that the simulated damage lengths are a little longer than the damage lengths obtained from the damage database analysis. The main reason for this difference is probably that the analysed vessels of a more recent date have a higher velocity, which results in longer damages.

## 4. A New Proposal for Damage Stability Regulation Using the Probabilistic Approach

Based on findings from the analysis of damage statistics of ship collisions, a new proposal for damage stability regulation using the probabilistic approach is made. The damage statistics, and not the simulation, is chosen for validation as the Monte Carlo based simulation shows a large variation in the results for different struck vessels. It is also decided to use the database with the reported data as it is, and not to include any more minor damages.

The main concept of the current probabilistic damage stability regulation from A.265 and SOLAS part B-1 is used for determination of the subdivision index $A$, where $A$ can be expressed by the formula

$$A = \sum p \cdot s \cdot v$$

The $p$-factor accounts for the probability that only one compartment or a group of compartments are flooded, disregarding the horizontal subdivision, $v$ is the factor accounting for the horizontal subdivision and $s$ for the probability of survival after flooding of the compartment. When wing compartments are fitted, the $p$-factor shall be obtained by multiplying by a factor $r$ for a wing compartment, and by multiplying by $(1 - r)$ for simultaneous flooding of a wing and adjacent inboard compartment.

Focus has been on validating the method for calculation of $A$ and determination of the $p-$, $r-$ and $v-$factors. The new proposal can be summarised as

The $p$-factor

The probability $p$ for cases where limits of neither compartment or group of compartments

under consideration coincide with the aft or the forward terminals:

$$J \leq \frac{1}{6} \qquad p_{i1} = -10 \cdot J^3 + \frac{21}{4} \cdot J^2$$

$$J > \frac{1}{6} \qquad p_{i2} = -\frac{13}{288} + \frac{13}{16} \cdot J + \frac{1}{2} \cdot J_n^3 - \frac{3}{4} \cdot J \cdot J_n^2 - \frac{3}{8} \cdot J_n^2 + \frac{3}{4} \cdot J \cdot J_n$$

The probability $p$ for cases where the forward limit of the compartment or group of compartments under consideration coincides with the forward terminal - or - where the aft limit of the compartment or group of compartments under consideration coincides with the aft terminal:

$$J \leq \frac{1}{6} \qquad p_{af} = \frac{1}{2}(p_{i1} + J)$$

$$J > \frac{1}{6} \qquad p_{af} = \frac{1}{2}(p_{i2} + J)$$

Where the compartment considered extends over the entire ship's length:

$$p = 1$$

For all the above expressions $J_n$ are defined as $\min(J, J_m)$, where $J$ is the length of the considered compartment, $J = \overline{x_2} - \overline{x_1}$, and $J_m$ is the largest expected non-dimensional damage length, $J_m = \frac{1}{2}$.

The $r$-factor

The factor $r$ shall be determined by the following formulas:

$$r = \frac{p \cdot r}{p} = 1 - \left[1 - C\left(\frac{b}{B}\right)\right] \cdot \left[1 - \frac{G}{p}\right]$$

The function $C$ is for all compartments defined as

$$C\left(\frac{b}{B}\right) = 12 \cdot J_b \cdot (-45 \cdot J_b + 4)$$

The function $G$ for cases where the considered compartment extends over the entire ship's length:

$$G_t = -30 \cdot J_b^2 + \frac{21}{2} \cdot J_b$$

The function $G$ for cases where limits of neither compartment or group of compartments under consideration coincide with the aft or the forward terminals:

$$G_i = 20 \cdot J_b^3 - \frac{21}{4} \cdot J_b^2 + G_t \cdot J$$

The function $G$ for cases where the forward limit of the compartment or group of compartments under consideration coincides with the forward terminal - or - where the aft limit

of the compartment or group of compartments under consideration coincides with the aft terminal:

$$G = \frac{1}{2}(G_i + G_t \cdot J)$$

The $v$-factor

Two proposals for the $v$-factor have been presented. The first proposal is based on bow height statistics. This proposal is dependent on the length of the struck vessel. The other proposal is based on the damage statistics from the damage database and is independent of the length of the struck vessel.

Proposal 1: Bow height statistics
The $v$-factor is dependent on the length of the vessel. The function is bi-linear with the knuckle point $v = 0.5$:

$$v = 0.0 \qquad (H - T) = 1.0 + \frac{1.1}{60} \cdot (L - 100)$$
$$(H - T)_{min} = 1.0 \qquad (H - T)_{max} = 2.1$$
$$v = 0.5 \qquad (H - T) = 4.5 + \frac{2.0}{60} \cdot (L - 100)$$
$$(H - T)_{min} = 4.5 \qquad (H - T)_{max} = 6.5$$
$$v = 1.0 \qquad (H - T) = 9.0 + \frac{4.2}{60} \cdot (L - 100)$$
$$(H - T)_{min} = 9.0 \qquad (H - T)_{max} = 13.2$$

Proposal 2: Damage statistics
The $v$-factor is independent on the length of the vessel. The function is bi-linear with the knuckle point $v = 0.8$:

$$v = 0.0 \qquad (H - T) = 0.0$$
$$v = 0.8 \qquad (H - T) = 7.8$$
$$v = 1.0 \qquad (H - T) = 12.5$$

A wide range of application examples for determination of the attained subdivision index has been presented. Most of the examples end up giving nearly the same attained subdivision index as the current regulations, especially when the parameters exerting most influence are the $p$- and $r$- factors. If the vessel has been designed with high horizontal subdivisions, the influence from the new $v$-factor will lower the attained subdivision index significantly.

This page is intentionally left blank.

# Bibliography


Abramowicz, W. (1994), Crush Resistance of 'T' 'Y' and 'X' Sections, Technical Report 24, Joint MIT-Industry Program on Tanker Safety.

Abramowicz, W. and Sinmao, M. (1999), User's Manual and Modeling Guide for the Program DAMAGE, Technical Report 66, Joint MIT-Industry Program on Tanker Safety.

Agerschou, H. and Lundgren, H. (1983), *Planning and Design of Ports and Marine Terminals*, A. Wiley - Interscience Publication.

Amdahl, J. (1982), *Energy Absorption in Ship - Platform Impact*, Ph.D. thesis, Department of Marine technology, Norwegian Institute of Technology.

Amdahl, J. and Kavlie, D. (1992), Experimental and Numerical Simulation of Double Hull Stranding, Technical report, DNV MIT Workshop on "Mechanics of Ship Collision and Grounding, DNV Høvik, Oslo.

Brown, A., Tikka, K., Daidola, J., Lützen, M., Choe, I. and Gooding, P. (2000), Structural Design and Response in Collision and Grounding, *SNAME Transactions*, 108.

Bruun, P. (1989), *Port Engineering, Vol. 1*, Library of Congress Catalog - in Publication Data, 4th edition.

Chen, D. (2000), *Simplified Collision Model (SIMCOL)*, Master's thesis, Dept. of Ocean Engineering, Virginia Tech.

Clausen, H. B., Lützen, M., Friis-Hansen, A. and Bjørneboe, N. (2001a), Bayesian and Neural Networks for Preliminary Ship Design, *Marine Technology*, 38(4).

Clausen, H. B., Lützen, M., Friis-Hansen, A. and Bjørneboe, N. (2001b), Bayesian and Neural Networks for Preliminary Ship Design, in *The Eighth International Symposium on Practical Design of Ships and Other Floating Structures (PRADS), Shanghai, China.*

Crake, K. (1995), *Probabilistic Evaluations of Tanker Ship Damage in Grounding Events*, Master's thesis, Naval Engineer thesis, MIT.

Demuth, H. and Beale, M. (1998), *Neural Network Toolbox for Use with MATLAB*, 3rd edition.

Denis, M. S. (1962), A Note on the Probabilistic Method of assessing Survivability to Collision Damage, *Schiffestechnik*, 9.

Derucher, K. N. (1983), Evaluation of Pier Fendering Systems, *The Dock and Harbour Authority.*

Dovre Safetec Ltd., C. (1996), COAST Database, Technical Report No. DST-95-CR-1110-02, Development of UKCS Vessel Traffic Database for DOT/UKOOA/HSE.

Foresee, F. D. and Hagen, M. T. (1997), Gauss-Newton Approximation to Bayesian Regularization, in *Proceedings of International Joint Conference on Neural Networks.*

Friis Hansen, P. and Pedersen, P. T. (1998), Risk Analysis of Conventional and Solo Watch Keeping, submitted to the Int. Maritime Organization (IMO) Marine Safety Committee by Denmark at the 69th Session.

Harder (2000), Harmonisation of Rules and Design Rationale,, Technical report, GRD1-1999-10721 (Fifth Framework Programme).

Herbert Engineering, C. (2001), Vertical Extent of Damage, Technical report, report prepared for Commandant (G-MSE-2) US Coast Guard Headquarters, Washington D.C.

Hughes, O. F. (1981), Design of Laterally Loaded Plating - Uniform Pressure Loads, *Journal of Ship Research*, 25(2).

Hutchison, B. L. (1986), Barge Collisions, Rammings and Groundings - an Engineering Assessment of the Potential for Damage to Radioactive Material Transport Casks, Technical Report SAND85-7165 TTC-05212.

Hysing, T. (1995), Safety of Passenger/Roro Vessels, Damage and Penetration Analysis, Technical Report Fl95-0419, Det Norske Veritas.

IMO (1971), *Resolution A.265 (VIII), Regulations on Subdivision and Stability of Passenger Ships.*

IMO (1995), Interim Guidelines for Approval of Alternative Methods of Design and Construction of Oil Tankers under Regulation 13F(5) of Annex I of MARPOL 73/78, *Resolution MEPC.66 (37) Adopted September 14, 1995.*

Jensen, J. J. (2000), Ship Design Part 1, *Department of Naval Architecture and Offshore Engineering, Technical University of Denmark.*

Jones, N. (1989), Structural Impact, *Cambridge University Press.*

Kirkegaard, H. (1993), *Ship Collisions with Icebergs*, Ph.D. thesis, Technical University of Denmark.

Kitamura, O. (2001), FEM Approach to the Simulation of Collision and Grounding Damage, in *Proceedings of 2nd International Conference on Collision and Grounding of Ships, Copenhagen, Denmark.*

Kuroiwa, T. (1996), Numerical Simulation of Actual Collision and Grounding Accidents, in *Proceedings of Int. Conference on Design and Methodologies for Collision and Grounding Protection of Ships, San Francisco, California.*

Lehmann, E. and Yu, X. (1995), Progressive Folding of Bulbous Bows, in *The Sixth International Symposium on Practical Design of Ships and Mobile Units (PRADS).*

LMIS (2000), Ship Characteristics, Technical report, Lloyd's Maritime Information Services.

Lützen, M. (2001), Damage Distributions, Technical Report 2-22-D-2001-01-1, EU-project GRD1-1999-10721 'HARDER'.

Lützen, M. (2001), Design against Minor Impacts, in *The Eighth International Symposium on Practical Design of Ships and Other Floating Structures (PRADS), Shanghai, China.*

Lützen, M. and Clausen, H. B. (2000), Collision Energy Distributions, Technical Report 2-21-D-2000-01-0, EU-project GRD1-1999-10721 'HARDER'.

Lützen, M. and Pedersen, P. T. (2000), Generation of Energy Dissipation Reference Values, Technical Report TD.09.00.12.00, EU-project G3RD-CT-2000-00253 'CRASH-COASTER'.

Lützen, M. and Rusaas, S. (2001), Derivation of Probability Distributions for Collision Energy for Use within a Harmonized Probabilistic Damage Stability Framework, in *Proceedings of 2nd International Conference on Collision and Grounding of Ships.*

Lützen, M., Simonsen, B. C. and Pedersen, P. T. (2000), Rapid Prediction of Damage to Struck and Striking Vessels in a Collision Event, in *Proceedings of Ship Structures for the New Millennium: Supporting Quality in Shipbuilding, Arlington.*

MacKay, D. J. C. (1992), Bayesian Interpolation, *Neural Computation*, 4(3).

McDermott, F., Kline, R. G., Jones, E. L., Maniar, N. and Chiang, W. P. (1974), Tanker Structural Analysis for Minor Collision, *SNAME Transactions*, 82.

Minorsky, V. (1959), An Analysis of Ship Collisions with Reference to Protection of Nuclear Power Ships, *Journal of Ship Research*, 3(2).

Motora, S. (1971), Equivalent Added Mass of Shops in Collision, *Society of Naval Architects, Japan*, 7.

Nagasawa, H. and Tani, M. (1977), A study on the Collapse of Ship Structure in Collision with Bridge Piers, *J. SNAJ.*, 142.

Paik, J. K., Chung, J. Y., Choe, I. H., Thayamballi, A. K., Pedersen, P. T. and Wang, G. (2000), On the Rational Design of Double Hull Tanker Structures against Collision, *SNAME Transactions*, 108.

Paik, J. K. and Pedersen, P. T. (1996), Modeling of the Internal Mechanics in Ship Collisions, *Ocean Engineering*, 23(2).

Pawlowski, M. (1996), Outline of the Probabilistic Concept of Ship Subdivision, Seminar on Practical Application of Probabilistic Subdivision Regulation in Ship Design, *Department of Naval Architecture and Offshore Engineering, Technical University of Denmark.*

Pedersen, P. and Zhang, S. (2000), Absorbed Energy in Ship Collisions and Grounding, *Journal of Ship Research*, 44(2).

Pedersen, P. T. (1995), Collision and Grounding Mechanics, *West European Confederation of Maritime Technology Societies (WEMT).*

Pedersen, P. T., Valsgaard, S., Olsen, D. and Spangenberg, S. (1993), Ship Impacts: Bow Collisions, *Int. J. of Impact Engineering*, 13(2).

Pedersen, P. T. and Zhang, S. (1998), On Impact Mechanics in Ship Collisions, *Marine Structures*, 11.

Pianc (1984), Report of the International Commission for Improving the Design of Fender Systems, Technical Report Supplement to Bulletin No. 45, Permanent International Association of Navigation Congress.

Rawson, C., Crake, K. and Brown, A. J. (1998), Assessing the Environmental Performance of Tankers in Accidental Grounding and Collision, *SNAME Annual Meeting.*

Sano, A., Muragishi, O., Yoshikawa, T., Murakami, A. and Motoi, T. (1996), Strength Analysis of a New Double Hull Structure for VLCC in Collision, in *Proceedings of Int. Conference on Design and Methodologies for Collision and Grounding Protection of Ships, San Francisco, California.*

Scharrer, M. (1996), Safety of Passenger/Roro Vessels, Analysis of Collision and Hole Sizes, Technical Report Fl96.099, Germanischer Lloyd.

Simonsen, B. and Ocakli, H. (1999), Experiments and Theory on Deck and Girder Crushing, *Thin-walled Structures*, 34.

Simonsen, B. C. (1999), Theory and Validation for the DAMAGE Collision Module, Technical Report 67, Joint MIT-Industry Program on Tanker Safety.

SOLAS (1990), *Chapter II, Part B-1, Subdivision and Damage Stability of Cargo Ships.*

Tagg, R., Bartzis, P., Papanikolaou, A., Spyrou, K. and Lützen, M. (2001), Updated Vertical Extent of Collision Damage, in *Proceedings of 2nd Internat ional Conference on Collision and Grounding of Ships.*

Wendel, K. (1960), Die Wahrscheunlichkeit des Ueberstehens von Verletzungen, *Schiffestechnik*, 7.

Wierzbicki, T. (1995), Concertina Tearing of Metal Plates, *Int. J. Solids Structures*, 32(19).

Wierzbicki, T. and Abramowicz, W. (1983), On the Crushing Mechanics of Thin-walled Structures, *Journal of Applied Mechanics*, 50.

Wierzbicki, T. and Simonsen, B. C. (1996), Global Structural Model of Bow Indentation into Ship Side, Rupture Analysis of Oil Tankers in a Side Collision, Technical Report 2, M.I.T.

Zhang, S. (1999), *The Mechanics of Ship Collisions*, Ph.D. thesis, Technical University of Denmark.

# Appendix A

# Main Particulars and Scantlings of Various Vessels

**Table Overview**



Table A.1: *Main Particulars and geometric bow-data for striking vessels*

| | | | Container Vessel | Bulk Carrier | General Cargo | Tanker | Coaster | Bulk Carrier |
|---|---|---|---|---|---|---|---|---|
| DWT | | $[mt]$ | 40,000 | 150,000 | 3,000 | 2,000 | 500 | 51,800 |
| Displacement | $\Delta$ | $[mt]$ | 54,000 | 174,850 | 4,594 | 3,016 | 886 | 70,000 |
| Length | $L_{pp}$ | $[m]$ | 211.5 | 274.0 | 78.0 | 69.0 | 41,0 | 205.25 |
| Breadth | $B$ | $[m]$ | 32.2 | 47.0 | 16.0 | 12.3 | 9.0 | 30.5 |
| Depth | $D$ | $[m]$ | 24.0 | 26.0 | 10.5 | 8.6 | 6.4 | 20.0 |
| Draft | $T$ | $[m]$ | 11.9 | 15.96 | 5.7 | 4.75 | 3.34 | 11.9 |
| Stem angle | $\phi$ | $[deg.]$ | 61.5 | 60.0 | 57.0 | 62.5 | 59.0 | 53.0 |
| Deck coeff. | $B_d$ | $[m^{-1}]$ | 0.109 | 0.0741 | 0.180 | 0.286 | 0.573 | 0.147 |
| Bottom coeff. | $B_b$ | $[m^{-1}]$ | 20.000 | 0.00299 | 0.180 | 0.286 | 0.573 | 0.076 |
| Bulb | | | | | | | | |
| Length | $R_L$ | $[m]$ | 7.5 | 7.5 | 2.9 | 2.2 | 1.8 | 8.5 |
| Vertical axis | $R_V$ | $[m]$ | 5.1 | 5.9 | 2.48 | 1.9 | 1.41 | 4.5 |
| Horisontal axis | $R_H$ | $[m]$ | 2.5 | 8.5 | 1.36 | 1.1 | 0.83 | 5.0 |
| Bulb start | $R_D$ | $[m]$ | 0.0 | 0.7 | 0.7 | 0.3 | 0.35 | 0.0 |

Table A.2: *Structural bow details of 51,800 DWT Bulk Carrier with transverse stiffened bow*

| | | |
|---|---|---|
| **Material** | | |
| Yield Stress 265 MPa | | |
| **Bulb** | | |
| **Frames** | | Spacing 610 mm |
| **Shell Plate** | Thickness 13.5 mm | |
| **Stringer Decks** | | |
| H = 2.000 m | Thickness 8.0 mm | |
| H = 4.000 m | Thickness 8.0 mm | |
| H = 5.875 m | Thickness 8.0 mm | |
| **Stringer Deck** : | H = 11.500 m, | H = 9.625 m |
| Thickness 8.0 mm | | |
| Stiffening Transv. | 230 x 9 | Spacing 610 mm |
| **Top of Bow** | | |
| **Shell Plate** | Thickness 13.5 mm | |
| **Forecastle Deck** : | H = 20.000 m | |
| Thickness 9.5 mm | | |
| Stiffening Long. | 400 x 120 x 11.5/23 | Spacing 3000 mm |
| **Peak Deck** : | H = 14.250 m | |
| Thickness 8.0 mm | | |
| Stiffening Long. | 400 x 120 x 11.5/23 | Spacing 3000 mm |
| Stiffening Transv. | 230 x 9 | Spacing 610 mm |
| **Upper Deck** : | H = 17.610 m | |
| Thickness 10.0 mm | | |
| Stiffening Long. | 400 x 120 x 11.5/23 | Spacing 3000 mm |
| **Centreline Bulkhead** | up to | 14.250 m |
| Thickness 7.5 mm | | |
| **Bottom** | | |
| Height of double bottom | 2.0 m | |
| Thickness | 15.5 mm | |
| Inner bottom Thickness | 15.5 mm | |
| Centreline Girder Thickness | 16.0 mm | |
| Girder Long. | Thickness 15.0 mm | Spacing 3.0 m |
| Floors | Thickness 13.5 mm | Spacing 610 mm |

Table A.3: *Structural data for cargo hold section of 150,000 DWT tanker*

| **Component** | | | **Material** |
|---|---|---|---|
| **Bottom** | | t = 17.2 mm | 2 |
| Long. Stiff. | Spacing 850 mm | 400 x 120 x 11.5/23 | 2 |
| **Inner Bottom** | H = 2300 mm | t = 17.0 mm | 2 |
| Long. Stiff. | Spacing 850 mm | 400 x 120 x 11.5/23 | 2 |
| **Floors** | Spacing = 3300 mm | t = 15.0 mm | 2 |
| **Bottom** Girders | Y = 5100, 10200 mm | t = 13.2 mm | 1 |
| | Y = 15300, 20400 mm | t = 14.0 mm | 1 |
| **Weather Deck** | | t = 19.0 mm | 1 |
| Long. Stiff. | Spacing 850 mm | Flat bar 400 x 28 | 1 |
| Transv. Stiff. | Spacing 3300 mm | Flat bar 500 x 24 | 1 |
| **Side Shell** | | t = 18.2 mm | 1 |
| Long. Stiff. | Spacing 850 mm | | 1 |
| | H = 0 - 7 m | 350 x 120 x 11.5/18 | 1 |
| | H = 7 - 10 m | 350 x 120 x 10.5/16 | 1 |
| | H = 10 - 14 m | 325 x 120 x 10.5/14 | 1 |
| | H = 14 - 21 m | 300 x 100 x 10.5/15 | 1 |
| | H = 21 - m | 250 x 90 x 11.5/16 | 1 |
| **Inner Side Shell** | Depth = 2000 mm | t = 17.9 mm | 1 |
| Long. Stiff. | Spacing 850 mm | | 1 |
| | H = 0 - 7 m | 375 x 120 x 10.5/18 | 1 |
| | H = 7 - 16 m | 350 x 120 x 10.5/16 | 1 |
| | H = 16 - m | 350 x 120 x 10.5/15 | 1 |
| **Long. Bulkhead** | Center | t = 16.2 mm | 1 |
| Long. Stiff. | Spacing 850 mm | | 1 |
| | H = 0 - 9 m | 350 x 120 x 10.5/16 | 1 |
| | H = 9 - 16 m | 325 x 120 x 10.5/14 | 1 |
| | H = 16 - m | 250 x 90 x 11.5/16 | 1 |
| Stringers | H = 4450, 8700, 13800, 18900 mm | 3500 x 700 x 20.3/24 | 2 |
| Vertical. Stiff. | Spacing 3300 mm | Flat bar 500 x 24 | 1 |
| **Web Frames** | Spacing = 3300 mmm | t = 20.3 mm | 1 |
| **Stringer Decks** | H = 4450, 8700, 13800, 18900 mm | t = 11.7 mm | 2 |
| **Transv. Bulkheads** | | t = 15.3 mm | 1 |
| Stringers aft part | H = 4450, 8700, 13800, 18900 mm | 3500 x 700 x 20.3/24 | 1 |
| Vertical. Stiff. | Spacing 850 mm | 413 x 118 x 24/23.2 | 1 |
| **Material** | | | |
| Material 1 | $E = 2.1 \cdot 10^{11} N/m^2$ | $\sigma_0 = 240 \cdot 10^6\ N/m^2$ $R_c = 3 \cdot 10^5 N/m$ | $\epsilon_c = 0.1$ |
| Material 2 | $E = 2.1 \cdot 10^{11} N/m^2$ | $\sigma_0 = 320 \cdot 10^6\ N/m^2$ $R_c = 3 \cdot 10^5 N/m$ | $\epsilon_c = 0.1$ |

Table A.4: *Structural data for cargo hold section of crude oil carrier, See also Figure 5.13*

| | | |
|---|---|---|
| **Material** | | |
| Yield Stress 310 MPa | | |
| **Frames** | | |
| Thickness 15 mm | | Spacing 3700 mm |
| **Floors** | | |
| Thickness 16 mm | | Spacing 3700 mm |
| **Stringer Decks** | | |
| H = 5600 mm | Thickness 15 mm | |
| H = 9650 mm | Thickness 15 mm | |
| H = 14510 mm | Thickness 14 mm | |
| **Deck Stiffeners** | | |
| Longitudinal: | 300 X 90 X 11/16 | Spacing 830 mm |
| Transverse : | 1500 X 12.5 | Spacing 3700 mm |
| **Side and Inner Side** | | |
| Side | Thickness 16.5 mm | |
| Inner Side | Thickness 15 mm | Depth 2500 mm |
| All Longitudinal with Spacing 810 mm | | |
| Between 0 and 5600 mm abl.: | 400 X 100 X 13/18 | |
| Between 5600 and 9650 mm abl.: | 400 X 100 X 11.5/16 | |
| Between 9650 and 14510 mm abl.: | 300 X 100 X 12/17 | |
| Between 14510 and 21000 mm abl.: | 300 X 90 X 11/16 | |
| **Bottom and Inner Bottom** | | |
| Thickness 17 mm | | Height 2300 mm |
| Longitudinal: | 450 X 125 X 11.5/18 | Spacing 830 mm |
| **Transverse Bulkhead** | | |
| Thickness 15 mm | | |
| Vertical Stiffeners : | 450 X 125 X 11.5/18 | Spacing 830 mm |
| Horizontal Stiffeners : | | |
| H = 14510, 9560 and 5600 mm abl. | 2000 X 150 X 12/12 | |

Table A.5: *Structural data for engine section of crude oil carrier, See also Figure 5.13*

| | | |
|---|---|---|
| **Material** | | |
| Yield Stress 310 MPa | | |
| **Frames** | | |
| | 400 X 12 | Spacing 800mm |
| **Floors** | | |
| Thickness = 17.6 mm | | Spacing 800mm |
| **Decks** | | |
| Thickness 11 mm | | |
| Weather deck | | |
| Longitudinal: | 700 X 150 X 11/15 | Spacing 830 mm |
| Transvers stiff.: | 700 X 11 | Spacing 800 mm |
| H = 9650 mm abl. | | |
| Longitudinal: | 300 X 11 | Spacing 830 mm |
| H = 14510 mm abl. | | |
| Longitudinal: | 300 X 11 | Spacing 830 mm |
| **Side Shell** | | |
| Thickness 16.5 mm | | |
| Longitudinal | 250 X 12 | Spacing 810 mm |
| **Bottom and Inner Bottom** | | |
| Bottom | Thickness 19.5 mm | |
| Inner Bottom | Thickness 16 mm | |
| Longitudinal: | 300 X 90 X 13/17 | Spacing 810 mm |
| **Longitudinal Bulkhead y=7000 mm** | | |
| Thickness 16 mm | | |
| Vertical Stiffeners : | 400 X 15 | Spacing 800 mm |
| **Longitudinal Bulkhead y=12500 mm** | | |
| Thickness 19.5 mm | | |
| Longitudinal Stiffeners : | 200 X 11 | Spacing 810 mm |

Table A.6: *Main particulars and structural data for three single hull tankers*

| | | Tanker 1 | Tanker 2 | Tanker 3 |
|---|---|---|---|---|
| Main Particulars | | | | |
| Length | $[m]$ | 103.0 | 198.0 | 317.0 |
| Breadth | $[m]$ | 15.5 | 29.9 | 56.6 |
| Depth | $[m]$ | 6.9 | 14.9 | 31.5 |
| Draught | $[m]$ | 5.8 | 11.1 | 22.5 |
| Mass | $[mt]$ | 7,400 | 52,400 | 330,300 |
| Material | | | | |
| Yield stress | $[MPa]$ | 250 | 250 | 250 |
| Plate thickness | | | | |
| Shell Plate | $[mm]$ | 14 | 19.5 | 20 |
| Bottom Plate | $[mm]$ | 12 | 15 | 20 |
| Deck Plate | $[mm]$ | 14 | 19.5 | 20 |
| Web frames | | | | |
| Spacing | $[mm]$ | 2900 | 3025 | 5400 |
| Thickness | $[mm]$ | 14 | 15 | 14 |
| Depth | $[mm]$ | 660 | 1000 | 3200 |
| Floors | | | | |
| Spacing | $[mm]$ | 2900 | 3025 | 5400 |
| Thickness | $[mm]$ | 10 | 11.5 | 15 |
| Depth | $[mm]$ | 885 | 1450 | 3200 |
| Stiffeners side and bottom | | | | |
| Web thickness | $[mm]$ | 10 | 12 | 15 |
| Web depth | $[mm]$ | 200 | 280 | 600 |
| Flange thickness | $[mm]$ | 10 | 15 | 15 |
| Flange width | $[mm]$ | 50 | 100 | 160 |
| Spacing | $[mm]$ | 720 | 760 | 950 |

# Appendix B

# Input for Collision Programs

## B.1 Damage of Struck Vessel

**Principal Structure**

**1** The ship bottom
**2** The inner bottom (if present)
**3** The weather deck
**4** The ship side
**5** The inner ship side (if present)
**6** Mid deck (if present, if more they are denoted 6.1,6.2,6.3 etc.)
**7** Transverse bulkhead (if present, if more they are denoted 7.1,7.2,7.3 etc.)
**8** Longitudinal bulkhead (if present, if more bulkheads, they are denoted 8.1,8.2, 8.3 etc.)

**Longitudinal Secondary Structure**

**9** Floors (if present, if more they are denoted 9.1,9.2,9.3 etc.)
**10** Stringers (if present, if more they are denoted 10.1,10.2,10.3 etc.)
**11** Stiffeners (if present, if calculated as beams then 11.1,11.2,11.3 etc.) 11.x can only be defined for stiffeners at side shell, rest are defined as 11

**Transverse Secondary Structure**

**12** Floors (if present, if more they are denoted 12.1,12.2,12.3 etc.)
**13** Girders (if present, if more they are denoted 13.1,13.2,13.3 etc.)
**14** Frames (if present, if more they are denoted 14.1,14.2,14.3 etc.)
**15** Stiffeners

### Coordinate System

All structure in struck vessel are described in a $x, y, z$ coordinate system. Origin is at the baseline and midship of the struck vessel, the $z$-axis pointing up and the $x$-axis is in the symmetry plane pointing forward.

### Input for data file

**type** Number, Item number

**Mat** Material

**Place** For secondary structure, type of principal structure the item is attached to

**Pos** Position according to above descreibed coordinate system

Principal Structure

| Item | | Data Input | | | |
|---|---|---|---|---|---|
| 1 | Bottom | Type | Mat | Pos ($z$) | $t_{plate}$ |
| 2 | Inner Bottom | Type | Mat | Pos ($z$) | $t_{plate}$ |
| 3 | Weather Deck | Type | Mat | Pos ($z$) | $t_{plate}$ |
| 4 | Side Shell | Type | Mat | Pos ($y$) | $t_{plate}$ |
| 5 | Inner Side | Type | Mat | Pos ($y$) | $t_{plate}$ |
| 6.x | Mid decks | Type | Mat | Pos ($z$) | $t_{plate}$ |
| 7.x | Transverse Bulkheads | Type | Mat | Pos ($x$) | $t_{plate}$ |
| 8.x | Longitudinal Bulkheads | Type | Mat | Pos ($y$) | $t_{plate}$ |

Longitudinal secondary Structure

| Item | | Data Input | | | | |
|---|---|---|---|---|---|---|
| 9.x | Girders at Bottom * | Type | Mat | Pos ($y$) | $t_{plate}$ | |
| 10.x | Stringer Decks A** | Type | Mat | Pos ($x$) | $t_{plate}$ | |
| 10.x | Stringer Decks B*** | Type | Mat | Pos ($x$) | $t_{plate}$ | Depth |

* Girders at bottom (9.01 9.02 ..) only if double bottom, if no double bottom, the girders are of type 11.

** Stringer deck A (10.01 10.02 ..) Between double side

***Stringer deck B (10.01 10.02 ..) Stringer deck not reaching the innerside or no inner side present

Longitudinal Stiffeners

| Item | | Data Input | | | | | | | |
|---|---|---|---|---|---|---|---|---|---|
| 11 | Stiffeners | Type | Mat | Place | Pos ($y/z$) | $t_{web}$ | $h_{web}$ | $t_{flange}$ | $h_{flange}$ |
| 11.x | Stiffeners** | Type | Mat | Place | Pos ($y/z$) | $t_{web}$ | $h_{web}$ | $t_{flange}$ | $h_{flange}$ |

* Stiffeners of type 11 are smeared out at plate when touched. ** Stiffeners of type 11.x are treated as beams. Use 11 for small stiffeners and 11.x for deep stiffners. 11.x can only be defined on the side shell

Transverse Secondary Structure

| Item | | Data Input | | | | | |
|---|---|---|---|---|---|---|---|
| 12.x | Floors | Type | Mat | Pos ($x$) | $t_{plate}$ | | |
| 13.x | Girders | Type | Mat | Pos ($x$) | $t_{plate}$ | | |
| 14.x | Frames at Side or Bottom | Type | Mat | Place | Pos ($x$) | $t_{plate}$ | Depth |

Girders : Plates between double side.

Transverse / Vertical Stiffeners

| Item | | Data Input | | | | | | | | |
|---|---|---|---|---|---|---|---|---|---|---|
| 15 | Stiffeners | Type | Mat | Place | Pos $(x/y)$ | $t_{web}$ | $h_{web}$ | $t_{flange}$ | $h_{flange}$ | |
| 15 | Stiffeners | Type | Mat | Place | Pos $(x/y)$ | $t_{web}$ | $h_{web}$ | $t_{flange}$ | $h_{flange}$ | Form Id |

Form Id only for stiffeners at transverse bulkheads. Vertical stiffeners form id=0, horisontal stiffener at aft part of bulk head form id = -1 and forward part form id = 1.

Material

| Item | Data Input | | | | |
|---|---|---|---|---|---|
| Material | Mat no. | $E$ | $\sigma_0$ | $R_c$ | $\epsilon_c$ |

Mat no. refer to the material number for the construction parts. $E$ is Young's modulus, $\sigma_0$ the flow stress, $R_c$ fracture toughness and $\epsilon_c$ the critical strain.

## B.2 Damage of Bow of Striking Vessel

**1** The ship bottom
**3** The weather deck
**4** The side shell
**6** Mid deck (if more they are denoted 6.1,6.2,6.3 etc.)
**8** Longitudinal bulkhead (iif more bulkheads, they are denoted 8.1,8.2, 8.3 etc.)

### Longitudinal Secondary Structure

**11** Stiffeners

### Transverse Secondary Structure

**14** Frames
**15** Stiffeners
**16** Frames only defined in bulb

### Coordinate System

All structure in struck vessel are described in a $x, y, z$ coordinate system. Origin is at the baseline and midship of the struck vessel, the $z$-axis pointing up and the $x$-axis is in the symmetry plane pointing forward.

### Input for data file

**type** Number, Item number
**Mat** Material
**Place** For secondary structure, type of principal structure the item is attached to
**Pos** Position according to above descreibed coordinate system

Principal Structure

| Item | | Data Input | | | | | | |
|---|---|---|---|---|---|---|---|---|
| 1 | Bottom | Type | Height ($z$) | $t_{plate}$ | | | | |
| 3 | Weather Deck | Type | Height ($z$) | $t_{plate}$ | | | | |
| 4 | Side Shell | Type | $h_{min}$ | $h_{max}$ | $t_{plate}$ | | | |
| 6.x | Mid decks | Type | Height ($z$) | $t_{plate}$ | | | | |
| 8.x | Longitudinal Bulkheads | Type | $h_{min}$ | $h_{max}$ | $x_{min}$ | $x_{max}$ | pos ($y$) | $t_{plate}$ |

$h_{min}$ and $h_{max}$ defined from bottom

$x_{min}$ and $x_{max}$ defined frm mid ship

Longitudinal Stiffeners

| Item | | Data Input | | | | | | | |
|---|---|---|---|---|---|---|---|---|---|
| 11 | Stiff. at side plating | Type | $h_{min}$ | $h_{max}$ | Spacing | $t_{web}$ | $h_{web}$ | $t_{flange}$ | $h_{flange}$ |
| 11 | Stiff. CL Girders | Type | Place | $t_{web}$ | $h_{web}$ | $t_{flange}$ | $h_{flange}$ | | |
| 11 | Stiff. all others | Type | Place | Spacing | $t_{web}$ | $h_{web}$ | $t_{flange}$ | $h_{flange}$ | |

Transverse Secondary Structure

| Item | | Data Input | | | | | |
|---|---|---|---|---|---|---|---|
| 14 | Frames | Type | Spacing | $t_{web}$ | $h_{web}$ | $t_{flange}$ | $h_{flange}$ |
| 16 | Frames only in Bottom | Type | Spacing | $t_{web}$ | $h_{web}$ | $t_{flange}$ | $h_{flange}$ |

Transverse / Vertical Stiffeners

| Item | | Data Input | | | | | | |
|---|---|---|---|---|---|---|---|---|
| 15 | Stiffeners | Type | Place | Spacing | $t_{web}$ | $h_{web}$ | $t_{flange}$ | $h_{flange}$ |

Material

| Item | Data Input |
|---|---|
| Material | $\sigma_0$ (flowstress) |

## B.3 Vessel and Collision Scenario files

**File describing the main particulars of the two vessels:**

The first line in the input file includes the main particulars of the struck vessel and the second line the main particulars of the striking vessel including the bow geometry data describing the conventional part of the bow. The third line is the bulb indication, 0 if no bulb is present, 1 if a bulb is present with prescribed bulb parameters and 2 if the vessel is equipped with a bulb where the bulb parameters is not known. If the bulb design is unknown the following bulb parameters is used, Zhang (1999)

$$R_L = 0.3 \cdot H_{deck} \qquad R_V = 0.125 \cdot H_{deck} \qquad R_H = 0.05 \cdot H_{deck}$$

See also Section 4.1. The fourth line includes the bulb parameters in case of a bulb indicator equal 1.

**line 1** $L\ H\ T\ M$

**line 2** $L\ H\ T\ M\ \phi\ B\ B_d\ B_b$

**line 3** bulb indicator

**line 4** $R_L\ R_V\ R_H\ R_D$

**File describing the collision scenario:**

This file includes the velocity of the struck and the striking vessel, the collision location, the collision angle and the angle at the struck ship side.

**line 1** $U_a\ U_b\ x_c\ y_c\ \beta\ \alpha$

This page is intentionally left blank.

# Appendix C

# Vessel Parameters, Neural Network

Relations between the loading capacity and the main particulars of ships of other types can be found by use of neural networks. The normalisation vectors, the weights and the biases for the neural network are given in the following.

**Bulk Carriers**
The training set consists of 766 ships with grain capacity [$m^3$] as input.

| Input $P[min\ max]$ | Output $\boldsymbol{T}[min\ max]$ |
|---|---|
| $\begin{bmatrix}1366 & 236559\end{bmatrix}$ | $\begin{bmatrix}69.0 & 312\\ 10.8 & 50.0\\ 9.00 & 19.9\\ 3.76 & 18.9\\ 4.60 & 25.9\\ 2200 & 236797\end{bmatrix}$ |

| Hidden layer | | Output layer | |
|---|---|---|---|
| Weight, $\boldsymbol{W^1}$ | Bias, $\boldsymbol{b^1}$ | Weight, $\boldsymbol{W^2}$ | Bias, $\boldsymbol{b^2}$ |
| $\begin{bmatrix}8.86632\\ -3.66334\\ 15.9613\end{bmatrix}$ | $\begin{pmatrix}5.15817\\ 0.75732\\ 17.6907\end{pmatrix}$ | $\begin{bmatrix}0.54202 & -0.74426 & 4.14808\\ 0.35881 & -0.92081 & 4.36273\\ 0.04983 & -0.00158 & 2.46594\\ 0.56203 & -0.84711 & 3.70895\\ 0.61517 & -0.72161 & 4.13998\\ 0.37825 & -1.39337 & 1.07635\end{bmatrix}$ | $\begin{pmatrix}-3.74877\\ -3.75530\\ -2.53032\\ -3.22797\\ -3.73190\\ -0.55488\end{pmatrix}$ |

**Cargo Ships**
The training set consists of 723 ships with grain capacity [$m^3$] as input.

| Input $P[min\ max]$ | Output $\boldsymbol{T}[min\ max]$ |
|---|---|
| $\begin{bmatrix}128 & 62403\end{bmatrix}$ | $\begin{bmatrix}34.8 & 199.7\\ 7.6 & 32.2\\ 9.0 & 20.5\\ 2.4 & 12.8\\ 3.25 & 19.3\\ 508 & 66557\end{bmatrix}$ |

| Hidden layer | | Output layer | |
|---|---|---|---|
| Weight, $\boldsymbol{W^1}$ | Bias, $\boldsymbol{b^1}$ | Weight, $\boldsymbol{W^2}$ | Bias, $\boldsymbol{b^2}$ |
| $\begin{bmatrix}5.68548\\ 13.11612\\ 14.96091\end{bmatrix}$ | $\begin{pmatrix}-2.29320\\ 5.01035\\ 12.2370\end{pmatrix}$ | $\begin{bmatrix}0.32858 & 0.62388 & 0.48401\\ 0.59685 & 0.46361 & 0.66787\\ -0.22801 & 0.27893 & 0.71612\\ 0.45486 & 0.43249 & 0.79339\\ 0.41907 & 0.40565 & 0.79370\\ 1.02008 & 0.51523 & 0.28028\end{bmatrix}$ | $\begin{pmatrix}-0.48787\\ -0.72654\\ -0.73241\\ -0.78605\\ -0.85900\\ -0.96607\end{pmatrix}$ |

### Chemical Tankers

The training set consists of 365 ships with liquid capacity [$m^3$] as input.

| Input $P[min\ max]$ | Output $\boldsymbol{T}[min\ max]$ |
|---|---|
| $\begin{bmatrix}472 & 88630\end{bmatrix}$ | $\begin{bmatrix}49.8 & 228.6\\ 9.00 & 32.26\\ 9.60 & 16.25\\ 3.51 & 16.08\\ 3.90 & 21.66\\ 1058 & 98870\end{bmatrix}$ |

| Hidden layer | | Output layer | |
|---|---|---|---|
| Weight, $\boldsymbol{W^1}$ | Bias, $\boldsymbol{b^1}$ | Weight, $\boldsymbol{W^2}$ | Bias, $\boldsymbol{b^2}$ |
| $\begin{bmatrix}6.57874\\ -5.09626\\ 17.8457\end{bmatrix}$ | $\begin{pmatrix}-1.82540\\ -3.48179\\ 19.2432\end{pmatrix}$ | $\begin{bmatrix}0.33521 & -1.08759 & 2.34884\\ 0.30798 & -1.66079 & 2.25891\\ -0.19688 & -0.60447 & 3.54896\\ 0.60327 & -0.81144 & 2.46268\\ 0.78726 & -1.00690 & 2.35051\\ 0.98202 & -0.97892 & 0.06603\end{bmatrix}$ | $\begin{pmatrix}-1.89631\\ -1.39018\\ -2.90985\\ -2.29481\\ -2.03953\\ -0.22365\end{pmatrix}$ |

### Gas Tankers

The training set consists of 182 ships with cubic feet gas capacity as input.

| Input $P[min\ max]$ | Output $\boldsymbol{T}[min\ max]$ |
|---|---|
| $\begin{bmatrix}186 & 137540\end{bmatrix}$ | $\begin{bmatrix}30.5 & 297.5\\ 7.60 & 48.20\\ 7.70 & 21.0\\ 1.61 & 13.40\\ 2.60 & 27.0\\ 375 & 114084\end{bmatrix}$ |

| Hidden layer | | Output layer | |
|---|---|---|---|
| Weight, $\boldsymbol{W^1}$ | Bias, $\boldsymbol{b^1}$ | Weight, $\boldsymbol{W^2}$ | Bias, $\boldsymbol{b^2}$ |
| $\begin{bmatrix}3.43242\\ -6.17059\\ -14.1235\end{bmatrix}$ | $\begin{pmatrix}-1.88171\\ -3.73901\\ -15.5372\end{pmatrix}$ | $\begin{bmatrix}0.75888 & -0.52865 & -3.27999\\ 0.86823 & -0.64486 & -2.51742\\ 0.71804 & 0.13493 & -4.33897\\ -0.03501 & -0.45258 & -5.64684\\ 0.74016 & -0.56400 & -3.97888\\ 1.02881 & -0.90095 & -1.12370\end{bmatrix}$ | $\begin{pmatrix}0.30084\\ 0.22484\\ 0.20462\\ 0.71293\\ 0.34420\\ 0.02400\end{pmatrix}$ |

### Passenger Ships

The training set consists of 58 ships with number of passengers as input. The data is scattered and therefore not very well represented by the fitted functions.

| Input $P[min\ max]$ | Output $\boldsymbol{T}[min\ max]$ |
|---|---|
| $\begin{bmatrix}30 & 2766\end{bmatrix}$ | $\begin{bmatrix}23.15 & 294.0\\ 5.9 & 32.2\\ 9.0 & 24.0\\ 1.15 & 8.2\\ 2.35 & 24.9\\ 62.0 & 44608\end{bmatrix}$ |

| Hidden layer | | Output layer | |
|---|---|---|---|
| Weight, $\boldsymbol{W^1}$ | Bias, $\boldsymbol{b^1}$ | Weight, $\boldsymbol{W^2}$ | Bias, $\boldsymbol{b^2}$ |
| $\begin{bmatrix}-0.92505\\ 3.72614\\ -3.50932\end{bmatrix}$ | $\begin{pmatrix}-0.11655\\ 3.33848\\ 2.34160\end{pmatrix}$ | $\begin{bmatrix}-0.04079 & 1.42519 & -1.175501\\ -0.34828 & 1.86807 & -0.82565\\ -0.90984 & 1.15251 & 0.18728\\ -0.50681 & 1.64595 & -0.63686\\ 0.30082 & 1.13518 & -1.38236\\ 0.03922 & 0.74035 & -1.71806\end{bmatrix}$ | $\begin{pmatrix}-0.27870\\ -0.55137\\ -0.53889\\ -0.41870\\ -0.15315\\ 0.38093\end{pmatrix}$ |

### Reefers

The training set consists of 179 ships with cubic feet capacity as input.

| Input $P[min\ max]$ | Output $\boldsymbol{T}[min\ max]$ |
|---|---|
| $\begin{bmatrix}22319 & 737865\end{bmatrix}$ | $\begin{bmatrix}54.9 & 178.5\\ 9.49 & 25.2\\ 10.5 & 22.3\\ 3.3 & 10.12\\ 4.1 & 15.7\\ 1250 & 24535\end{bmatrix}$ |

| Hidden layer | | Output layer | |
|---|---|---|---|
| Weight, $\boldsymbol{W^1}$ | Bias, $\boldsymbol{b^1}$ | Weight, $\boldsymbol{W^2}$ | Bias, $\boldsymbol{b^2}$ |
| $\begin{bmatrix}2.51652\\ 2.77303\\ 3.37369\end{bmatrix}$ | $\begin{pmatrix}-1.45905\\ 1.03138\\ 3.08111\end{pmatrix}$ | $\begin{bmatrix}0.76381 & 0.33075 & 1.44361\\ 0.91034 & 0.58453 & 1.10445\\ -0.53015 & 2.03037 & 0.45384\\ 0.22466 & 0.93268 & 1.44355\\ 1.16802 & -0.24266 & 1.82602\\ 1.49795 & 0.46138 & 0.85162\end{bmatrix}$ | $\begin{pmatrix}-1.46795\\ -1.32521\\ -1.36829\\ -1.63560\\ -1.47494\\ -1.44744\end{pmatrix}$ |

### Tankers

The training set consists of 684 ships with oil capacity [$m^3$] as input.

| Input $P[min\ max]$ | Output $\boldsymbol{T}[min\ max]$ |
|---|---|
| $\begin{bmatrix}268 & 351673\end{bmatrix}$ | $\begin{bmatrix}29.5 & 343.7\\ 7.0 & 60.04\\ 7.5 & 18.50\\ 2.6 & 22.70\\ 3.0 & 31.8\\ 480 & 352992\end{bmatrix}$ |

| Hidden layer | | Output layer | |
|---|---|---|---|
| Weight, $\boldsymbol{W^1}$ | Bias, $\boldsymbol{b^1}$ | Weight, $\boldsymbol{W^2}$ | Bias, $\boldsymbol{b^2}$ |
| $\begin{bmatrix}-1.07863\\ 2.18246\\ 15.5047\end{bmatrix}$ | $\begin{pmatrix}2.16449\\ 2.28212\\ 17.4847\end{pmatrix}$ | $\begin{bmatrix}-1.38730 & 2.06591 & 4.04733\\ -1.42566 & 2.34321 & 3.61948\\ -0.76058 & 0.00814 & 5.50097\\ -2.92933 & 1.34807 & 4.65261\\ -2.71442 & 1.35533 & 5.76455\\ -5.88845 & 1.60895 & -0.16969\end{bmatrix}$ | $\begin{pmatrix}-4.09242\\ -3.92194\\ -4.52830\\ -2.87217\\ -4.10988\\ 3.98024\end{pmatrix}$ |

### Fishing Vessels

The training set consists of 642 ships with deadweight [tonnes] as input.

| Input $P[min\ max]$ | Output $\boldsymbol{T}[min\ max]$ |
|---|---|
| $\begin{bmatrix}26 & 9360\end{bmatrix}$ | $\begin{bmatrix}21.0 & 152.95\\ 6.01 & 22.20\\ 9.00 & 19.20\\ 1.81 & 9.20\\ 2.79 & 14.70\\ 128.0 & 16758\end{bmatrix}$ |

| Hidden layer | | Output layer | |
|---|---|---|---|
| Weight, $\boldsymbol{W^1}$ | Bias, $\boldsymbol{b^1}$ | Weight, $\boldsymbol{W^2}$ | Bias, $\boldsymbol{b^2}$ |
| $\begin{bmatrix}5.29085\\ -3.80136\\ -87.1545\end{bmatrix}$ | $\begin{pmatrix}2.05811\\ -1.88821\\ -85.515\end{pmatrix}$ | $\begin{bmatrix}-3.80292 & -5.85790 & -0.29510\\ -3.15950 & -5.41227 & -0.28429\\ -5.06314 & -6.68153 & -0.43759\\ -3.10186 & -4.90533 & -0.45088\\ -2.49829 & -4.79540 & -0.28419\\ -0.79686 & -2.62789 & -0.03157\end{bmatrix}$ | $\begin{pmatrix}4.54883\\ 4.15525\\ 5.47331\\ 3.88317\\ 3.56876\\ 1.34740\end{pmatrix}$ |

**Ro-Ro Vessels**

The training set consists of 140 ships with lane meters as input. To ensure a reasonable number of data, ships from 1980 and on are used.

| Input $P[min\ max]$ | Output $\boldsymbol{T}[min\ max]$ |
|---|---|
| $\begin{bmatrix} 31 & 5700 \end{bmatrix}$ | $\begin{bmatrix} 34.45 & 291.92 \\ 8.23 & 32.28 \\ 11.0 & 22.0 \\ 1.71 & 11.9 \\ 2.16 & 31.2 \\ 289 & 61182 \end{bmatrix}$ |

| Hidden layer | | Output layer | |
|---|---|---|---|
| Weight, $\boldsymbol{W^1}$ | Bias, $\boldsymbol{b^1}$ | Weight, $\boldsymbol{W^2}$ | Bias, $\boldsymbol{b^2}$ |
| $\begin{bmatrix} 4.45355 \\ 3.01456 \\ 2.41768 \end{bmatrix}$ | $\begin{pmatrix} -0.33269 \\ 1.74831 \\ -1.99689 \end{pmatrix}$ | $\begin{bmatrix} 0.34490 & 1.04506 & -0.54273 \\ 0.57809 & 1.24673 & -0.28530 \\ -1.35365 & 2.24761 & 1.69343 \\ 0.54400 & 0.85244 & -0.31102 \\ 0.62901 & 0.55796 & -1.08153 \\ 1.71875 & 0.48272 & -1.83213 \end{bmatrix}$ | $\begin{pmatrix} -0.76470 \\ -0.64829 \\ -1.20903 \\ -0.55565 \\ -0.60831 \\ -0.92284 \end{pmatrix}$ |

# Appendix D

# Damage Relations

### Relation Between the Non-dimensional Damage Length and the Non-dimensional Penetration, Simulation, Analysis 1

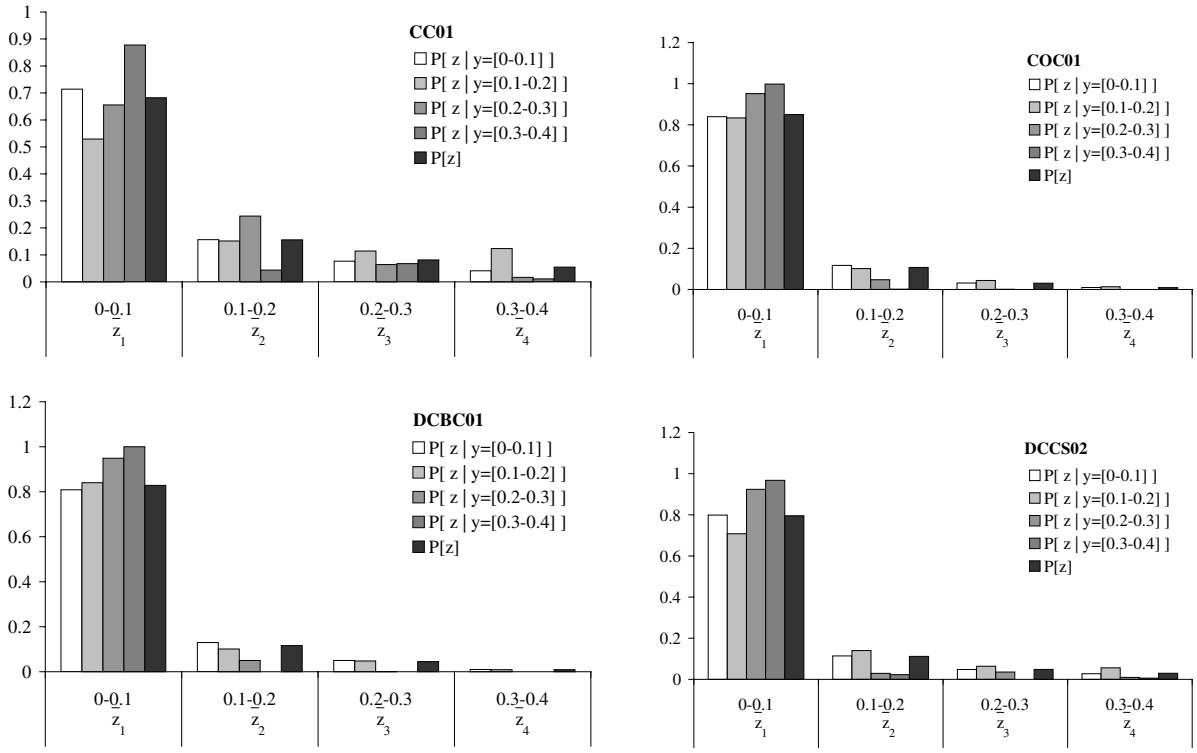

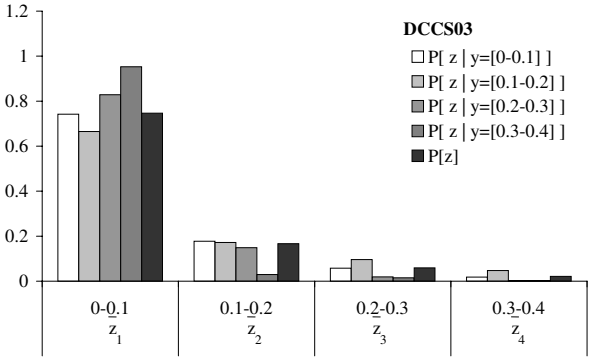
DCCS03
P[ z | y=[0-0.1] ]
P[ z | y=[0.1-0.2] ]
P[ z | y=[0.2-0.3] ]
P[ z | y=[0.3-0.4] ]
P[z]
0-0.1
z1
0.1-0.2
z2
0.2-0.3
z3
0.3-0.4
z4

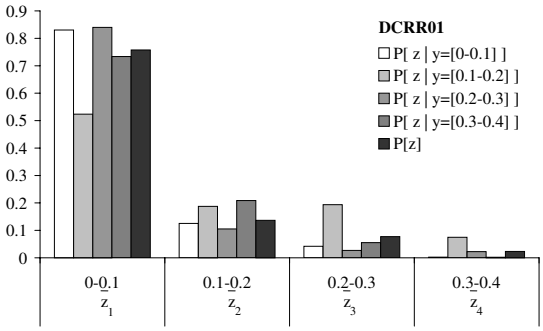
DCRR01
P[ z | y=[0-0.1] ]
P[ z | y=[0.1-0.2] ]
P[ z | y=[0.2-0.3] ]
P[ z | y=[0.3-0.4] ]
P[z]
0-0.1
z1
0.1-0.2
z2
0.2-0.3
z3
0.3-0.4
z4

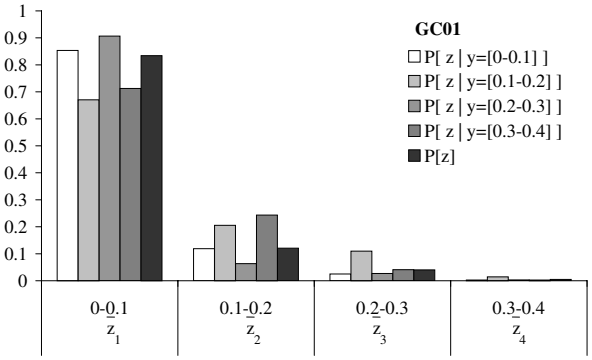
GC01
P[ z | y=[0-0.1] ]
P[ z | y=[0.1-0.2] ]
P[ z | y=[0.2-0.3] ]
P[ z | y=[0.3-0.4] ]
P[z]
0-0.1
z1
0.1-0.2
z2
0.2-0.3
z3
0.3-0.4
z4

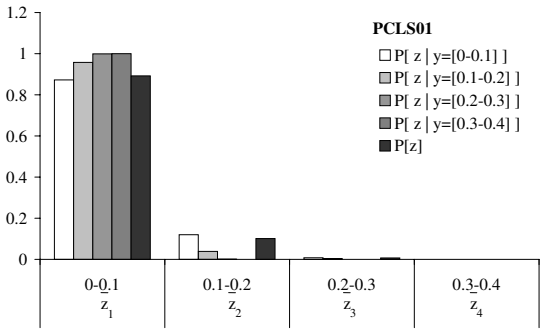
PCLS01
P[ z | y=[0-0.1] ]
P[ z | y=[0.1-0.2] ]
P[ z | y=[0.2-0.3] ]
P[ z | y=[0.3-0.4] ]
P[z]
0-0.1
z1
0.1-0.2
z2
0.2-0.3
z3
0.3-0.4
z4

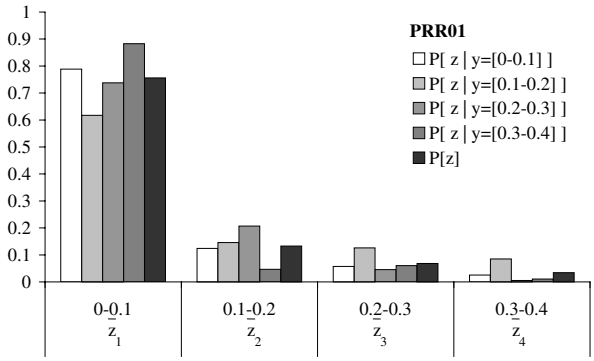
PRR01
P[ z | y=[0-0.1] ]
P[ z | y=[0.1-0.2] ]
P[ z | y=[0.2-0.3] ]
P[ z | y=[0.3-0.4] ]
P[z]
0-0.1
z1
0.1-0.2
z2
0.2-0.3
z3
0.3-0.4
z4

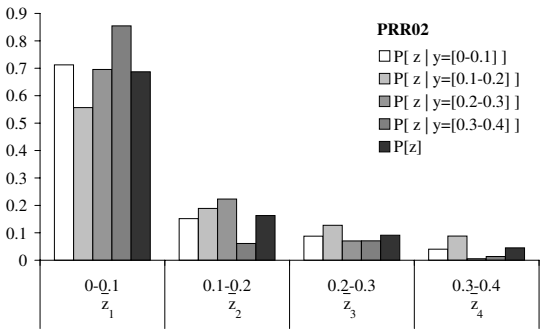
PRR02
P[ z | y=[0-0.1] ]
P[ z | y=[0.1-0.2] ]
P[ z | y=[0.2-0.3] ]
P[ z | y=[0.3-0.4] ]
P[z]
0-0.1
z1
0.1-0.2
z2
0.2-0.3
z3
0.3-0.4
z4

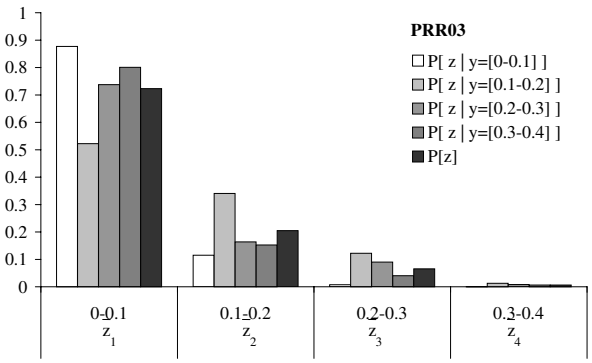
PRR03
P[ z | y=[0-0.1] ]
P[ z | y=[0.1-0.2] ]
P[ z | y=[0.2-0.3] ]
P[ z | y=[0.3-0.4] ]
P[z]
0-0.1
z1
0.1-0.2
z2
0.2-0.3
z3
0.3-0.4
z4

## Relation Between the Non-dimensional Damage Length and the Non-dimensional Penetration, Simulation, Analysis 2

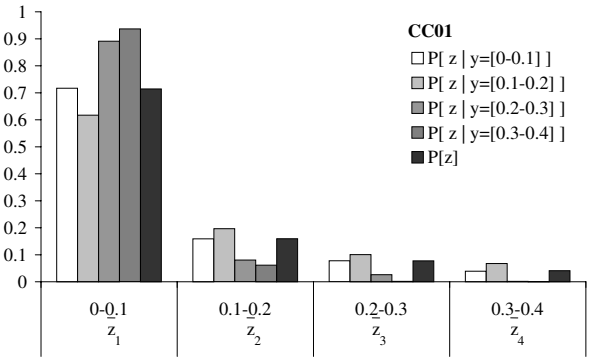


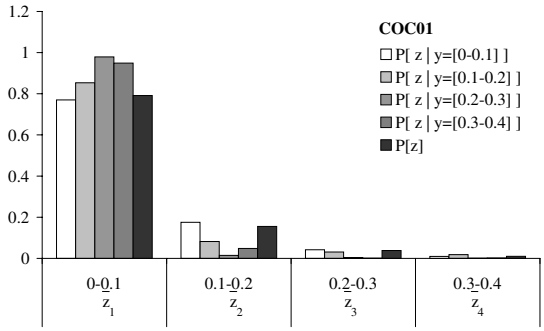


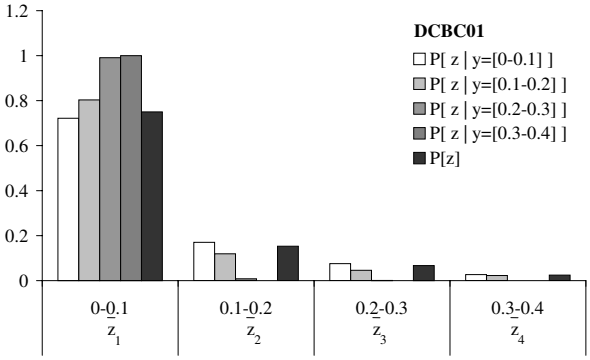


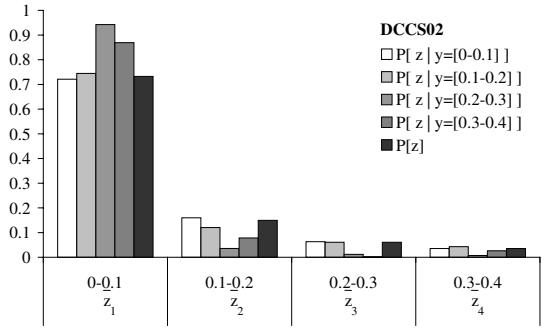


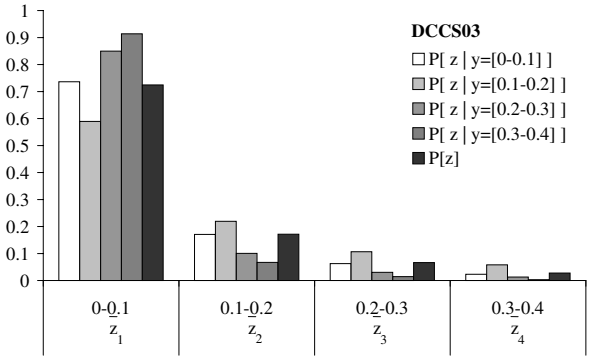


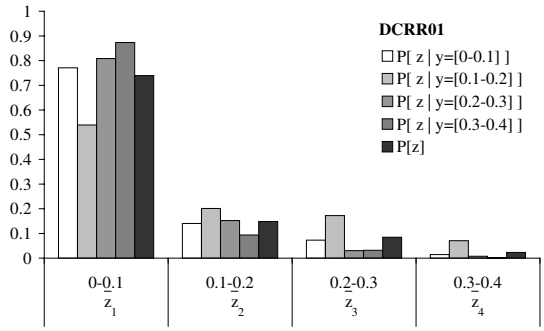

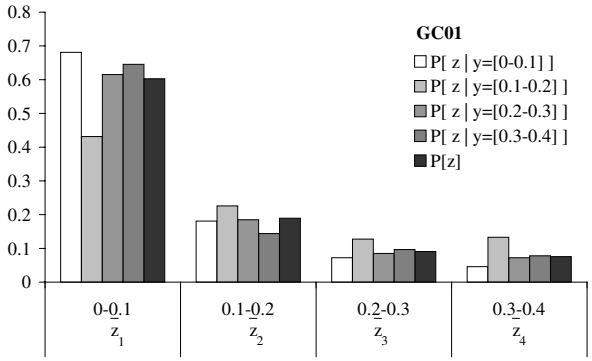
GC01
P[ z | y=[0-0.1] ]
P[ z | y=[0.1-0.2] ]
P[ z | y=[0.2-0.3] ]
P[ z | y=[0.3-0.4] ]
P[z]
0-0.1
z1
0.1-0.2
z2
0.2-0.3
z3
0.3-0.4
z4

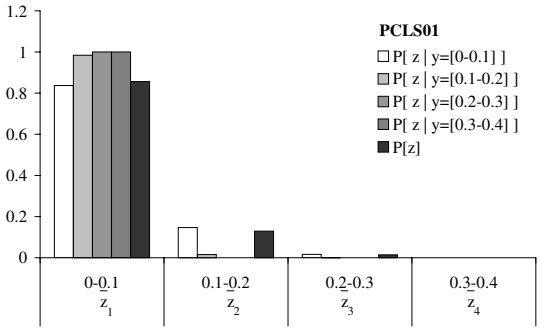
PCLS01
P[ z | y=[0-0.1] ]
P[ z | y=[0.1-0.2] ]
P[ z | y=[0.2-0.3] ]
P[ z | y=[0.3-0.4] ]
P[z]
0-0.1
z1
0.1-0.2
z2
0.2-0.3
z3
0.3-0.4
z4

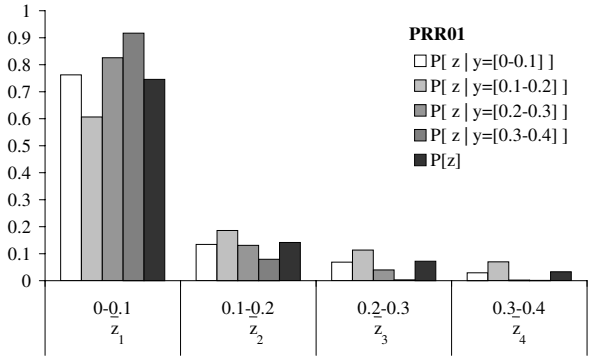
PRR01
P[ z | y=[0-0.1] ]
P[ z | y=[0.1-0.2] ]
P[ z | y=[0.2-0.3] ]
P[ z | y=[0.3-0.4] ]
P[z]
0-0.1
z1
0.1-0.2
z2
0.2-0.3
z3
0.3-0.4
z4

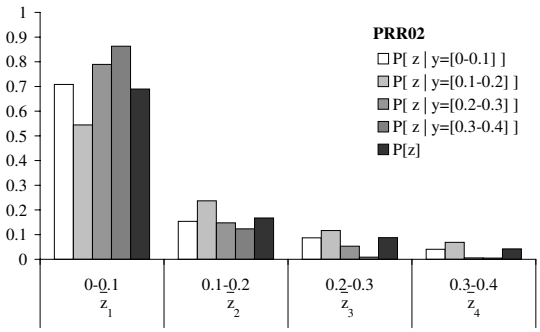
PRR02
P[ z | y=[0-0.1] ]
P[ z | y=[0.1-0.2] ]
P[ z | y=[0.2-0.3] ]
P[ z | y=[0.3-0.4] ]
P[z]
0-0.1
z1
0.1-0.2
z2
0.2-0.3
z3
0.3-0.4
z4

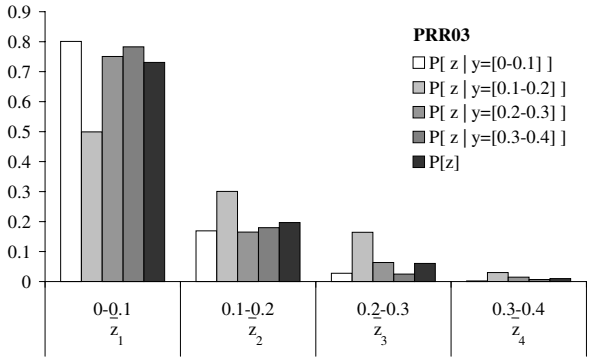
PRR03
P[ z | y=[0-0.1] ]
P[ z | y=[0.1-0.2] ]
P[ z | y=[0.2-0.3] ]
P[ z | y=[0.3-0.4] ]
P[z]
0-0.1
z1
0.1-0.2
z2
0.2-0.3
z3
0.3-0.4
z4

# Appendix E

# Expressions for Determination of $p$

### Inside Compartment

| | Aft part of vessel $\overline{x_2} \leq \overline{x_k}$ | Damage over mid-length of vessel $\overline{x_1} \leq \overline{x_k} < \overline{x_2}$ | | Forward part of vessel $\overline{x_1} > \overline{x_k}$ |
|---|---|---|---|---|
| | | $\overline{x_k} \leq \overline{x_m}$ $J' = 2(\overline{x_k} - \overline{x_1})$ | $\overline{x_k} > \overline{x_m}$ $J' = 2(\overline{x_2} - \overline{x_k})$ | |
| $J \leq J_k$ | $i1)$ | $i5)$ | $i8)$ | $i3)$ |
| $J > J_k$ $J' \leq J_k$ | $i2)$ | $i6)$ | $i9)$ | $i4)$ |
| $J > J_k$ $J' > J_k$ | | $i7)$ | $i10)$ | |

$i1)$ $$p = \int_0^{J} b_1 \int_{\overline{x_1}+\frac{\overline{y}}{2}}^{\overline{x_2}-\frac{\overline{y}}{2}} a_1 \; d\overline{x}d\overline{y}$$

$i2)$ $$p = \int_0^{J_k} b_1 \int_{\overline{x_1}+\frac{\overline{y}}{2}}^{\overline{x_2}-\frac{\overline{y}}{2}} a_1 \; d\overline{x}d\overline{y} + \int_{J_k}^{\min(J,J_m)} b_2 \int_{\overline{x_1}+\frac{\overline{y}}{2}}^{\overline{x_2}-\frac{\overline{y}}{2}} a_1 \; d\overline{x}d\overline{y}$$

$i3)$ $$p = \int_0^{J} b_1 \int_{\overline{x_1}+\frac{\overline{y}}{2}}^{\overline{x_2}-\frac{\overline{y}}{2}} a_2 \; d\overline{x}d\overline{y}$$

$i4)$ $$p = \int_0^{J_k} b_1 \int_{\overline{x_1}+\frac{\overline{y}}{2}}^{\overline{x_2}-\frac{\overline{y}}{2}} a_2 \; d\overline{x}d\overline{y} + \int_{J_k}^{\min(J,J_m)} b_2 \int_{\overline{x_1}+\frac{\overline{y}}{2}}^{\overline{x_2}-\frac{\overline{y}}{2}} a_2 \; d\overline{x}d\overline{y}$$

$i5)$ $$p = \int_0^{J} b_1 \int_{\overline{x_1}+\frac{\overline{y}}{2}}^{\overline{x_2}-\frac{\overline{y}}{2}} a_2 \; d\overline{x}d\overline{y} - \int_0^{\min(J',J_m)} b_1 \int_{\overline{x_1}+\frac{\overline{y}}{2}}^{\overline{x_k}} (a_2 - a_1) \; d\overline{x}d\overline{y}$$

$i6)$ $$p = \int_0^{J_k} b_1 \int_{\overline{x_1}+\frac{\overline{y}}{2}}^{\overline{x_2}-\frac{\overline{y}}{2}} a_2 \; d\overline{x}d\overline{y} + \int_{J_k}^{\min(J,J_m)} b_2 \int_{\overline{x_1}+\frac{\overline{y}}{2}}^{\overline{x_2}-\frac{\overline{y}}{2}} a_2 \; d\overline{x}d\overline{y} + \int_0^{\min(J',J_m)} b_1 \int_{\overline{x_1}+\frac{\overline{y}}{2}}^{\overline{x_k}} (a_2 - a_1) \; d\overline{x}d\overline{y}$$

$i7)$ $$p = \int_0^{J_k} b_1 \int_{\overline{x_1}+\frac{\overline{y}}{2}}^{\overline{x_2}-\frac{\overline{y}}{2}} a_2 \; d\overline{x}d\overline{y} + \int_{J_k}^{\min(J,J_m)} b_2 \int_{\overline{x_1}+\frac{\overline{y}}{2}}^{\overline{x_2}-\frac{\overline{y}}{2}} a_2 \; d\overline{x}d\overline{y} - \int_0^{J_k} b_1 \int_{\overline{x_1}+\frac{\overline{y}}{2}}^{\overline{x_k}} (a_2 - a_1) \; d\overline{x}d\overline{y} - \int_{J_k}^{\min(J',J_m)} b_2 \int_{\overline{x_1}+\frac{\overline{y}}{2}}^{\overline{x_k}} (a_2 - a_1) \; d\overline{x}d\overline{y}$$

$i8)$ $$p = \int_0^{J} b_1 \int_{\overline{x_1}+\frac{\overline{y}}{2}}^{\overline{x_2}-\frac{\overline{y}}{2}} a_1 \; d\overline{x}d\overline{y} + \int_0^{\min(J',J_m)} b_1 \int_{\overline{x_k}}^{\overline{x_2}-\frac{\overline{y}}{2}} (a_2 - a_1) \; d\overline{x}d\overline{y}$$

$i9)$ $$p = \int_0^{J_k} b_1 \int_{\overline{x_1}+\frac{\overline{y}}{2}}^{\overline{x_2}-\frac{\overline{y}}{2}} a_1 \; d\overline{x}d\overline{y} + \int_{J_k}^{\min(J,J_m)} b_2 \int_{\overline{x_1}+\frac{\overline{y}}{2}}^{\overline{x_2}-\frac{\overline{y}}{2}} a_1 \; d\overline{x}d\overline{y} + \int_0^{\min(J',J_m)} b_1 \int_{\overline{x_k}}^{\overline{x_2}-\frac{\overline{y}}{2}} (a_2 - a_1) \; d\overline{x}d\overline{y}$$

$i10)$ $$p = \int_0^{J_k} b_1 \int_{\overline{x_1}+\frac{\overline{y}}{2}}^{\overline{x_2}-\frac{\overline{y}}{2}} a_1 \; d\overline{x}d\overline{y} + \int_{J_k}^{\min(J,J_m)} b_2 \int_{\overline{x_1}+\frac{\overline{y}}{2}}^{\overline{x_2}-\frac{\overline{y}}{2}} a_1 \; d\overline{x}d\overline{y} + \int_0^{J_k} b_1 \int_{\overline{x_1}+\frac{\overline{y}}{2}}^{\overline{x_2}-\frac{\overline{y}}{2}} (a_2 - a_1) \; d\overline{x}d\overline{y} + \int_{J_k}^{(J',J_m)} b_2 \int_{\overline{x_k}}^{\overline{x_2}-\frac{\overline{y}}{2}} (a_2 - a_1) \; d\overline{x}d\overline{y}$$

## Aft Compartment

| | Aft of knuckle point $\overline{x_k} > \overline{x_2}$ | Knuckle point in compartment $\overline{x_2} \geq \overline{x_k}$ | |
|---|---|---|---|
| | | $\overline{x_k} \leq J/2$ | $\overline{x_k} > J/2$ |
| $J \leq J_k$ | $a1)$ | $a3)$ | $a5)$ |
| $J > J_k$ $2(J-\overline{x_k}) \leq J_k$ | $a2)$ | $a4)$ | $a6)$ |
| $J > J_k$ $2(J-\overline{x_k}) > J_k$ | | | $a7)$ |

$$a1) \quad p = \int_0^J b_1 \int_0^{J-\frac{\overline{y}}{2}} a_1 \; d\overline{x}d\overline{y} + \int_J^{J_k} b_1 \int_0^{\frac{J}{2}} a_1 \; d\overline{x}d\overline{y} + \int_{J_k}^{J_m} b_2 \int_0^{\frac{J}{2}} a_1 \; d\overline{x}d\overline{y}$$

$$a2) \quad p = \int_0^{J_k} b_1 \int_0^{J-\frac{\overline{y}}{2}} a_1 \; d\overline{x}d\overline{y} + \int_{J_k}^{\min(J,J_m)} b_2 \int_{\frac{J}{2}}^{J-\frac{\overline{y}}{2}} a_1 \; d\overline{x}d\overline{y} + \int_{J_k}^{J_m} b_2 \int_0^{\frac{J}{2}} a_1 \; d\overline{x}d\overline{y}$$

$$a3) \quad p = \int_0^{J_k} b_1 \int_0^{\frac{J}{2}} a_1 \; d\overline{x}d\overline{y} + \int_{J_k}^{J_m} b_2 \int_0^{\frac{J}{2}} a_1 \; d\overline{x}d\overline{y} + \int_0^{J} b_1 \int_{\frac{J}{2}}^{J-\frac{\overline{y}}{2}} a_2 \; d\overline{x}d\overline{y}$$
$$+ \int_0^{J_k} b_1 \int_{\overline{x_k}}^{\frac{J}{2}} (a_2 - a_1) \; d\overline{x}d\overline{y} + \int_{J_k}^{J_m} b_2 \int_{\overline{x_k}}^{\frac{J}{2}} (a_2 - a_1) \; d\overline{x}d\overline{y}$$

$$a4) \quad p = \int_0^{J_k} b_1 \int_0^{\frac{J}{2}} a_1 \; d\overline{x}d\overline{y} + \int_{J_k}^{J_m} b_2 \int_0^{\frac{J}{2}} a_1 \; d\overline{x}d\overline{y} + \int_0^{J_k} b_1 \int_{\frac{J}{2}}^{J-\frac{\overline{y}}{2}} a_1 \; d\overline{x}d\overline{y}$$
$$+ \int_{J_k}^{\min(J,J_m)} b_2 \int_{\frac{J}{2}}^{J-\frac{\overline{y}}{2}} a_2 \; d\overline{x}d\overline{y} + \int_0^{J_k} b_1 \int_{\overline{x_k}}^{\frac{J}{2}} (a_2 - a_1) \; d\overline{x}d\overline{y}$$
$$+ \int_{J_k}^{J_m} b_2 \int_{\overline{x_k}}^{\frac{J}{2}} (a_2 - a_1) \; d\overline{x}d\overline{y}$$

$$a5) \quad p = \int_0^{J_k} b_1 \int_0^{\frac{J}{2}} a_1 \; d\overline{x}d\overline{y} + \int_0^{J} b_1 \int_{\frac{J}{2}}^{J-\frac{y}{2}} a_1 \; d\overline{x}d\overline{y} + \int_{J_k}^{J_m} b_2 \int_0^{\frac{J}{2}} a_1 \; d\overline{x}d\overline{y}$$
$$+ \int_0^{2(J-\overline{x_k})} b_1 \int_{\overline{x_k}}^{J-\frac{\overline{y}}{2}} (a_2 - a_1) \; d\overline{x}d\overline{y}$$

$$a6) \qquad p = \int_0^{J_k} b_1 \int_0^{\frac{J}{2}} a_1 \; d\overline{x}d\overline{y} + \int_{J_k}^{J_m} b_2 \int_0^{\frac{J}{2}} a_1 \; d\overline{x}d\overline{y} + \int_0^{J_k} b_1 \int_{\frac{J}{2}}^{J-\frac{\overline{y}}{2}} a_1 \; d\overline{x}d\overline{y}$$
$$+ \int_{J_k}^{\min(J,J_m)} b_2 \int_{\frac{J}{2}}^{J-\frac{\overline{y}}{2}} a_1 \; d\overline{x}d\overline{y} + \int_0^{2(J-\overline{x_k})} b_1 \int_{\overline{x_k}}^{J-\frac{\overline{y}}{2}} (a_2 - a_1) \; d\overline{x}d\overline{y}$$

$$a7) \qquad p = \int_0^{J_k} b_1 \int_0^{\frac{J}{2}} a_1 \; d\overline{x}d\overline{y} + \int_{J_k}^{J_m} b_2 \int_0^{\frac{J}{2}} a_1 \; d\overline{x}d\overline{y} + \int_0^{J_k} b_1 \int_{\frac{J}{2}}^{J-\frac{\overline{y}}{2}} a_1 \; d\overline{x}d\overline{y}$$
$$+ \int_{J_k}^{\min(J,J_m)} b_2 \int_{\frac{J}{2}}^{J-\frac{\overline{y}}{2}} a_1 \; d\overline{x}d\overline{y} + \int_0^{J_k} b_1 \int_{\overline{x_k}}^{J-\frac{\overline{y}}{2}} (a_2 - a_1) \; d\overline{x}d\overline{y}$$
$$+ \int_{J_k}^{2(J-\overline{x_k})} b_2 \int_{\overline{x_k}}^{J-\frac{\overline{y}}{2}} (a_2 - a_1) \; d\overline{x}d\overline{y}$$

**Forward Compartment**

| | Forward of knuckle point $\overline{x_1} > \overline{x_k}$ | Knuckle point in compartment $\overline{x_1} \leq \overline{x_k}$ | |
|---|---|---|---|
| | | $\overline{x_k} \leq 1 - J/2$ | $\overline{x_k} > 1 - J/2$ |
| $J \leq J_k$ | $f1)$ | $f3)$ | $f6)$ |
| $J > J_k$, $2(\overline{x_k} - \overline{x_1}) \leq J_k$ | $f2)$ | $f4)$ | $f7)$ |
| $J > J_k$, $2(\overline{x_k} - \overline{x_1}) > J_k$ | | $f5)$ | |

$$f1) \quad p = \int_0^{J} b_1 \int_{\overline{x_1}+\frac{y}{2}}^{1} a_2 \; d\overline{x}d\overline{y} + \int_{J}^{J_k} b_1 \int_{1-\frac{J}{2}}^{1} a_2 \; d\overline{x}d\overline{y} + \int_{J_k}^{J_m} b_2 \int_{1-\frac{J}{2}}^{1} a_2 \; d\overline{x}d\overline{y}$$

$$f2) \quad p = \int_0^{J_k} b_1 \int_{\overline{x_1}+\frac{y}{2}}^{1} a_2 \; d\overline{x}d\overline{y} + \int_{J_k}^{\min(J,J_m)} b_2 \int_{\overline{x_1}+\frac{y}{2}}^{1-\frac{y}{2}} a_2 \; d\overline{x}d\overline{y} + \int_{J_k}^{J_m} b_2 \int_{1-\frac{J}{2}}^{1} a_2 \; d\overline{x}d\overline{y}$$

$$f3) \quad p = \int_0^{J} b_1 \int_{\overline{x_1}+\frac{y}{2}}^{1-\frac{J}{2}} a_2 \; d\overline{x}d\overline{y} + \int_{J_k}^{J_m} b_2 \int_{1-\frac{J}{2}}^{\frac{J}{2}} a_2 \; d\overline{x}d\overline{y} + \int_0^{J_k} b_1 \int_{1-\frac{J}{2}}^{1} a_2 \; d\overline{x}d\overline{y}$$
$$- \int_0^{2(\overline{x_k}-\overline{x_1})} b_1 \int_{\overline{x_1}-\frac{y}{2}}^{\overline{x_k}} (a_2 - a_1) \; d\overline{x}d\overline{y}$$

$$f4) \quad p = \int_0^{J_k} b_1 \int_{\overline{x_1}+\frac{y}{2}}^{1-\frac{J}{2}} a_2 \; d\overline{x}d\overline{y} + \int_{J_k}^{\min(J,J_m)} b_2 \int_{\overline{x_1}-\frac{y}{2}}^{1-\frac{J}{2}} a_2 \; d\overline{x}d\overline{y} + \int_0^{J_k} b_1 \int_{1-\frac{J}{2}}^{1} a_2 \; d\overline{x}d\overline{y}$$
$$+ \int_{J_k}^{J_m} b_2 \int_{1-\frac{J}{2}}^{1} a_2 \; d\overline{x}d\overline{y} - \int_0^{2(\overline{x_k}-\overline{x_1})} b_1 \int_{\overline{x_1}+\frac{y}{2}}^{\overline{x_k}} (a_2 - a_1) \; d\overline{x}d\overline{y}$$

$$f5) \quad p = \int_0^{J_k} b_1 \int_{\overline{x_1}+\frac{y}{2}}^{1-\frac{J}{2}} a_2 \; d\overline{x}d\overline{y} + \int_{J_k}^{\min(J,J_m)} b_2 \int_{\overline{x_1}-\frac{y}{2}}^{1-\frac{J}{2}} a_2 \; d\overline{x}d\overline{y} + \int_0^{J_k} b_1 \int_{1-\frac{J}{2}}^{1} a_2 \; d\overline{x}d\overline{y}$$
$$+ \int_{J_k}^{J_m} b_2 \int_{1-\frac{J}{2}}^{1} a_2 \; d\overline{x}d\overline{y} - \int_0^{2(\overline{x_k}-\overline{x_1})} b_1 \int_{\overline{x_1}+\frac{y}{2}}^{\overline{x_k}} (a_2 - a_1) \; d\overline{x}d\overline{y}$$

$$f6) \quad p = \int_0^{J} b_1 \int_{\overline{x_1}+\frac{y}{2}}^{1-\frac{J}{2}} a_1 \; d\overline{x}d\overline{y} + \int_{J_k}^{J_m} b_2 \int_{1-\frac{y}{2}}^{1} a_1 \; d\overline{x}d\overline{y} + \int_0^{J_k} b_1 \int_{1-\frac{J}{2}}^{1} a_1 \; d\overline{x}d\overline{y}$$
$$+ \int_0^{J_k} b_1 \int_{\overline{x_k}}^{1} (a_2 - a_1) \; d\overline{x}d\overline{y} + \int_{J_k}^{J_m} b_2 \int_{\overline{x_k}}^{1} (a_2 - a_1) \; d\overline{x}d\overline{y}$$

$$f7) \quad p = \int_0^{J_k} b_1 \int_{\overline{x_1}+\frac{y}{2}}^{1-\frac{J}{2}} a_1 \; d\overline{x}d\overline{y} + \int_{J_k}^{\min(J,J_m)} b_2 \int_{\overline{x_1}-\frac{y}{2}}^{1-\frac{J}{2}} a_1 \; d\overline{x}d\overline{y} + \int_0^{J_k} b_1 \int_{1-\frac{J}{2}}^{1} a_1 \; d\overline{x}d\overline{y}$$
$$+ \int_{J_k}^{J_m} b_2 \int_{1-\frac{J}{2}}^{1} a_1 \; d\overline{x}d\overline{y} + \int_0^{J_k} b_1 \int_{\overline{x_k}}^{1} (a_2 - a_1) \; d\overline{x}d\overline{y}$$
$$+ \int_{J_k}^{J_m} b_2 \int_{\overline{x_k}}^{1} (a_2 - a_1) \; d\overline{x}d\overline{y}$$

This page is intentionally left blank.

# Appendix F

# The SLF 43/3/2 Proposal

SUBCOMMITTEE ON STABILITY AND LOAD LINES AND ON FISHING VESSELS SAFETY
43rd session
Agenda item 3

## Development of Revised SOLAS Chapter II-1 Parts A, B and B-1

**Regulation 7-1**
Calculation of the factor $p$

1. The factor $p$ shall be calculated in accordance with paragraph 1.1 using the following notation:

   $x_1$ the distance from the aft terminal of $L_s$ to the foremost portion of the aft end of the compartment or compartment group being considered;

   $x_2$ the distance from the aft terminal of $L_s$ to the aftermost portion of the forward end of the compartment or compartment group being considered;

   $E_1 = x_1/L_s$

   $E_2 = x_2/L_s$

   $E = E_1 + E_2$

   $J$ the non-dimensional length of a compartment, given by the formula: $J = E_2 - E_1$

   $J_{max}$ the maximum non-dimensional damage length, given by the formula: $J_{max} = 48/L_s$ but is not to be taken as greater than 0.24;

   $a$ the assumed distribution density of damage location along the ship's length, given by the formula: $a = 0.6 + 0.4E$

   $F$ the assumed distribution function of damage location along the ship's length, given by the formula: $F = 0.25E(0.6 + a)$

$y$ normalised length of a compartment, given by the formula: $y = J/J_m$

$y_1 = 1 - y$ but is not to be taken as less than zero

$F_0 = 1 - y_1^2$

$F_1 = y - 1/3(1 - y_1^3)$

$F_2 = 1/2y^2 - 1/3y + 1/12(1 - y_1^4)$

$p = F_1 J_{max}$

$q = 0.2F_2 J_{max}^2$

1.1 The factor $p$ is to be determined for each compartment or group of compartments, treated as a single flooded space, according to the following formulae.

1.1.1 Where the aft limit of the compartment or group of compartments under consideration coincides with the aft terminal:
$p = F + 0.5ap + q$

1.1.2 Where the forward limit of the compartment or group of compartments under consideration coincides with the forward terminal:
$p = F + 0.5ap - q$

1.1.3 Where neither limit of the compartment or group of compartments under consideration coincides with the aft or forward terminal:
$p = ap$

1.1.4 Where the compartment considered extends over the entire ship length $L_s$:
$p = F + 0.5ap - q$

2 Where wing compartments are fitted the $p$ value for the wing compartment shall be obtained by multiplying the value, as determined in paragraph 3, by a factor $r$ as determined by paragraph 2.2, which represents the probability that the inboard spaces will not be flooded.

2.1 The $p$ value for the case of simultaneous flooding of a wing and adjacent inboard compartment shall be obtained by using the formula of paragraph 1.1, multiplied by an increase of the factor $r$ due to the increase in the breadth of penetration $b$.

2.2 The factor $r$ shall be determined by the following formulae:
$r = 1$, if $J \leq J_0$ or $w \geq 0.5$ and
$r = 1 - [1 - F_0(z)]r'$ in other cases where the following notation applies:
$b$ is the mean transverse distance in metres measured at right angles to the centreline at the deepest subdivision loadline between the shell and a plane through the outermost portion of and parallel to that part of the longitudinal bulkhead which extends between the longitudinal limit used in calculating the factor $p$. This vertical plane shall be so orientated that the mean transverse distance to the shell is a maximum, but not more than twice the least distance between the plane and the shell;

$w \quad = b/B$

$J_0 \; = 0.12w$

$y_0 \; = J_0/J_{max}$

$w_{max} \; = 2.75J_{max}$

$z \quad = w/w_{max}$

$r'$ The factor $r'$ shall be determined by the following formulae:

$r' = (1 - F_0(y_0))(1 - J_0)$ if $J = 1$ and where $J$ is less than 1:

$r' = 1 - \frac{y_0 + F_1(y_0) + 2(y - y_0)F_0(y_0)}{y + F_1(y)}$ if $E_1 = 0$ or $E_2 = 1$,

$r' = 1 - \frac{F_1(y_0) + (y - y_0)F_0(y_0)}{F_1(y)}$ in all other cases.

In calculating $F_0$ (and $F_1$) in this paragraph, $y$ and $y_1$ shall be replaced by $y_0$ and $(1 - y_0)$ or $z$ and $(1 - z)$, as appropriate.

# PhD Theses
# Department of Naval Architecture and Offshore Engineering
# Technical University of Denmark · Kgs. Lyngby

**1961** **Strøm-Tejsen, J.**
*Damage Stability Calculations on the Computer DASK.*

**1963** **Silovic, V.**
*A Five Hole Spherical Pilot Tube for three Dimensional Wake Measurements.*

**1964** **Chomchuenchit, V.**
*Determination of the Weight Distribution of Ship Models.*

**1965** **Chislett, M.S.**
*A Planar Motion Mechanism.*

**1965** **Nicordhanon, P.**
*A Phase Changer in the HyA Planar Motion Mechanism and Calculation of Phase Angle.*

**1966** **Jensen, B.**
*Anvendelse af statistiske metoder til kontrol af forskellige eksisterende tilnærmelsesformler og udarbejdelse af nye til bestemmelse af skibes tonnage og stabilitet.*

**1968** **Aage, C.**
*Eksperimentel og beregningsmæssig bestemmelse af vindkræfter på skibe.*

**1972** **Prytz, K.**
*Datamatorienterede studier af planende bådes fremdrivningsforhold.*

**1977** **Hee, J.M.**
*Store sideportes indflydelse på langskibs styrke.*

**1977** **Madsen, N.F.**
*Vibrations in Ships.*

**1978** **Andersen, P.**
*Bølgeinducerede bevægelser og belastninger for skib på lægt vand.*

**1978** **Römeling, J.U.**
*Buling af afstivede pladepaneler.*

**1978** **Sørensen, H.H.**
*Sammenkobling af rotations-symmetriske og generelle tre-dimensionale konstruktioner i elementmetode-beregninger.*

**1980** **Fabian, O.**
*Elastic-Plastic Collapse of Long Tubes under Combined Bending and Pressure Load.*

**1980 Petersen, M.J.**
*Ship Collisions.*

**1981 Gong, J.**
*A Rational Approach to Automatic Design of Ship Sections.*

**1982 Nielsen, K.**
*Bølgeenergimaskiner.*

**1984 Nielsen, N.J.R.**
*Structural Optimization of Ship Structures.*

**1984 Liebst, J.**
*Torsion of Container Ships.*

**1985 Gjersøe-Fog, N.**
*Mathematical Definition of Ship Hull Surfaces using B-splines.*

**1985 Jensen, P.S.**
*Stationære skibsbølger.*

**1986 Nedergaard, H.**
*Collapse of Offshore Platforms.*

**1986 Yan, J.-Q.**
*3-D Analysis of Pipelines during Laying.*

**1987 Holt-Madsen, A.**
*A Quadratic Theory for the Fatigue Life Estimation of Offshore Structures.*

**1989 Andersen, S.V.**
*Numerical Treatment of the Design-Analysis Problem of Ship Propellers using Vortex Lattice Methods.*

**1989 Rasmussen, J.**
*Structural Design of Sandwich Structures.*

**1990 Baatrup, J.**
*Structural Analysis of Marine Structures.*

**1990 Wedel-Heinen, J.**
*Vibration Analysis of Imperfect Elements in Marine Structures.*

**1991 Almlund, J.**
*Life Cycle Model for Offshore Installations for Use in Prospect Evaluation.*

**1991 Back-Pedersen, A.**
*Analysis of Slender Marine Structures.*

**1992 Bendiksen, E.**
*Hull Girder Collapse.*

**1992 Petersen, J.B.**
*Non-Linear Strip Theories for Ship Response in Waves.*

**1992 Schalck, S.**
*Ship Design Using B-spline Patches.*

**1993 Kierkegaard, H.**
*Ship Collisions with Icebergs.*

**1994 Pedersen, B.**
*A Free-Surface Analysis of a Two-Dimensional Moving Surface-Piercing Body.*

**1994 Hansen, P.F.**
*Reliability Analysis of a Midship Section.*

**1994 Michelsen, J.**
*A Free-Form Geometric Modelling Approach with Ship Design Applications.*

**1995 Hansen, A.M.**
*Reliability Methods for the Longitudinal Strength of Ships.*

**1995 Branner, K.**
*Capacity and Lifetime of Foam Core Sandwich Structures.*

**1995 Schack, C.**
*Skrogudvikling af hurtiggående færger med henblik på sødygtighed og lav modstand.*

**1997 Simonsen, B.C.**
*Mechanics of Ship Grounding.*

**1997 Olesen, N.A.**
*Turbulent Flow past Ship Hulls.*

**1997 Riber, H.J.**
*Response Analysis of Dynamically Loaded Composite Panels.*

**1998 Andersen, M.R.**
*Fatigue Crack Initiation and Growth in Ship Structures.*

**1998 Nielsen, L.P.**
*Structural Capacity of the Hull Girder.*

**1999 Zhang, S.**
*The Mechanics of Ship Collisions.*

**1999 Birk-Sørensen, M.**
*Simulation of Welding Distortions of Ship Sections.*

**1999 Jensen, K.**
*Analysis and Documentation of Ancient Ships.*

**2000 Wang, Z.**
*Hydroelastic Analysis of High-Speed Ships.*

**2000 Petersen, T.**
*Wave Load Prediction—a Design Tool.*

**2000 Banke, L.**
*Flexible Pipe End Fitting.*

**2000 Simonsen, C.D.**
*Rudder, Propeller and Hull Interaction by RANS.*

**2000 Clausen, H.B.**
*Plate Forming by Line Heating.*

**2000 Krishnaswamy, P.**
*Flow Modelling for Partially Cavitating Hydrofoils.*

**2000 Andersen, L.F.**
*Residual Stresses and Deformations in Steel Structures.*

**2000 Friis-Hansen, A.**
*Bayesian Networks as a Decision Support Tool in Marine Applications.*

**Maritim Teknik**

**Institut for Mekanik, Energi og Konstruktion**

**Danmarks Tekniske Universitet**

Studentertorvet, Building 101E
DK-2800 Kongens Lyngby
Denmark
Phone + 45 4525 1360
Fax + 45 4588 4325
info.mt@mek.dtu.dk
www.mek.dtu.dk

ISBN 87-89502-60-4